K-SHELL EXCITATION OF MOLECULES BY FAST ELECTRON IMPACT

by

GORDON ROBERT WIGHT

B.Sc. Hons., Memorial University of Newfoundland, 1970.

A THESIS SUBMITTED IN PARTIAL FULFILMENT OF
THE REQUIREMENTS FOR THE DEGREE OF

DOCTOR OF PHILOSOPHY

in the Department of

CHEMISTRY

We accept this thesis as conforming to the
required standard

THE UNIVERSITY OF BRITISH COLUMBIA

August, 1974.

In presenting this thesis in partial fulfilment of the requirements for an advanced degree at the University of British Columbia, I agree that the Library shall make it freely available for reference and study. I further agree that permission for extensive copying of this thesis for scholarly purposes may be granted by the Head of my Department or by his representatives. It is understood that copying or publication of this thesis for financial gain shall not be allowed without my written permission.

Department of Chemistry

The University of British Columbia
Vancouver 8, Canada

Date August 15, 1974

ABSTRACT

Energy loss spectra of 2.5 keV electrons, scattered by molecular targets through small angles, have been studied in the regions of the respective carbon, nitrogen, oxygen and fluorine K-edges and the sulfur $L_{II,III}$ edges. Electron energy loss spectra for diatomic, triatomic and polyatomic molecules have been studied. Discrete excitations have been interpreted in terms of the promotion of the respective K-shell electron to unfilled valence molecular orbitals and Rydberg orbitals. Most spectra show considerable structure above the respective K-edge, in addition to the normal K-continuum. This structure represents the simultaneous transitions of a K-shell and valence shell electrons (i.e. shake-up and shake-off events following the creation of an inner hole). In the case of molecular nitrogen and carbon monoxide, a simple core model was shown to provide an accurate description for the K-shell excited molecule. On the basis of this model, excitation and ionization energies for some exotic chemical species have been predicted from the relative energies observed in the K-shell energy loss spectra of a number of molecules. The agreement between the estimated (core analogy) and observed K-shell excitation energies for larger molecules is less satisfactory, possibly because of the large changes in molecular geometry which occur as a result of an election promotion. Finally, the carbon K-shell energy loss spectra of carbon disulfide, carbonyl sulfide and carbon tetrafluoride show features which are possibly associated with the existence of an effective potential barrier in these molecules.

TABLE OF CONTENTS

Page

Page

Page

LIST OF FIGURES

LIST OF PLATES

LIST OF TABLES

ACKNOWLEDGEMENTS

I would like to thank sincerely Dr. C. E. Brion for his interest, encouragement and assistance and Dr. M. J. van der Wiel for the stimulus he injected into the work.

I also acknowledge many helpful discussions with Dr. A. J. Merer and thank him for his interest. In addition, the many discussions with Mr. W.-C. Tam and Mr. S. Tong Lee were most helpful and are appreciated.

The capable staff of the mechanical and electronics workshops were a tremendous asset during all phases of this work; in particular, Mr. E. Gomm and Mr. J. Shim.

Financial support in the form of a National Research Council Science Scholarship is also acknowledged.

Finally, from my wife, daughter and myself, thank you to all who have contributed to an enjoyable stay in Vancouver, especially;

Ron and Bea Thompson

Chris and Elizabeth Brion

Bill and Marilyn Henderson

Frank and Joyce Roberts.

CHAPTER ONE

INTRODUCTION

Electron impact excitation has been used as a spectroscopic technique since the beginning of this century. Indeed, the first experimental demonstration of the quantization of atomic and molecular systems was provided by an energy loss measurement of electrons, inelastically scattered by mercury atoms, in the classic Franck-Hertz experiment[1]. The electron energy loss measurements of Rudberg[2] in 1930 are quite impressive in view of the limited development of electron optics, electron energy analysers and signal processing electronics at that time. However, until the early 1960's there were few experiments in electron impact spectroscopy. At that time, there was a rapid growth in both the quantity and quality of data, largely due to the stimulus provided by two groups; that of Boersch, Geiger et al. and that of Lassettre et al. In fact, as early as 1966, an electron spectrometer with a resolution $\leq$ 0.010 eV was in operation. This was sufficient to resolve rotational structure in the electron energy loss spectrum[3] for molecular hydrogen. Since these measurements, the resolution of electron energy loss spectrometers has not been improved. However, in terms of quantitative measurements, there has been a continual improvement in determinations of generalized oscillator strengths and portions of the Bethe surface. Recently, the dependence of excitation cross-sections on impact energy (the "excitation function") and scattering angle has been

used to identify the nature of atomic and molecular transitions. In particular many electric dipole forbidden transitions have been identified in this manner using low impact energies. The developments and current status of experiments are discussed in a number of reviews[4-9].

In electron energy loss spectroscopy a "monoenergetic" beam of electrons is used to excite the target species. Excitations are detected as energy losses in the scattered electron beam. The process may be represented as follows;

$$X + e \rightarrow X^* + e$$

where X is the target species, e is the "colliding" electron and X^* is the discrete state of the target which is excited by the collision. Discrete electron energy losses occur for every accessible state of the target. Therefore, electron energy loss spectroscopy is an alternative to the use of photoabsorption for investigating the excited states of atoms and molecules. In addition, the scattered intensities observed for fast electron impact and small angle scattering may be quantitatively related to optical oscillator strengths[10,11]. Under these conditions the impinging electron simulates a virtual photon field and electric dipole transitions are dominant. Dipole selection rules do not apply for low impact energies, particularly at large scattering angles, and magnetic dipole, electric quadrupole and spin forbidden processes may be observed. Electron impact excitation is particularly useful at short wavelengths (high excitation energies) where useful photon continuua are difficult to produce.

This thesis describes the application of fast electron impact to a study of the high energy discrete states in the regions of inner shell excitations of small molecules. These high energy states result from the

promotion of an inner shell electron, for example a 1s (K) electron (which for most molecules is nonbonding and mainly atomic in character) to unfilled molecular orbitals and Rydberg orbitals of the molecule. Little information is available about these high energy states.

To excite a molecule to a discrete state by photoabsorption, the photon energy must be exactly equal to the energy required for the transition. In the energy region for K-shell excitation, two continuum light sources exist: (i) Bremsstrahlung and (ii) electron synchrotron radiation. Bremsstrahlung continua are difficult sources for photoabsorption studies because they are usually weak. An electron synchrotron produces a useful continuum, but it is a very expensive facility and of limited availability. K-shell absorptions were first observed for molecular nitrogen using Bremsstrahlung continua[12,13]. Since then, Bremsstrahlung continua have been used to obtain a number of inner shell absorption spectra, although the results are mainly in the regions of sulfur and fluorine inner shell edges[14-26]. Although synchrotron radiation has been available for some time, only K-shell absorption spectra for molecular nitrogen[27] and methane[28] have been reported.

Recently, electron impact has been used for the excitation of inner shell electrons. Low resolution, K-shell electron energy loss spectra of nitrogen and carbon monoxide have been measured at an impact energy of 10 keV[29] and further measurements have been made in coincidence with specific ion products[30]. Also, the K-shell energy loss spectra of some nucleic acid bases have been observed by passing 25 keV electrons through thin solid samples[31].

Further evidence on the discrete excitation of inner shell electrons has been provided by the occurrence of high energy autoionization lines in

Auger electron spectra excited by (i) electron impact[32-36], and, (ii) a carefully selected X-ray line[36]. High energy contributions to the K_α emission spectra of nitrogen[37-39] and (as pointed out by Siegbahn[32]) in carbon monoxide[40], have been attributed to resonance emission from neutral states.

The data presently available on the discrete excitation of inner shell electrons is extremely limited and incomplete. Molecular nitrogen[27] and methane[28] are the only common gases for which reasonable K-shell absorption spectra have been obtained. The object of this research is to obtain and interpret inner shell "absorption" spectra for a variety of gaseous molecules using fast electron impact.

CHAPTER TWO

THEORY OF FAST ELECTRON IMPACT.

2.1. Electron Energy Loss Spectroscopy.

In electron energy loss spectroscopy a beam of "monoenergetic" electrons is used to excite discrete states of an atomic or molecular target. Excitations are detected as electron energy losses in the scattered electron beam. The process may be represented as follows;

$$X + e(E_o) \rightarrow X^*(E_n) + e(E_1,\theta)$$

where X is the target atom or molecule in its ground electronic state, E_o is the kinetic energy of the incident electron beam, X^* is the n^{th} excited state of the target which has energy E_n with respect to the ground state and E_1 is the kinetic energy of an electron which is inelastically scattered through angle θ (with respect to the incident beam) in a collision in which the target is excited to the n^{th} state. The energy equation is given by;

$$E_o = E_1 + E_n + E_t$$

where E_t is the kinetic energy of the projectile electron which is transferred to translational energy of the target during the collision. Using the conservation of energy and momentum, it has been shown[41] that

$$E_t \sim (2mE_o/M)\left[1 - (E_n/2E_o) - \left\{1 - (E_n/E_o)\right\}^{1/2}\cos\theta\right] \quad (2.1.1)$$

where m and M are the masses of the incident electron and target molecule respectively. Because of the large mass disparity between the electron and target, this term is very small and may be neglected. For example, $E_t \sim 10^{-3}$ eV for the promotion of a nitrogen K-shell electron ($E_n \sim 400$ eV)

with experimental conditions used for this study (E_o = 2500 eV and $\theta \sim 0^\circ$). Therefore, the electron energy loss, $E_o - E_1$, is equal to the energy required to excite the n^{th} excited state of the target, E_n. A measurement of the discrete energy losses of the scattered electrons produces the electron energy loss spectrum which gives the energy absorption spectrum of the target. Experimentally, the magnitude of the scattered electron current measured at a given energy loss, $E_o - E_1 = E_n$ and scattering angle θ, is proportional to the differential cross-section,

$$\frac{d\sigma_{on}}{d\Omega}(E_o,\theta)$$

for the excitation of the n^{th} state of the target. It has already been stated that for high impact energies and small scattering angles, there is a quantitative relationship between electron impact cross-sections and optical data[10,11]. The following semiclassical treatment shows why a relationship should exist.

2.2. The Virtual Photon Model.

In fast charged particle impact, excitations are generally produced by distant (or glancing) collisions in which the impact parameter, b, is larger than the dimensions of the atomic or molecular target [see Figure 1(a)]. The electric field experienced by the target in a distant collision with a fast electron (or any structureless charged particle) is sharply pulsed in time and uniform in space. The frequency components of this impulsive field may be obtained from the fourier transform relationship:

$$E(t) = \int I(\omega)e^{i\omega t}\, d\omega; \quad I(\omega) = \int E(t)e^{-i\omega t}\, dt$$

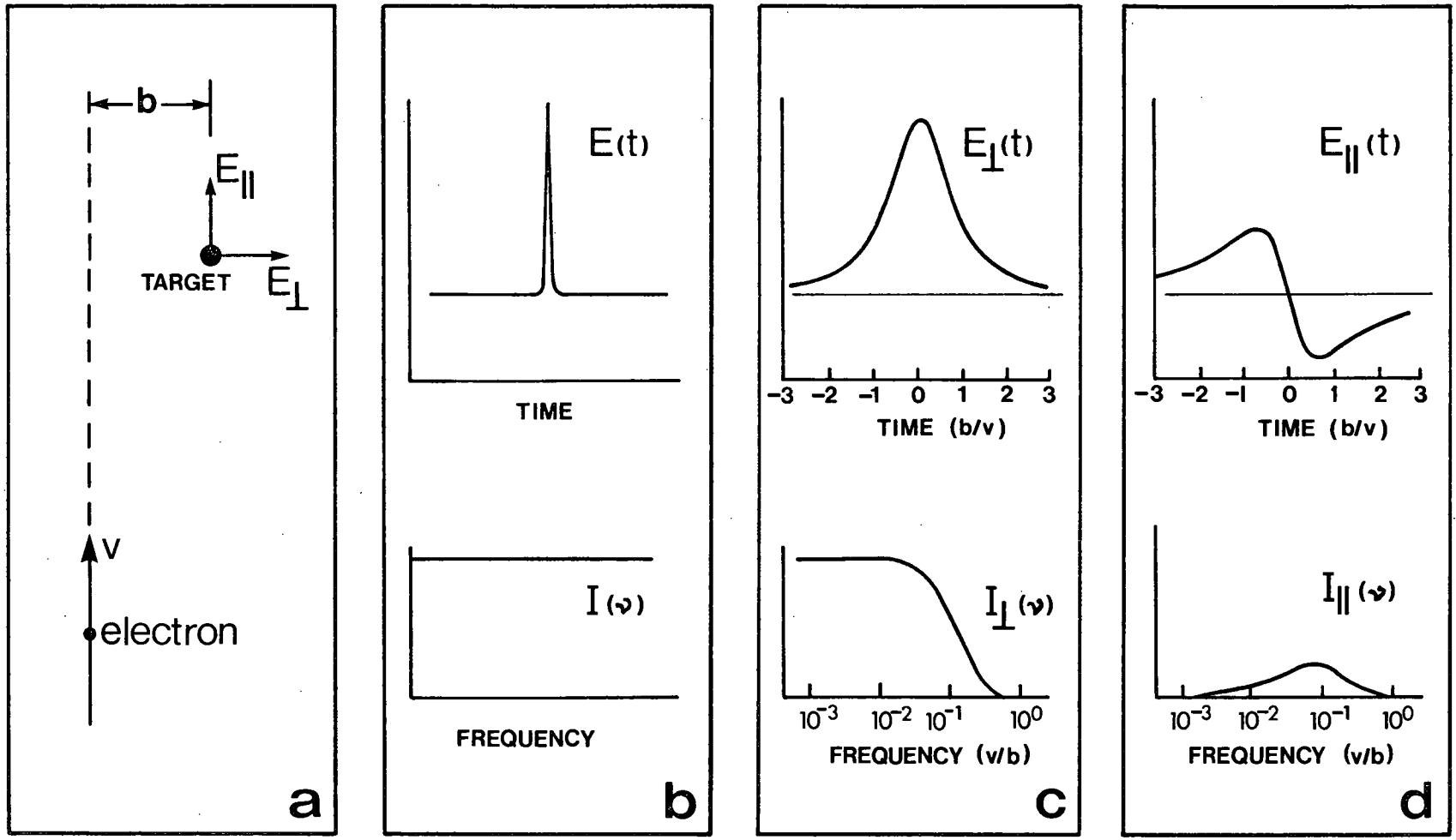

FIGURE 1. Electric field, E(t), and corresponding frequency spectrum, I(ν), associated with a distant collision of a fast electron and molecular target.
a. Collision parameters; v, electron velocity and b, impact parameters.
b. Idealized case for a very fast electron.
c. and d. realistic picture.

where E(t) is the time dependence of the electric field and $I(\omega)$, where $\omega = 2\pi\nu$, is the intensity distribution of the frequency components of the electric field. The faster the incident projectile, the more E(t) resembles a delta function and in this hypothetical limit the fourier transform of the electric field, $I(\omega)$, has equal coefficients at all frequencies [see Figure 1(b)]. Therefore the electric field experienced by the target in a distant collision with a fast electron is similar to the electric field associated with a beam of white light. The interaction of the electron and target may be viewed as the creation of a virtual photon field.

In practice, the electric field pulse has a finite width and therefore $I(\omega)$ is not constant over the entire range of frequencies. This problem has been considered by Christophorou[42]. The results are illustrated in Figure 1(c) and 1(d) where the components of the electric field intensities as a function of time in units of b/v and the frequency spectra $I(\nu)$ have been plotted. Figure 1(c) shows that the intensity perpendicular to the direction of incidence, $I_{\perp}(\nu)$, is a constant over a large range of frequencies (or energies since energy = $h\nu$ where h is Planck's constant) starting at zero frequency and then declines sharply as ν approaches the "cut-off" frequency, v/b. Figure 1(d) shows that the parallel component, $I_{||}(\nu)$ is much less intense and has a peaked intensity distribution. Therefore, $I(\nu) \sim I_{\perp}(\nu)$ and is essentially constant over the range of frequencies normally involved in the excitation of atoms and molecules. The white light analogy is still maintained.

It has been shown[42] that the number of virtual photons ($N\omega$) at frequency ω, is approximately inversely proportional to the energy;

$$N_{\omega} \sim \text{const.}\ (1/\hbar\omega) .$$

The number of electronic transitions, N_n, induced by these virtual photons is proportional to the number of photons with energy equal to the transition energy, E_n, and the optical oscillator strength, f_n, of the transition. Therefore in this "optical approximation";

$$N_n \sim N_\omega \cdot f_n \sim \text{const.}\ (f_n/E_n) \qquad (2.2.1)$$

For fast electron impact and large oscillator strength transitions (i.e. electric dipole allowed), the optical approximation gives a reasonable estimate for the number of primary excitations[42]. One implication of equation (2.2.1) is that valence shell electron excitation predominates over inner shell electron excitation since E_n is much larger for the latter.

For a quantitative relationship between optical oscillator strengths and fast electron impact cross-section data, a quantum mechanical treatment is required. In the derivations which follow, it will be shown that such a relationship does exist and moreover that the optical approximation is in approximate agreement with the quantum results.

2.3. The First Born Approximation.

A theoretical description of fast electron impact excitation was initially derived by Bethe[43] in the 1930's. A recent review which gives more physical insight into the Bethe theory has been written by Inokuti[11]. The basis of the Bethe theory is the first Born approximation which assumes that the interaction between the electron and the target is weak and therefore the incident wave is negligibly distorted by the interaction. The criterion for the validity of this approximation is somewhat arbitrary, but generally the first Born approximation is assumed to be valid if the kinetic energy of the incident electron is some 5-7 times the excitation energy of a particular

transition and the scattering angle is small. Alternatively, the momentum which is transferred in the collision should be small. This condition is also satisfied by fast electron impact and small angle scattering. In order to illustrate the first Born approximation, the simplest electron-atom scattering problem will be considered. The results will then be generalized to more complex atom and molecule scattering.

2.4. Electron-Hydrogen Atom Scattering.

Even this is a three body problem and approximations are necessary. The following derivation is based on that given by Massey and Burhop[44]. The treatment by Moiseiwitsch and Smith is also informative[45].

The Schrödinger equation for the system is

$$\left\{ \nabla_1^2 + \nabla_2^2 + \frac{2m}{\hbar^2}\left[E + \frac{e^2}{r_1} + \frac{e^2}{r_2} - \frac{e^2}{r_{12}} \right] \right\} \Psi(\vec{r}_1, \vec{r}_2) = 0 \qquad (2.4.1)$$

where subscripts 1 and 2 are associated with the incident and atomic electron respectively, $E = E_o + E_t$ is the total energy of the system, where E_o is the energy of the ground state of the hydrogen atom and E_t is the kinetic energy of the incident electron, $\vec{r}_1$ and $\vec{r}_2$ are respectively the position vectors of the incident and atomic electrons with respect to the nucleus (essentially the centre of mass), r_{12} is the interelectron distance and $\Psi(\vec{r}_1, \vec{r}_2)$ is a wavefunction describing the two electrons.

The total wavefunction $\Psi(\vec{r}_1, \vec{r}_2)$ may be expressed in the form,

$$\Psi(\vec{r}_1, \vec{r}_2) = e^{i\vec{k}_o \cdot \vec{r}_1} \cdot \psi_o(\vec{r}_2) + \phi(\vec{r}_1, \vec{r}_2) \qquad (2.4.2)$$

where the first term on the RHS of equation (2.4.2) represents the wavefunction in the absence of any interaction (i.e. an asymptotic solution of

equation (2.4.1), $r_1 \to \infty$) and consists of the product of an incident plane wave describing the incident electron and the electronic wavefunction of the ground state of the hydrogen atom, $\psi_o(\vec{r}_2)$. The wave number k_o is given by

$$k_o^2 = 2mE_t/\hbar^2 .$$

The second term on the RHS of equation (2.4.2) represents terms introduced by the interaction.

The wavefunction $\phi(\vec{r}_1, \vec{r}_2)$ may be expanded in terms of a complete set of states of the hydrogen atom,

$$\phi(\vec{r}_1, \vec{r}_2) \sim \left[\sum_n + \int\right] F_n(\vec{r}_1)\cdot\psi_n(\vec{r}_2) \qquad (2.4.3)$$

where the sum and integral are over the discrete and continuum states respectively. Substitution into (2.4.2), then into (2.4.1) and using the fact that

$$\left[\nabla_2^2 + \frac{2m}{\hbar^2}\left(E_n + \frac{e^2}{r^2}\right)\right] \psi_n(\vec{r}_2) = 0 \qquad (2.4.4)$$

implies:

$$\left[\sum_n + \int\right] (\nabla_1^2 + k_n^2)\, F_n(\vec{r}_1)\, \psi_n(\vec{r}_2) =$$

$$\frac{2me^2}{\hbar^2}\left\{\left(\frac{1}{r_{12}} - \frac{1}{r_1}\right) e^{i\vec{k}_o\cdot\vec{r}_1}\, \psi_o(\vec{r}_2) + \left[\sum_n + \int\right]\left(\frac{1}{r_{12}} - \frac{1}{r_1}\right)\right\}\cdot$$

$$F_n(\vec{r}_1)\, \psi_n(\vec{r}_2) \qquad (2.4.5)$$

where $k_n^2 = (2m/\hbar^2)(E_t - E_n + E_o)$ (2.4.6)

and E_n is the energy of the n^{th} atomic state.

Multiplying both sides of (2.4.5) by $\psi_n^*(\vec{r}_2)$, integrating over $\vec{r}_2$ and using the orthoganality of the atomic functions,

$$\int \psi_n^* (\vec{r}_2)\, \psi_i(\vec{r}_2)\, d\vec{r}_2 = 0 \quad , \quad (n \neq i)$$

gives;

$$(\nabla_1^2 + k_n^2)\, F_n(\vec{r}_1) = U_{no}\, e^{i\vec{k}_o\cdot\vec{r}_1} + \left(\sum_m + \int\right) U_{nm}(\vec{r}_1)\, F_m(\vec{r}_1) \tag{2.4.7}$$

where

$$U_{nm} = \frac{2me^2}{\hbar^2} \int \psi_n^*(r_2) \left(\frac{1}{r_{12}} - \frac{1}{r_1}\right) \psi_m(\vec{r}_2)\, d\vec{r}_2 \tag{2.4.8}$$

$$= (2m/\hbar^2) V_{nm} .$$

Equation (2.4.7) represents an infinite set of coupled differential equations and approximations must be used. In the first Born approximation, the interaction is assumed to be weak and therefore the scattering amplitudes, $F_m(\vec{r}_1)$, are small. Therefore, on the RHS of equation (2.4.7) we neglect the terms in $U_{nm}\cdot F_m$, $m \neq 0$, since they are small in comparison with the first term which involves the incident wave. Hence the essence of the first Born approximation is that the incident wave is negligibly distorted by the weak interaction.

We then must solve

$$(\nabla_1^2 + k_n^2)\, F_n(\vec{r}_1) = U_{on}(\vec{r}_1)\, e^{i\vec{k}_o\cdot\vec{r}_1}, \tag{2.4.9}$$

and we require an asymptotic solution of the form

$$F_n(\vec{r}_1) = r^{-1}\, f_n(\theta,\phi)\, e^{i\vec{k}_n\vec{r}_1} \tag{2.4.10}$$

which is an outgoing spherical wave. $f_n(\theta,\phi)$ is the scattering amplitude corresponding to the excitation of the n^{th} state of the hydrogen atom where the electron is scattered at polar angles θ and ϕ with respect to the direction of incidence. The differential cross-section for the excitation is given by the ratio of the scattered to the incident flux;

$$\frac{d\sigma_{on}}{d\Omega}(\theta,\phi) = I_{on}(\theta,\phi) = \frac{k_n}{k_o} \mid f_n(\theta,\phi) \mid^2 \qquad (2.4.11)$$

where the factor k_n/k_o is in the ratio of the scattered to incident velocity ($V = \hbar k/m$).

To determine $f_n(\theta,\phi)$ a solution of (2.4.9) is required such that the asymptotic form of $F_n(\vec{r}_1)$ is given by (2.4.10). This may be done using the method of Green's Function and gives[45,46]

$$f_n(\theta,\phi) = -(4\pi)^{-1} \int U_{on}\, e^{i(\vec{k}_o - \vec{k}_n)\cdot\vec{r}_1}\, d\vec{r}_1 \qquad (2.4.12)$$

Substitution of (2.4.12) into (2.4.11) gives the following expression for the differential cross-section,

$$I_{on}(\theta,\phi) = (4\pi)^{-2} \frac{k_n}{k_o} \left| \int U_{on}(\vec{r}_1)\, e^{i(\vec{k}_o - \vec{k}_n)\cdot\vec{r}_1}\, d\vec{r}_1 \right|^2 \qquad (2.4.13)$$

It is convenient to introduce the momentum transfer variable $\hbar\vec{K}$ where,

$$\hbar\vec{K} = \hbar\vec{k}_o - \hbar k_n ,$$

the momentum transfer in the collision and $\hbar k_o$ and $\hbar k_n$ are the momenta of the incident and scattered electron respectively. The magnitude of K is given by,

$$K^2 = k_o^2 + k_n^2 - 2k_o k_n \cos\theta \qquad (2.4.14)$$

where θ is the scattering angle.

The differential cross-section (2.4.13) is then

$$I_{on}(\theta,\phi) = (4\pi)^{-2} \frac{k_n}{k_o} \left| \int U_{on}(\vec{r}_1)\, e^{i\vec{K}\cdot\vec{r}_1}\, d\vec{r}_1 \right|^2 \qquad (2.4.15)$$

The total cross-section, Q_{on}, may be obtained by integrating (2.4.15),

$$Q_{on} = \iint I_{on}(\theta,\phi)\, \sin\theta d\theta d\phi.$$

2.5 Generalization to Scattering by Complex Atoms.

If the interaction between the projectile and the atom is Coulombic, then the interaction potential is

$$V = -e^2 \sum_{s=1}^{N} (\vec{r} - \vec{r}_s)^{-1} + \frac{Z_N}{r} \qquad (2.5.1)$$

where $\vec{r}_s$ is the position vector of the s^{th} atomic electron, $\vec{r}$ is the position vector of the incident electron with respect to the nucleus (essentially the centre of mass), Z_N is the nuclear charge and the sum extends over all N atomic electrons. The differential cross-section is then given by (2.4.15) with $U_{on}(\vec{r}_1)$ given by

$$U_{on} = \frac{2me^2}{\hbar^2} \int \psi_n^* \left[- \sum_{s=1}^{N} (\vec{r} - \vec{r}_s)^{-1} + \frac{Z_N}{r} \right] \psi_o \, d\vec{r}_1 \ldots\ldots\ldots d\vec{r}_N \qquad (2.5.2)$$

The expression for the differential cross-section may be simplified by integrating over the coordinates of the incident electron ($\vec{r}$) using the relation[43] (Bethe's integral),

$$\int |\vec{r} - \vec{r}_s|^{-1} e^{i\vec{K}\cdot\vec{r}}\, d\vec{r} = 4\pi K^{-2} e^{i\vec{K}\cdot\vec{r}_s} \qquad (2.5.3)$$

If the atomic wavefunctions are orthogonal, the nuclear term does not contribute to the differential cross-section. The nuclear term will therefore be omitted in the following discussion and if the wavefunctions are not orthogonal, it is a trivial task to add this term.

The differential cross-section then becomes

$$I_{on}(\theta,\phi) = \frac{m^2e^4}{4\pi^2\hbar^4}\frac{k_n}{k_o}\left|\frac{4\pi}{K^2}\int \psi_n^* \sum_{s=1}^{N} e^{i\vec{K}\cdot\vec{r}_s}\ \psi_o\ d\tau_N\right|^2 \quad (2.5.4)$$

where $d\tau_N$ indicates integration over all the coordinates of the N atomic electrons. It is convenient to express (2.5.4) in the following form,

$$I_{on}(\theta,\phi) = \frac{4m^2e^4}{\hbar^4}(k_n/k_o)\,K^{-4}\,|\varepsilon_{on}(\vec{K})|^2 \quad (2.5.5)$$

where the matrix elements, $\varepsilon_{on}(\vec{K})$, are given by

$$\varepsilon_{on}(\vec{K}) = \int \psi_n^* \sum_{s=1}^{N} e^{i\vec{K}\cdot\vec{r}_s}\ \psi_o\ d\tau_N \quad (2.5.6)$$

For most excitations the differential cross-section is only a function of θ [i.e. $I_{on}(\theta,\phi) = I_{on}(\theta)$] because[11]; either the initial state ψ_o is spatially symmetric or the target atoms are randomly oriented. Under these conditions $|\varepsilon_{on}(\vec{K})|^2$ is only a function of $|\vec{K}|$.

From an experimental view, it is more convenient to express the differential cross-section as a function of K rather than θ. Differentiating (2.4.14) where k_o and k_n are constant, gives;

$$d(K^2) = 2k_ok_n\sin\theta d\theta = k_ok_n\frac{d\Omega}{\pi} \quad (2.5.7)$$

Since $I_{on}(\theta,\phi) = \frac{d\sigma_{on}}{d\Omega}(\theta,\phi)$ we replace $d\Omega$ by $2\pi\sin\theta d\theta = \pi d(K^2)/k_ok_n$ and finally obtain from (2.5.5)

$$d\sigma_{on}(K) = \frac{4\pi m^2 e^4}{\hbar^4} k_o^{-2} K^{-4} |\varepsilon_{on}(K)|^2 d(K^2) \qquad (2.5.8)$$

It is relatively easy to generalize (2.5.8) to the case of electron-molecule scattering. Consider a molecule having M nuclei and N electrons. In this case the differential cross-section for the excitation of the n^{th} state is given by (2.5.8) where $\varepsilon_{on}(K)$ is defined by;

$$\varepsilon_{on}(K) = \int \psi_n^* \sum_{m=1}^{M} Z_m e^{i\vec{K}\cdot\vec{R}_m} - \sum_{s=1}^{N} e^{i\vec{K}\cdot\vec{r}_s} \psi_o \, d\vec{\tau}_M d\vec{\tau}_N \qquad (2.5.9)$$

where the ψ's denote molecular wavefunctions which are functions of electronic, vibrational and rotational quantum numbers, $\vec{R}_m$ and $\vec{r}_s$ are respectively the position vectors of the m^{th} nucleus and s^{th} molecular electron with respect to the centre of mass, Z_m is the nuclear charge of the m^{th} nucleus and $d\vec{\tau}_M$ indicates integration over all nuclear coordinates. In terms of the Born-Oppenheimer approximation, the molecular wavefunctions are expressed as the product of an electronic wavefunction depending only on the positions of the electrons (at a fixed nuclear separation) and a wavefunction depending on the nuclear motion. Therefore

$$\psi_{evr}(\vec{r},\vec{Q}) = \psi_e(\vec{r},Q_o)\cdot\psi_{vr}(\vec{Q}) \qquad (2.5.10)$$

where ψ_{evr} designates the total wavefunction describing the electronic (e), vibrational (v) and rotational (r) motions, $\vec{r}$ are the coordinates of the electrons, $\vec{Q}$ the coordinates of the nuclei and Q_o a fixed nuclear configuration. The nuclear terms in (2.5.9) will vanish upon integration over the electronic coordinates if the electronic wavefunctions are orthogonal. The intensities of vibrational excitation accompanying a given electronic transition is simply given by the Franck-Condon factors which are proportional to the overlap between the initial and final vibrational wavefunctions

(see References 11 and 47). It should be noted that the first Born approximation has been assumed to be valid. However, experimentally, it has been found[48,49] that the Franck-Condon factors derived from electron impact data are in agreement with optical values even when the excitation energy is such that the first Born approximation no longer applies. In addition, the relative intensities of vibrational peaks belonging to the same electronic transition are almost independent of scattering angle[49]. These facts may be used to advantage in electron impact spectroscopy and one specific example is the identification of the "C" state of ammonia[50]. A comprehensive, theoretical treatment of the excitation of vibrational levels by electron impact has been given by Bonham and Geiger[51].

2.6. Generalized Oscillator Strengths.

In discussing electron impact excitation it is convenient to use the generalized oscillator strength, $f_n(K)$, which was first introduced by Bethe[43].

$$f_n(K) = (E_n/Q) \, |\varepsilon_{on}(K)|^2 \qquad (2.6.1)$$

where $Q = \hbar^2K^2/2m$ and has the units of energy. Using[11] the Bohr radius, $a_o = \hbar^2/me^2 = 0.52918 \times 10^{-8}$ cm and the Rydberg energy, $R = me^4/2\hbar^2 =$ 13.606 eV, (2.6.1) becomes;

$$f_n(K) = (E_n/R \, (Ka_o)^{-2} \, |\varepsilon_{on}(K)|^2 \qquad (2.6.2)$$

$f_n(K)$ is then a generalization of the optical oscillator strength defined by

$$f_n = (E_n/R) \, M_{on}^2 \qquad (2.6.3)$$

where

$$M_{on}^2 = a_o^{-2} \left| \int \psi_n^* \sum_{s=1}^{N} \vec{r}_s \, \psi_o \, d\tau_N \right|^2 \qquad (2.6.4)$$

M_{on}^2 is the dipole matrix element squared and f_n is proportional to the cross-section for the excitation of the n^{th} state by photoabsorption (dipole approximation).

Consider the case when $\vec{K}$ is directed along the z axis and let z_s be the z coordinate of the s^{th} atomic electron, $\vec{K}\cdot\vec{r}_s = Kz_s$ in (2.5.6). Equation (2.6.2) becomes

$$f_n(K) = (E_n/R)\,(Ka_o)^{-2} \left| \int \psi_n^* \sum_{s=1}^{N} e^{iKz_s} \, \psi_o \, d\tau_N \right|^2 \qquad (2.6.5)$$

For small $\vec{K}$, the exponential in (2.6.5) may be expanded in a power series in K,

$$e^{iKz_s} \sim 1 + (iKz_s) + \tfrac{1}{2}(iKz_s)^2 + \ldots + \tfrac{1}{n!}(iKz_s)^n \qquad (2.6.6)$$

Assuming that ψ_n and ψ_o are orthogonal we obtain[4],

$$\varepsilon_{on}(K) \sim \varepsilon_1(iK) + \varepsilon_2(iK)^2 + \varepsilon_3(iK)^3 + \ldots \qquad (2.6.7)$$

and

$$f_n(K) = (E_n/R)\, a_o^{-2} \left[\varepsilon_1^{\,2} + (\varepsilon_2^{\,2} - 2\varepsilon_1\varepsilon_3)\, K^2 + \ldots + O(K^4) \right] \qquad (2.6.8)$$

where

$$\varepsilon_\ell = \frac{1}{\ell!} \int \psi_n^* \sum_{s=1}^{N} z_s^\ell \, \psi_o \, d\tau_N \qquad (2.6.9)$$

In expressing $f_n(K)$ as a function of even powers of K in (2.6.8) it has been assumed that the wavefunctions ψ_n and ψ_o are real (odd powers of K in $\varepsilon^*\varepsilon$, (2.6.7) substituted into (2.6.5), are imaginary.

For very small momentum transfers, as $K \to 0$, the right side of (2.6.8) is dominated by the first term and

$$\lim_{K \to 0} f_n(K) = (E_n/R)\, a_o^{-2}\, \varepsilon_1^{\,2} = f_n \qquad (2.6.10)$$

where f_n is the optical oscillator strength defined in (2.6.3). Lassettre et al.[52] have shown that (2.6.10) applies regardless of the first Born approximation. However, extrapolations of $f_n(K)$ from relatively large values of K^2, to $K^2 = 0$, may be subject to considerable error. For example, minima may occur in the generalized oscillator strength function at small values of K^2 as illustrated by the $X\ ^1\Sigma^+ \to B\ ^1\Sigma^+$ transition of carbon monoxide[53].

On the basis of (2.6.10) it is easy to distinguish between electric dipole allowed and forbidden transitions:

$$\lim_{K \to 0} f_n(K) \to f_n > 0 \to \text{electric dipole allowed}$$

$$\lim_{K \to 0} f_n(K) \to f_n \simeq 0 \to \text{electric dipole forbidden}$$

In electron impact spectroscopy it is conventional to define an allowed transition as one which is rigorously allowed by electric dipole selection rules even at low energies and large scattering angles where the first Born approximation does not hold. Transitions for which $\varepsilon_1 = 0$ and $\varepsilon_2 \neq 0$ in (2.6.8) are termed "electric quadrupole" transitions. However, the "quadrupole moment", ε_2, is not identical to the electric quadrupole moment which occurs in optical spectroscopy[5]. Expressing z^2 as $r^2/3 + (z^2 - r^2/3)$, ε_2 becomes

$$\varepsilon_2 = 1/3 \int \psi_n^* \sum_{s=1}^{N} r_s^2\, \psi_o\, d\tau_N + \int \psi_n^* \sum_{s=1}^{N} (z_s^2 - r_s^2/3)\, \psi_o\, d\tau_N \qquad (2.6.11)$$

In optical spectroscopy only the second term on the RHS of (2.6.11) contributes to the intensity of electric quadrupole transitions[5]; there is no analogue to the first term. The Lyman-Birge-Hopfield bands of molecular nitrogen provide an example where only the second term of (2.6.11) is nonzero while for the $1^1S \rightarrow 2^1S$ transition in helium only the first term is nonzero[5]. Recently,[54] some group theoretical selection rules have been derived which are valid for all impact energies.

The relationship between the generalized oscillator strength and the optical oscillator strength (2.6.10) has important implications for electron impact spectroscopy;

1. for small momentum transfers, electric dipole selection rules apply to the excitation of atoms and molecules by electron impact

2. optical oscillator strengths may be deduced from electron impact data and

3. optical oscillator strengths may be used to normalize experimental electron impact data.

Three classes of electron impact experiments have been used to derive optical oscillator strengths:

1. Fix the incident energy, E_o, vary θ and extrapolate $f_n(K)$ to $K^2 \rightarrow 0$ (recall that $K^2 = k_o^2 + k_n^2 - 2k_o k_n \cos\theta$ from (2.4.14). This method has been used extensively by Lassettre and co-workers (for examples see References 53,55 and 56).

2. Fix the scattering angle θ, vary E_o and extrapolate $f_n(K)$ to $K^2 \rightarrow 0$. This method has been used by Hertel and Ross[57,58].

3. Use high incident energies ($k_o \sim k_n$) and small scattering angles such that $K^2 = 0$, the generalized oscillator strength is equal to the optical

oscillator strength. This method has been used extensively by Geiger et al. (see References 3, 59-62) and van der Wiel (see Reference 63).

When the first Born approximation is valid, the generalized oscillator strength can be directly related to the differential cross-section. Using (2.6.2) and (2.5.5),

$$f_n(K) = \frac{\hbar^2}{2me^4} E_n(k_o/k_n) K^2 \frac{d\sigma_{on}}{d\Omega} \qquad (2.6.11)$$

It is convenient to introduce[11] an effective generalized oscillator strength $f'_n(K,E_o)$ which can be calculated entirely from experimental measurements regardless of the validity of the first Born approximation.

$$f'_n(K,E_o) = (4a_o^2)^{-1} \left[1 - \frac{E_n}{E_o}\right]^{-1/2} (Ka_o)^2 \frac{E_n}{R} \frac{d\sigma_{on}}{d\Omega} \qquad (2.6.12)$$

When the first Born approximation is valid (large E_o) we can use the Born expression for the differential cross-section (2.5.5) to show,

$$f'_n(K,E_o) \rightarrow f_n(K) \quad , \text{ large } E_o \qquad (2.6.13)$$

where $f_n(K)$ is the generalized oscillator strength defined by (2.6.2). A necessary, although not sufficient, condition[11] for the validity of the first Born approximation is that the effective generalized oscillator strength $f'_n(K,E_o)$ should have the same K dependence at different incident energies, E_o. Therefore, if $f'_n(K,E_o)$ is a different function of K at different impact energies, E_o, the first Born approximation is clearly invalid. On this basis, Skerbele and Lassettre have found transitions in nitrogen[64] and carbon monoxide[53] where deviations are apparent even when the incident energies are high enough to expect the first Born approximation to apply. On the basis of a survey of a number of atomic and molecular transitions, it has been found[53] that deviations from the first Born

approximation are observed when the term symbols of the initial and final states are identical. Therefore, the deviations are dependent on an operator which is totally symmetric.

Experimentally, in an electron energy loss measurement, the differential cross-section for the transition is measured at a fixed incident energy, E_o, and scattering angle θ. Using (2.6.12) and assuming that the first Born approximation applies such that $f_n'(K,E_o) = f_n(K)$,

$$\frac{d\sigma_{on}}{d\Omega} = 4a_o^2 \left[1 - \frac{E_n}{E_o}\right]^{1/2} (Ka_o)^{-2} (R/E_n) f_n(K) \qquad (2.6.14)$$

At $\theta = 0°$ such that Ka_o is a minimum and $E_n << E_o$, it has been shown[11] that,

$$\frac{d\sigma_{on}}{d\Omega} = 16a_o^2 R^2 E_o E_n^{-3} f_n \qquad (2.6.15)$$

where f_n is the optical oscillator strength and E_n is the excitation energy or equivalently the electron energy loss.

CHAPTER THREE

EXPERIMENTAL METHODS FOR INNER-SHELL EXCITATION STUDIES

For molecules composed of second row elements, the inner shell (or core) electrons are the 1s (K) electrons which are nonbonding and mainly atomic in character. Transitions involving the discrete excitation of a K-shell electron occur in the approximate energy regions; 200 eV (62 Å) for boron, 300 eV (41 Å) for carbon, 400 eV (31 Å) for nitrogen, 550 eV (22.5 Å) for oxygen and 690 eV (18 Å) for fluorine. The 2s (L_I) and 2p ($L_{II,III}$) electrons of third row elements are also core electrons when these elements are incorporated in a molecular environment. For sulfur-containing molecules, inner shell excitations require approximately 2475 eV (5 Å) for sulfur K, 220 eV (56 Å) for sulfur L_I and 160 eV (77.5 Å) for sulfur $L_{II,III}$.

A bibliography of inner shell excitation studies has previously been given in Chapter I. Information on discrete excitations has been provided by four types of experiments; photoabsorption, Auger electron spectroscopy, X-ray emission spectroscopy and electron energy loss spectroscopy. Each of these techniques has certain limitations.

Discrete excitation by photoabsorption requires a photon with an energy exactly equal to the energy required for the transition. The difficulty of producing a useful photon continuum in the energy region required for K-shell excitations (soft X-ray) has previously been mentioned; Bremsstrahlung continuua are weak (particularly below 1000 eV) and electron

synchrotron facilities are not readily available. In addition, an electron synchrotron produces a large intensity of photons having energies higher than that required for K-shell excitation and order overlapping in the spectrograph seems to be a problem. In the case of the K-shell absorption spectrum of nitrogen[27], an excess of oxygen (which has strong absorption below 20 Å) had to be included in order to suppress this effect. The design and construction of monochromators for the soft X-ray region is also difficult. Surface reflectivities are extremely poor at such short wavelengths and grazing incidence monochromators must be used. Also, since resolution is on a wavelength scale, it becomes progressively more difficult to obtain high energy resolution in the short wavelength region of the energy spectrum. Since resolution is gained at the expense of intensity, there is a practical limit to the resolution which can be obtained in the soft X-ray region.

In order to discuss the application of Auger electron spectroscopy to inner shell excitation studies it is convenient to give a brief introduction to the technique. The ejection of an inner shell electron by X-ray absorption, electron impact or other methods, results in the production of a highly unstable species. The dominant relaxation process, for molecules composed of second row elements, is by Auger electron ejection[65]. The process may be represented as follows;

i. $X \xrightarrow[\text{or } h\nu]{e} X^{K+} + e$ Initial Ionization

ii. $X^{K+}(E^{K+}) \rightarrow X^{++}(E^{++}) + e(E_1)$

where (i) represents the initial ionization of a K-shell electron and (ii) represents the Auger relaxation process in which the inner shell "hole" is

filled by a valence shell electron and the energy liberated in the process appears as kinetic energy (E_1) of a second valence shell electron (the Auger electron) which is ejected in the process. The kinetic energy of the Auger electron is given by;

$$E_1 = E^{K+} - E^{++}$$

where E^{K+} is the energy of the initial K-shell ion state and E^{++} is the energy of a doubly ionized state of the molecule (both vacancies in the valence shell). If the initial K-shell "hole" state in (ii) is neutral, then the main relaxation process is autoionization which produces a singly charged final state:

$$\text{iii.} \quad X^{K*} (E^{K*}) \rightarrow X^{+} (E^{+}) + e (E_2)$$

where X^{+} represents a singly charged ion state with the vacancy in one of the valence shells. The kinetic energy of the ejected electron, E_2, is equal to the difference in energy between the initial K-shell excited state and the singly charged ion state;

$$E_2 = E^{K*} - E^{+}$$

Referring to processes (ii) and (iii), the energies of the initial K-shell ion (ii) and discrete states (iii) usually differ by less than 10 eV while the doubly charged ion states in (ii) are typically 20 - 30 eV higher in energy than the singly charged states in (iii). Therefore, autoionization processes can be identified since the kinetic energies of the ejected electrons are higher than the maximum energy which can be taken up by an Auger electron. It is also possible for "excited" K-shell ion states (produced by the shake-up of valence electrons in conjunction with K-shell ionization)

to give rise to high energy Auger peaks. However, it can be established that the initial state is neutral and not an "excited" K-shell ion state by comparing the results of excitation by electron impact and X-ray absorption[33-36]. The discrete states are not excited by an X-ray line with energy far in excess of the transition energies and the corresponding autoionization lines are absent from the Auger spectrum. However, the energy of an autoionization line is equal to the energy difference between the initial neutral excited state and some final state of the singly charged species. Therefore, an ambiguity in peak assignment may arise unless one of the states involved in the process can be positively identified.

A competitive relaxation process for a molecule with an inner shell vacancy, is X-ray emission, in which the "hole" is filled by a valence shell electron and the liberated energy appears as a photon (X-ray fluorescence). If the initial state is neutral, then the energy of the emitted photon is equal to the excitation energy of the discrete state (resonance emission). Recently, Siegbahn et al.[38,39,66], have constructed a high resolution X-ray emission spectrometer (ΔE (FWHM) $\simeq$ 0.1 eV) which is capable of resolving some of the vibrational structure of emission bands. The resonance emission from the lowest K-shell excited state of molecular nitrogen has been clearly observed[38,39]. However, emission bands from the higher energy K-shell excited states (observed in Reference 27) have not been reported. In addition, high energy satellite lines in the K-shell X-ray emission spectrum of carbon monoxide have very low intensities and energies and assignments of these lines have not been given[66]. However, for low atomic numbers, emission intensities are expected to be small since

the competition between Auger emission and X-ray fluorescence is dominated by the nonradiative process (see Reference 65). In addition, as in the case of autoionization, an ambiguity in peak assignment may arise, since the final state involved in the emission process may either be the ground electronic state or any of the neutral, valence shell excited states of the molecule.

The only condition for the excitation of a neutral state by electron impact is that the kinetic energy of the incident electron must be greater than the transition energy. Since the kinetic energy of the incident electron is determined by the potential difference between the electron source and collision region, the problems of an energy source for K-shell excitations encountered in photoabsorption studies, do not exist. In addition, the lifetimes of these high energy states are relatively short and therefore the natural line widths are large. The uncertainty broadening of the excited states in the regions of the respective carbon, nitrogen and oxygen K-edges is probably[39] around 0.1 eV. This estimate is supported by the clear resolution of vibrational structure (0.26 eV spacings) in the high energy autoionization band of carbon monoxide[32]. In principle the resolution obtainable in electron energy loss spectroscopy is an order of magnitude lower than the natural line widths (see for example Reference 3) and therefore, electron impact spectroscopy can potentially provide as much information about these states as optical absorption spectroscopy. Also, with the use of a suitable retarding lens, electrons can be energy analysed at constant energy, E, and the resolution ($\Delta E/E$) is constant over the entire energy loss spectrum. Therefore, even for incident electrons with energies in the keV range, and energy losses in the 300 - 700 eV energy

region, "high" resolution can be obtained by preretarding the scattered electrons and energy analysing at a sufficiently low energy. Figure 2 shows the parameters relevant to a comparison of resolution on a wavelength and energy basis and is helpful in comparing and contrasting photoabsorption and electron impact spectroscopy. In Figure 2 the resolution, $\Delta\lambda$ (Å), corresponding to fixed values of resolution, ΔE (eV), has been plotted as a function of energy. To illustrate the use of Figure 2, consider the following examples; for carbon K-shell excitation, $\sim$ 300 eV (41 Å), a resolution, ΔE, of 0.5 eV corresponds to a resolution $\Delta\lambda$ of $\sim$ 0.1 Å, while for fluorine K-shell excitation, $\sim$ 700 eV (18 Å), a resolution of 0.5 eV corresponds to a resolution, $\Delta\lambda$, of 0.02 Å. The K-shell photoabsorption spectrum of nitrogen[27] was obtained with a resolution $<$ 0.03 Å which corresponds to a resolution $<$ 0.4 eV at 400 eV (31 Å). In the case of electron impact, a resolution of $\sim$ 0.1 eV can be obtained with only modest "monochromation" of the incident beam. This, and the fact that there is no difficulty in obtaining an energy source in electron impact spectroscopy, suggests that there are advantages to the use of electron impact over photoabsorption methods in the soft X-ray and X-ray regions.

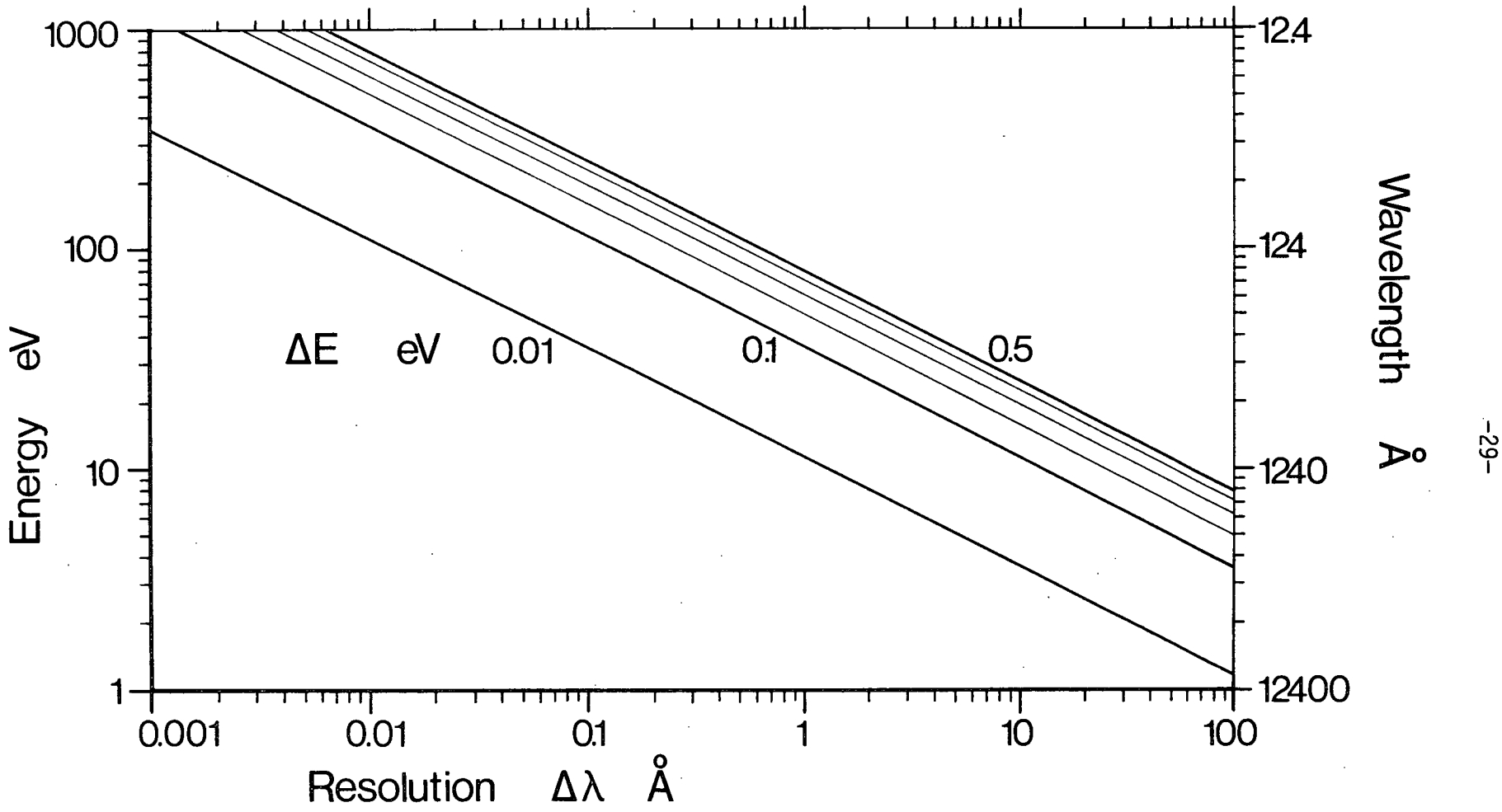

FIGURE 2. Resolution, $\Delta\lambda$ (Å), plotted against energy for fixed values of resolution, ΔE (0.01 to 0.05 eV).

CHAPTER FOUR

EXPERIMENTAL

4.1. 180° Electrostatic Analyser.

One of the most important components of an electron spectrometer is the electron energy, or momentum analyser. The kinetic energies of scattered electrons are usually measured by deflecting the electrons in an electric or magnetic field. Alternatively, a combination of electric and magnetic fields may be used. The properties and relative merits of different types of electron energy analysers have been discussed in a number of review articles.[8,9,67-69]

A hemispherical electrostatic analyser was selected for this work for the following reasons; (i) electrostatic deflection was chosen over magnetic deflection because uniform magnetic fields are more difficult to produce and control than electrostatic fields. In addition, problems of fringe fields are more severe in the case of a magnetic analyser. (ii) the two dimensional focusing properties of the hemispherical electrostatic analyser are ideally suited for coupling to strongly decelerating lenses of axial symmetry.

The properties of hemispherical electrostatic analysers have been discussed by Purcell[70], Simpson[71], Simpson and Kuyatt[72,73] and Sar-El[68]. A schematic diagram is shown in Figure 3. Electrons are deflected by the $1/r^2$ electrostatic field produced by the potential difference, V_{12}, between the two hemispherical surfaces with radii $r_2 > r_1$. The magnitude

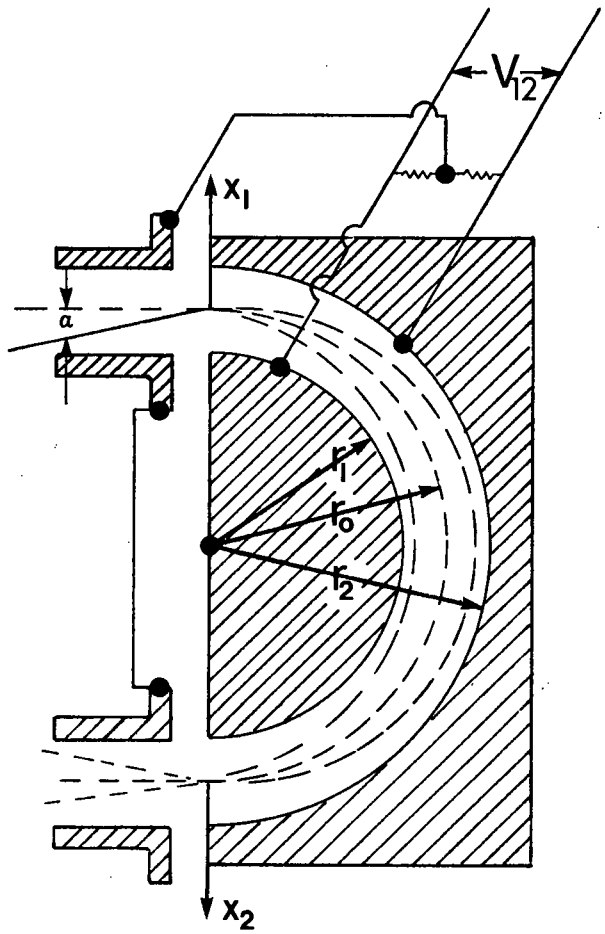

FIGURE 3. Schematic diagram of a hemispherical electron energy analyser.

of the electrostatic field is given by

$$\xi(r) = C/r^2 \qquad (4.1.1)$$

where C is a constant. Consider an electron with kinetic energy $E_o = mu_o^2/2$ which enters the analyser at the point $x_1 = 0$ and at an angle $\alpha = 0°$. In order for the electron to follow a circular path with radius r_o, the centrifugal force must be equal to the electrostatic force, e , at r_o;

$$mu_o^2/r_o = e\xi(r_o) = eC/r_o^2 \qquad (4.1.2)$$

Since the kinetic energy, $mu_o^2/2$ is equal to eV_o in electron volts; from (4.1.2),

$$C = 2r_oV_o = (r_1 + r_2)V_o \qquad (4.1.3)$$

where r_o is chosen as the midpoint. The potential at point r is given by;

$$V(r) = \frac{C}{r} + B \qquad (4.1.4)$$

where B is a constant. The potentials of the inner and outer hemispheres with respect to point r_o are then

$$V(r_1) - V(r_o) = C/r_1 - C/r_o \qquad (4.1.5)$$

$$V(r_o) - V(r_2) = C/r_o - C/r_2 \qquad (4.1.6)$$

and therefore the potential difference across the hemispheres is given by

$$V(r_1) - V(r_2) = C/r_1 - C/r_2$$

$$= V_o \left[(r_2/r_1) - (r_1/r_2)\right] \qquad (4.1.7)$$

Let x_1 be the radial distance from r_o of an electron entering the analyser at angle α and energy E. It has been shown[73] that the deviation, x_2, of the transmitted electron from the radial path, r_o, is given by;

$$(x_2/r_o) = -(x_1/r_o) + 2(\Delta E/E_o) - 2\alpha^2 \qquad (4.1.8)$$

where $\Delta E = E - E_o$. Since there is no linear term in α, the analyser has first order angular focusing (the angular focusing is perfect at 360°)[74]. In addition, because of the spherical symmetry, the analyser has two dimensional focusing properties.

The energy resoltuion (i.e. the transmission of electrons as a function of energy taking into account the distribution of incident electrons over space and angle can be approximated by[73]

$$\Delta E(FWHM)/E_o = S/2r_o \qquad (4.1.9)$$

where $\Delta E(FWHM)$ is the full width at half maximum of the transmitted beam and S is the slit width or diameter for a circular aperture. Expression (4.1.9) neglects a term in α^2 and is only applicable if $\alpha^2 << S/2r_o$.

The analyser used for this research has the following dimensions;

$r_1 = 1.5$ inches

$r_o = 2.0$ inches

$r_2 = 2.5$ inches

$S = 0.050$ inches

The ratio of the potential dividing resistors R_2/R_1) is given by the ratio of the potentials V_2/V_1 and for the dimensions of our analyser using (4.1.5) and (4.1.6):

$$R_2/R_1 = V_2/V_1 = 3/5 \qquad (4.1.10)$$

The theoretical resolution (neglecting the α^2 term) is given by (4.1.9),

$$\Delta E/E_o = S/2r_o = 0.0125 = 1.25\% \qquad (4.1.11)$$

In order to test the performance of the analyser, the resolution,

(i.e. ΔE(FWHM), as a function of electron energy, $E_o = eV_o$) was measured at 0° scattering with helium as a target gas. The results are shown in Figure 4. The ΔE(obs) curve is a convolution of the energy spread of the gun and energy transmission function of the analyser. By extrapolating to $E_o = 0$, the gun spread was estimated as $\sim$ 0.28 eV. The lower curve represents the energy transmission width of the analyser and was obtained by corrected ΔE(obs) for the gun spread (the energy distributions were assumed to be approximately Gaussian[73]). The experimental resolution of the analyser is 1.23%, in good agreement with the theoretical estimate of 1.25% (see 4.1.11). An additional check of the analyser was performed by plotting the focus potential, V_{12}, of the hemispheres as a function of electron energy eV_o. The experimental plot was a straight line, $V_{12} = 1.07\ V_o$, in exact agreement with the theoretical value calculated using (4.1.7) and the dimensions of our analyser.

4.2. The Electron Source.

The electron source for the spectrometer was a Philips 6AW59 television gun consisting of an indirectly heated oxide cathode (BaSrO), grid, anode and focusing element (Einzel lens). A circuit diagram of the electron gun power supply is shown in Figure 5. The advantage of an oxide cathode source is that a reasonably monoenergetic beam, ΔE(FWHM) $\sim$ 0.25 eV , can be produced without using an energy selector. This is a result of the low work function of the mixed oxide cathodes, which means that they can be operated at much lower temperatures than other emitters. For a thermionic cathode[67,72], ΔE(FWHM) = 2.54 kT where k is the Boltzmann constant (1/11600 eV/^oK). This implies a ΔE(FWHM) of $\sim$ 0.25 eV for a normal

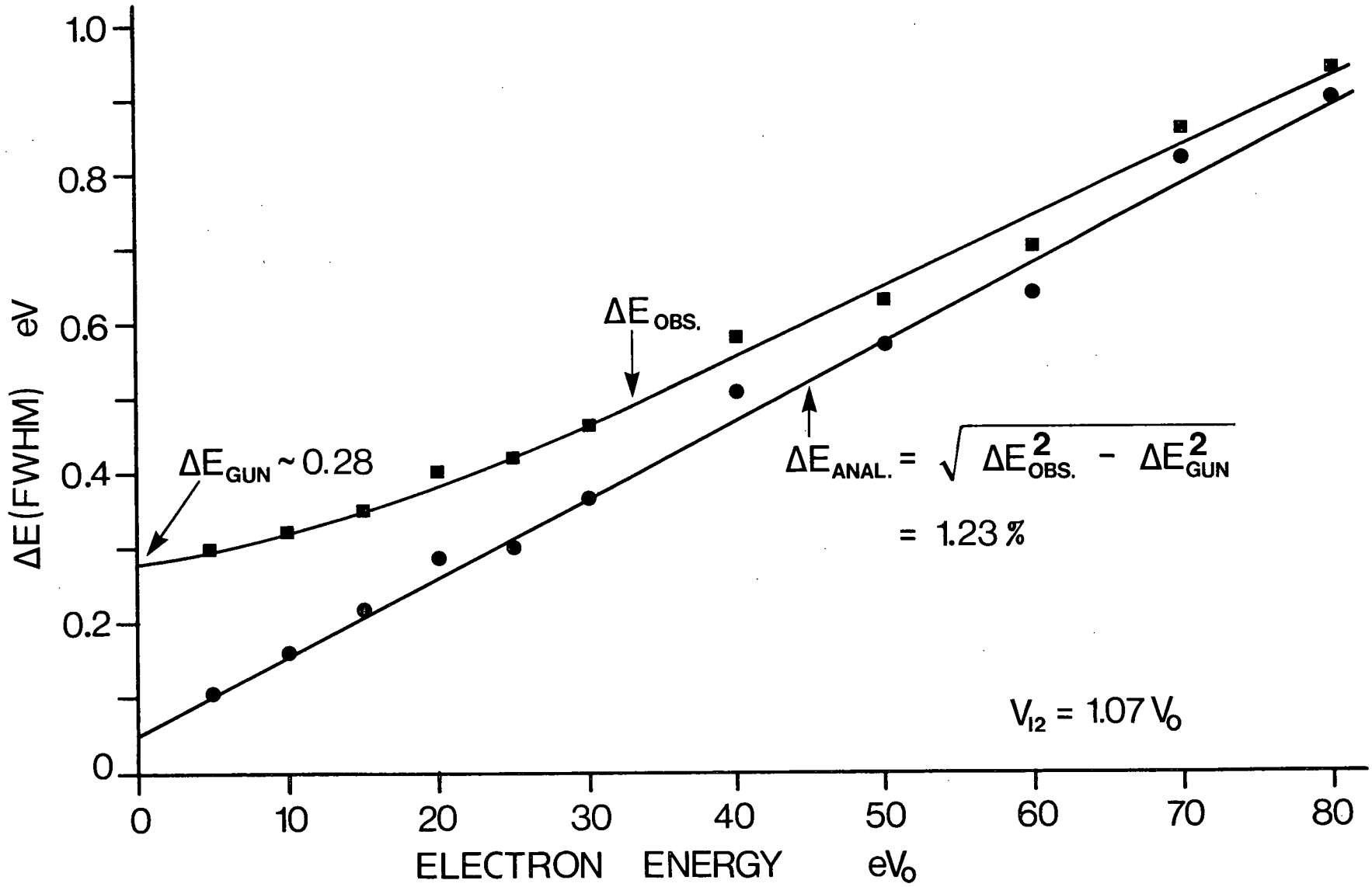

FIGURE 4. Resolution, ΔE (FWHM), vs. electron energy for the 180° electron energy analyser: ■ observed (convolution of gun and analyser spreads), ● analyser only (gun spread subtracted).

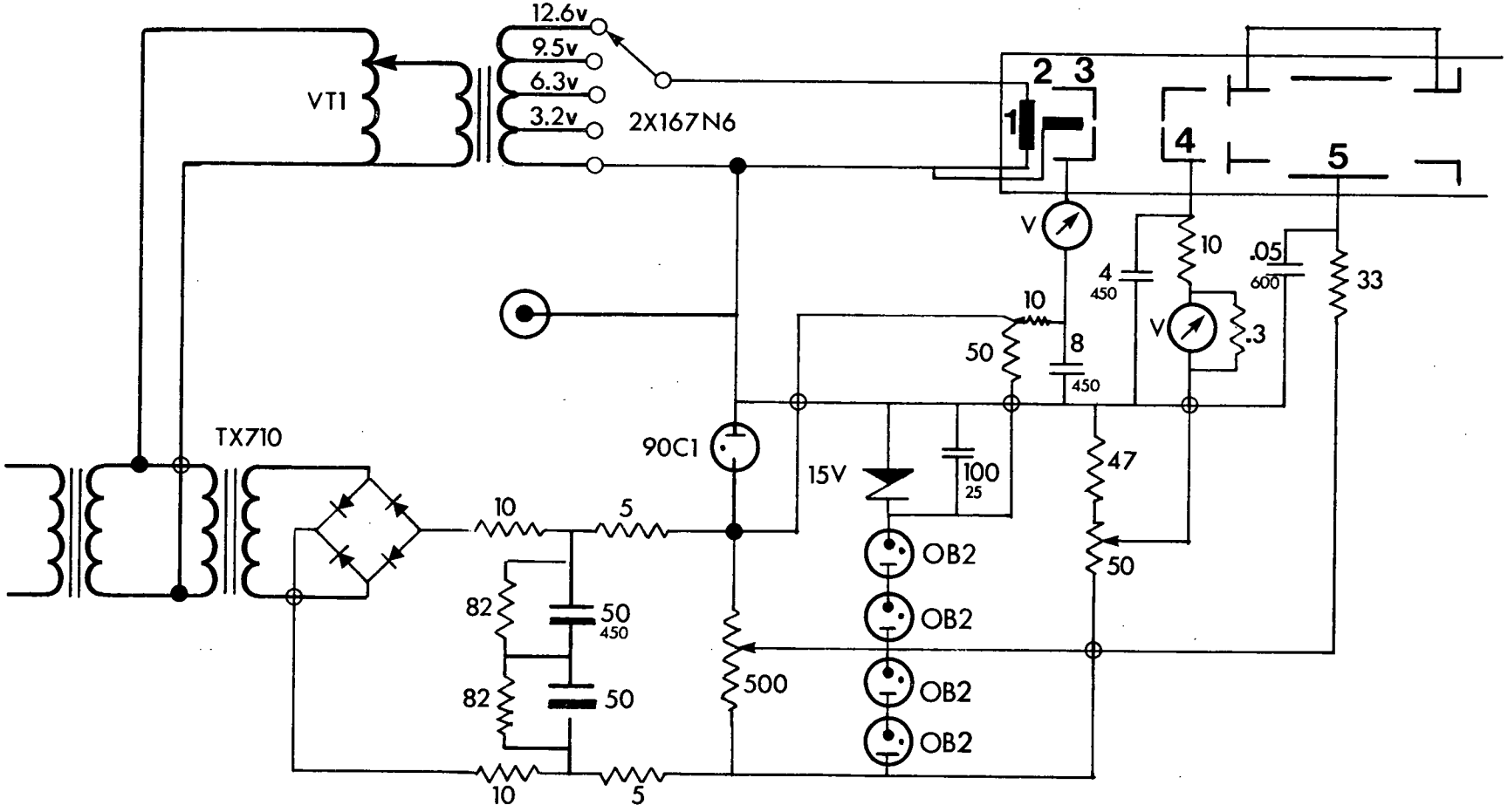

FIGURE 5. Electron gun power supply; 1. filament, 2. cathode, 3. grid, 4. anode and 5. focus. Resistors are in KΩ and capacitors in μF.

operating temperature of approximately 1100 ^{o}K. The experimental value obtained by extrapolation of the observed ΔE(FWHM) is $\sim$ 0.28 eV (see Figure 4). In addition, the television gun produces a well focused beam. However, a major disadvantage is that the oxide cathode is readily poisoned by most gases, particularly by strong oxidizers such as oxygen and nitric oxide. In the present experiment, this difficulty was partially overcome by operating the gun with a higher filament voltage which tended to reduce its useful lifetime. A more satisfactory solution would be to build a differentially pumped source.

4.3. The Spectrometer.

Plate 1 is a photograph of the spectrometer and Figure 6 shows a schematic diagram. The main components are: A, the electron gun (oxide cathode) and Einzel lens; B and F, quadrupole electric deflection plates; c, collision chamber operated at typical gas pressures of 10^{-4} torr; D, gas inlet; E, angular selection plate; G, decelerating lens; H, hemispherical analyser; and I, channel electron multiplier.

4.3.1. Spectrometer Construction.

The spectrometer was constructed from brass with the exception of the angular selection plate, E, and the aperture plates of the analyser, which were machined from molybdenum. The deflection plates were 0.4" x 0.6" and the angular selection plate and analyser "slit" plates have apertures of 0.050". The lens, G, is an equal diameter (D = 1.9") two tube cylindrical lens with a high voltage element (length 1.21 D), a gap of 0.16 D and a low voltage element (length 0.84 D), (the lens para-

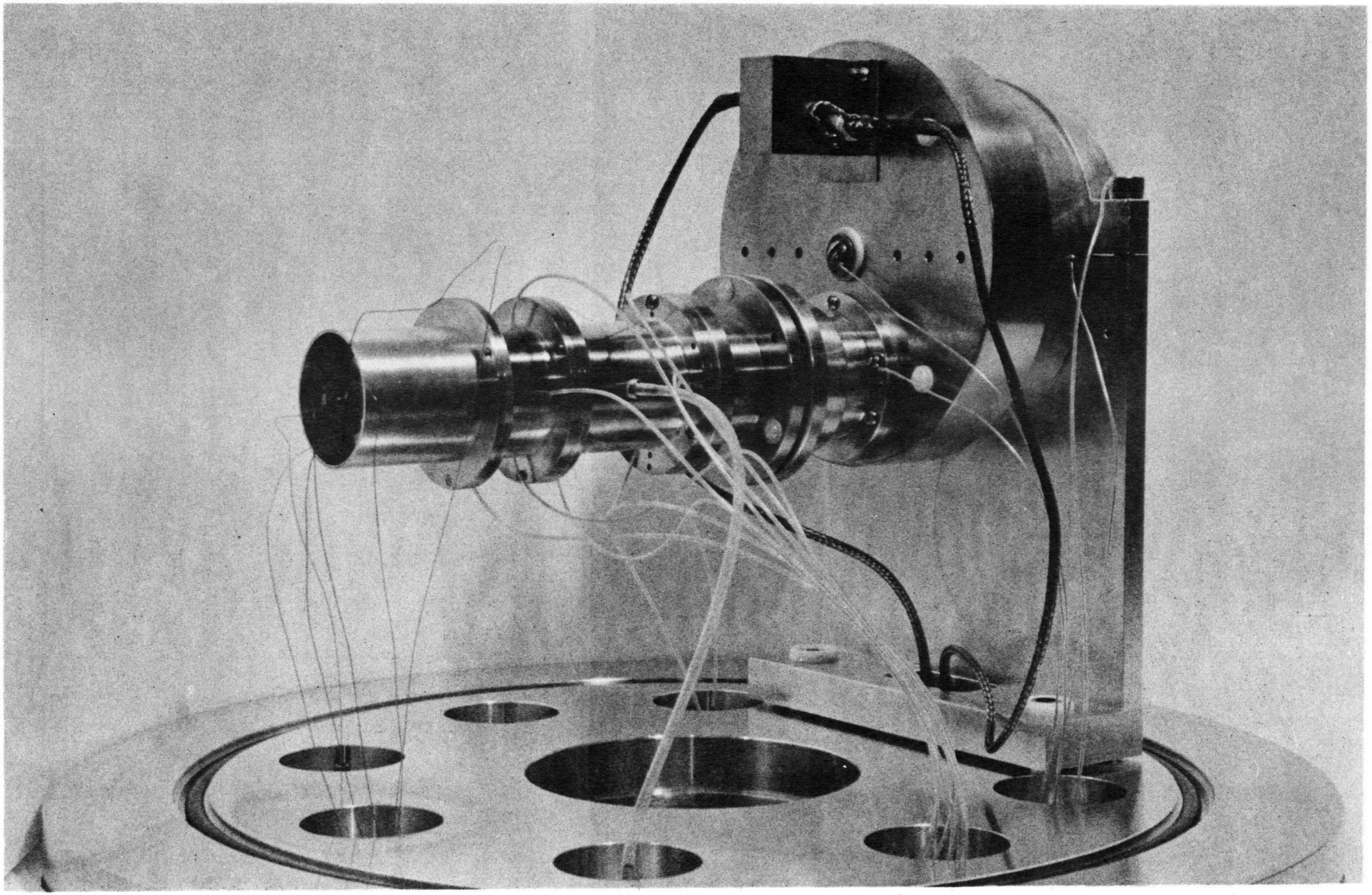

PLATE 1 The Spectrometer.

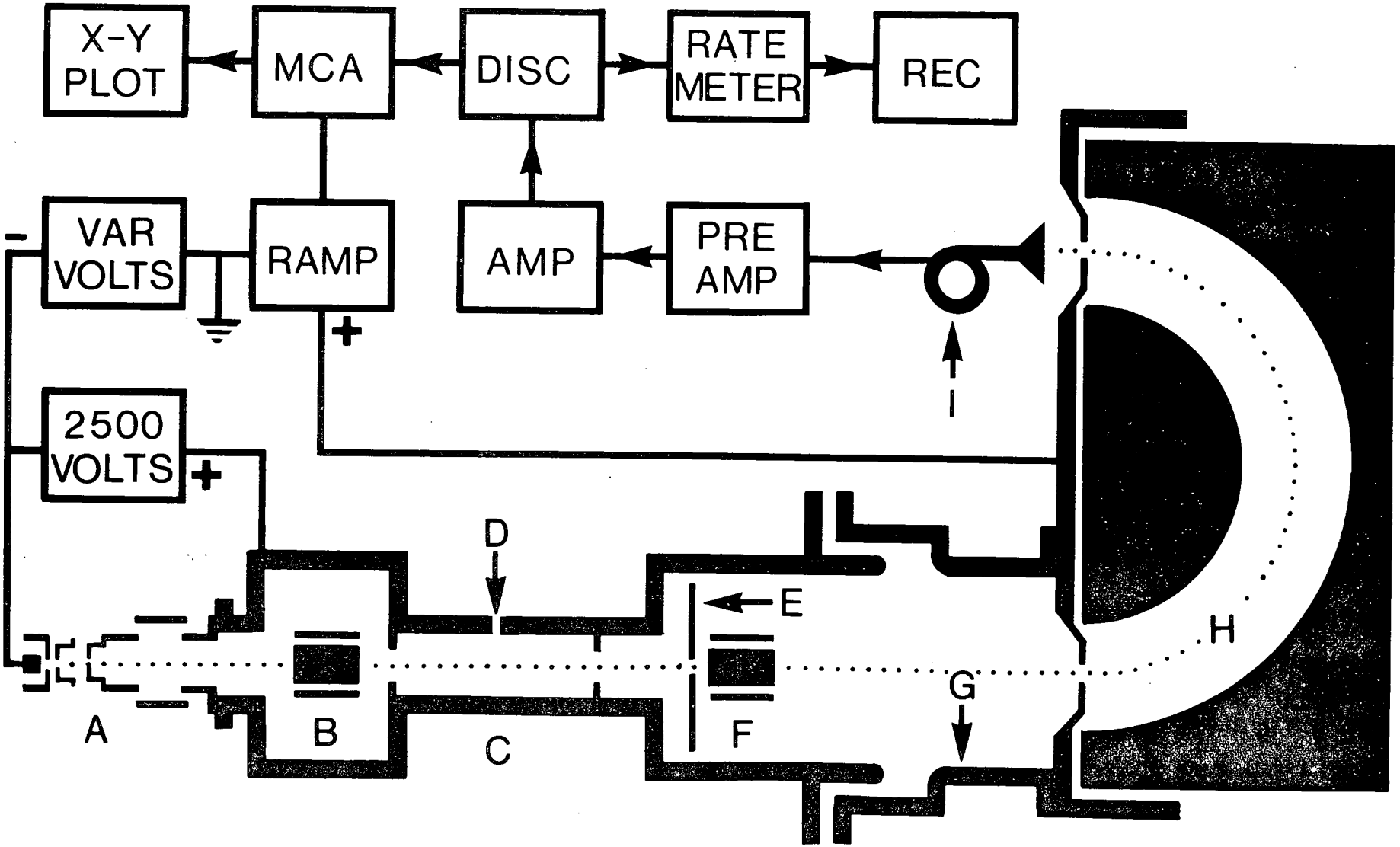

FIGURE 6. Schematic diagram of the apparatus.

meters are essentially those used by van der Wiel[63]). Electrical insulation between components operating at different potentials was initially provided by boron nitride spacers. However, these proved to be very brittle, which was an inconvenience when the machine was dismantled for cleaning. This problem was overcome by rebuilding the spectrometer using precision sapphire balls (located in undersized holes) as insulators. An additional advantage is that the balls also serve as accurate locaters. Initially all brass surfaces were gold plated to provide a uniform surface potential. However, it was found that the performance of the spectrometer was not degraded by the omission of this step. The surfaces of the hemispheres and aperture plates were coated with a uniform layer of benzene soot to minimize the number of surface scattered electrons. In addition, a slot (0.13" x 2.8") was milled in the back hemisphere (behind the entrance slit) to reduce the number of back-scattered and secondary emitted electrons. The performance of the analyser was not impaired by this modification.

4.3.2. Spectrometer Operation.

The electron beam was accelerated towards the collision region by a 2.5 kV potential difference. The quadrupole deflection plates B and F were used to control the beam direction and the electron current was monitered by deflecting the beam onto the angular selection plate, E, which was floated, through a precision electrometer, by the high voltage power supply. For K-shell energy loss measurements, it was not possible to obtain spectra at a 0° scattering angle because of the large intensity (even with the slot) of scattered and secondary emitted electrons produced by the fast primary electron beam colliding with the back hemisphere. The

primary beam was therefore deflected by the plates, B, such that it was intercepted by the angular selection plate, E. Electrons having an average scattering angle of 2×10^{-2} radians passed through the angular selection plate aperture into the decelerating lens. Energy loss spectra were obtained by scanning the electric potential applied to the decelerating lens (usually from ground to +40 V) while the cathode potential was floated at a negative voltage (corresponding to the approximate K-shell energy loss; e.g. for nitrogen K-shell, -425 V). The accuracy of the energy scale obtained was $\pm$ 0.02 eV. The transmission energy of the analyser was set at 25 eV and the resolution [ΔE(FWHM)] was $\sim$ 0.5 eV. Output pulses from the multiplier were processed by standard pulse electronics (see Figure 6) and stored in a multiscaler, whose channel advance was synchronous with the scanning voltage applied to the decelerating lens. The zero of the energy scale for each spectrum was determined by recording the peak from elastically scattered electrons (measured as a d.c. current using the electron multiplier as a Faraday cup) and the K-shell spectrum (pulse counting) under identical experimental conditions (beam intensity, deflection angle and target gas pressure). The elastic peak was too intense to record in the pulse counting mode. In order to measure the valence shell energy loss spectrum, the beam intensity was reduced such that the pulse counting mode could be used. K-shell energy loss spectra, were usually obtained using primary beams intensities of 0.1 μA to 1 μA. Although some structure was usually apparent after a single scan, it was usually necessary to signal average for some hours (typically overnight) in order to obtain a spectrum with a good signal to noise ratio for the weaker intensity structures.

4.3.3. Energy Calibration.

The energy scale was usually fixed with respect to the elastic peak as described in Section (4.3.2). The voltages were measured using a digital voltmeter with an accuracy of ± 0.1 volt on the 1000 volt range. Since a calibrated voltage source in the 200 - 700 volt region was not continuously available, the lowest energy discrete peaks in the K-shell energy loss spectra of molecular nitrogen and carbon monoxide (both carbon and oxygen K-shells) were measured with a Fluke 343 A calibration power supply. This provided three internal energy standards (N_K = 400.93 ± 0.05 eV, C_K = 287.28 ± 0.05 eV and O_K = 534.0 ± 0.1 eV) which were periodically used to calibrate the digital voltmeter. Absolute energies were determined for the ammonia spectrum by recording the nitrogen K-shell spectrum of several mixtures containing different partial pressures of methane and molecular nitrogen and calibrating the ammonia peaks with respect to the intense 400.93 eV peak of nitrogen (see Figure 7). The carbon K-shell energy loss spectrum of methane was similarly calibrated against the first discrete peak observed in the K-shell energy loss spectrum of carbon dioxide (290.7 ± 0.2 eV), (see Figure 7). The absolute energies are accurate to ± 0.2 eV for all K-shell spectra unless otherwise stated.

4.3.4. Vacuum System.

The complete experimental arrangement is shown in Plate 2. The vacuum chamber consists of a 16" outside diameter aluminum tube, 16" in height with a 1/2"-thick wall. The bottom of the tube rests on a viton O-ring located in a machined groove in the baseplate (see Plate 1). The top of the chamber is similarly closed with an aluminum lid (containing an air

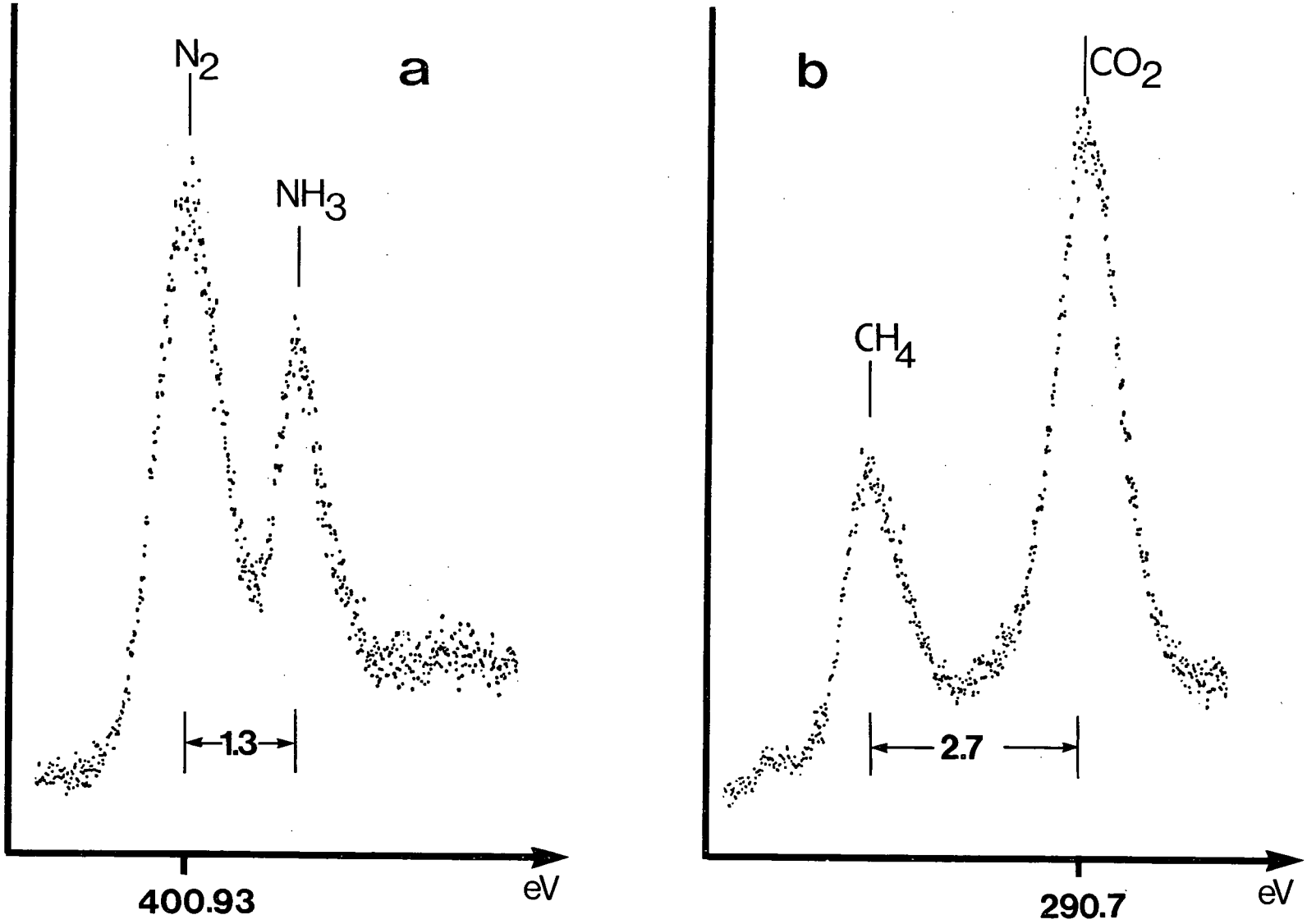

FIGURE 7. Energy calibration of K-shell spectra;
a. ammonia calibrated using molecular nitrogen (400.93 eV peak),
b. methane calibrated using carbon dioxide (290.7 eV peak).

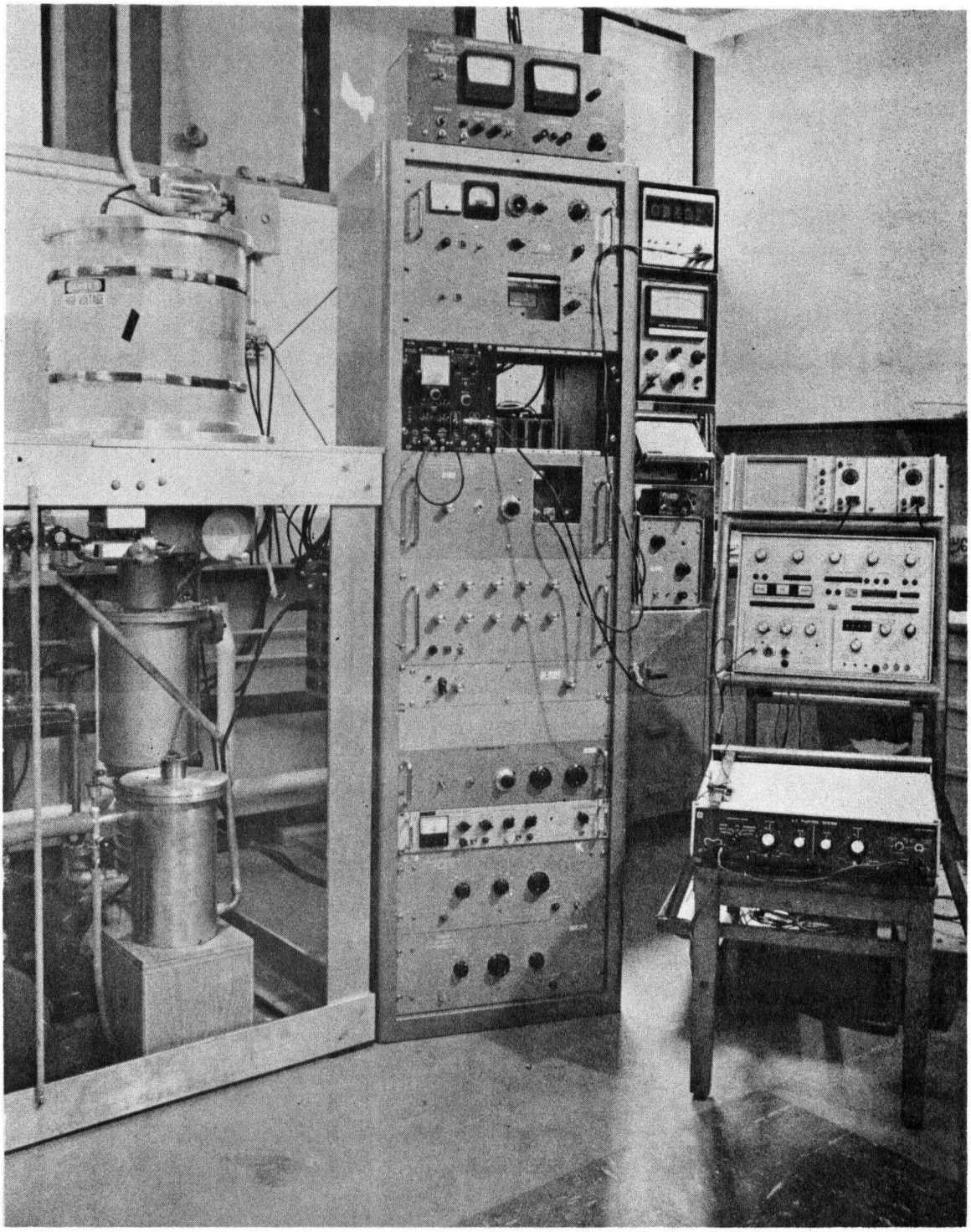

PLATE 2 Complete Experimental Arrangement.

inlet valve and ionization gauge head) and O-ring seal. All electrical connections are made via high voltage ceramic octal-plugs or single feed-throughs. These are soldered into flanges which are bolted to the lower side of the baseplate and sealed with viton O-rings. The lid and vacuum chamber may therefore be easily removed (no bolts are used on the main chamber) to provide ready access to the spectrometer.

The vacuum chamber is screened from magnetic fields by a mu-metal shield (not shown in Plate 2).

The vacuum is produced by an NRC 4" diffusion pump (using Convalex 10 polyphenyl ether) with a water baffle, liquid nitrogen trap, and 5" gate valve between the pump and vacuum chamber. The typical base pressure of the system is $\sim 1 \times 10^{-6}$ torr.

4.4. Sample Purity.

All chemical samples used in this study were commercially purchased and used without further purification. For liquid samples the normal degassing procedure was followed. The stated minimum purity of the samples was as follows:

N_2	99.99%	CH_4	99.99%
CO	99.5%	NH_3	99.99%
O_2	99%	H_2O	DISTILLED
NO	98.5%	CH_3OH	99.9%
CO_2	99.99%	CH_3OCH_3	99.9%
N_2O	98%	CH_3NH_2	98%
CS_2	FISHER SPECTROANALYSED	CF_4	99.7%
COS	97.5%	CH_3COCH_3	FISHER SPECTROANALYSED

CHAPTER FIVE

DIATOMIC MOLECULES

5.1. Nitrogen and Carbon Monoxide

5.1.1. Nitrogen.

The ground state electron configuration of the nitrogen molecule is

$$(1s\sigma_g)^2\ (1s\sigma_u)^2\ (2s\sigma_g)^2\ (2s\sigma_u)^2\ (2p\pi_u)^4\ (2p\sigma_g)^2,\ {}^1\Sigma_g^+.$$

a. Valence Shell Spectrum.

The valence shell electron energy loss spectrum is well known and was recorded to test the spectrometer performance and also to provide a purity check of the sample. In addition, some indication of the possibility of forbidden transitions contributing to the K-shell spectrum may be obtained. The valence shell electron energy loss spectrum of molecular nitrogen is shown in Figure 8. Molecular nitrogen has been thoroughly studied in this energy region by both optical (see Reference 75) and electron energy loss spectroscopy (see Reference 5). An electron energy loss spectrum has been obtained[62] with 25 keV incident energy electrons and a resolution, ΔE(FWHM), of 0.01 eV. The locations of the peaks observed in our low resolution spectrum (ΔE(FWHM) 0.5 eV) are consistent with the higher resolution results. Peak A with a maximum at 9.2 eV in our spectrum is associated with the Lyman-Birge-Hopfield bands, ${}^1\Sigma_g^+ \rightarrow a\ {}^1\Pi_g$ $(2p\sigma_g \rightarrow 2p\pi_g)$. This transition is forbidden by electric dipole selection rules ($g \nleftrightarrow g$), although it gives rise to weak photoabsorption because of magnetic dipole and electric quadrupole interactions (see Reference 76). The transition is

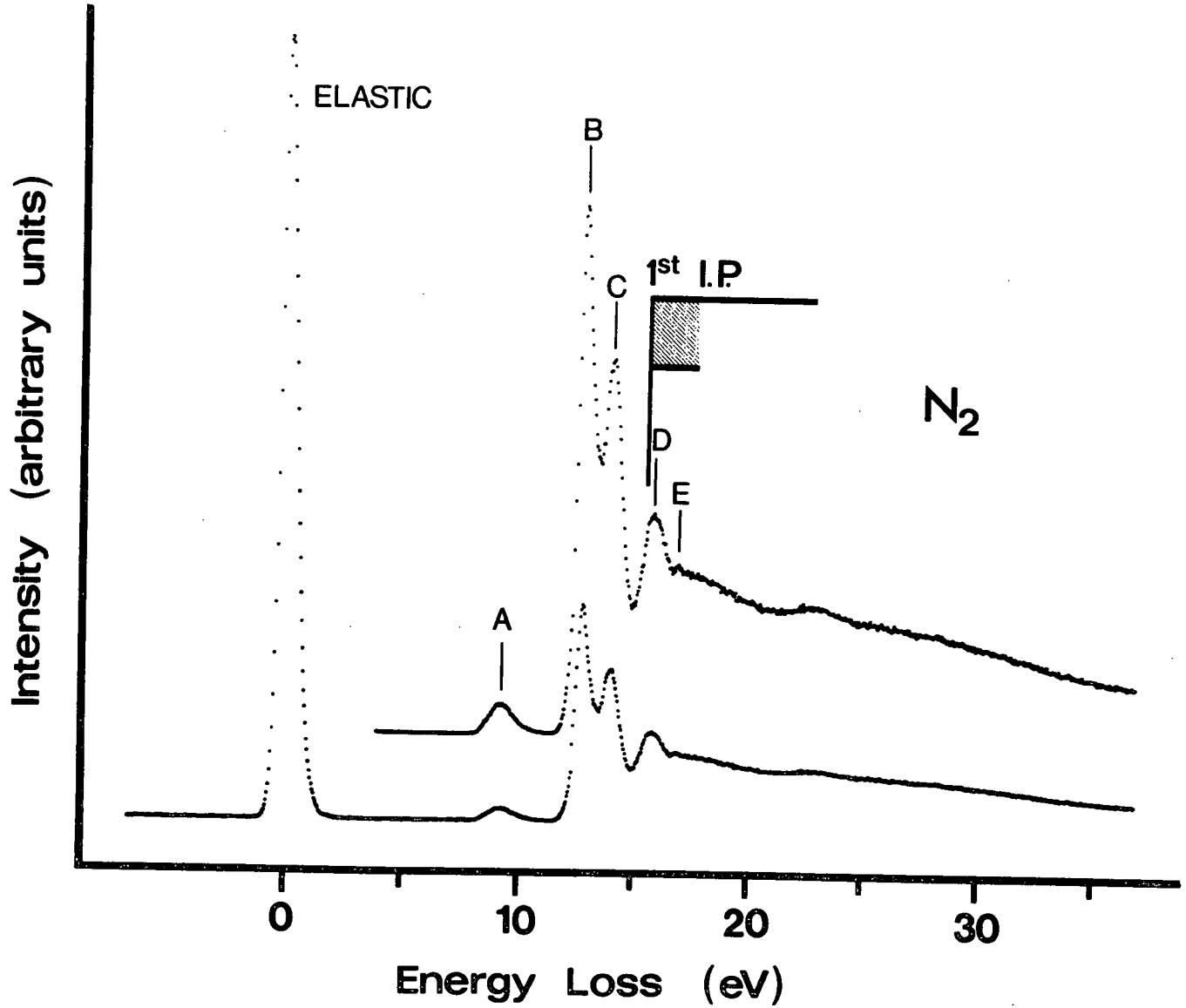

FIGURE 8. Valence shell energy loss spectrum of molecular nitrogen.

also forbidden in our experiment since the first Born approximation should be valid (i.e. $E_o(2500\ eV) >> E_n$ and $\theta_{aver.} \sim 0°$). In electron impact excitation the interaction between the incident and target electrons is assumed to be purely electrostatic and therefore, the transition is only associated with an electric quadrupole interaction. Since the term symbol of the initial and final states differ, only the second term in equation (2.6.11) contributes (i.e. the same matrix element associated with electric quadrupole transitions by photoabsorption). For forward scattering and fast electron impact, the ratio of dipole to quadrupole cross-sections has been given[5] as

$$\sigma_d/\sigma_q = 2\bar{E}\varepsilon_1^2/E_n^2\varepsilon_2^2 \quad \text{where} \quad \bar{E} = E_o - (E_n/2)$$

and ε_1 and ε_2 are the dipole and quadrupole matrix elements respectively [see (2.6.9)]. This implies that the dipole to quadrupole intensity ratio increases linearly with incident energy. At 48 eV incident energy and $\theta = 0°$, the ratio[49] is $\sim$ 16. The ratio observed in our spectrum, 2500 eV incident energy and $\theta_{aver.} \sim 0.02$ rad. is $\sim$ 18. Although our results were not for forward scattering, we still expect much less intensity to be associated with a quadrupole transition. The reason for this discrepancy is not clear. In fact, Bonham[77], using 10 keV electron impact has also observed the Lyman-Birge-Hopfield bands, while Geiger at 25 keV and $\theta = 0$ has not (see Reference 5). The main intensity of peak B (12.8 eV) is associated with the excitation of the $b\ ^1\Pi_u$ state (12.84 eV, $\nu' = 4$ Reference 62). The higher energy peaks (C = 14.0 eV, D = 15.8 eV and E = E = 16.9 eV) result from the excitation of a number of electronic states (see References 60 and 62). The location of the first ionization potential in our spectrum is based on the experimental value[75,78] of 15.57 eV.

b. Nitrogen K-shell Excitation.

The $1s\sigma_g$ and $1s\sigma_u$ electrons are indistinguishable in X-ray PES studies[32] although in theory there should be a small energy difference between the two orbitals[32]. The electrons filling these orbitals are essentially nonbonding and are designated "K-shell" electrons because of their atomic character. The removal of a K-shell electron which is localized on one nitrogen nucleus produces a nitric oxide type "core"[12]. (The "core" includes the two nuclei and their K-shells.) It should be noted that all states having a K-shell hole are intermediate states that only exist for approximately 10^{-14} seconds before they decay by Auger emission (relaxation via a radiative transition has a very low probability for elements of low atomic number[65]). If the K-shell electron is promoted to the first unoccupied molecular orbital of nitrogen, the antibonding $2p\pi_g$, the resulting outer electronic configuration is the same as that of the ground state of nitric oxide. Similarly, promotion of the K-shell electron in nitrogen to higher energy orbitals produces species resembling nitric oxide in excited states. Only those excited states of nitric oxide which are produced by the promotion of the $2p\pi^*$ electron can be correlated with the states of nitrogen produced by the single transition of a K-shell electron. These include the dissociative, non-Rydberg, $A'^2\Sigma^+$ state and all of the Rydberg states of nitric oxide which converge to the ground ionic state. Complete ejection of the K-electron produces a state analogous to the ground state of NO^+. Therefore, the energy positions of the structure observed in the nitrogen K-shell spectrum relative to the first discrete peak, should reproduce the energy levels of the first Rydberg series of the nitric oxide molecule. Nakamura et al.[27] have successfully used this analogy with nitric oxide to interpret

the discrete structure observed in the optical absorption spectrum of nitrogen, which was obtained using synchrotron radiation.

The K-shell electron energy loss spectrum of N_2 is shown in Figure 9 and the peak positions are listed in Table 1. The relative energies of the nitric oxide molecule[79] have been drawn above the spectrum in Figure 9 such that the first Rydberg level of nitric oxide matches up with the second discrete peak in our spectrum. A difficulty in applying this analogy is that we are dealing with excitation in the Frank-Condon region of the nitrogen ground state to "NO-like" states. Therefore vibrational populations are uncertain. The second discrete peak was chosen as a reference point for two reasons: (i) the first discrete peak is broad and it has been suggested that it represents transitions to two final states[36] and, (ii) the second peak, which represents excitation to a Rydberg orbital ($3s\sigma$) is expected to have an internuclear separation close to that of the nitrogen ground state and therefore should have less vibrational excitation. The spectrum has been divided into three regions on the basis of the relative energy levels of nitric oxide (see Figure 9). Region I includes all of the discrete structure and extends up to the first ionization potential of nitric oxide (which corresponds to the K-edge of nitrogen), Region II extends from the first to the second ionization potential of nitric oxide and Region III includes all the structure above the second ionization potential. The discrete part of the spectrum (Region I) is in good agreement with the relative nitric oxide levels and also with the photoabsorption spectrum[27] (see Figure 10). The ground vibrational state of nitric oxide corresponds to an energy 0.4 eV below the maximum of the first discrete peak in our spectrum (see Figure 9), whereas in the photoabsorption spect-

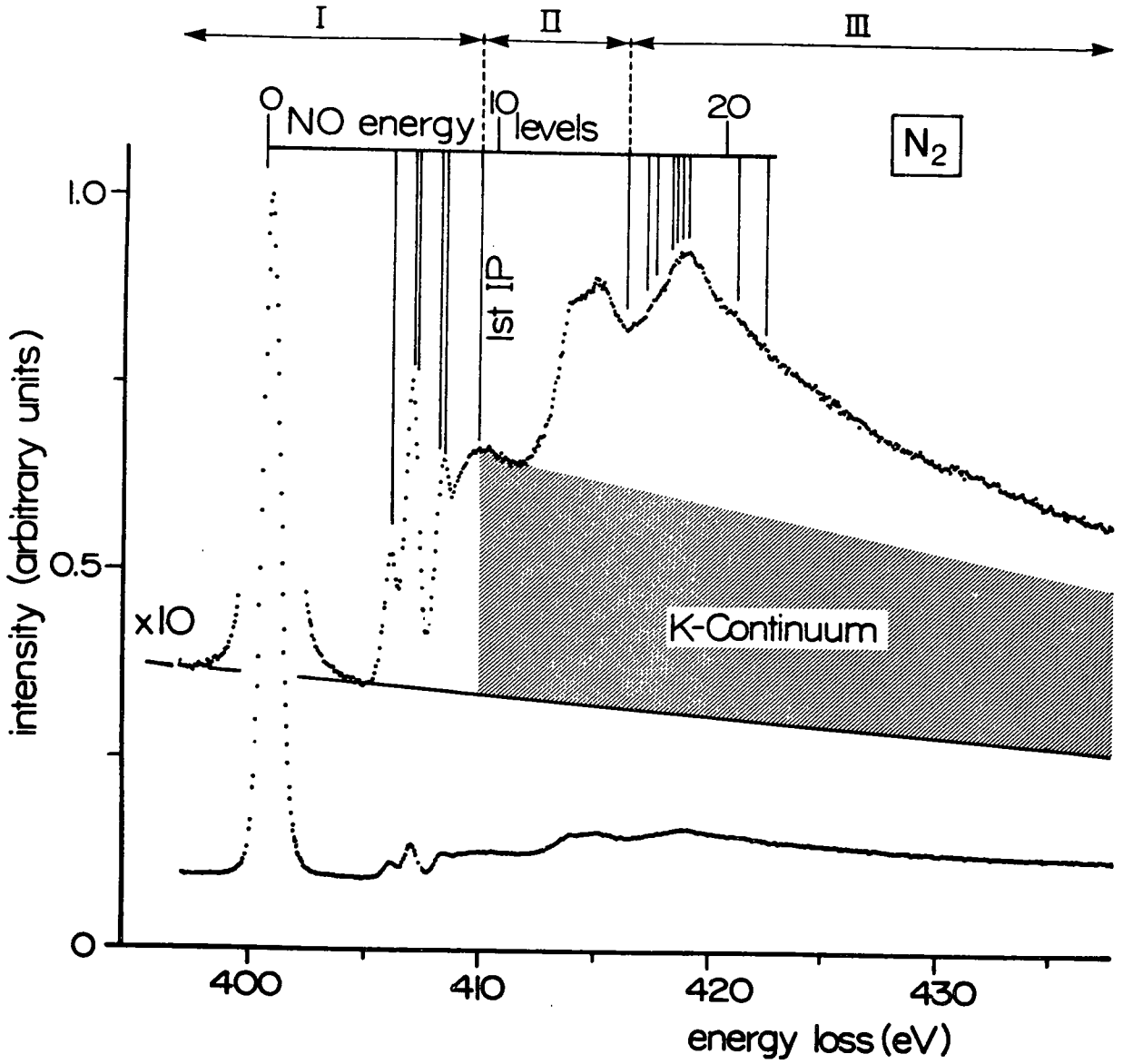

FIGURE 9. K-shell energy loss spectrum of molecular nitrogen.

TABLE 1

ABSOLUTE ENERGIES (eV), RELATIVE ENERGIES AND ASSIGNMENTS OF PEAKS OBSERVED IN REGION I OF THE K-SHELL SPECTRA OF N_2 AND CO (CARBON K-SHELL).

Peak	Nitrogen				CO(C_K-shell)		Assignment[e]		Nitric oxide (ref. 79)	
	This work		Optical[27]		This work					
	Energy	ΔE	Energy	ΔE	Energy	ΔE	Orbital[g]	State	State	Energy
1	400.62[a]	0	400.11[c]		286.86[d]	0	$2p\pi_g$	$^1\Pi_u$	$X^2\Pi$	0
2	406.10	5.48[b]	405.59	5.48[b]	292.34	5.48[b]	$3s\sigma_g$	$^1\Sigma_u^+$	$A^2\Sigma^+$	5.48
3.	407.00	6.38	406.50	6.39	293.31	6.45	$3p\pi_u$	$^1\Pi_u$	$C^2\Pi$	6.49
			406.72	6.61			$3p\sigma_u$	$^1\Sigma_u^+$	$D^2\Sigma^+$	6.61
4.	408.39	7.77	407.66	7.55	294.77	7.91	$4s\sigma_g$	$^1\Sigma_u^+$	$E^2\Sigma^+$	7.55
			407.90	7.79			$3d\pi_g$	$^1\Pi_u$	$H'^2\Pi$	7.88
							$3d\sigma_g$	$^1\Sigma_u^+$	$H^2\Sigma^+$	7.88
K-edge[f]	409.9		409.5		296.1					

a Peak maximum at 400.93 ± 0.05 eV.
b The second peak was used to position the relative nitric oxide levels.
c Centre of truncated peak at 400.84 eV.
d Peak maximum at 287.28 ± 0.05 eV.
e Omit the g and the u for carbon monoxide states.
f Values from ESCA[32]: N_2, 409.9 eV; CO, carbon-K 295.9 eV.
g Only the outer orbitals involved in the K-excitations have been included.

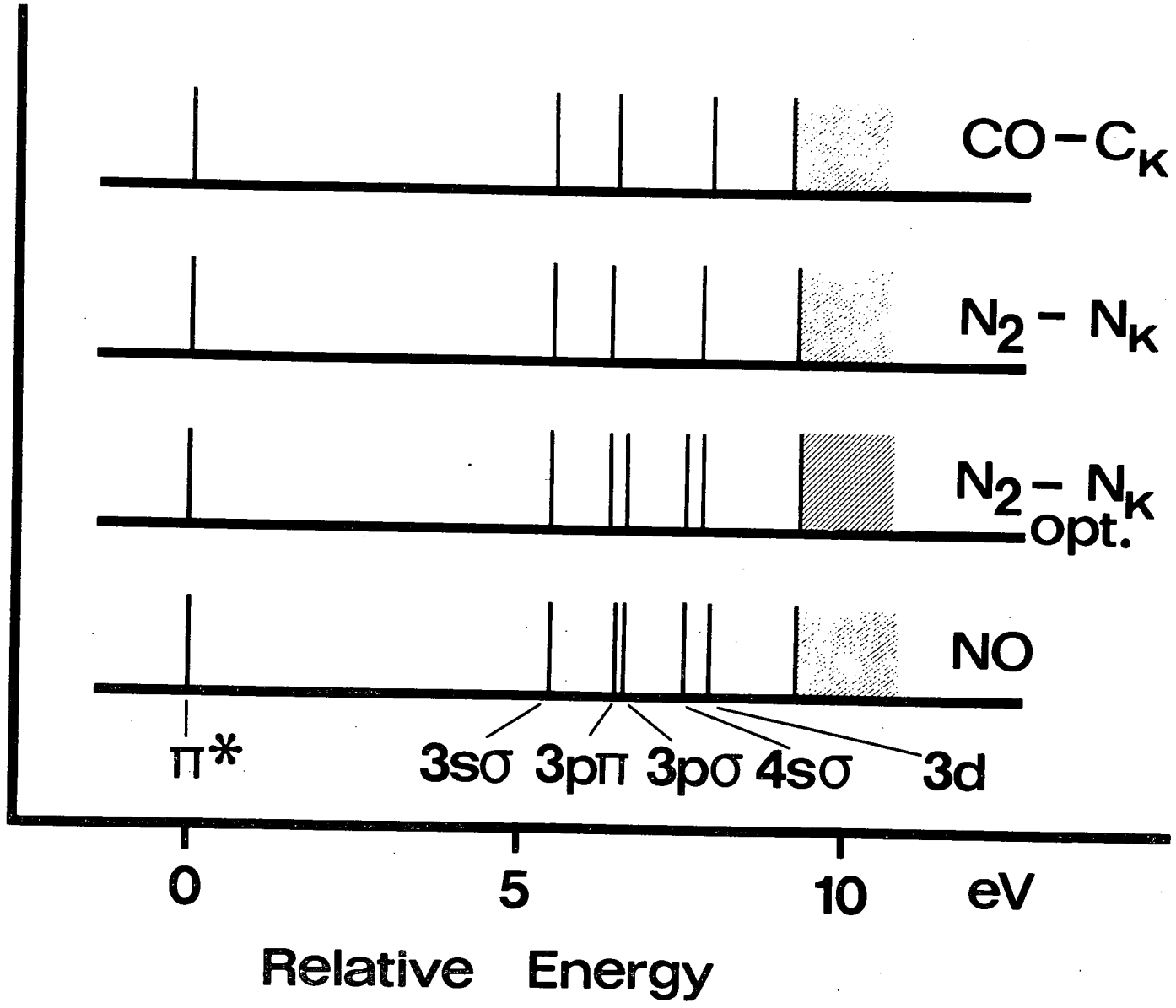

FIGURE 10. Comparison of the relative energies of valence excited states of nitric oxide and K-shell excited states of nitrogen and carbon monoxide (carbon K).

rum[27] the ground vibrational state was 0.6 eV below the centre of the truncated first discrete peak. The difference is partially explained by the asymmetric shape we find for this peak. A comparison of the nitrogen K-shell energy loss spectrum obtained with a resolution [ΔE(FWHM)] of 0.5 eV (this work) and the photoabsorption spectrum[27] [ΔE(FWHM) < 0.2 eV] is shown in Figure 11. The first discrete peak observed in the photoabsorption spectrum is "truncated" because of total absorption of the available radiation[30]. The discrete part of the spectrum has already been assigned by Nakamura et al.[27] (see Table 1), with the intense peak we observe at 400.93 ± 0.05 eV being attributed to the promotion of a $1s\sigma_u$ electron to the lowest unfilled molecular orbital of nitrogen, the antibonding $2p\pi_g$.

$$N_2\ (1s\sigma_g)^2\ (1s\sigma_u)^2\ .....\ (2p\sigma_g)^2,\ X\,^1\Sigma_g^+ \rightarrow$$

$$(1s\sigma_g)^2\ (1s\sigma_u)^1\ .....\ (2p\sigma_g)^2\ (2p\pi_g)^1,\ ^1\Pi_u$$

From a consideration of electron-ion coincidence spectra[29,30], and the photoabsorption data[27], Wuilleumier and Krause[36] have concluded that two excited states contribute to the first peak, the $^1\Pi_u$ and the $^1\Sigma_u^+$ states. The $^1\Sigma_u^+$ state results from the promotion of a $1s\sigma_g$ electron to the $2p\sigma_u$ orbital and is analogous to the dissociative $A'\,^2\Sigma^+$ state of the nitric oxide molecule. From the sharp Auger peaks resulting from the decay of these states, it was concluded that a maximum of two vibrational levels of the $^1\Pi_u$ state were excited. Therefore, in the energy loss spectrum there should be one or two vibrational transitions to the $^1\Pi_u$ state and a broader continuum contribution to the higher energy side of the peak from the $^1\Sigma_u^+$ state. Our results show that the first discrete peak has a FWHM

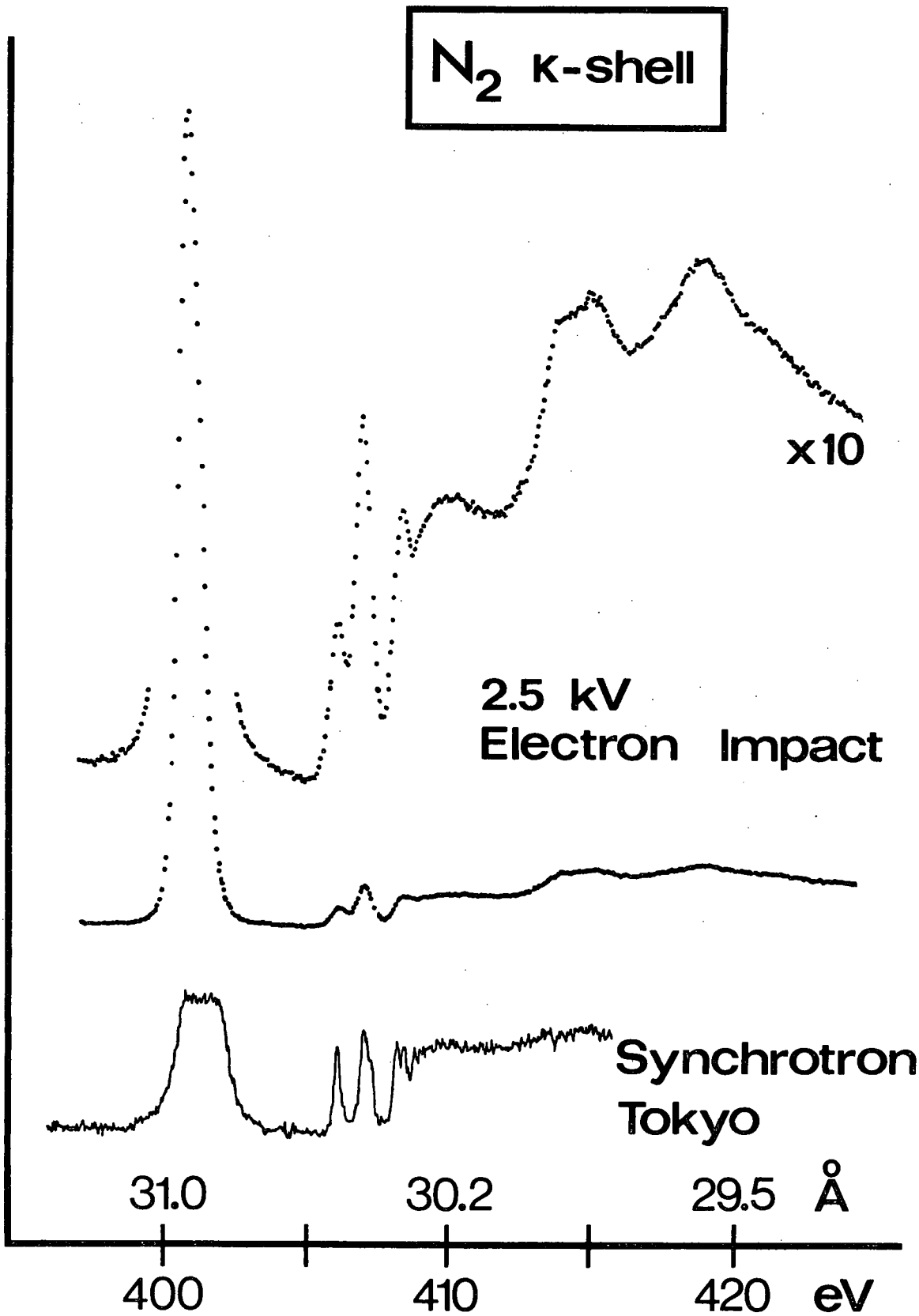

FIGURE 11. Comparison of the K-shell energy loss spectra of molecular nitrogen obtained using electron impact and synchrotron radiation.

of 0.8 eV, which is significantly more than the 0.5 eV FWHM of the peak from the elastically scattered electrons under identical experimental conditions. Furthermore, the peak is slightly asymmetric on the high energy side. We are not able to make any definite new conclusion from our results. However, we observe a base width (at 5% of the peak height) of about 2 eV in contrast to the 3 eV reported by van der Wiel and El-Sherbini[30] at an impact energy of 10 keV and also, if there are two states, they must be less than 0.5 eV[36] apart. It is possible that the relative cross sections for the two processes are significantly different at 2.5 and 10 keV.

A value of 409.9 eV was derived for the K-shell binding energy from the relative nitric oxide levels and this is in excellent agreement with the X-ray PES value[32]. We have derived an approximate continuum shape by using semiempirical X-ray mass absorption coefficients[80] for nitrogen† (see the hatched region in Figure 9). Structure is observed above the K-edge instead of a smooth continuous decrease. This structure represents a variety of multiple electron transitions involving one K-electron and one or more valence electrons. The following two-electron transitions are

† The relationship between high impact energy loss spectra and photoabsorption data has been derived in Chapter Two. For our experimental conditions the conversion factor is approximately (energy loss)$^{-3}$ (see 2.6.15), (if at a momentum transfer, K, of about 1 au, the higher terms in K in the generalized oscillator strength (2.6.8) can be neglected). This factor was used to obtain the relative behaviour of the extrapolated mass absorption coefficients in the region of our spectrum. The absorption coefficients have a contribution from shake-up and shake-off processes, but at energies far above the K-edge we expect this contribution to be a constant fraction of the K-continuum. The K-continuum was constructed by normalizing the data to the height of our spectrum at the K-edge.

expected to make the largest contributions:

i. double excitation; i.e., shake-up of a valence electron in conjunction with K-shell excitation, designated by $(N_2^{K-1})^{**}$ where the superscript K-1 denotes a hole in the K-shell. It is interesting to note that these states should correlate with the Rydberg and non-Rydberg states of nitric oxide produced by the excitation of a $2p\sigma_g$ or $2p\pi_u$ electron.

ii. excitation and ionization; involving an electron from both the K- and valence shell, where one of the electrons is ejected and the other remains behind in a higher unfilled orbital, designated by $(N_2^{K-1})^{+*}$. The simultaneous ionization of a K-electron and a valence electron required an energy outside the range of the spectrum.

The broad band observed in our spectrum in Region II must be associated with discrete structure arising from double excitations, i.e. $(N_2^{K-1})^{**}$ states, since from the nitric oxide analogy, the lowest possible $(N_2^{K-1})^{+*}$ state should correspond to the first excited ion state of nitric oxide ($a\ ^3\Sigma^+$) which is 6.4 eV[79] above the ground ionic state. It is interesting to note that a number of autoionizing states of nitric oxide[79] has been observed between the first and the second ionization potentials which are analogous to the $(N_2^{K-1})^{**}$ states. The intensity of the first bump above the K-edge is approximately 5% of that of the discrete peak at 401 eV which is a reasonable ratio for shake-up events (for example see Reference 81). This suggests that the $2p\pi_g$ orbital is involved in these excitations. The second rise starting $\sim$ 6 eV above the K-edge is then identified with onsets of ionization to a series of $(N_2^{K-1})^{+*}$ states analogous to NO^{+*} states whose thresholds (known from PES)[79] are too close together to observe them separ-

ately. However, as shown in Figure 9, the position of the second bump correlates with these states (it is possible that doubly excited states, $(N_2^{K-1})^{**}$, also contribute to the intensity in Region III). These $(N_2^{K-1})^{+*}$ states should give rise to a series of satellite peaks in an X-ray photoelectron spectrum at the low energy side of the nitrogen K-shell peak. It is therefore interesting to compare the structure we observe above 416 eV with the satellite peaks observed by Carlson et al.[81]. The scatter of data points at the base of the intense K-shell peak of Reference 81 does not allow a conclusion about the possible presence of satellites around 6 eV below the K-shell peak. In our spectrum higher onsets are not distinct enough to compare with the satellite lines observed in Reference 81. (However, in carbon monoxide, onsets are clearly observed and correlate with the satellite peaks.) In order to compare the intensities we observe for the $(N_2^{K-1})^{+*}$ continua with the line intensities in the ESCA spectrum[81], we note the following features of our spectrum:

(i) The height of the jumps in Regions II and III are of the same magnitude as that of the K-jump.

(ii) At the high energy limit of our spectrum the structure has decreased to a height which is roughly 30% higher than the K-continuum, $(N_2^{K-1})^{+}$. Since Carlson et al.[81] observed a total satellite intensity of approximately 15% of the K-shell peak at a photon energy of 1487 eV, our data at the high energy side of the spectrum are consistent with this earlier work. However, it has been found in a wide range of cases (see for instance Reference 82) where ejection of a deep inner electron is involved, that the intensity ratio of double transitions (one inner and one outer shell electron) relative to single transitions (inner electron) as a

function of photon energy rises steeply from threshold and then becomes constant. On this basis we would expect the structures to have heights of only a few percent of the K-jump throughout Region III. The fact that much larger structures are present suggests that there is a strong contribution from a series of $(N_2^{K-1})^{**}$ states converging to each of the indicated thresholds. An alternative explanation would take account of the indistinguishability of the electrons, due to which a shake-off in conjunction with discrete K-excitation gives rise to the same $(N_2^{K-1})^{+*}$ state as a shake-up "following" K-ionization. However, the first process might have more of the characteristics of a resonance transition and therefore might locally enhance the "normal" intensity of the $(N_2^{K-1})^{+*}$ continua.

The onset of the increase in intensity beyond the K-edge in the photoabsorption spectrum of nitrogen[27] agrees with the onset of structure in Region I of our spectrum (see Figure 11). Also, the structure we observe above the K-edge is qualitatively similar to that observed in the electron energy loss spectrum of nitrogen measured in coincidence with the N_2^{++} (plus N^+) ions[30] produced by Auger decay. (From the similarity with the coincidence studies of carbon monoxide where an ambiguity of ionic states does not exist, we can conclude that most of the intensity is due to N_2^{++} ions.) A normal Auger decay of the doubly excited states would produce a singly charged ion, of which the coincidence spectrum shows no appreciable intensity in this energy range. The inference that N_2^{++} is the predominant product indicates that the $(N_2^{K-1})^{**}$ states first autoionize to form $(N_2^{K-1})^{+}$, which then undergo a normal Auger decay. This is supported by the fact that the decay rate of the first autoionizing step will certainly be faster than that of an Auger transition.

5.1.2. Carbon Monoxide.

Carbon monoxide is isoelectronic with nitrogen and has a ground state electron configuration of

$$(1s\sigma_O)^2\ (1s\sigma_C)^2\ (2s\sigma)^2\ (2s\sigma^*)^2\ (2p\pi)^4\ (2p\sigma)^2,\ ^1\Sigma^+.$$

We have studied both the carbon and oxygen K-shell energy loss spectra. The valence shell spectrum has also been recorded.

a. Valence Shell Spectrum.

The valence shell electron energy loss spectrum of carbon monoxide is shown in Figure 12. The locations of peaks are consistent with higher resolution energy loss spectra[48,53,55,83] and optical data[75]. Peak A with a maximum at 8.4 eV is associated with the "fourth positive group" of carbon monoxide, which is analogous to the forbidden Lyman-Birge-Hopfield bands of nitrogen. However, in the case of carbon monoxide, the transition is allowed, $^1\Sigma^+ \rightarrow A\ ^1\Pi$ ($2p\sigma \rightarrow \pi^*$) and this is reflected in the much higher intensity of this peak compared with peak A in the nitrogen valence shell spectrum (Figure 8). Peaks B (10.7 eV) and C (11.3 eV) are associated with the B $^1\Sigma^+$ and C $^1\Sigma^+/E\ ^1\Pi$ Rydberg states respectively (see References 55 and 75). The higher energy peaks, D (13.4 eV), E (16.3 eV) and F (17.0 eV) are associated with a number of overlapping excitations. The location of the first ionization potential on the spectrum is based on the optical[75] and UV-PES[78] value of 14.00 eV.

b. Carbon K-shell Excitation.

The production of a carbon K-shell "hole" should produce a nitric oxide type core and therefore we would expect the carbon K-shell spectrum of carbon monoxide to be similar to the K-shell spectrum of nitrogen. As is shown in Figure 13, this is the case, and the relative energies of the

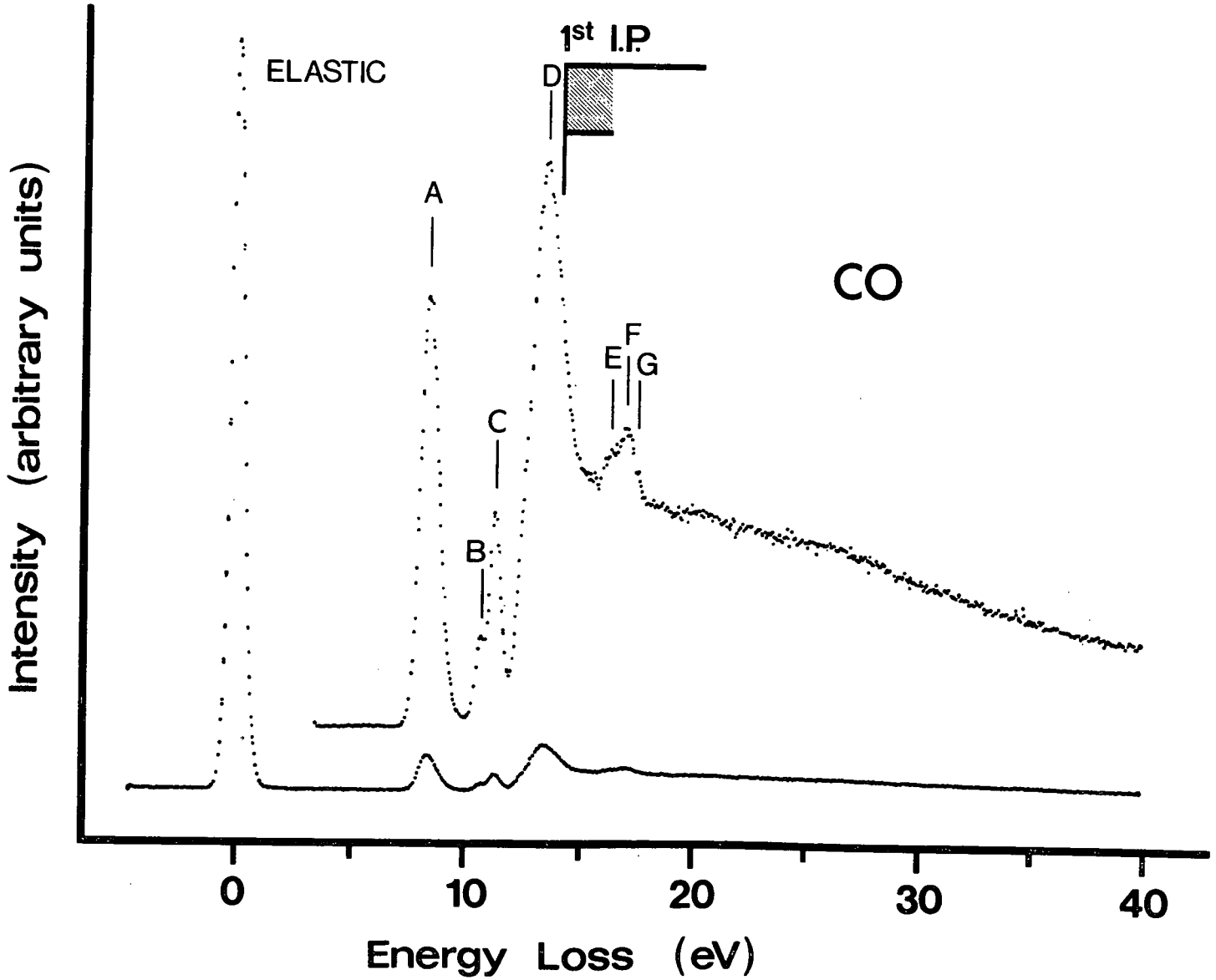

FIGURE 12. Valence shell energy loss spectrum of carbon monoxide.

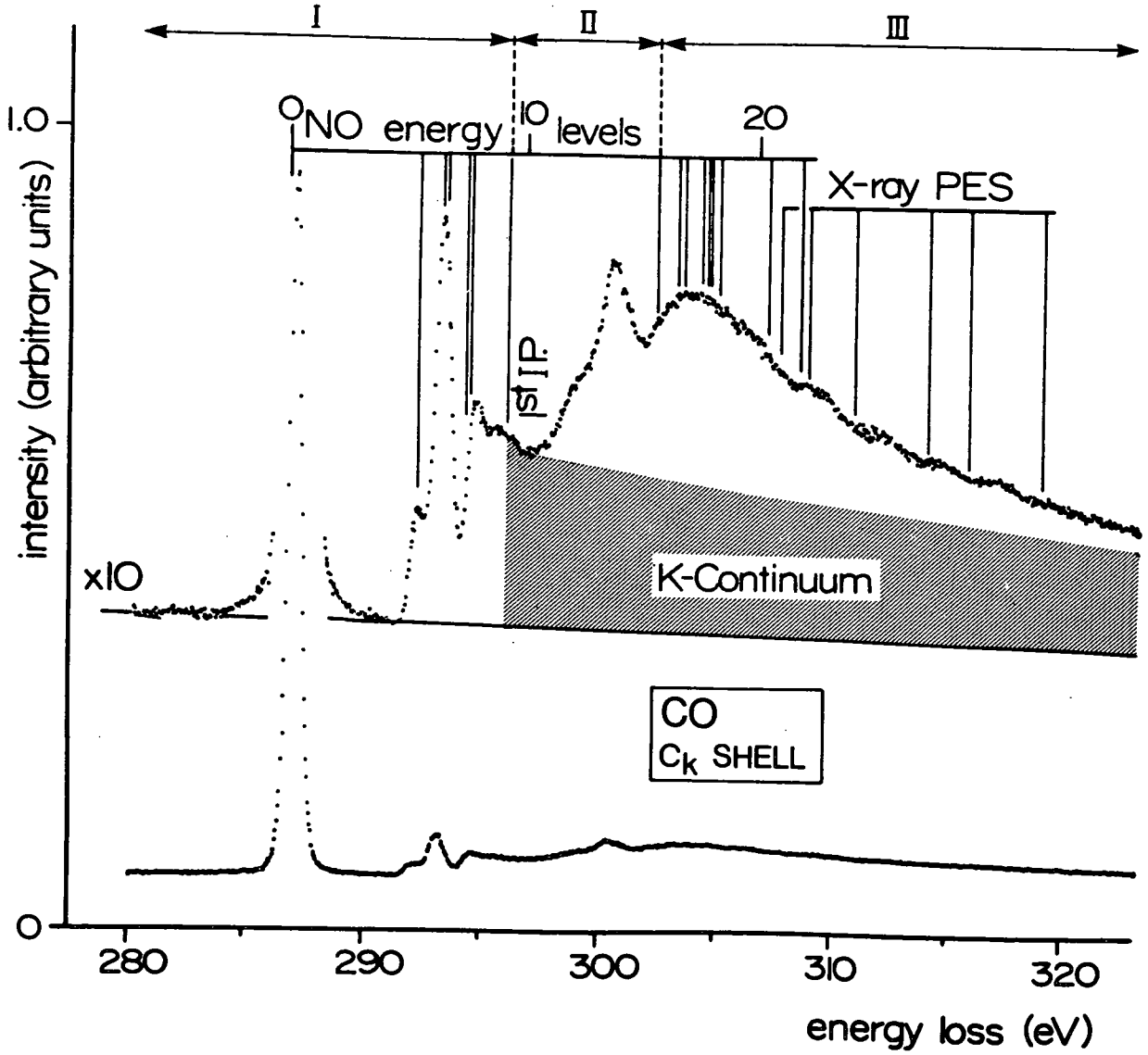

FIGURE 13. Carbon K-shell energy loss spectrum of carbon monoxide.

peaks are in good agreement with those of the nitric oxide levels (see Figure 10). Therefore we have assigned the discrete peaks in Region I by analogy with the Rydberg states of nitric oxide (Table 1). The interpretation of both the discrete and continuum part of the spectrum is the same as that for nitrogen and therefore the arguments for peak assignments will not be repeated. Instead we will discuss the differences between the two spectra.

The relative intensities of the peaks in Region I of the two spectra are slightly different. A further difference is that the first discrete peak at 287.28 ± 0.05 eV in the carbon K-shell spectrum has a FWHM of 0.56 eV and is symmetric, indicating that only one or two vibrational levels of the $^1\Pi$ state are excited. This is in excellent agreement with the Auger results[32] where the vibrational spacings of the final CO^+ states (produced by autoionization of the $^1\Pi$ state) have been resolved. The base width (at 5% of the peak height) of the first peak is only 1.5 eV, rather than the 3 eV reported in Reference 30. (The coincidence spectra[30] produced the same broad asymmetric shape for the first peak in both nitrogen and carbon monoxide.) This might indicate that the relative excitation cross-sections for the states represented by the first peak are quite different at 2.5 and 10 keV.

An energy of 296.1 eV was derived for the K-edge, which is in good agreement with the X-ray PES value[32] of 295.9 eV. The approximate continuum shape (hatched region in Figure 13) was constructed by smoothly joining the extrapolated behaviour for the X-ray absorption coefficients of methane and methylal[84] (mainly carbon-K) to the continuum decrease near the K-edge. The structure observed in Region II is associated with discrete

states, $(C^{K-1}O)^{**}$ (i.e. carbon K-excitation and valence shake-up). Shaw and Thomas[85] have investigated the X-ray PES spectrum in the energy region 5.4 to 6 eV below the main carbon K-shell peak and have put a limit for the intensity of any satellite structures (from $C^{K-1}O)^{+*}$ states) as 0.4% of the carbon K-shell peak. This supports our assignment of the structure in Region II. The structure in Region III represents $(C^{K-1}O)^{+*}$ states and there is probably a large contribution from doubly excited states $(C^{K-1}O)^{**}$. The energies of the NO^{+*} states as given by PES[79] correlate with the first broad bump in Region III. Onsets have been resolved where the ionization potentials are sufficiently far apart. The energies of the satellite lines obtained by Carlson et al.[81] using an X-ray energy of 1487 eV are in excellent agreement with the onsets observed in our spectrum (see Figure 13, X-ray PES lines). The lowest satellite line observed by Carlson et al. is at 8.5 eV below the K-shell peak, but the scatter of data points would probably mask a broad band of satellite lines close to the intense K-shell peak. There are obvious differences between the structures observed above the K-edge in the nitrogen spectrum and the carbon K-shell spectrum of carbon monoxide. In Region II the components making up the discrete structures do not have the same relative intensities as in nitrogen. In carbon monoxide the structure is generally more intense relative to the K-jump and the higher onsets in Region III are clearly resolved. It is reasonable to expect different shake-up and shake-off probabilities in the two molecules, nitrogen and carbon monoxide. Carbon monoxide has two different nuclei, and therefore, each molecular orbital will generally have unequal "carbon and oxygen" electron densities. A change in the screening of the carbon nucleus by the production of a carbon K-shell hole, should

preferentially produce shake-up and shake-off of electrons from molecular orbitals with the higher "carbon" electron densities. Also if a direct interaction between the inner and the valence electrons is involved to a significant extent, we would expect this effect to contribute more to the carbon K-shell spectrum than the nitrogen spectrum since the carbon K-orbital is closer in energy to the valence shell.

The continuum structure is qualitatively the same as that observed in the carbon K-shell energy loss spectrum of carbon monoxide measured in coincidence with CO^{++} ions produced by Auger decay[30]. As in the case of nitrogen, the doubly excited states observed in Region II do not contribute to the CO^{+} coincidence spectrum implying that these $(C^{K-1}O)^{**}$ states first autoionize to form $(C^{K-1}O)^{+}$ which then undergo a normal Auger decay to CO^{++}.

c. Oxygen K-shell Excitation.

From the close agreement observed in both the nitrogen K-shell spectrum and the carbon K-shell spectrum of carbon monoxide with the relative nitric oxide levels, we expect the oxygen K-shell spectrum to reproduce the relative energy spacings of the states of the CF radical (the production of an oxygen K-shell hole should produce a CF type core). Three states of the carbon monofluoride radical are well known from spectroscopic studies[86,89]; the ground $X^2\Pi$, the $A^2\Sigma^+$ and the $B^2\Delta$ states. Recently a $D^2\Pi$ and possibly a $C^2\Sigma^+$ state have been observed (see Reference 90 for details). The ionization potential of CF has been derived in a wide range of experiments with estimates from spectroscopic data[89,91] and calculated values[90,92], in fair agreement (see Reference 92 for a complete review).

The oxygen K-shell energy loss spectrum of carbon monoxide is shown

in Figure 14. The relative energies of those states of CF which have outer electronic configurations identical to those produced by a single transition of a K-electron in CO, are also shown (the $B^2\Delta$ state has therefore not been included in the correlation). The results are listed in Table 2 and tentative assignments of the discrete structures have been made on the basis of the carbon monofluoride states. The second discrete peak has been used to normalize the relative CF energy levels. Also included in Figure 14 are the three higher discrete peaks in the spectrum on an expanded scale (insert a). (The full spectrum and the insert are from different data runs.) As shown by Figure 14, the relative energies of the presently known states of CF agree with the peaks in our spectrum. The intense peak observed at 534.0 ± 0.1 eV (analogous to the ground $X^2\Pi$ state of CF) has a FWHM of 1.3 eV and therefore we conclude that a number of vibrational levels are populated (5 to 7). This is supported by the fact that the relative CF energy scale implies that the ground vibrational state is ∿ 0.5 eV below the centre of the first discrete peak (see Figure 14).

The ionization potential of CF, estimated as 8.9 ± 0.1 eV from spectroscopic data[89,91] and 9.2 ± 0.5 eV from a Hartree-Fock SCF calculation[92] leads to values of 542.4 eV and 542.7 eV respectively for the oxygen K-edge of carbon monoxide. These values compare favourably with the experimental[32] X-ray PES energy of 542.1 eV. An approximate K-continuum as indicated by the hatched region in Figure 14 was constructed by extrapolating X-ray mass absorption coefficients for oxygen[80] (corrected by an $(\text{energy loss})^{-3}$ factor) to the K-edge. Broad structure is observed above the K-edge which represents shake-up and shake-off events associated

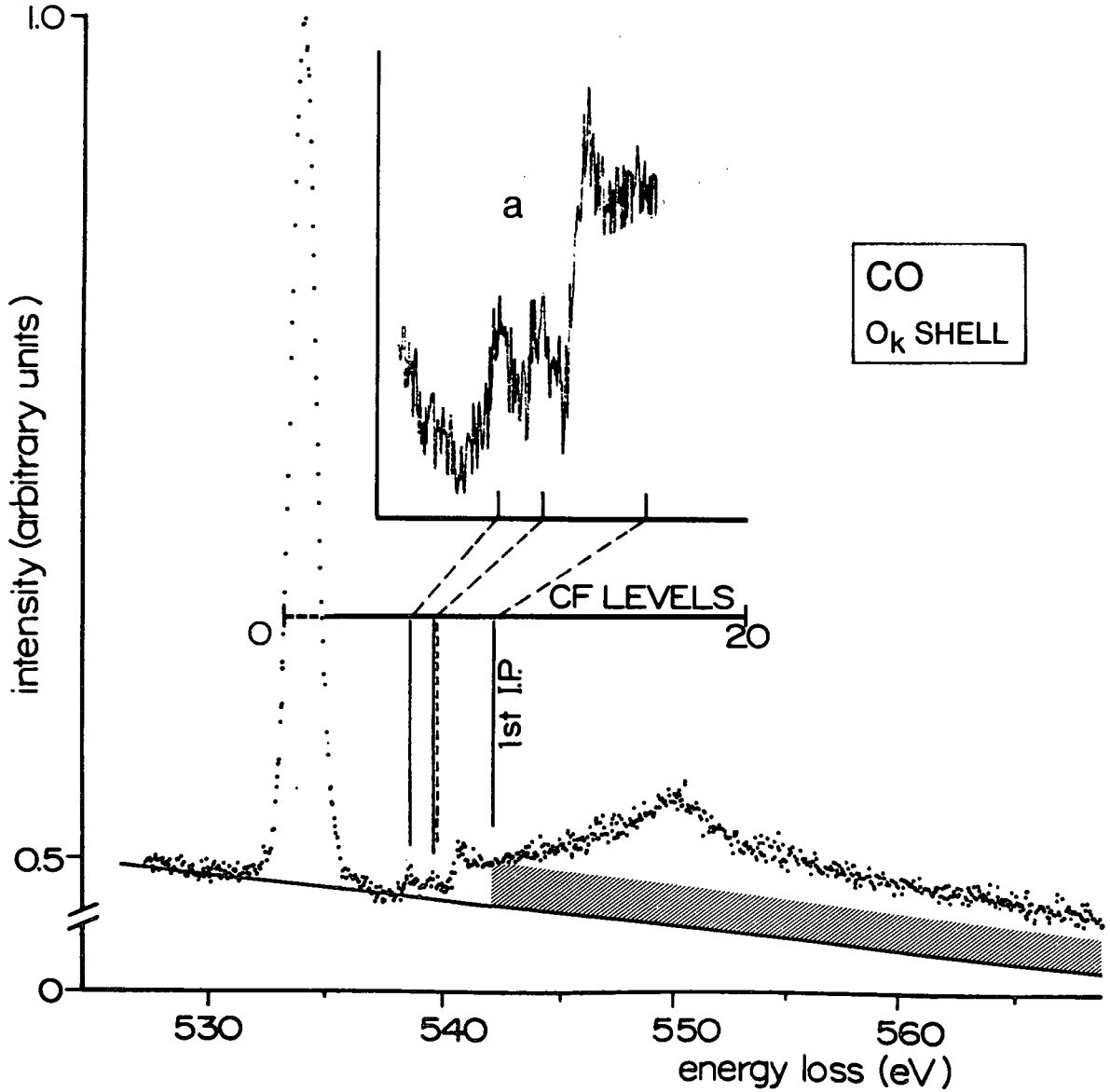

FIGURE 14. Oxygen K-shell energy loss spectrum of carbon monoxide. Insert a (taken from a separate data run) shows the three higher discrete peaks on an expanded scale.

TABLE 2

ABSOLUTE ENERGIES (eV), RELATIVE ENERGIES AND POSSIBLE ASSIGNMENTS OF PEAKS OBSERVED IN REGION I OF THE OXYGEN K-SHELL SPECTRUM OF CARBON MONOXIDE.

Peak	CO(O_K-shell) this work		Possible assignments		CF[86-90]	
	Energy	ΔE	Orbital[d]	State	State	Energy
1	533.5[a]	0	$2p\pi^*$	$^1\Pi$	$X^2\Pi$	0
2	538.8	5.3[b]	$3s\sigma$	$^1\Sigma^+$	$A^2\Sigma^+$	5.32
3	539.8	6.3	$3p\pi$	$^1\Pi$	$D^2\Pi$	6.40
4			$3p\sigma$	$^1\Sigma^+$	$C^2\Sigma^+$?	6.65
4	540.9	7.4	-	-	-	-
K-edge[c]	542.4					

a. Peak maximum at 534.0 ± 0.1 eV.
b. The second peak was used to position the CF levels.
c. ESCA[32] value, 542.1 eV.
d. Only the outer orbitals involved in the K-excitations have been included.

with K-excitation and ionization. Relative to the K-jump, this structure is more intense than in either of the previous spectra.

5.2. Nitric Oxide and Oxygen.

5.2.1. Nitric Oxide.

The ground electronic state of the nitric oxide molecule has the electron configuration

$$(1s\sigma_O)^2\ (1s\sigma_N)^2\ (2s\sigma)^2\ (2s\sigma^*)^2\ (2p\sigma)^2\ (2p\pi)^4\ (2p\pi^*)^1,\ ^2\Pi.$$

A valence shell spectrum was not recorded. The $1s\sigma_O$ and $1s\sigma_N$ molecular orbitals, formed from the oxygen K-shell and nitrogen K-shell atomic orbitals respectively, are nonbonding and mainly atomic in character. The excitation or ionization of an inner shell electron results in a number of electronic states for each orbital configuration because of the coupling of unpaired electron spins between the core and valence shell (see Table 3). Thus the ionization of a nitrogen 1s electron or oxygen 1s electron results in $^3\Pi$ and $^1\Pi$ molecular ion states. Using X-ray PES, $^3\Pi$ - $^1\Pi$ energy splittings (exchange splittings) of 1.42 eV and 0.55 eV have been observed[93,94] for nitrogen 1s ionization and oxygen 1s ionization respectively. On the basis of the core analogy model we expect the promotion of a nitrogen 1s electron in nitric oxide to discrete levels below the 1s ionization limit, to produce a nitric oxide species with relative energy levels similar to those of molecular oxygen in its ground and valence shell excited states (produced by the excitation of an O_2, $2p\pi_g$ electron). Ionization of the nitrogen 1s electron should produce a nitric oxide species similar to oxygen in its ground ionic state. Similarly the promotion of an oxygen 1s electron in nitric oxide should produce an

TABLE 3

ELECTRON CONFIGURATIONS AND ELECTRONIC STATES OF K-SHELL EXCITED NITRIC OXIDE AND MOLECULAR OXYGEN.

NITRIC[a] OXIDE	ELECTRON CONFIGURATION							RYDBERG ORBITALS			MOLECULAR STATES[b]
	$1s\sigma_O$	$1s\sigma_N$	$2s\sigma$	$2s\sigma^*$	$2p\sigma$	$2p\pi$	$2p\pi^*$	$n\sigma$	$n\pi$	∞	
NO	2	2	2	2	2	4	1				$X\,^2\Pi$
$N^{K*}O$	2	1	2	2	2	4	2				$^4\Sigma^-$, $^2\Sigma^-$, $^2\Delta$, $^2\Sigma^+$
$N^{K*}O$	2	1	2	2	2	4	1	1			$^4\Pi$, $^2\Pi$, $^2\Pi$
$N^{K*}O$	2	1	2	2	2	4	1		1		$^4\Sigma^-$, $^4\Delta$, $^4\Sigma^+$, $^2\Sigma^-(2)$, $^2\Delta(2)$, $^2\Sigma^+(2)$
$N^{K+}O$	2	1	2	2	2	4	1			1	$^3\Pi$, $^1\Pi$
OXYGEN[c]	$1s\sigma_g$	$1s\sigma_u$	$2s\sigma_g$	$2s\sigma_u$	$2p\sigma_g$	$2o\pi_u$	$2p\pi_g$				
O_2	2	2	2	2	2	4	2				$X\,^3\Sigma_g^-$, a $^1\Delta_g$, b $^1\Sigma_g^+$
O_2^{K*}	2	1	2	2	2	4	3				$^3\Pi$, $^1\Pi$
O_2^{K*}	2	1	2	2	2	4	2	1			$^5\Sigma^-$, $^3\Sigma^-(2)$, $^3\Delta$, $^3\Sigma^+$, $^1\Sigma^-$, $^1\Delta$, $^1\Sigma^+$
O_2^{K*}	2	1	2	2	2	2	2		1		$^5\Pi$, $^3\Pi(4)$, $^3\Phi$, $^1\Pi(3)$, $^1\Phi$
O_2^{K+}	2	1	2	2	2	2	2			1	$^4\Sigma^-$, $^2\Sigma^-$, $^2\Delta$, $^2\Sigma^+$

a The same molecular states are obtained by oxygen 1s excitation in NO
b The numbers in brackets refer to the number of states of that symmetry.
c g, u designations do not apply to an oxygen molecule with a localized 1s hole.

"NF-like" species.

a. Nitrogen K-shell Excitation.

The nitrogen K-shell electron energy loss spectrum of nitric oxide is shown in Figure 15 and the energies and possible assignments of peaks are listed in Table 4. The general appearance of the spectrum is similar to that observed for the diatomic molecules nitrogen and carbon monoxide in that the spectrum is dominated by the first discrete peak. This intense peak, located at 399.1 eV is interpreted as arising from the promotion of a nitrogen 1s electron to the lowest available molecular orbital, the $2p\pi^*$. The resulting electron configuration can give rise to $^4\Sigma^-$, $^2\Sigma^-$, $^2\Delta$ and $^2\Sigma^+$ electronic states (see Table 3). Electric dipole selection rules apply to electron impact excitation for high incident energies and small scattering angles (i.e. when the first Born approximation is valid)[4]. Although the first Born approximation may not always apply to our experiment (the incident energy is six times the excitation energy for nitrogen K-shell promotion while the ratio decreases to 4.5 for oxygen K-shell promotion) the experimental conditions are such that spin forbidden transitions should not be observed. Therefore, the $^4\Sigma^-$ state is not expected to contribute to our spectrum. The $^2\Sigma^-$, $^2\Delta$ and $^2\Sigma^+$ states are all dipole connected to the ground $^2\Pi$ state and peaks associated with the excitation of these states should be observed in our spectrum. The first discrete peak has a ΔE(FWHM) of 1.0 eV compared with a ΔE(FWHM) of 0.4 eV observed for the peak associated with elastic scattered electrons and is symmetric (the slight asymmetry on the tail of the peak is instrumental). This suggests that the energy spacings of the three doublet states is less than 1 eV. Since this first peak is by far the most intense

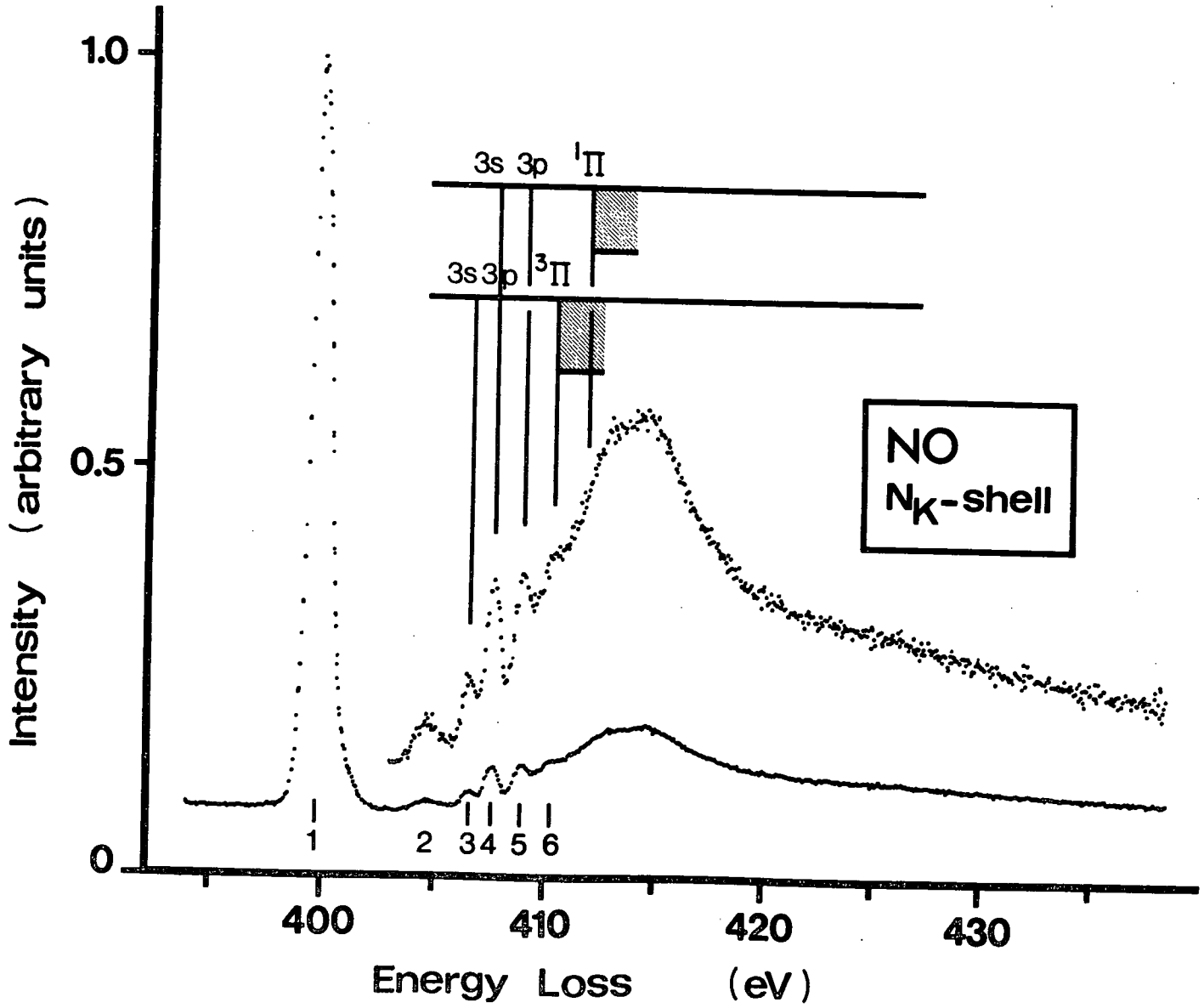

FIGURE 15. Nitrogen K-shell energy loss spectrum of nitric oxide.

TABLE 4

ABSOLUTE ENERGIES (eV), RELATIVE ENERGIES AND POSSIBLE ASSIGNMENTS OF PEAKS OBSERVED IN THE K-SHELL ENERGY LOSS SPECTRA OF NO (NITROGEN AND OXYGEN K-SHELLS).

N_K-SHELL			ORBITAL[a] ASSIGNMENT	STATES	O_K-SHELL		
PEAK	ENERGY	ΔE			PEAK	ENERGY	ΔE
1	399.7	0	$2p\pi^*$	$^2\Sigma^-$, $^2\Delta$, $^2\Sigma^+$	1	532.7	0
2	404.7	5.0	$2p\sigma^*$	$^2\Pi$, $^2\Pi$			
3	406.6	6.9	$3s\sigma$	$^2\Pi$	2	540.2	7.5
4	407.6	7.9	$3s\sigma$, $3p\pi$	$^2\Pi$, ?			
5	409.0	9.3	3p				
	~ 409.8	~ 10.1					
K-EDGE[b]	410.3	10.6	∞	$^3\Pi$	K-EDGE[b]	543.3	10.6
6	~ 410.4	~ 10.7					
K-EDGE[b]	411.8	12.1	∞	$^1\Pi$	K-EDGE[b]	544.0	11.3
	413.1	13.4	SHAKE-UP AND SHAKE-OFF			546.3	13.6
	414.5	14.8					

a Only the outer orbitals involved in the K-excitations have been included.
b These values are from X-ray PES.[32]

structure in the spectrum, we expect these discrete levels to give the largest contribution to the high energy autoionization lines observed in the Auger spectrum of nitric oxide excited by electron impact[35].

A theoretical estimate of the energy differences between the $^4\Sigma^-$, $^2\Sigma^-$, $^2\Delta$ and $^2\Sigma^+$ states (arising from the transition $1s\sigma_N \rightarrow 2p\pi^*$) can be made on the basis that the orbital wavefunctions of the four states are identical (frozen orbital approximation). Omitting the filled orbitals, the $^4\Sigma^-$ and $^2\Delta$ states can be represented by the single determinants,

$$\psi(^4\Sigma^-) = |1s\ \pi^{+*}\pi^{-*}|$$

$$\psi(^2\Delta) = |1s\ \pi^{+*}\overline{\pi^{+*}}|$$

where the orbitals have been written in complex form and the bar represents β spin. The $^2\Sigma$ states are associated with linear combinations of the three single determinants,

$$\phi_A = |1s\ \pi^{+*}\overline{\pi^{-*}}|,\ \phi_B = |1s\ \overline{\pi^{+*}}\pi^{-*}| \text{ and } \phi_C = |\overline{1s}\ \pi^{+*}\pi^{-*}|$$

Linear combinations which are eigenfunctions of S^2, the total spin angular momentum operator, can be found by the Nesbet method[95]. Combinations which satisfy the above condition and have the correct reflection symmetry are

$$\psi(^2\Sigma^-) = \frac{1}{\sqrt{6}}(2\phi_C - \phi_A - \phi_B)$$

$$\psi(^2\Sigma^+) = \frac{1}{\sqrt{2}}(\phi_A - \phi_B)$$

From the total energy expressions for the four states and the fact that $K_{1s\pi^+*} = K_{1s\pi^-*}$ the energy differences are

$$E(^2\Sigma^-) = E(^4\Sigma^-) + 3K_{1s\pi^+*} \quad \ldots\ (5.2.1)$$

$$E(^2\Delta) = E(^4\Sigma^-) + K_{1s\pi^+*} + K_{\pi^+*\pi^-*} \quad \ldots\ (5.2.2)$$

$$E(^2\Sigma^+) = (E^4\Sigma^-) + K_{1s\pi^+*} + 2K_{\pi^+*\pi^-*} \quad \ldots \quad (5.2.3)$$

where K_{ij} is the exchange integral between orbitals i and j. On the basis of the core analogy model, nitrogen 1s excitation in nitric oxide (i.e. production of $N^{K*}O$ states) is expected to produce molecular oxygen like states. Therefore we assume that the charge distributions of valence molecular orbitals for $N^{K*}O$ states have an equal contribution from both atomic centres. The $2p\pi^*$ orbital in $N^{K*}O$ is then approximated by the wavefunction $\phi(2p\pi^*) = 0.707p\pi_{NK^*} - 0.707p\pi_O$ where $p\pi_{NK^*}$ and $p\pi_O$ represent the atomic $p\pi$ orbitals associated with the nitrogen nucleus with a 1s hole and the oxygen nucleus respectively in $N^{K*}O$. Since $p\pi_{NK^*} \sim p\pi_O$ and $1s_{NK^*} \sim 1s_O$, one-centre exchange integrals for atomic oxygen[96] may be used to calculate the exchange integrals in equations (5.2.1) to (5.2.3). The two-centre exchange integrals are typically an order of magnitude smaller[94] and have been neglected (see Reference 94 where an analogous procedure has been used to estimate the exchange splitting for 1s ionization in open shell systems). The results are shown in Figure 16(a) where the experimental energy levels[75] of the three states of molecular oxygen ($X^3\Sigma_g^-$, $a^1\Delta_g$ and $b^1\Sigma_g^+$) arising from the same valence electron configuration (.... $2p\pi_u^4\ 2p\pi_g^2$) have been included. On the basis of the core analogy model the $^3\Sigma_g^-$ state of molecular oxygen gives rise to corresponding $^4\Sigma^-$ and $^2\Sigma^-$ states in $N^{K*}O$ while the energy difference between the $^1\Delta_g$ and $^1\Sigma_g^+$ states is expected to be similar to the energy difference between the $^2\Delta$ and $^2\Sigma^+$ states of $N^{K*}O$. The calculation suggests that the $^2\Sigma^-$ and $^2\Delta$ states should be close in energy and approximately 1 eV below the $^2\Sigma^+$ state. This result is in qualitative agreement with the corresponding experimental oxygen energy levels. The experimental FWHM of 1.0 eV

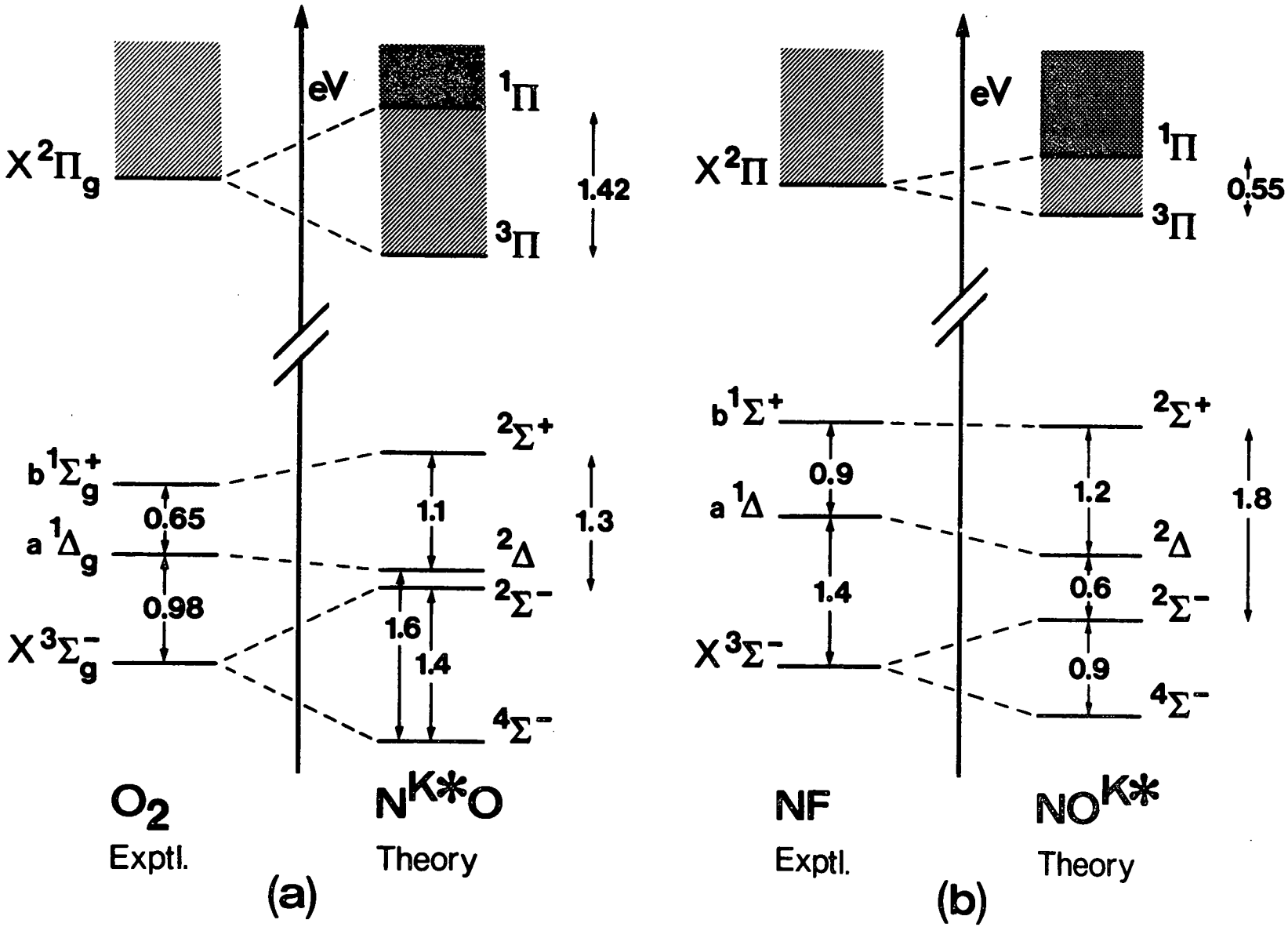

FIGURE 16. Comparison of the relative energies of: (a) valence O_2 states (experimental) and N^{K*} states (theoretical); (b) valence NF states (experimental) and NO^{K*} states (theoretical). $N^{K+}O$ and NO^{K+} splittings are from X-ray PES data.

for the first discrete peak and the symmetric peak shape indicates that if all three doublet states are excited with approximately equal intensity, their energy spacings must be smaller than those calculated.

Our assignment of the first discrete peak ($1s\sigma_N \rightarrow 2p\pi^*$) is supported by the close agreement between the observed peak energy, 399.7 ± 0.2 eV, and the value of 399.8 eV estimated using the concept of equivalent cores and the thermochemical method[97-99]. The following reaction scheme was used:

1.	$NO(X^2\Pi) \rightarrow N^{K+}O(^3\Pi) + e$	ΔE_1	= 410.3 eV[32]
2.	$N^{K+}O(^3\Pi) \rightarrow N^{K+}O(W)$	ΔE_2	= 0.4
3.	$N^{K+}O(W) + O^{6+} \rightarrow O_2^+(W) + N^{6+}$	ΔE_3	= δ
4.	$O_2^+(W) \rightarrow O_2^+(X)$	ΔE_4	= -0.01
5.	$O_2^+(X) + e \rightarrow O_2(X^3\Sigma_g^-)$	ΔE_5	= -12.07[100]
6.	$O_2(X^3\Sigma_g^-) \rightarrow O_2(W)$	ΔE_6	= 0.6
7.	$O_2(W) + N^{6+} \rightarrow N^{K*}O(W) + O^{6+}$	ΔE_7	= $-\delta'$
8.	$N^{K*}O(W) \rightarrow N^{K*}O(w)$	ΔE_8	$\sim$ 0.6

$$NO(X^2\Pi) \rightarrow N^{K*}O(w) \qquad \Delta E = 399.8 + \delta - \delta' \sim 399.8 \text{ eV}$$

where (X) indicates the ground state species; $N^{K+}O(W)$, $O_2^+(W)$, $O_2(W)$ and $N^{K*}O(W)$ respectively represent the weighted averages of the $^3\Pi$ and $^1\Pi$ $N^{K+}O$ states, the ground ionic states ($^2\Pi_{3/2}$, $^2\Pi_{1/2}$) of O_2, the $X^3\Sigma_g^-$, a $^1\Delta_g$ and b $^1\Sigma_g^+$ states of O_2 and the $^4\Sigma^-$, $^2\Sigma^-$, $^2\Delta$ and $^2\Sigma^+$ states of $N^{K*}O$. $N^{K*}O(w)$ is the weighted average of the doublet $N^{K*}O$ states in $N^{K*}O(W)$, cf. Figure 16(a). The weighted averages have been calculated from the relative energies shown in Figure 16(a), except ΔE_4 which is based on the $^2\Pi_{3/2}$, $^2\Pi_{1/2}$ splitting of the ground state O_2^+ species[100]. In the equivalent cores approximation,

$\delta \sim \delta'$ (see Reference 98).

The broad band of structure with a maximum at $\sim$ 404.7 eV is too high in energy to be associated with promotion to the $2p\pi^*$ orbital and too low in energy to be associated with the lowest Rydberg excitation. A possible explanation of this band is that it represents the excitation of a nitrogen 1s electron to the antibonding $2p\sigma^*$ valence orbital. The broad nature of the peak could be associated with excitation of the two $^2\Pi$ states (see Table 3) resulting from this electron configuration (the $^4\Pi$ state is forbidden). The resulting states are expected to have some dissociative character since the corresponding valence shell excitation in nitric oxide results in a dissociative $A'\ ^2\Sigma^+$ state[101]. This dissociative character would contribute to the broadening of the structure. Since all the valence orbitals have been accounted for, the higher discrete peaks in the spectrum are probably associated with the promotion of a nitrogen 1s electron to Rydberg orbitals. This assignment is supported by the magnitudes of the derived quantum defects. The promotion of a $1s\sigma$ electron to either $ns\sigma$ or $np\sigma$ Rydberg orbitals results in three separate Rydberg series ($^4\Pi$, $^2\Pi$ and $^2\Pi$). Two of these series, the $^4\Pi$ and one of the $^2\Pi$ series will converge to the $^3\Pi$ K-shell ion state while the remaining $^2\Pi$ series converges to the $^1\Pi$ K-shell ion state. Only the $^2\Pi$ states are expected to contribute to our spectrum. The first Rydberg transition, $1s\sigma_N \rightarrow 3s\sigma$, should result in two $^2\Pi$ states, one converging at the $^3\Pi$ ionic limit and the other converging to the $^1\Pi$ ionic limit. The third peak located at 406.6 eV is assigned to the $^2\Pi$ state which is associated with the $^3\Pi$ limit. Using the observed peak energy and the X-ray PES value of 410.3 eV for the $^3\Pi$ limit[32], we deduce a quantum defect of 1.08, which compares favourably with the quantum

defects observed for 3s Rydberg excitation in the valence shell spectrum of nitric oxide[79,101], $2p\pi^* \rightarrow 3s\sigma$, $\delta = 0.97$ and the valence shell spectrum of molecular oxygen[102], $2p\pi_g \rightarrow 3s\sigma_g$, $\delta = 1.1$. The fourth peak observed at an energy of 407.6 eV has a quantum defect of 1.2 with respect to the $^1\Pi$ ion state. This peak could then have a contribution from the remaining $^2\Pi$ state produced by the excitation of a $1s\sigma_N$ electron to the $3s\sigma$ Rydberg orbital. The much larger intensity of peak four compared to peak three could result from a contribution from the transition $1s\sigma_N \rightarrow 3p\pi$ where the ionization limit is the $^3\Pi$ ion state. The quantum defect of peak four with respect to the $^3\Pi$ limit is 0.75 and is consistent with the quantum defect, $\delta = 0.76$[79], observed for the corresponding valence shell transition in nitric oxide ($2p\pi^* \rightarrow 3p\pi$). Similarly peak five observed at 409.0 eV has a quantum defect of 0.80 with respect to the $^1\Pi$ limit which is consistent with what we would expect for 3p excitation where the Rydberg state converges to the $^1\Pi$ limit. However, the promotion of a $1s\sigma_N$ electron to the $3p\pi$ and $3p\sigma$ Rydberg levels results in six and two dipole allowed final states respectively (see Table 3) and the assignments of these higher Rydberg peaks are clearly uncertain. Peak six observed at $\sim$ 410.4 eV is probably associated with Rydberg states which converge to the $^1\Pi$ ion state.

The positions of the $^3\Pi$ and $^1\Pi$ K-edges in our spectrum are based on the experimental X-ray PES values[32] of 410.3 and 411.8 eV respectively. The broad band of structure with maxima at approximately 413.1 eV and 414.5 eV is associated with the shake-up and shake-off of valence electrons in conjunction with K-shell excitation.

On the basis of the core analogy model we expect the energy spacing between the average energy of the $^4\Sigma^-$ and $^2\Sigma^-$ states resulting from $1s\sigma_N$

promotion to the $2p\pi^*$ orbital and the average energy of the $^3\Pi$ and $^1\Pi$ $N^{K+}O$ states in nitric oxide to reproduce the energy spacing between the ground state and first ion state of molecular oxygen, 12.07 eV[100] [see Figure 16(a)]. Using the first peak maximum as an indication of the $^2\Sigma^-$ energy level and our estimate of the $^4\Sigma^-$ - $^2\Sigma^-$ splitting of 1.4 eV, yields an energy spacing of 12.0 ± 0.4 eV in qualitative agreement with the predicted value. The splitting† between the $^3\Pi$ and $^1\Pi$ ion states produced by ionization of a nitrogen 1s electron in nitric oxide is 1.42 eV[93,94]. Using the same approximation assumed in deriving equations (5.2.1) to (5.2.3), the $^3\Pi$, $^1\Pi$ energy spacing is equal to $2K_{1s\pi^{+*}}$[32,94]. Using the value of $K_{1s\pi^{+*}}$ calculated with one-centre atomic oxygen exchange integrals gives a value of 0.96 eV for the ESCA splitting.

b. Oxygen K-shell Excitation.

The oxygen K-shell electron energy loss spectrum of nitric oxide is shown in Figure 17 and the energies and possible assignments of structure are listed in Table 4. The poor signal to noise ratio compared with that of the nitrogen K-shell spectrum of nitric oxide (Figure 15) reflects the fact that the inelastic scattering intensity of fast electrons for forward scattering decreases[11] by a factor, $\propto$ (energy loss)$^{-3}$. The interpretation of the first discrete peak observed at 532.7 eV is analogous to that of the first peak in the nitrogen K-shell spectrum of nitric oxide (see Table 4). The peak is very broad and has a FWHM of 2.1 eV compared with an elastic FWHM of 0.4 eV. This result suggests that the three doublet NO^{K*} states associated with this peak have a wider energy spacing than the corresponding

† Absolute binding energies in References 93 and 94 are only ± 0.5 eV. Therefore in Table 4 the $N^{K+}O$ energies are from Reference 32.

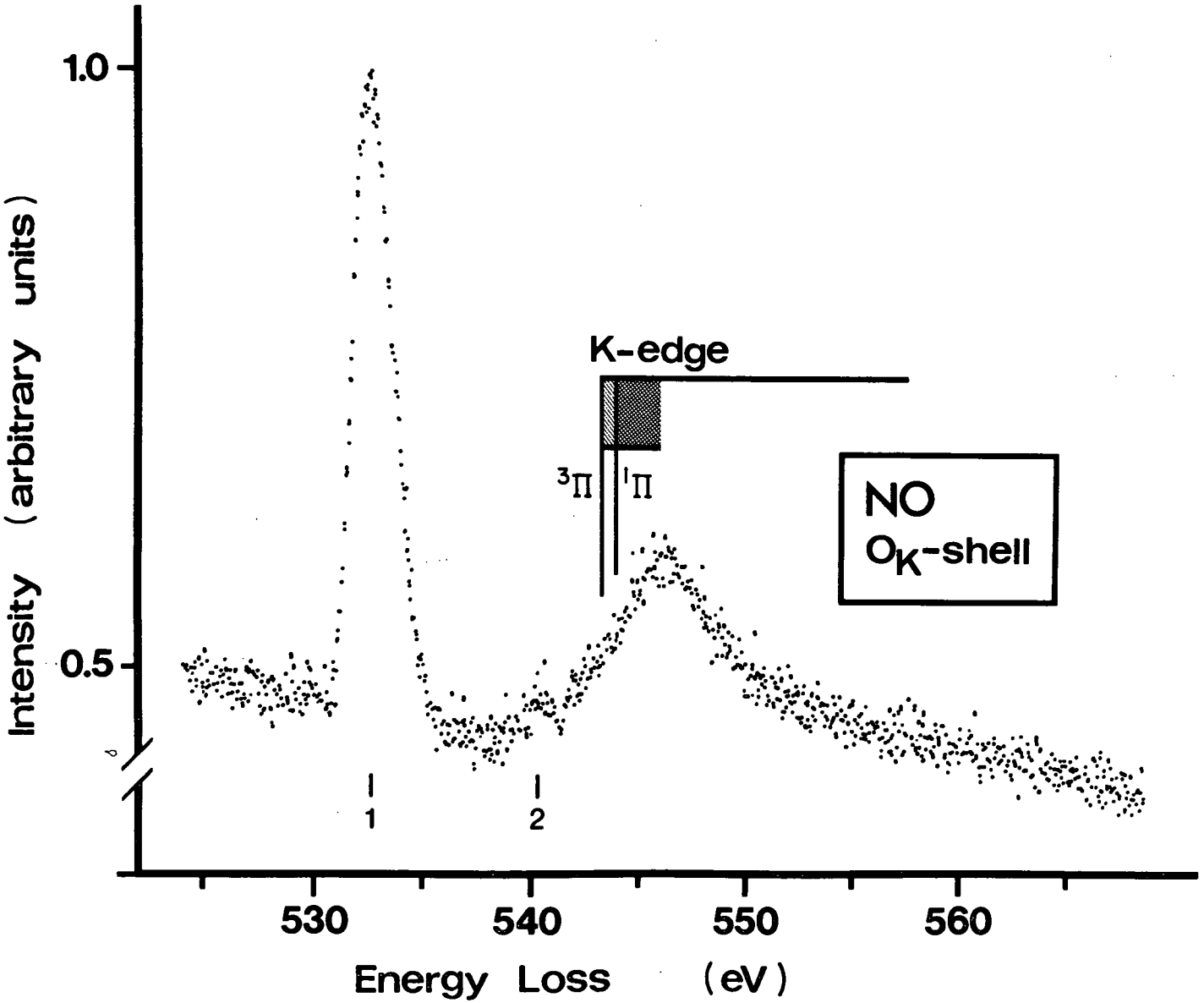

FIGURE 17. Oxygen K-shell energy loss spectrum of nitric oxide.

$N^{K*}O$ states. The intensity of the first peak relative to the others indicates that these discrete levels are expected to give the largest contribution to the high energy autoionization lines observed in the oxygen K-shell Auger spectrum of nitric oxide excited by electron impact[35].

Oxygen 1s excitation in nitric oxide should produce an "NF-like" species. In analogy to the case of nitrogen 1s electron promotion, we have theoretically estimated the relative energy spacings of the $^4\Sigma^-$, $^2\Sigma^-$, $^2\Delta$ and $^2\Sigma^+$ states as a result of oxygen 1s promotion to the $2p\pi^*$ molecular orbital. A wave function for the $2p\pi^*$ orbital in NO^{K*} was calculated using an INDO calculation[103] (unrestricted Hartree-Fock with one-centre exchange) for NF with an internuclear separation equal to that of nitric oxide. Using the resulting wavefunction, $\phi(2p\pi^*) \sim 0.859p\pi_N - 0.512p\pi_{OK^*}$, $p\pi_{OK^*} \sim p\pi_F$, $1s_{OK^*} \sim 1s_F$ and the one-centre atomic fluorine exchange integrals[96], the calculated energy spacings shown in Figure 16(b) were obtained.† The experimental energy spacings[104,105] of the $X^3\Sigma^-$, a $^1\Delta$ and b $^1\Sigma^+$ states of NF (larger than the corresponding spacings in oxygen) are in qualitative agreement with the estimated values for NO^{K*} [see Figure 16(b)]. The calculation suggests that the three doublet states produced by oxygen 1s promotion to the $2p\pi^*$ molecular orbital in nitric oxide, have an energy spacing of $\sim$ 1.8 eV in good agreement with the experimental FWHM of the first discrete peak (Figure 17). The energy required for the transition $1s\sigma_O \rightarrow 2p\pi^*$ can be estimated using the equivalent cores approximation and the thermochemical method in exact analogy to the

† The energy spacings were also calculated using a wavefunction calculated for NF with r_e = 1.3173 A, the experimental internuclear separation[104] of NF, $X^3\Sigma^-$. The largest deviation from the energy differences shown in Figure 16(b) was < 0.1 eV.

method used for the nitrogen K-shell case, $1s\sigma_N \rightarrow 2p\pi^*$. The estimated value of $\sim$ 531.9 eV is in good agreement with the observed peak energy, 532.7 eV, considering that the observed FWHM of the peak is 2.1 eV.

There appears to be a broad band of structure with a maximum at approximately 540.2 eV. The quantum defects with respect to the $^3\Pi$ and $^1\Pi$ ionization limits are consistent with those expected for excitation of an oxygen 1s electron to Rydberg states with quantum number three.

The positions of the $^3\Pi$ and $^1\Pi$ K-edges in our spectrum are based on the experimental X-ray PES values[32] of 543.3 eV and 544.0 eV respectively. The broad band of structure with a maximum at approximately 546 eV represents the shake-up and shake-off of valence electrons in conjunction with $1s\sigma_O$ excitation.

The core analogy model suggests that the energy difference between the average energies of the $^3\Pi$ and $^1\Pi$ NO^{K+} states and the $^4\Sigma^-$ and $^2\Sigma^-$ NO^{K*} states [see Figure 16(b)] should have a magnitude similar to the first ionization potential of NF. Assuming that the onset of the first discrete peak in the NO^{K*} spectrum corresponds to excitation of the $^2\Sigma^-$ state, we derive a value of $\sim$ 13 eV for the ionization potential of NF. The value of 13.1 $\pm$ 0.2 eV derived[106] from experimental appearance potentials[107,108] and the theoretical value[106] of 13.2 $\pm$ 0.3 eV are in reasonable agreement with this prediction.

The magnitude of the molecular exchange integral, $K_{1s_F\pi^*_F}$ derived from the INDO $2p\pi^*$ wavefunction for NO^{K*}, implies that the exchange splitting (to the same degree of approximation as in the case of the discrete multiplet splittings) of the $^3\Pi$ and $^1\Pi$ NO^{K+} states is 0.6 eV. This compares favourably with the experimental value[93,94] of 0.55 eV.

5.2.2. Oxygen.

The ground electronic state of the oxygen molecule has the electron configuration:

$$(1s\sigma_g)^2\ (1s\sigma_u)^2\ (2s\sigma_g)^2\ (2s\sigma_u)^2\ (2p\sigma_g)^2\ (2p\pi_u)^4\ (2p\pi_g)^2,\ {}^3\Sigma_g^-$$

a. Valence Shell Spectrum.

The valence shell energy loss spectrum of molecular oxygen is shown in Figure 18. A high resolution spectrum, $\Delta E(FWHM) = 0.01$ eV, in the 6.8 to 21 eV energy region, has been obtained[61] using 25 keV incident electrons. In addition, assignments of optically forbidden transitions and some Rydberg states have been made on the basis of angular dependence studies using lower impact energies[102,116]. The locations of peaks in our spectrum are consistent with these higher resolution measurements. The first excitation in oxygen is $2p\pi_u \rightarrow 2p\pi_g$ resulting in six possible final electronic states; ${}^{1,3}\Sigma_u^+$, ${}^{1,3}\Delta_u$ and ${}^{1,3}\Sigma_u^-$. The only optically allowed transition is $X\ {}^3\Sigma_g^- \rightarrow B\ {}^3\Sigma_u^-$ (the Schuman-Runge continuum). Peak B in our spectrum (maximum 8.3 eV) is associated with this transition (the vertical transition energy from other workers is 8.6 eV; see Reference 116). The broad band A with a maximum at approximately 6.0 eV is in the energy region where the forbidden $A^3\Sigma_u^+$, $C^3\Delta_u$ and $c^1\Sigma_u^-$ states occur (see Reference 16). The $+\leftarrow|\rightarrow-$ selection rule is not rigorous for nonaxial scattering in electron impact[54] and the intensity of the A band is probably associated with the $A^3\Sigma_u^+$ state. The ${}^3\Delta_u$ and ${}^1\Sigma_u^-$ excitations are less probable at impact energy of 2.5 keV since the first involves $\Delta\Lambda = 2$ and the second involves a spin forbidden transition. The ${}^1\Sigma_u^+$ and ${}^1\Delta_u$ states have not been observed in either electron impact or optical studies. Peak C (10.0 eV) and shoulder D (10.9 eV) are associated with the "longest"

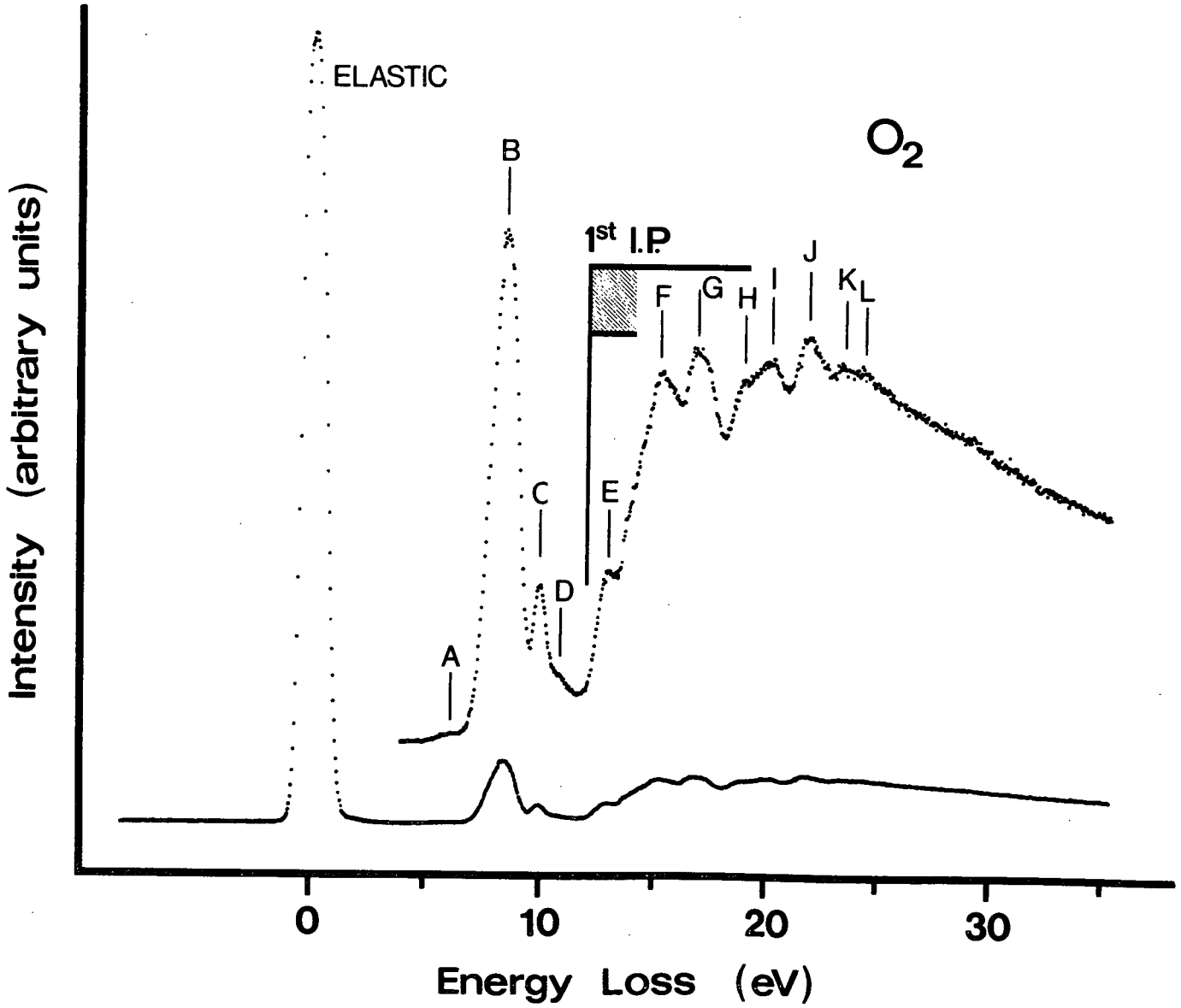

FIGURE 18. Valence shell energy loss spectrum of molecular oxygen.

(9.97 eV[61]) and "second" (10.29 eV[61]) band respectively. The higher energy peaks, E (13.0 eV), F (15.3 eV) G (16.9 eV), H (19.0 eV), I (20.1 eV), J (21.8 eV), K (23.5 eV) and L (24.5 eV) are associated with a large number of overlapping transitions (see Reference 61). The location of the first ionization potential shown in our spectrum is based on the experimental[100] UV PES value of 12.07 eV.

b. Oxygen K-shell Excitation.

In general, the promotion of a core electron ($1s\sigma \equiv$ oxygen K) to discrete levels results in a number of possible final states for a given electron configuration (see Table 3).† The exchange splitting between the multiplet components can be quite large as shown by the experimental value[109] of 1.11 eV measured by X-ray PES for the splitting between $^4\Sigma^-$ and $^2\Sigma^-$ ion states produced by 1s ionization in molecular oxygen.

The K-shell electron energy loss spectrum of oxygen is shown in Figure 19 and the energies and possible assignments of peaks are listed in Table 5. The first discrete peak observed at 530.8 eV is attributed to the promotion of an oxygen $1s\sigma$ electron to the lowest unfilled molecular orbital, the $2p\pi_g$. The resulting configuration:

$$(1s\sigma)^1 \ldots\ldots\ldots (2p\pi)^4\ (2p\pi^*)^3$$

gives rise to a $^3\Pi$ and a $^1\Pi$ state and only the triplet state is expected to contribute to our spectrum.. The observed peak has a FWHM of 0.5 eV, indicating the excitation of a number of vibrational levels. Since the intensity of this peak is much larger than the higher energy discrete peaks observed in the spectrum, excitation to the $^3\Pi$ state is expected to give

† Formally, g and u symmetry does not apply to an oxygen molecule with a localized 1s hole (for example see Reference 117).

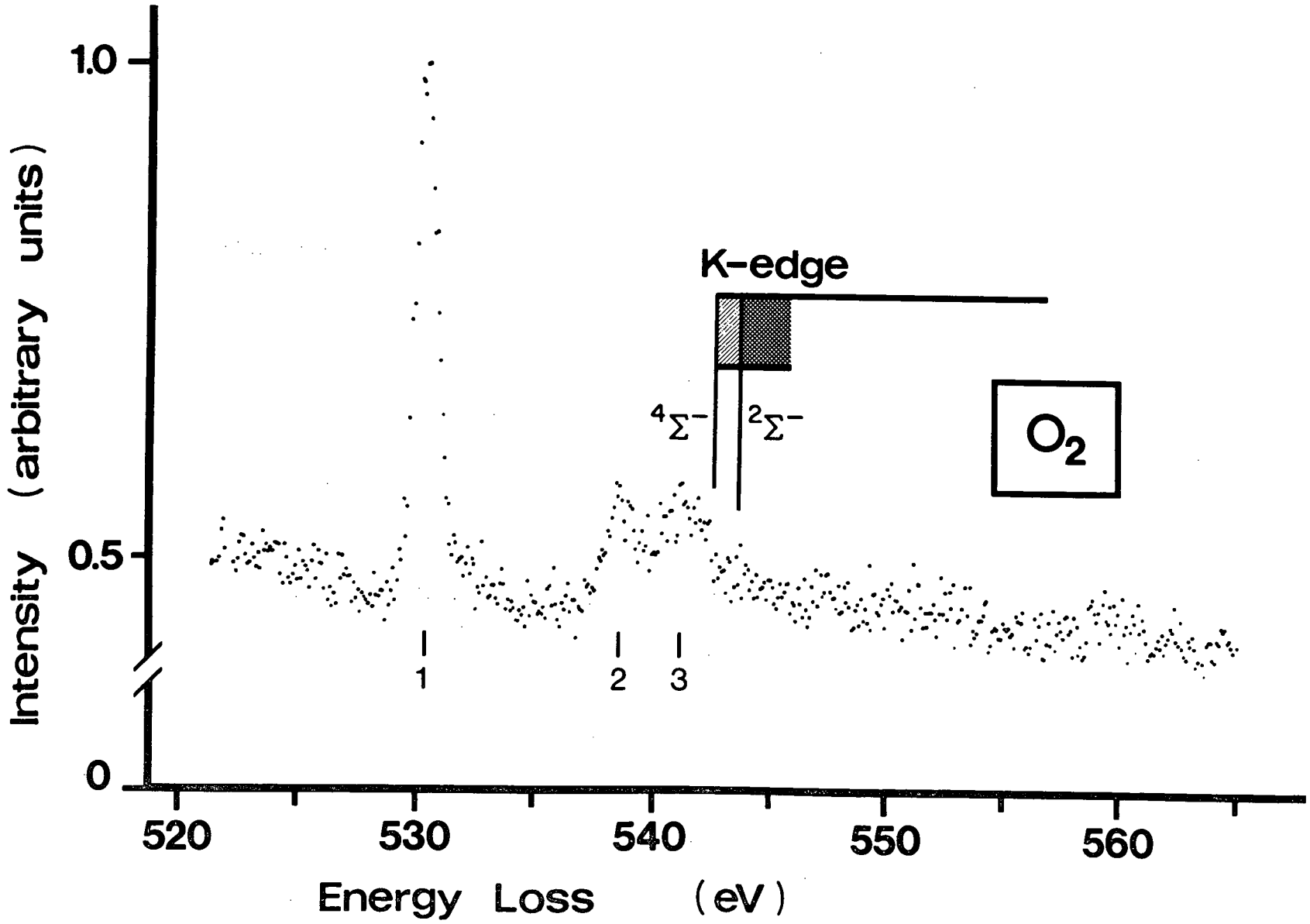

FIGURE 19. K-shell energy loss spectrum of molecular oxygen.

TABLE 5

ABSOLUTE ENERGIES (eV), RELATIVE ENERGIES AND POSSIBLE ASSIGNMENTS OF PEAKS OBSERVED IN THE K-SHELL ENERGY LOSS SPECTRUM OF O_2.

PEAK	ENERGY	ΔE	ASSIGNMENT[a]	
			ORBITAL	STATES
1	530.8	0	$2p\pi_g$	$^3\Pi$
2	539.2	8.4	$3s\sigma_g$	$^3\Sigma^-(2)$, $^3\Sigma^+$
3	541.9	11.1	3p, 3d, etc	
K-EDGE[b]	543.1	12.3	∞	$^4\Sigma^-$
K-EDGE[b]	544.2	13.4	∞	$^2\Sigma^-$

a Only the final orbital involved in the excitation and molecular states dipole connected to the ground $^3\Sigma_g^-$ state have been included. However, the $^3\Sigma^+$ state has been included since the $-\not\leftrightarrow+$ rule does not apply to electron impact for non-axial scattering.[54]

b As determined by X-ray PES.[32]

the largest contribution to the high energy autoionization lines observed in the oxygen 1s Auger spectrum excited by electron impact[32,35]. The second and third peaks with maxima at 539.2 and approximately 541.9 eV respectively are probably associated with the excitation of a $1s\sigma$ electron to the 3s, 3p and higher energy Rydberg levels. A quantum defect of 1.25 is derived from the observed energy position of the second peak and the experimental[32] X-ray PES values for the K-edges. The magnitude of the quantum defect is similar to that deduced from the reported excitation energy for the corresponding valence shell transition in oxygen[102], $2p\pi_g \rightarrow 3s\sigma_g$, for which $\delta = 1.1$.

The positions of the $^4\Sigma^-$ and $^2\Sigma^-$ K-edges in our spectrum are based on the X-ray PES values[32] of 543.1 eV and 544.2 eV respectively.

On the basis of the core analogy model we expect K-shell excitations in molecular oxygen to produce an "OF-like" species. The existence of the oxygen monofluoride radical has been firmly established by matrix techniques[110,112], and recently, gas phase detection has been claimed[113]. An ionization potential of 13.1 ± 0.5 eV has been calculated[114], which agrees with the value of 13.1 ± 0.3 eV estimated[114] from the appearance potential[115] of OF^+ from O_2F_2. From the energy difference between the average energy of the $^4\Sigma^-$ and $^2\Sigma^-$ O_2^{K+} states and the estimated energy of the $^3\Pi$ and $^1\Pi$ O_2^{K*} states, we deduce a value of 12.7 ± 0.4 eV for the ionization potential of OF. Our estimated value is in reasonable agreement with the theoretical and "experimental" values.

CHAPTER SIX

TRIATOMIC MOLECULES

6.1. Carbon Dioxide and Nitrous Oxide.

6.1.1. Carbon Dioxide.

The carbon dioxide molecule is linear in its ground electronic state and has the electron configuration

$$(1\sigma_g)^2\ (1\sigma_u)^2\ (2\sigma_g)^2\ (3\sigma_g)^2\ (2\sigma_u)^2\ (4\sigma_g)^2\ (3\sigma_u)^2\ (1\pi_u)^4\ (1\pi_g)^4,\ {}^1\Sigma_g^+.$$

The $1\sigma_g$ and $1\sigma_u$ orbitals are linear combinations of oxygen 1s atomic orbitals, while the $2\sigma_g$ orbital is formed from the carbon 1s atomic orbital. The $1\sigma_g$, $1\sigma_u$ and $2\sigma_g$ orbitals are essentially localized† on their nuclei and are therefore nonbonding. To indicate their "atomic" character, the electrons filling these orbitals are designated oxygen K-shell and carbon K-shell electrons. We have studied both the carbon and oxygen K-shell energy loss spectra. A valence shell spectrum has also been recorded.

a. Valence Shell Spectrum.

The valence shell energy loss spectrum of carbon dioxide is shown in Figure 20. The observed locations of peaks are consistent with high resolution electron impact spectra[5,49,118] and a "high" resolution optical spectrum[119]. The broad peak A with a maximum at approximately 9 eV is associated with $1\pi_g \rightarrow 2\pi_u$ (π^*) transitions. In the photoabsorption

† Recent quantum mechanical calculations on the 1s-hole states of the O_2^+ molecular ion[117] have been interpreted as an indication that the core holes are localized.

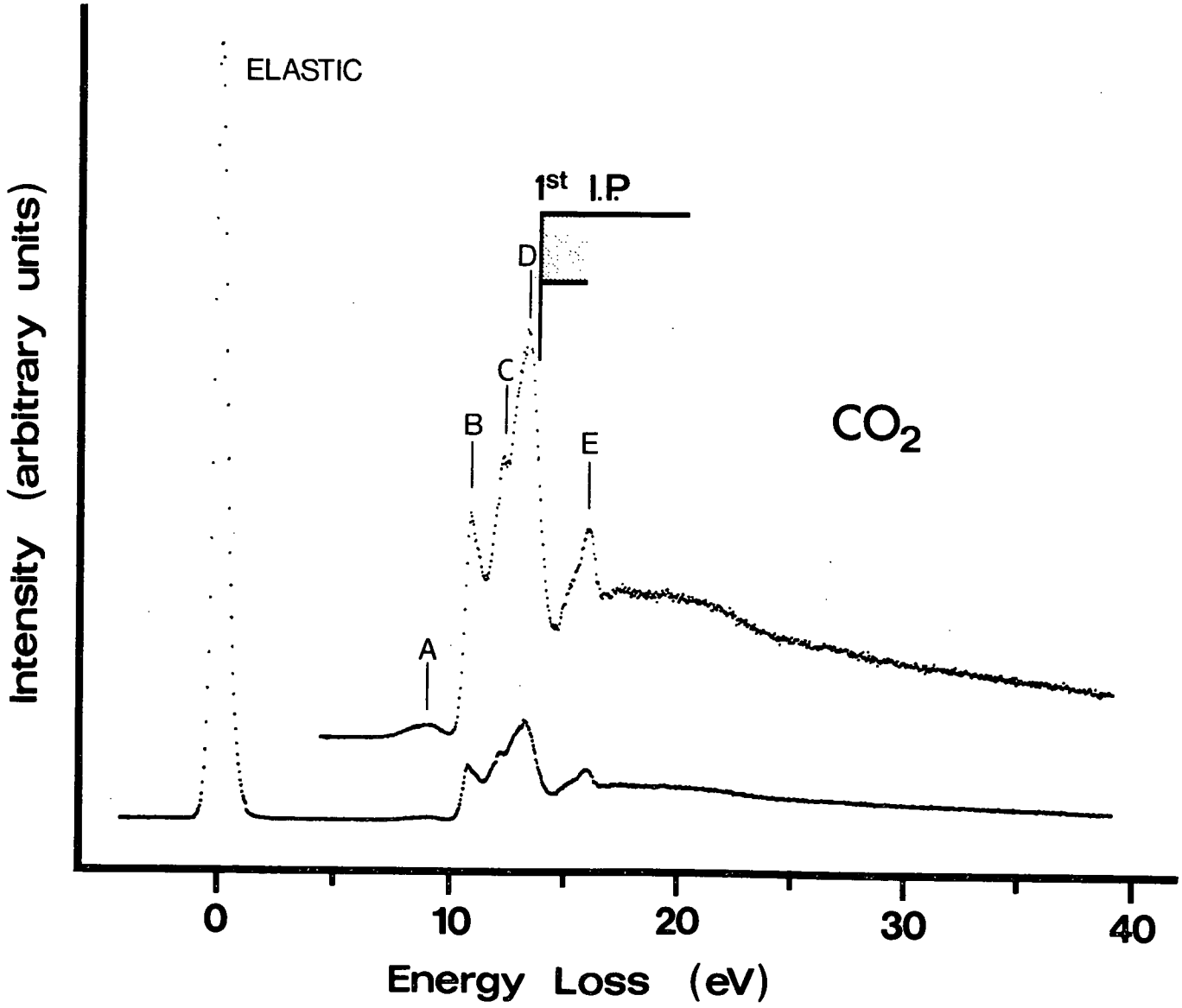

FIGURE 20. Valence shell energy loss spectrum of carbon dioxide.

spectrum[119], two overlapping bands have been observed in this energy region; one (peak maximum at 8.41 eV) assigned to the $^1\Sigma_g^+ \rightarrow {}^1\Delta_u$ ($^1B_2$) transition and the second (peak maximum at 9.31 eV) assigned to the $^1\Sigma_g^+ \rightarrow {}^1\Pi_g$ transition. Both transitions are forbidden in $D_{\infty h}$ symmetry, but in C_{2v} symmetry they each have an allowed $^1B_2$ component. The higher energy peaks in our spectrum; B (10.9 eV, shoulder $\sim$ 11.2 eV), C (12.3 eV), D (13.3 eV) and E (16.0 eV) are probably associated with Rydberg transitions. The higher resolution electron energy loss spectrum[118] has been interpreted on the basis of a Rydberg assignment. The location of the first ionization potential shown in Figure 20 is based on the experimental value[78,120] of 13.77 eV.

b. Carbon K-shell Excitation.

The K-shell spectra of the diatomic molecules (Chapter Five) were interpreted on the basis of a simple "equivalent core" model, in which a hole in the K-shell is considered to have the same effect on the potential experienced by the outer valence electrons as one more positive charge on the nucleus.

If the core analogy model is valid for carbon dioxide, we would expect the relative energies of the peaks observed in the carbon K-shell spectrum (with respect to the lowest energy discrete peak) to reproduce those observed in the excitation of the $6a_1$ electron to Rydberg states in nitrogen dioxide. However, before comparing data from the two molecules, several factors should be considered.

i. The ground electronic state of the nitrogen dioxide molecule, X^2A_1, is bent (the equilibrium bond angle is 134°) and the extent of vibrational excitation accompanying electron promotion is determined by

the overlap of the final and initial state vibrational wavefunctions (i.e. the Franck-Condon factors). Therefore, the promotion of the $6a_1$ electron to the linear Rydberg states and the ion state is expected to excite many vibrational quanta (particularly of the bending mode, ν_2). This is illustrated in Figure 21, where a qualitative representation of some of the states of nitrogen dioxide has been drawn in the bending coordinate. It should be noted that the independent stretching coordinate also contributes to the vibrational structure of excited states.

ii. In carbon K-shell excitations in carbon dioxide, vibrational populations are determined by the Franck-Condon region of the linear ground state. This is shown in Figure 21, where it has been assumed that the K-shell excited states of carbon dioxide have the same relative energies as those states of nitrogen dioxide resulting from the promotion of a $6a_1$ valence electron.

In order to compare the two sets of data, the nitrogen dioxide energies must be corrected by subtracting both the barrier to linearity of nitrogen dioxide (1.83 eV)[121] and the excess vibrational population of the upper states. The latter quantity can be estimated as being approximately 1.6 eV on the basis of the difference between the vertical (11.25 eV)[122] and the adiabatic ($\leq$ 9.62 eV)[123] values for the first ionization potential of nitrogen dioxide. We expect a similar correction to apply to the Rydberg states.

The carbon K-shell energy loss spectrum of carbon dioxide is shown in Figure 22 and the energies and tentative assignments of structure are listed in Table 6. Although complete data on the valence shell excitation of nitrogen dioxide is not available, the corrected relative energies of

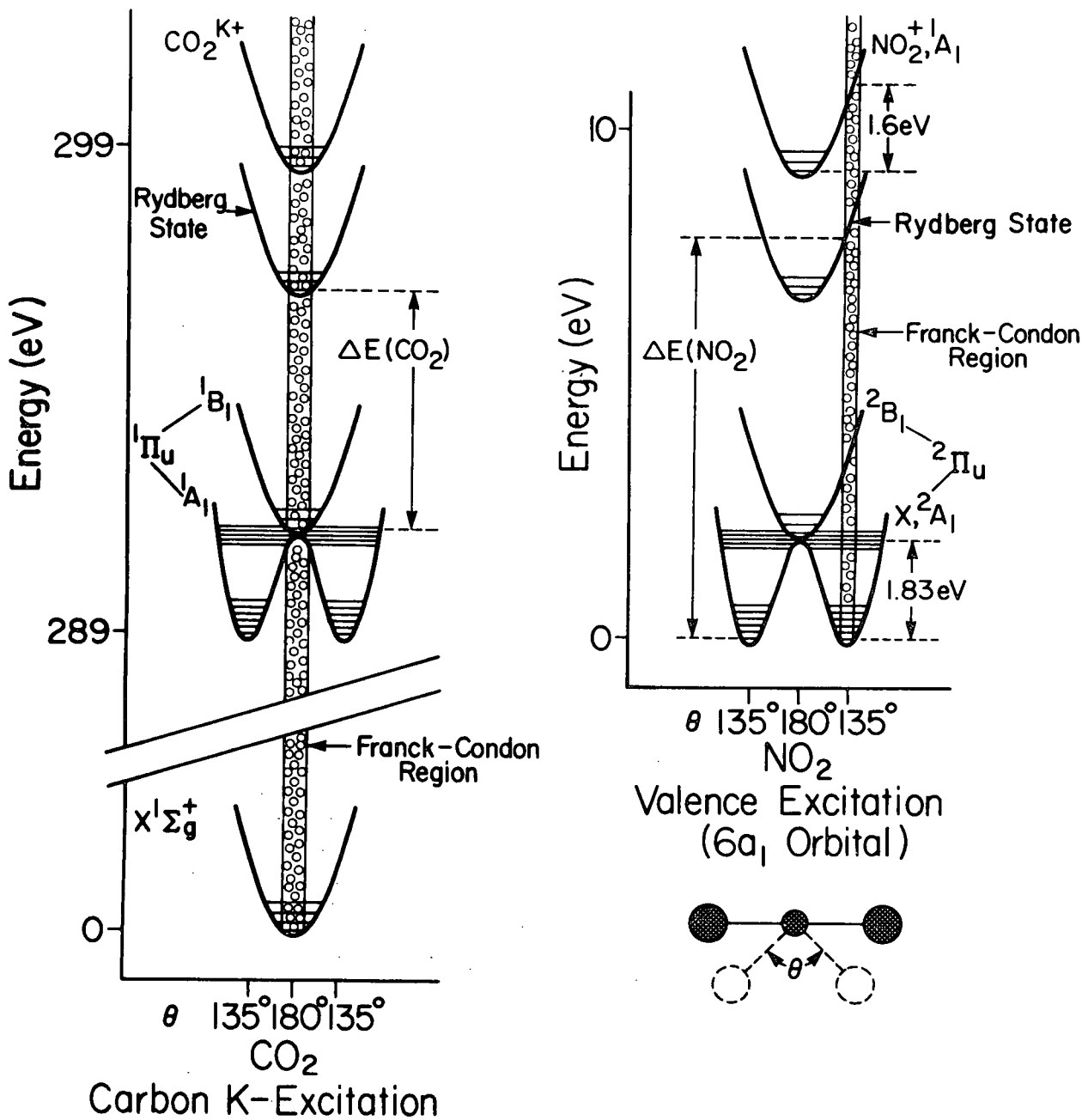

FIGURE 21. Qualitative representation (not to scale) of the potential energy surfaces, as a function of the bending coordinate, of some states of nitrogen dioxide and K-shell excited carbon dioxide. Note: These indicate the nature of the energy corrections which would have to be applied in order to compare data from the two molecules on the basis of the core analogy model.

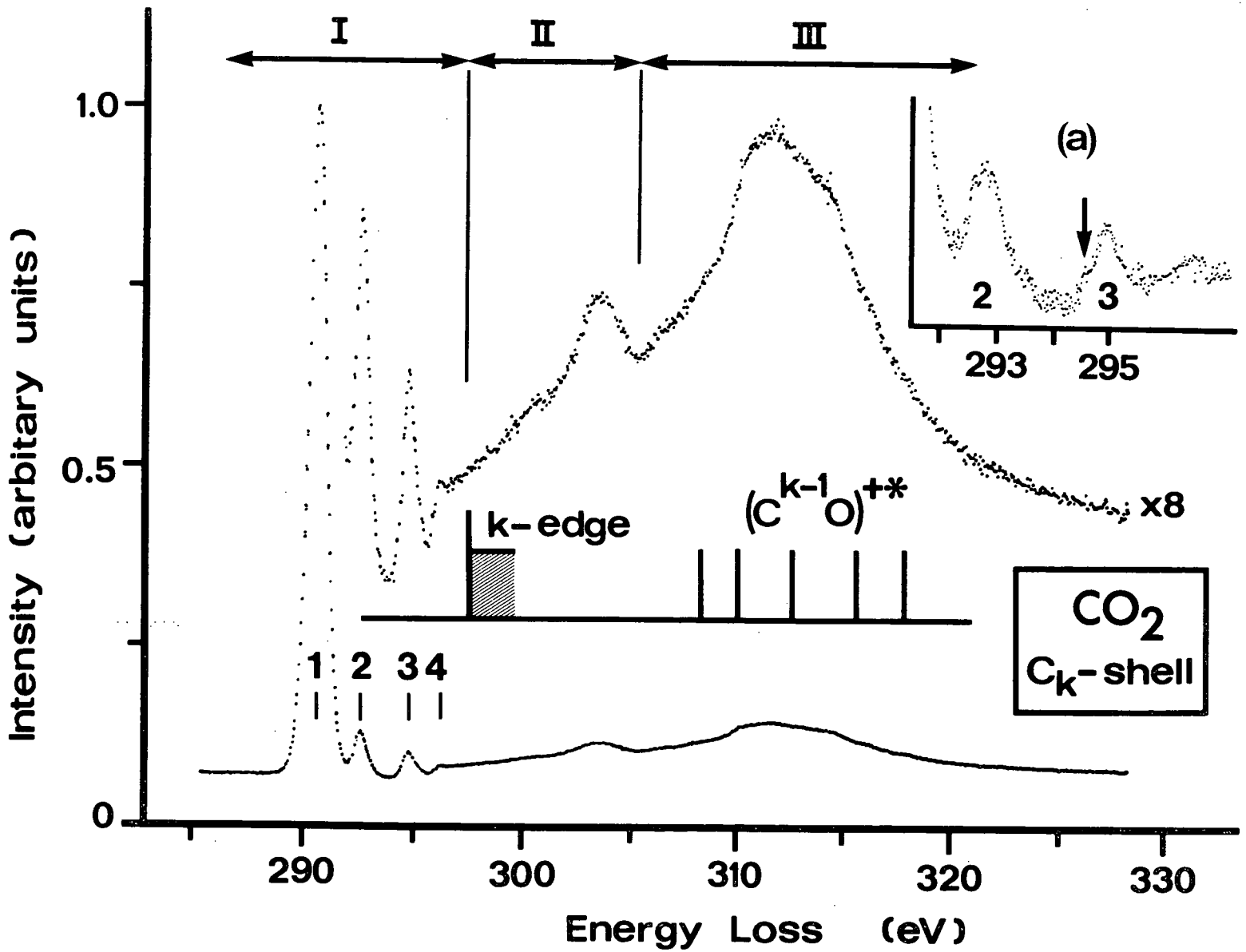

FIGURE 22. The carbon K-shell energy loss spectrum of carbon dioxide.

TABLE 6

ABSOLUTE ENERGIES (eV), RELATIVE ENERGIES AND POSSIBLE ASSIGNMENTS OF PEAKS OBSERVED IN THE CARBON AND OXYGEN K-SHELL SPECTRA OF CARBON DIOXIDE.

PEAK	CARBON K-SHELL			OXYGEN K-SHELL			POSSIBLE ASSIGNMENT[b]
	ENERGY	ΔE	CALCULATED VALUE[a]	ENERGY	ΔE	CALCULATED ENERGY[a]	
1	290.7	0	-	535.4	0	-	$1\pi_u$ $(6a_1 + 1b_1)$
2	292.7	2.0	294.1	MASKED[c]	?	537.7	$3s\sigma_g$
3	(294.5)[d]	(3.8)	294.9	538.7	3.3	538.5	$3p\sigma_u$
	294.9	4.2	295.2			538.8	$3p\pi_u$
			296.0			539.6	$4s\sigma_g$
4	296.3	5.6	296.2	539.9	4.5	539.8	$4p\sigma_u$
			296.4			539.9	$4p\pi_u$
K-EDGE[e]	297.5	6.8	-	541.1	5.4	-	∞
5	∿301	∿10	-				$1\pi_u$ + SHAKE-UP
6	∿314	∿13	-				$1\pi_u$ + SHAKE-UP

a. Calculated using the Rydberg formula; $E_n = A - R/(n-\delta)^2$, where E_n is the excitation energy; A, the K-shell ionization energy of CO_2; R, the Rydberg constant; n, the quantum number; and δ, the quantum defect. The quantum defects used were those from the valence shell Rydberg series of carbon dioxide[124] with; $\delta(ns\sigma)=1.0$, $\delta(np\sigma)=0.71$, and $\delta(np\pi)=0.56$.

b. Only the final orbital/s involved in the K-excitations have been included. If the hole states are localized (see text) the g and u designations should be omitted for oxygen K-shell excitations since the molecule would have $C_{\infty v}$ symmetry.

c. The intense first discrete peak probably includes the first Rydberg transition (see the text).

d. This extra peak is from a higher resolution scan. Figure 2 (insert a).

e. These values are from X-ray PES measurements.[125]

the identified Rydberg states[122] which converge to the first ion state do not match the data from the carbon K-shell spectrum (see the correlation diagram, Figure 23). Qualitatively, the spectrum is very similar to those previously observed for nitrogen and carbon monoxide, with the discrete structure dominated by the lowest energy peak. This intense peak observed at 290.7 ± 0.2 eV is interpreted as arising from the promotion of a carbon K-shell electron ($2\sigma_g$) to the lowest unfilled molecular orbital of carbon dioxide, the $2\pi_u$.

$$CO_2\ (1\sigma_g)^2\ (1\sigma_u)^2\ (2\sigma_g)^2\ \ldots\ (1\pi_g)^4,\ X\,^1\Sigma_g^+ \rightarrow$$
$$(1\sigma_g)^2\ (1\sigma_u)^2\ (2\sigma_g)^1\ \ldots\ (1\pi_g)^4\ (2\pi_u)^1,\ ^1\Pi_u.$$

For linear states of carbon dioxide, the $2\pi_u$ orbital is doubly degenerate. This degeneracy is removed in bent states with the production of the $6a_1$ and the $1b_1$ Renner-Teller components (see Figure 21). A reasonable estimation for the equilibrium bond angle of a state produced by exciting a carbon K-shell electron ($2\sigma_g$ becomes $2a_1$ in C_{2v} symmetry) to the $6a_1$ orbital is approximately 135°. This estimation is based on two facts; a bond angle of 134° for the ground state of nitrogen dioxide, and a bond angle of 122° for the first valence excited state of carbon dioxide[120] which results from the transition $1\pi_g(4b_2) \rightarrow 1\pi_u(6a_1)$. The analogous carbon K-shell excited state resulting from the transition $2a_1 \rightarrow 6a_1$ is expected to have a bond angle larger than 122° since the $4b_2$ orbital is now filled and on the basis of a Walsh diagram[120] this orbital favours larger bond angles. The peak which we have associated with the transitions $2a_1 \rightarrow 6a_1$ and $2\sigma_g \rightarrow 2\pi_u$ ($6a_1 + 1b_1$) has a FWHM of 0.9 eV (elastic peak 0.5 eV) indicating that a number of vibrations are excited. In the bending coordinate,

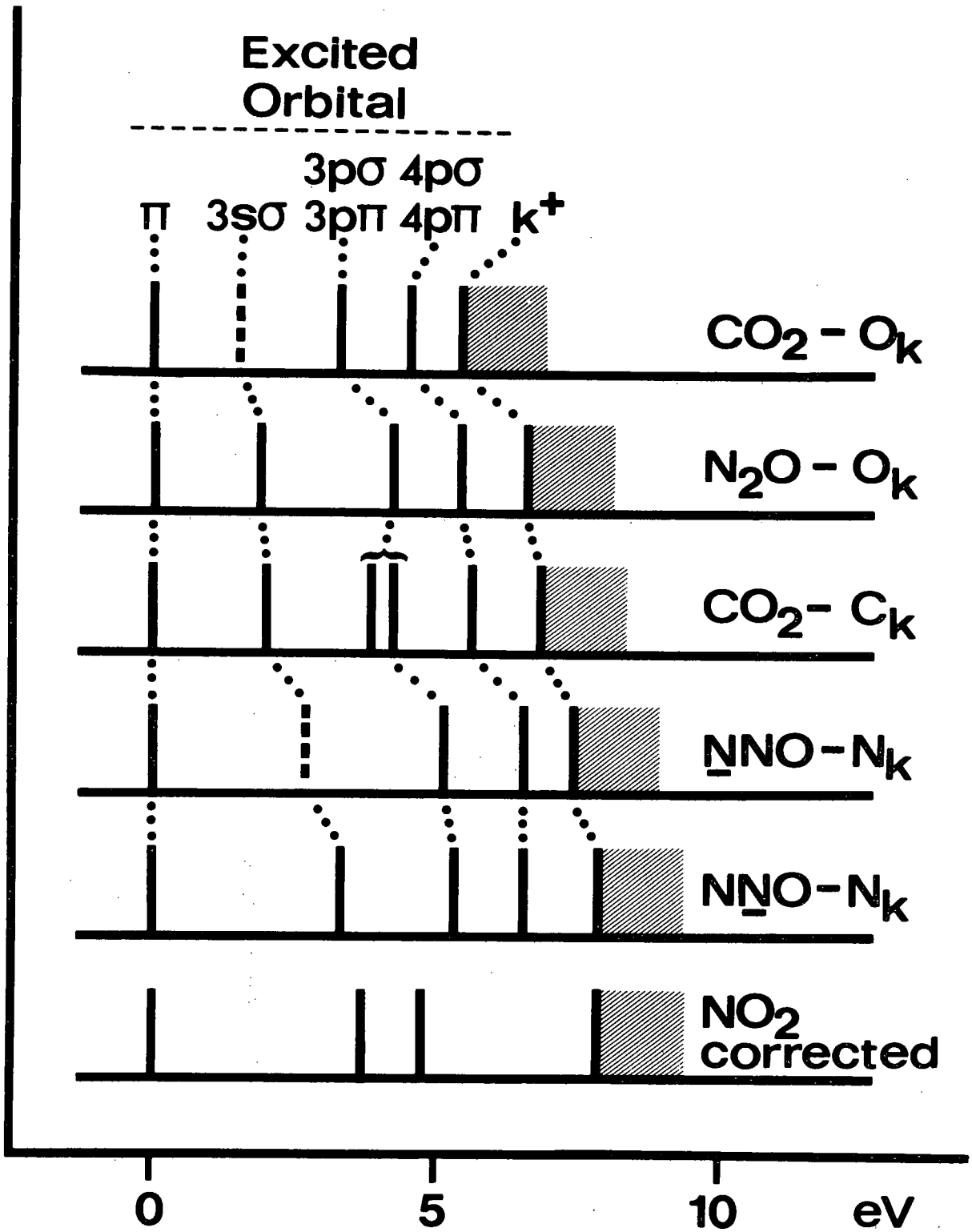

FIGURE 23. Correlation of the observed peaks in the K-shell energy loss spectra of carbon dioxide and nitrous oxide (both carbon and oxygen K-shells). The dashed lines represent the expected positions of unresolved peaks (see the text). The relative energies (corrected) of appropriate states from the valence shell spectrum of nitrogen dioxide have also been included for comparison.

maximum Franck-Condon overlap is expected for the $0 \rightarrow 0$ transition to the linear $1b_1$ component. Therefore, most of the observed intensity is probably associated with vibrational excitation of the lower members of the linear component while some of the intensity on the low energy side of the peak, could be excitation of the higher vibrational levels of the bent $6a_1$ component below the barrier to linearity. These "hole" states decay by Auger emission in a much shorter time than that required for a vibration and therefore the excited molecule does not reach the bent equilibrium conformation. However, such transitions may still occur since the wave-functions are finite, although small, at the linear position (i.e. between the two wells). In Auger emission studies the K-shell excited states are observed when they decay by autoionizing to singly charged ion states. The energies of the ejected electrons are higher than the maximum energy which can be taken up by a "normal" Auger electron. In the carbon K-shell Auger spectrum of carbon dioxide[35], two high energy peaks at 272.6 ± 0.5 eV and 268.2 ± 0.5 eV have been observed. Assuming that the first discrete state at 290.7 ± 0.2 eV is the initial neutral excited state implies that singly charged ion states of carbon dioxide occur at 18.1 eV and 22.5 eV. The first energy agrees with that necessary[78] to remove a $3\sigma_u$ electron, while the second probably represents shake-up in conjunction with the ionization of a valence electron. The higher energy discrete peaks in the spectrum are associated with states produced by promoting a carbon K-shell electron to Rydberg orbitals, producing states which converge to the carbon K-shell ionization limit. The much lower intensity, with respect to that of the first discrete peak, is expected, since the first discrete peak is associated

with the promotion of a K-shell electron to a valence molecular orbital with a principal quantum number of two, while the higher energy discrete peaks are associated with higher quantum number (n = 3,4) Rydberg orbitals. Two orbitals which are sometimes included in the valence shell, the $5\sigma_g$ and the $4\sigma_u$, are expected to correspond with outer Rydberg orbitals[119]. Energy values calculated using quantum defects from the valence shell Rydberg series of carbon dioxide[124] and a series limit of 297.5 eV as determined by X-ray PES[125], and in good agreement with peaks observed in the spectrum (see Table 6). The largest deviation is found for the peak at 292.7 eV, which is assigned to the first Rydberg transition, $2\sigma_g \rightarrow 3s\sigma_g$. However, this is expected since the $3s\sigma_g$ orbital is very close to the valence shell and is probably not a "true" Rydberg orbital. This transition is optically forbidden by the selection rule $g \nleftrightarrow g$ and is also forbidden in our experiment if the first Born approximation is valid. However, in electron impact spectroscopy symmetry forbidden transitions have been observed even at higher energies where the first Born approximation is normally expected to be valid. In fact, Skerbele and Lassettre[53] have proposed the selection rule that deviations from the first Born approximation are largest when the excited state and the ground state belong to the same symmetry species, i.e. the deviation depends upon a totally symmetric operator (see Reference 126). In this case, both states have a $^1\Sigma_g^+$ term manifold and therefore deviations from the Born theory are to be expected. The third peak at 294.9 eV is assigned to the Rydberg transitions $2\sigma_g \rightarrow 3p\sigma_u$, $3p\pi_u$. A higher resolution scan is shown in Figure 22 (insert a) and indicates that this band is composed of a number of peaks. The quantum defect calculations are in good agreement with these assignments, giving

values of 294.9 eV for the $3p\sigma_u$ peak and 295.2 eV for the $3p\pi_u$ peak. It is possible that the high energy shoulder has a contribution from the transition $2\sigma_g \rightarrow 4s\sigma_g$ (calculated value 296.0 eV). The fourth discrete band with a maximum at 296.4 eV is probably associated with $2\sigma_g \rightarrow 4p$ Rydberg transitions.

A value of 297.5 eV has been obtained for the carbon K-shell binding energy by X-ray PES[125]. An ionization potential of 298.0 eV is obtained using the core analogy model (energy of the onset of the first discrete peak in the carbon K-shell spectrum, plus a corrected value for the ionization potential of nitrogen dioxide) which is only in fair agreement with the experimental value (see Figure 23). Structure is observed above the K-edge representing a variety of multiple electron transitions involving one K-shell electron and one or more valence shell electrons. The following two electron transitions are expected to make the largest contributions;

i. double excitation; i.e. shake-up of a valence electron in conjunction with K-shell excitation, designated by $(C^{K-1}O_2)^{**}$ where the superscript K-1 denotes a hole in the carbon K-shell.

ii. excitation and ionization; involving an electron from both the carbon K- and valence shells, where one of the electrons is ejected and the other remains behind in a higher unfilled orbital, designated by $(C^{K-1}O_2)^{+*}$.

The broad structure observed in Region II of the carbon K-shell spectrum is associated with discrete structure arising from double excitations, i.e. $(C^{K-1}O_2)^{**}$ states. The intensity of these bands is roughly the same as that of the K-jump and a few percent of the intensity of the first discrete peak at 290.7 eV. This suggests that most of the intensity arises

from the shake-up of valence electrons in conjunction with carbon K-shell promotion to the $2\pi_u$ molecular orbital. Discrete states resulting from the promotion of a carbon K-shell electron to the Rydberg orbitals are much less intense and therefore we expect shake-up associated with these transitions to contribute little intensity to the observed shake-up structure. Contributions to the intensity of this structure from $(C^{K-1}O_2)^{+*}$ states are improbable since the lowest shake-up state associated with K-shell ionization, as determined by X-ray PES[125], should start at 10.8 eV above the K-edge. The structure observed in Region III of the carbon K-shell spectrum is identified with the onsets of ionization to $(C^{K-1}O_2)^{+*}$ states. These $(C^{K-1}O_2)^{+*}$ states should give rise to a series of shake-up peaks in the X-ray PES spectrum on the low kinetic energy side of the carbon K-shell peak. In Figure 22 we have drawn the shake-up peaks associated with carbon K-ionization of carbon dioxide observed by Siegbahn et al.[125] and Carlson et al.[81]. It can be seen that the energy region of the band observed in our spectrum correlates with the shake-up peaks. The total shake-up intensity observed in the X-ray PES experiments is roughly 20% of that of the K-shell peak, while the intensity of structure in Region III of our spectrum is at least twice that of the K-jump. The large shake-up intensity observed in Region III of our spectrum probably has a significant contribution from a series of $(C^{K-1}O_2)^{**}$ states, which converge to each of the indicated thresholds [cf. the nitrogen K-shell spectrum of molecular nitrogen (5.1.1).

c. Oxygen K-shell Excitation.

The oxygen K-shell energy loss spectrum of carbon dioxide is shown in Figure 24 and tentative assignments of observed structures are

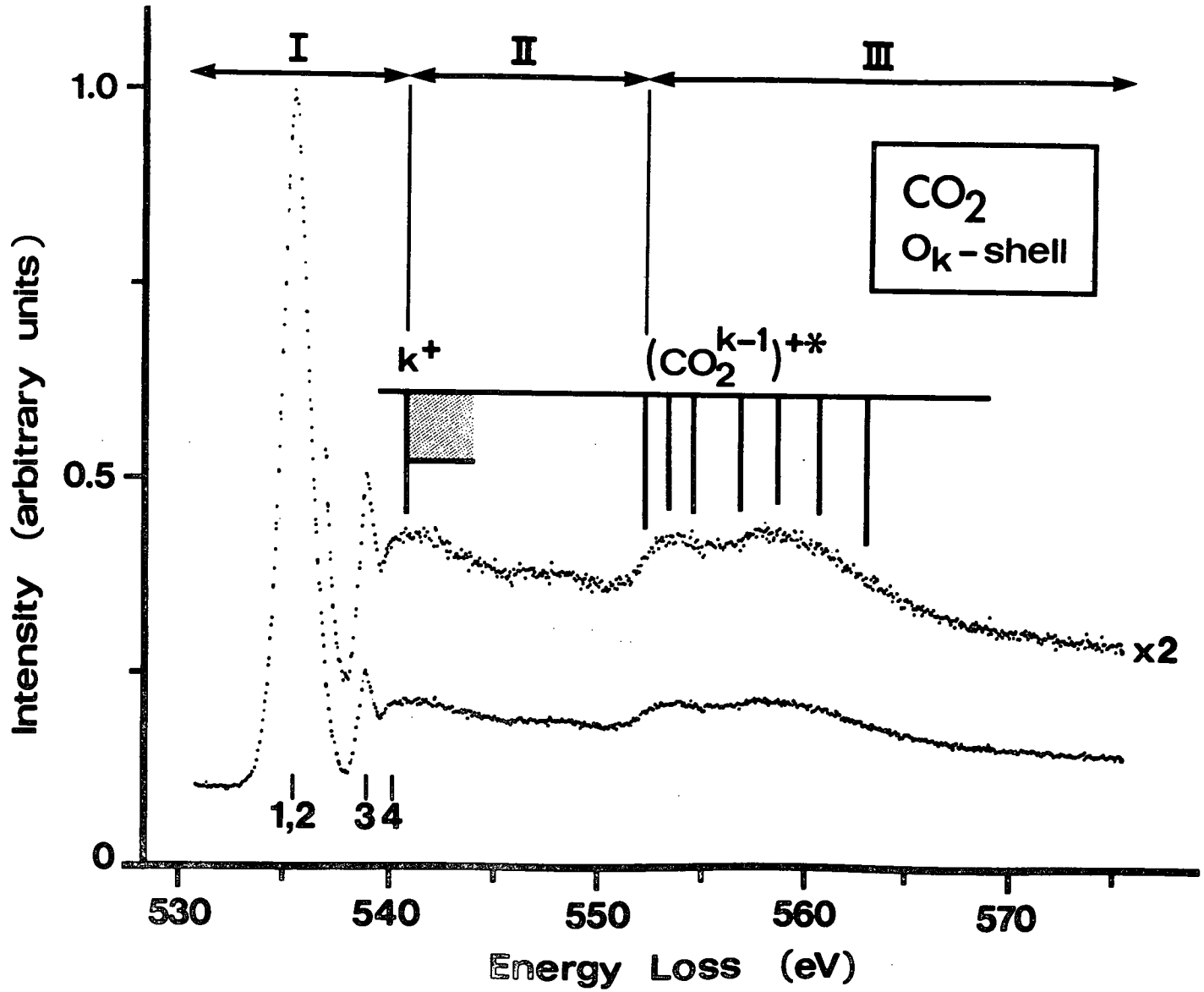

FIGURE 24. The oxygen K-shell energy loss spectrum of carbon dioxide.

listed in Table 6. The interpretation of the spectrum is analogous to that of the carbon K-shell and therefore only differences will be discussed in detail. The first discrete peak at 535.4 ± 0.2 eV has a FWHM of 1.4 eV compared with the elastic peak FWHM of 0.55 eV. In addition to the promotion of an oxygen K-shell electron to the two components of the $2\pi_u$ orbital, the $6a_1$ and the $1b_1$, it is possible that some of the line broadening and intensity on the high energy side of the peak is associated with the lowest energy Rydberg transition, $1\sigma_u \rightarrow 3s\sigma_g$. This transition is optically allowed (in contrast to the corresponding transition involving a carbon K-shell electron) since formally one oxygen K-shell orbital has σ_g symmetry and the other has σ_u symmetry. The results of the correlation diagram shown in Figure 23 are consistent with the possibility that the first discrete peak includes the first Rydberg transition. The assignments of the remaining discrete peaks follow those of the carbon K-shell as shown by Table 6 and Figure 23. The energy positions of these discrete peaks are in good agreement with those expected on the basis of calculations involving quantum defects from the valence shell spectra of carbon dioxide[124] and a series limit of 541.1 eV[125] (see Table 6).

In the oxygen K-shell Auger spectrum of carbon dioxide[35], a peak has been observed at 511.3 ± 0.3 eV which is too high in energy to attribute to a "normal" Auger process. The assumption that the first discrete state observed at 535.4 eV in our spectrum, is the initial neutral excited state, implies the existence of a singly charged state of carbon dioxide at an energy of 24.1 eV. The closest known ion state of carbon dioxide[78] is at 19.4 eV, arising from the ejection of a $4\sigma_g$ electron. Therefore, the final state probably arises from the shake-up of a valence electron in conjunction

with the ionization of a second valence electron.

A value of 541.1 eV has been obtained for the oxygen K-shell binding energy by X-ray PES[125]. Above this edge the spectrum has been divided into two regions; Region II extends from the K-edge up to the lowest energy where $(CO_2^{K-1})^{+*}$ states have been observed by X-ray PES[81,125], and Region III extends from this point to the high energy limit of the spectrum. Thus in Region II we would expect to observe discrete excitations, $(CO_2^{K-1})^{**}$ states, while in Region III the structures probably arise from both discrete states, $(CO_2^{K-1})^{**}$, and continuum states, $(CO_2^{K-1})^{+*}$ (cf. the carbon K-shell spectrum). The intensities of shake-up structures observed in Region II, relative to the intensities of Region III and the K-jump, appear to be small. In Figure 24 we have indicated the energy positions where states arising from shake-up associated with oxygen K-shell ionization of carbon dioxide have been observed by X-ray PES[81,125]. The broad region of structure observed in Region III of our spectrum correlates with the shake-up peaks.

6.1.2. Nitrous Oxide (N_2O).

The nitrous oxide molecule is isoelectronic with carbon dioxide and the linear ground electronic state has the electronic configuration

$$(1\sigma)^2\ (2\sigma)^2\ (3\sigma)^2\ (4\sigma)^2\ (5\sigma)^2\ (6\sigma)^2\ (7\sigma)^2\ (1\pi)^4\ (2\pi)^4,\ {}^1\Sigma^+.$$

The 1σ orbital is essentially the oxygen K-shell orbital and the 2σ and 3σ orbitals represent nitrogen K-shell orbitals. We have studied both the nitrogen and the oxygen K-shell energy loss spectra. A valence shell spectrum has also been recorded.

a. Valence Shell Spectrum.

The valence shell energy loss spectrum of nitrous oxide is shown

in Figure 25. The locations of peaks are consistent with higher resolution spectra[49,118,119]. The weak band with a maximum at ∿ 7.0 eV (peak A) is probably associated with a $\pi \rightarrow \pi^*$ transition, analogous to the first band in the carbon dioxide valence shell spectrum (see Figure 20). In a higher resolution photoabsorption spectrum[119], a broad, weak band with a maximum at 6.81 eV has been assigned to the forbidden, $^1\Sigma^+ \rightarrow {}^1\Delta$ transition. In C_s symmetry, both Renner-Teller components, A' and A", are allowed, which explains why the transition is observed in our spectrum. The higher energy peaks observed in our spectrum, B (8.5 eV), C (9.6 eV), D(11.2 eV), E (12.3 eV), F(14.1 eV), G (14.8 eV), H (16.0 eV) and I (18.5 eV) are probably associated with Rydberg transitions. A Rydberg interpretation of the higher resolution electron impact spectrum[118] has been suggested, although in the photoabsorption spectrum[119], the peak corresponding to B in our spectrum has been assigned to the transition $^1\Sigma^+ \rightarrow {}^1\Pi$ ($\sigma \rightarrow \pi^*$). The location of the first ionization potential shown on our spectrum is based on the experimental value[78,120] of 12.89 eV.

b. Nitrogen K-shell Excitation.

If we assume that the core electrons are localized on their nuclei, the 2σ and 3σ molecular orbitals represent central nitrogen and terminal nitrogen K-shell orbitals respectively. On the basis of the core analogy model, excitation of a terminal nitrogen K-shell electron in nitrous oxide should produce states analogous to appropriate states of nitrogen dioxide.

The nitrogen K-shell energy loss spectrum is shown in Figure 26 and tentative peak assignments are listed in Table 7. The assignments are analogous to those previously given for the corresponding peaks in the

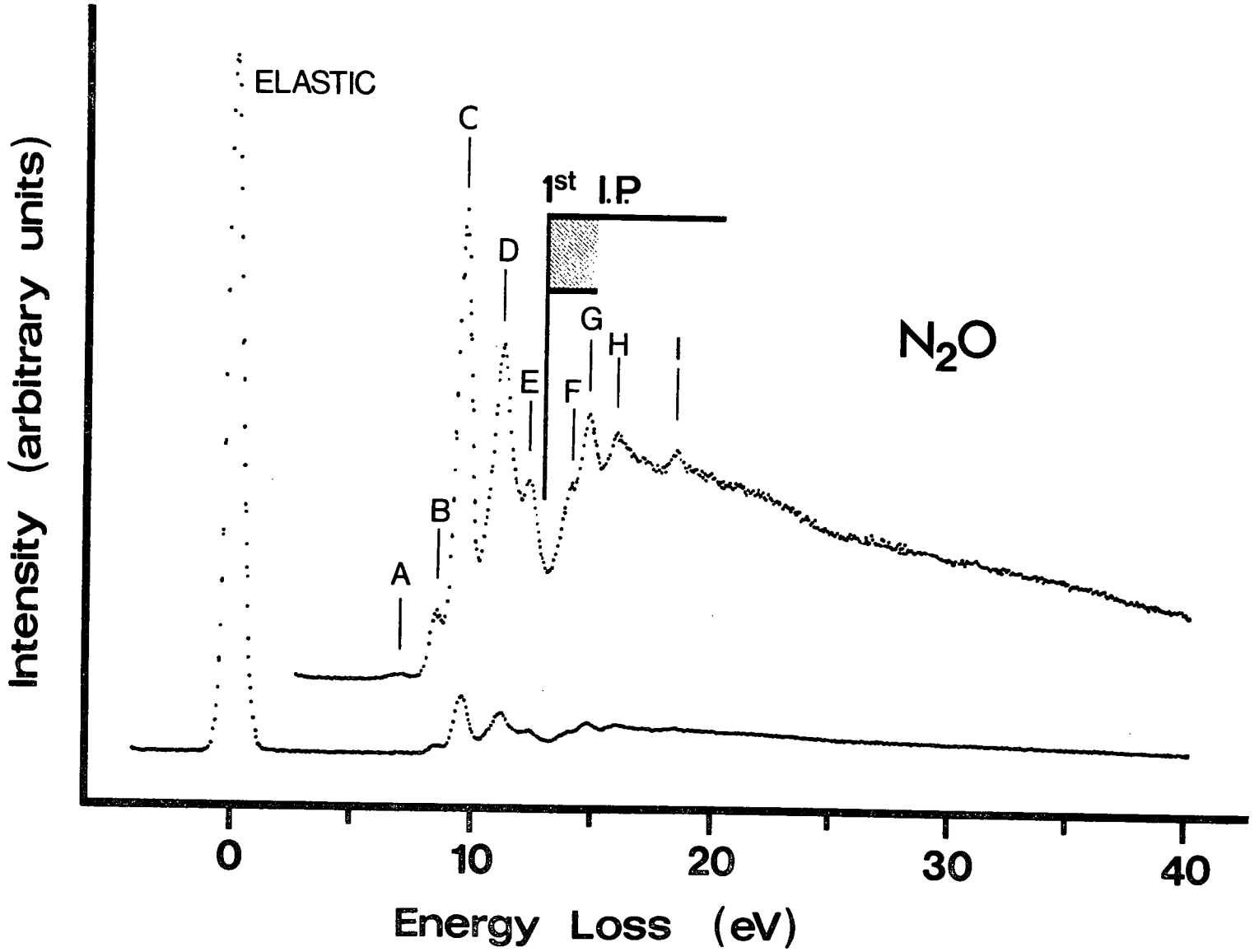

FIGURE 25. Valence shell energy loss spectrum of nitrous oxide.

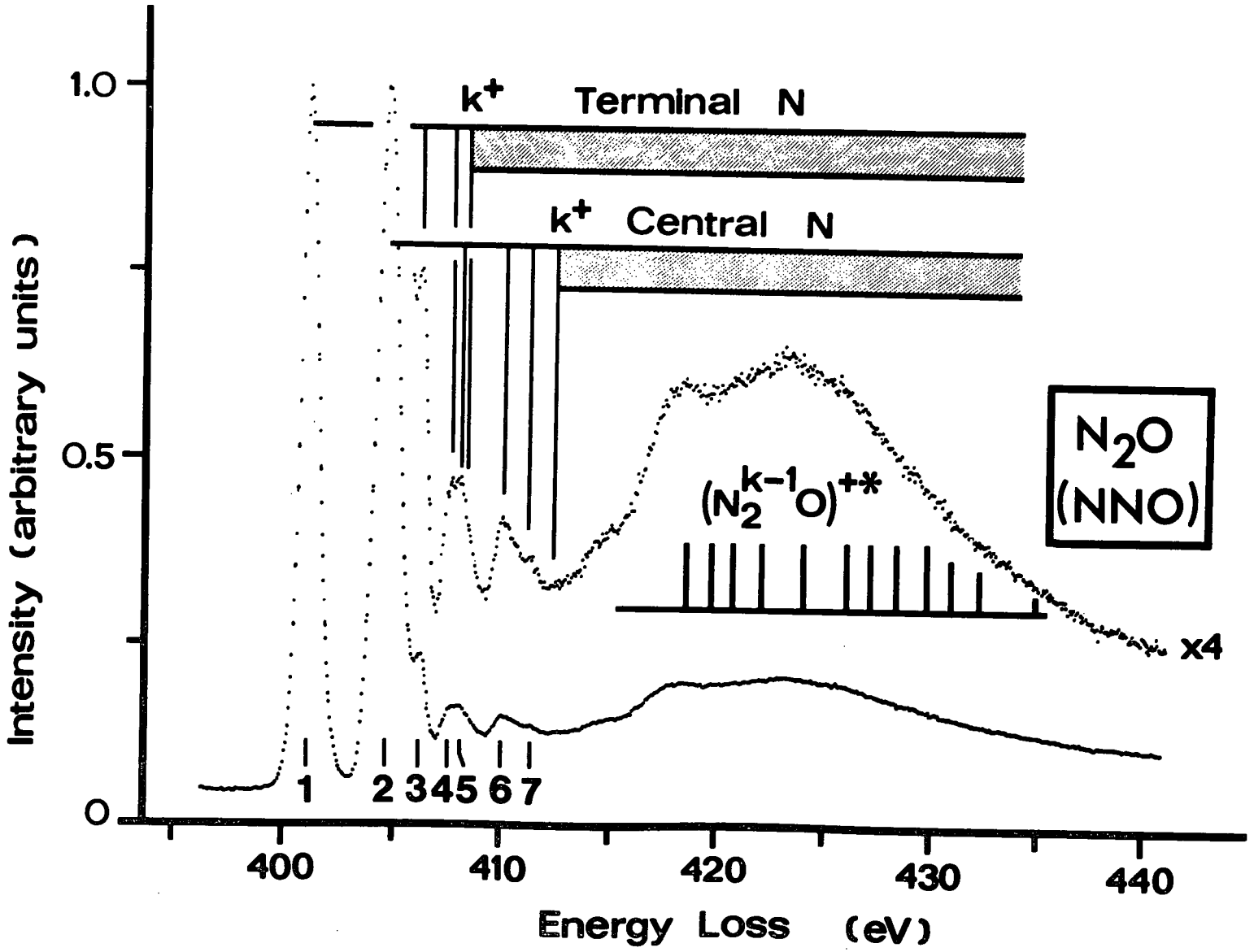

FIGURE 26. The nitrogen K-shell energy loss spectrum of nitrous oxide.

TABLE 7

ABSOLUTE ENERGIES (eV), RELATIVE ENERGIES AND POSSIBLE ASSIGNMENTS OF PEAKS OBSERVED IN THE NITROGEN K-SHELL SPECTRUM OF NITROUS OXIDE.

PEAK	ENERGY	ΔE	ASSIGNMENT[a]	CALCULATED VALUE[b]
1	401.1	0	$N_T \rightarrow 3\pi(a' + a'')$	-
2	404.7	3.6[c]	$N_C \rightarrow 3\pi(a' + a'')$	-
			$N_T \rightarrow 3s\sigma$?	405.1
3	406.2	5.1	$N_T \rightarrow 3p\sigma$	406.0
			$3p\pi$	406.2
			$N_T \rightarrow 3d\sigma$	406.7
			$3d\pi$	406.9
			$N_T \rightarrow 4s\sigma$	407.0
4	407.6	6.5	$N_T \rightarrow 4p\sigma, 4p\pi$	407.3
			$4d\sigma$	407.5
			$4d\pi$	407.6
5	408.0	6.9	$N_C \rightarrow 3s\sigma$	409.1
TERMINAL[d] K-EDGE	408.5	7.4	$N_T \rightarrow \infty$	-
6	410.0	8.9	$N_C \rightarrow 3p\sigma$	410.0
			$3p\pi$	410.2
			$N_C \quad 3d\sigma$	410.7
			$3d\pi$	410.9
			$N_C \rightarrow 4s\sigma$	411.0
7	411.2	10.1	$N_C \rightarrow 4p\sigma, 4p\pi$	411.3
			$4d\sigma$	411.5
			$4d\pi$	411.6
CENTRAL[d] K-EDGE	412.5	11.4	$N_C \rightarrow \infty$	-

a Only the final orbital/s involved in the K-excitations have been included.
b Calculated using the Rydberg formula. The quantum defects used were those from the valence shell Rydberg series of nitrous oxide[127] (averaged values) with $\delta(ns\sigma)=1.0$, $\delta(np\sigma)=0.68$, $\delta(np\pi)=0.57$, $\delta(nd\sigma)=0.29$ and $\delta(nd\pi)=0.07$
c A more accurate determination is 3.62 ± 0.05 eV (from a different data run).
d These values are from X-ray PES experiments[32].

carbon dioxide spectra (see Figure 23), although the nitrous oxide spectrum is more complex since two separate spectra are overlapped. Therefore, we will discuss the separation of the spectrum into its two component parts and any features which are unique to the nitrous oxide spectrum. The spectrum is dominated by the first two discrete peaks which have approximately equal intensities. The lowest energy peak is attributed to the promotion of a terminal nitrogen K-shell electron to the lowest unfilled molecular orbital, the 3π. The higher energy peak is then associated with the corresponding transition involving a central nitrogen K-shell electron. The observed energy difference between the two discrete states produced by these transitions is 3.62 ± 0.05 eV. The two discrete peaks have different widths, with the peak associated with the terminal nitrogen having a FWHM of 1.1 eV while the corresponding peak associated with the central nitrogen has a FWHM of 1.3 eV. These are much larger than the width of the peak from elastically scattered electrons (FWHM of 0.5 eV) and indicate K-shell excitation to a number of vibrational levels of both components, a' and a", of the 3π level (π degeneracies in nitrous oxide are lifted in C_s symmetry with the formation of a' and a" components). It is possible that the first Rydberg transition associated with the promotion of a terminal nitrogen K-shell electron is masked by the intense second discrete peak and therefore, may contribute to its width. It is interesting that the widths of the peaks associated with the corresponding ion states (separated by 4.0 eV), observed by X-ray PES[32], follow the reverse order in that ionization of a terminal nitrogen K-shell electron gives rise to a peak with a FWHM of 1.05 eV, while ionization of a central nitrogen K-shell electron produces a peak having a FWHM of 0.95 eV. The absolute magnitudes of the FWHM's

measured in the two different experiments are not directly comparable, since the large natural line widths of the incident X-rays are the main contributor to the FWHM's of the peaks associated with the ion states. The separation of the higher energy discrete peaks in the spectrum into peaks associated with each of the nitrogen inner shells has been made on the basis that the energy splitting observed between corresponding Rydberg states (i.e. one associated with the promotion of a terminal nitrogen K-shell electron and the other associated with the promotion of a central nitrogen K-shell electron to the same final orbital) should be from 3.6 to 4.0 eV. In fact, for a "true" Rydberg type orbital, we would expect an energy splitting closer to the 4.0 eV separation of the ion states. Peaks 6 and 7 lie above the terminal nitrogen K-edge and are assigned to Rydberg transitions involving the central nitrogen (see Table 7). However, it is possible that in this energy region there could be a contribution from doubly excited $(N^{K-1}NO)^{**}$ states. On the basis of the first assignment it is possible to tentatively assign the other discrete peaks. The energy positions of the assigned peaks are in good agreement with those expected on the basis of calculated values using quantum defects from the valence shell spectra of nitrous oxide[127] and series limits as provided by X-ray PES[32] (see Table 7). The energy difference between all of the corresponding states is within the range 3.6 to 4.0 eV and the spectrum associated with each shell correlates with those of carbon dioxide (see Figure 23). The association of the peak at 408.0 eV with the first Rydberg transition involving a central nitrogen K-shell electron ($2\sigma \rightarrow 3s\sigma$), indicates that the peak from the corresponding transition involving a terminal nitrogen K-shell electron should be in the energy region of the intense second discrete peak. In some regions it is

impossible to specify which Rydberg transitions are responsible for the main intensity (for example 3p or 3d). For instance, in the valence shell spectra, $\sigma \rightarrow 3d\pi$ Rydberg transitions are usually intense[127]. The relative energies of the peaks assigned to the promotion of a terminal nitrogen K-shell electron do not match those observed in the carbon K-shell spectrum of carbon dioxide or the corrected relative energies of the nitrogen dioxide molecule (see Figure 23). Therefore, the description of the K-shell excited states of these triatomic molecules in terms of the core analogy model is not as accurate as that for the diatomics. This result is not surprising in view of the additional molecular complexities of the triatomic molecules.

The energy positions of the terminal and central nitrogen K-edges, shown in Figure 26, are those obtained by X-ray PES[32]. Structures observed between the two edges cannot be assigned with certainty, although the correlation diagram, Figure 23, is consistent with the discrete assignment. Above the central nitrogen K-edge the observed structures correspond to the shake-up and shake-off of valence electrons in conjunction with K-shell excitation or ionization of either a terminal or central nitrogen K-shell electron. The first band of structure observed at $\sim$ 414 eV in our spectrum is probably associated with $(N^{K-1}NO)^{**}$ states, while the band centred around 418 eV could have a contribution from $(NN^{K-1}O)^{**}$ states. The position of $(N^{K-1}NO)^{+*}$ and $(NN^{K-1}O)^{+*}$ states as determined by X-ray PES[128] have been included in Figure 26.

c. Oxygen K-shell Excitation.

The oxygen K-shell energy loss spectrum of nitrous oxide is shown in Figure 27 and tentative peak assignments are listed in Table 8. The interpretation of the spectrum is analogous to that of each nitrogen

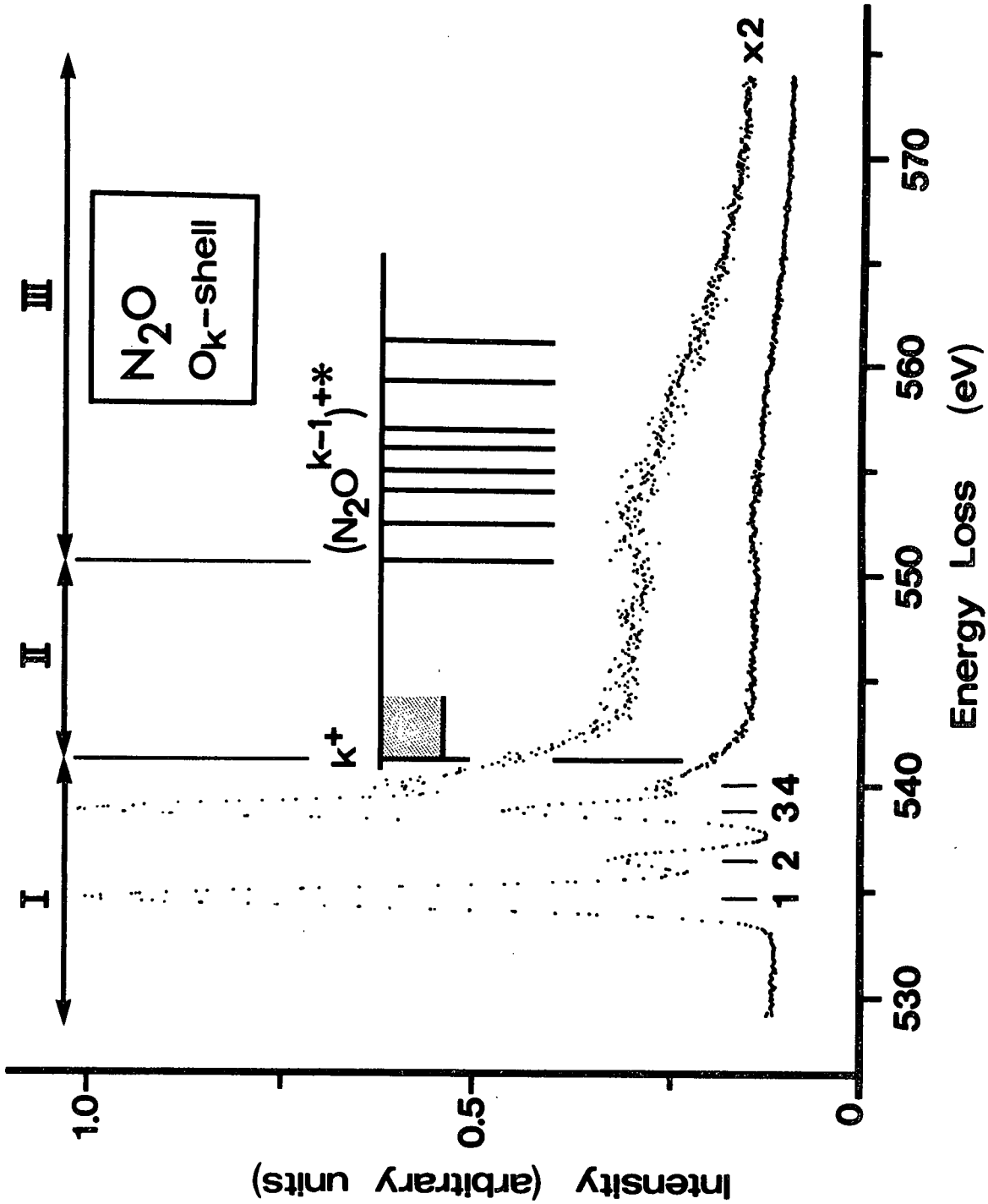

FIGURE 27. The oxygen K-shell energy loss spectrum of nitrous oxide.

TABLE 8

ABSOLUTE ENERGIES (eV), RELATIVE ENERGIES AND POSSIBLE ASSIGNMENTS OF PEAKS OBSERVED IN THE OXYGEN K-SHELL SPECTRUM OF NITROUS OXIDE.

PEAK	ENERGY	ΔE	ASSIGNMENT[a]	CALCULATED VALUE[b]
1	534.6	0	$3\pi(a' + a'')$	-
2	536.5	1.9	$3s\sigma$	537.8
3	538.8	4.2	$3p\sigma$	538.7
			$3p\pi$	538.9
			$3d\sigma$	539.3
			$3d\pi$	539.6
			$4s\sigma$	539.7
4	540.0	5.4	$4p\sigma$, $4p\pi$	540.0
			$4d\sigma$	540.2
			$4d\pi$	540.3
K-EDGE[c]	541.2	6.6	∞	-

a. Only the final orbital/s involved in the K-excitations have been included.

b. Calculated using the Rydberg formula. The quantum defects used were those from the valence shell Rydberg series of nitrous oxide[127] with $\delta(ns\sigma) = 1.0$, $\delta(np\sigma) = 0.68$, $\delta(np\pi) = 0.57$, $\delta(nd\sigma) = 0.29$ and $\delta(nd\sigma) = 0.07$.

c. This value is from X-ray PES[32].

K-shell spectrum and therefore only differences and interesting features will be discussed. The first discrete peak has a FWHM of 1.2 eV, which is similar to those observed for the corresponding peaks in the nitrogen spectrum of nitrous oxide. (In contrast, for carbon dioxide, the FWHM's were 0.9 eV for the carbon K-shell and 1.4 eV for the oxygen K-shell. This provides some reinforcement of the suggestion that the first peak in the oxygen K-shell spectrum of carbon dioxide has a contribution from a transition to the $3s\sigma_g$ Rydberg orbital.) The intensities of the higher energy discrete peaks in the spectrum, relative to that of the first discrete peak, are larger than those observed in either of the previous spectra. Part of this intensity may be associated with transitions to d-type Rydberg orbitals since the valence shell spectrum has a strong contribution from sigma to nd Rydberg orbitals[127]. However, we would also expect this to occur in the case of the nitrogen K-shell spectrum of nitrous oxide, where a "normal" intensity was observed. A sharp decrease in intensity is observed after the K-edge. In the nitrogen K-shell spectrum it is difficult to conclude whether a similar situation occurs because both K-regions are obscured, one by discrete structure and the other by a continuum.

The position of the oxygen K-edge in Figure 27,is based on the experimental value provided by X-ray PES[32]. A surprising feature above the K-edge is the extremely small intensity of structures associated with $(N_2O^{K-1})^{**}$ and $(N_2O^{K-1})^{+*}$ states. The energy positions where shake-up in conjunction with K-shell ionization (i.e. $(N_2O^{K-1})^{+*}$ states) have been observed by X-ray PES[128] are included in Figure 27.

6.2. Carbon Disulfide and Carbonyl Sulfide.

6.2.1. Carbon Disulfide.

The carbon disulfide molecule is linear in its ground electronic state and has the electron configuration:

$$1s_{1s}^4\ 1s_{1s}^2\ 1s_{2s}^4\ 1s_{2p}^{12}\ (5\sigma_g)^2\ (4\sigma_u)^2\ (6\sigma_g)^2\ (5\sigma_u)^2\ (2\pi_u)^4\ (2\pi_g)^4,\ {}^1\Sigma_g^+.$$

We have studied the carbon 1s (K) and sulfur 2p ($L_{II,III}$) energy loss spectra. Cross-sections for discrete transitions in the region of the sulfur 2s (L_I) edge appear to be small and a spectrum was not recorded. The valence shell of carbon disulfide is isoelectronic with those of carbon dioxide and nitrous oxide.

a. Valence Shell Spectrum.

The valence shell energy loss spectrum of carbon disulfide is shown in Figure 28. The observed locations of peaks are consistent with a higher resolution spectrum[118]. Peak A, with a maximum at 4.1 eV, is associated with the $^1B_2$ Renner-Teller component of the $^1\Delta_u$ state which results from the transition, $2\pi_g \rightarrow 3\pi_u$ (π^*). This transition has been positively identified in the corresponding energy region of a high resolution optical spectrum[129]. The weak intensity of this band is associated with the forbidden nature of the transition in $D_{\infty h}$ symmetry. The intense peak, B, with a maximum at 6.2 eV is associated with the $2\pi_g \rightarrow 3\pi_u$ (π^*), $^1\Sigma_u^+$ ($^1B_2$) transition (see the interpretation of the optical spectra[119,129]). This transition is electric dipole allowed in both $D_{\infty h}$ and C_{2v} symmetry, which accounts for its strong intensity relative to peak A. The locations of higher energy peaks in our spectrum are; C (8.5 eV), D (9.3 eV), E (11.1 eV), F (11.9 eV), G (13.4 eV) and H (15.1 eV). In the photoabsorption spectrum[119] and a higher resolution

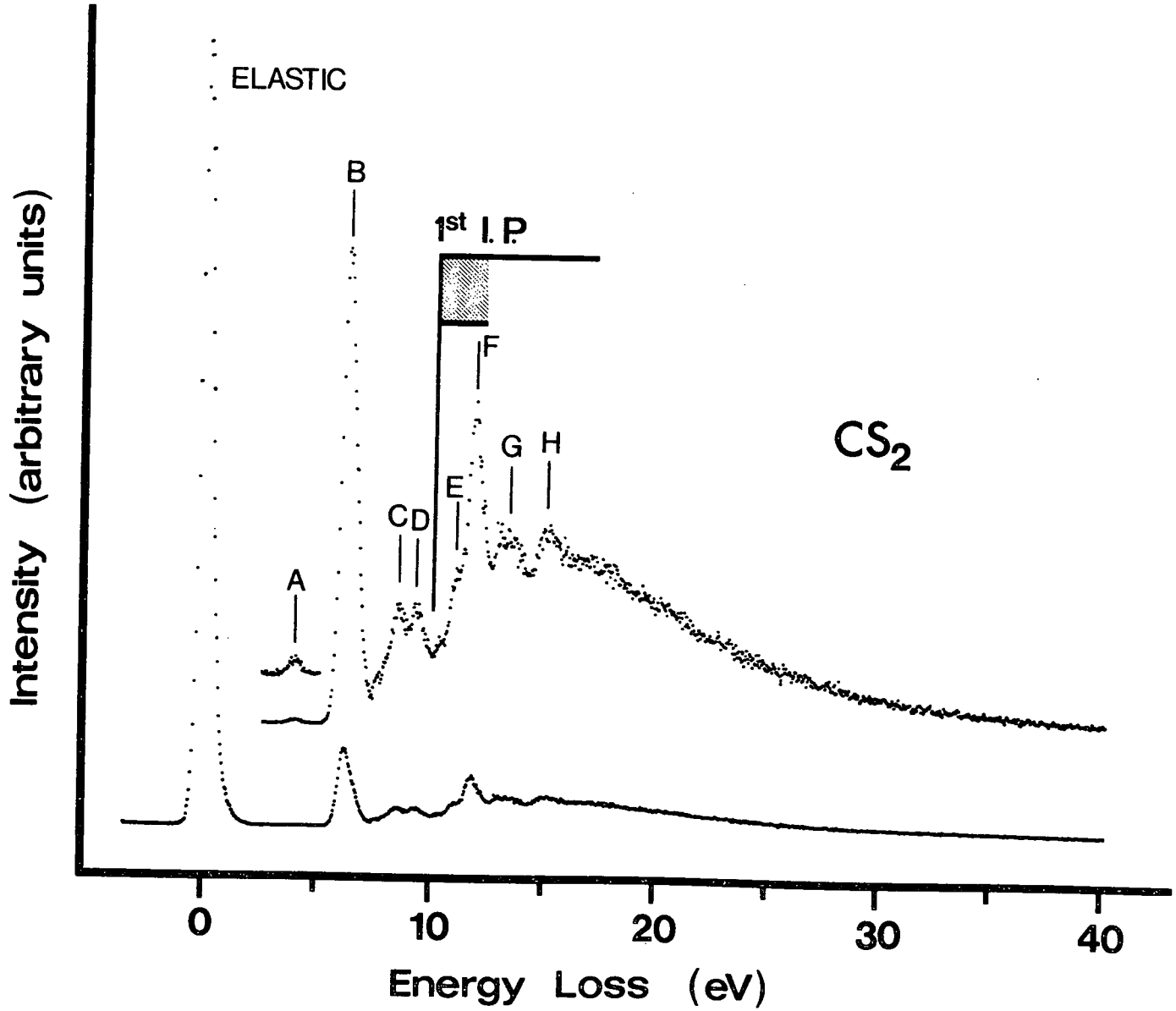

FIGURE 28. Valence shell energy loss spectrum of carbon disulfide.

electron impact spectrum[118], corresponding peaks have been assigned to Rydberg excitations. The location of the first ionization potential shown in our spectrum is based on the UV-PES value[78] of 10.06 eV.

b. Carbon K-shell Excitation.

The carbon K-shell energy loss spectrum of carbon disulfide is shown in Figure 29 and the energies and possible assignments of peaks are listed in Table 9. The intense peak observed at 286.1 eV is interpreted as arising from the promotion of a carbon K-shell electron to the lowest unfilled molecular orbital, the $3\pi_u$ (π^*). The peak has a FWHM of 0.56 eV compared with a FWHM of 0.38 eV for the peak associated with elastically scattered electrons. This indicates the excitation of a number of vibrational levels. This peak is analogous to the first discrete peak observed in the carbon K-shell spectrum of carbon dioxide. The second and third peaks located at $\sim$ 289.6 eV and 290.6 eV respectively, are probably associated with the promotion of a carbon K-shell electron to Rydberg orbitals. Since carbon and sulfur belong to different rows of the periodic table, a choice of principal quantum numbers exists. The lowest Rydberg orbital may be designated 3s appropriate for carbon or 4s appropriate for sulfur. The quantum defects may be appreciably different from those derived for molecules containing only second row atoms (see Reference 130). The quantum defects (assuming n = 3) derived from the experimental energies of peaks two and three and the X-ray PES value for the carbon K-edge in carbon disulfide[125] are 1.03 and 0.67 respectively. If a Rydberg assignment is correct, peak two is probably associated with 3s excitation and peak three with 3p excitation. The broad shoulder on the low energy side of peak four may also be associated with Rydberg transitions.

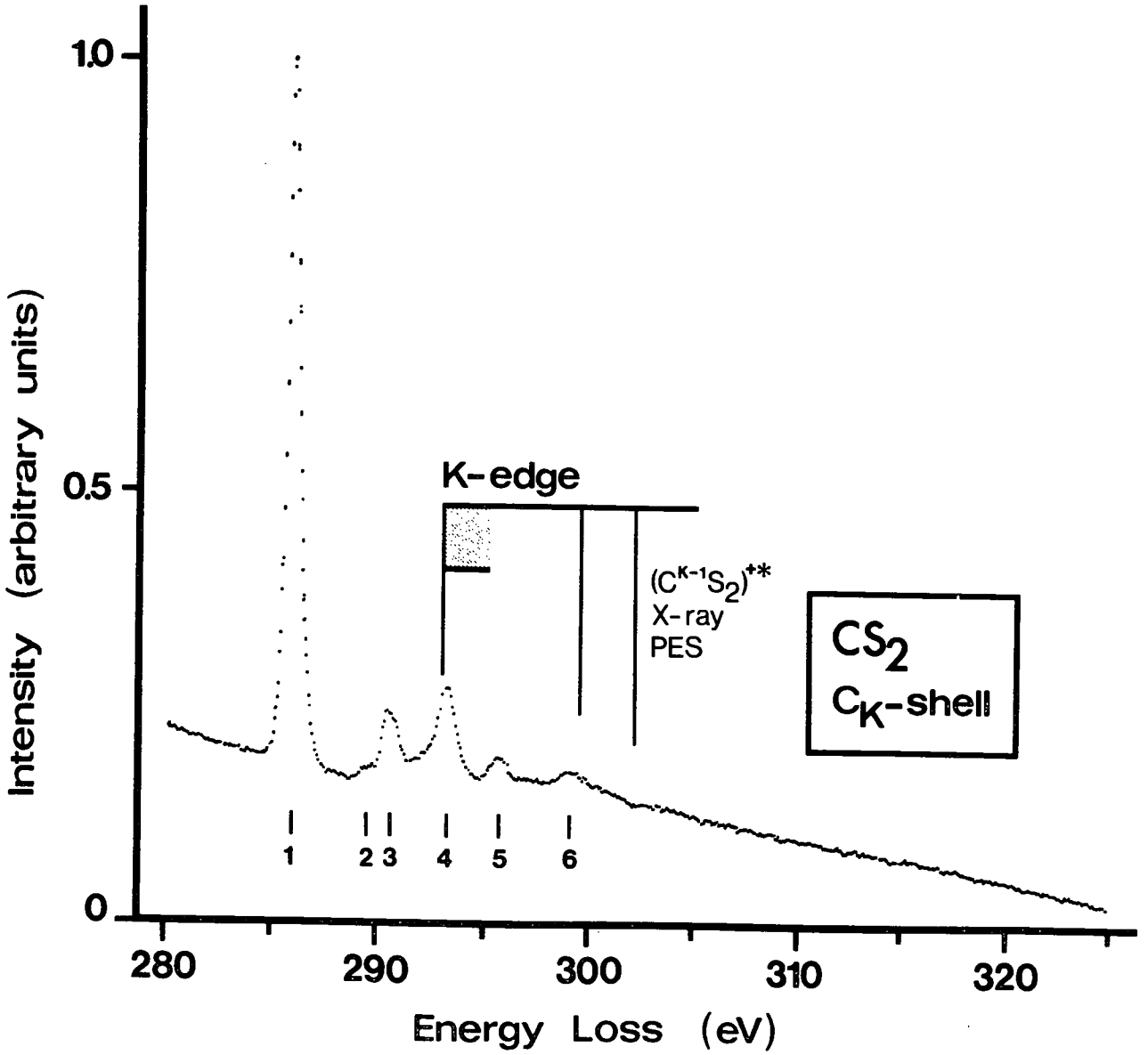

FIGURE 29. Carbon K-shell energy loss spectrum of carbon disulfide.

TABLE 9

ABSOLUTE ENERGIES (eV), RELATIVE ENERGIES AND POSSIBLE ASSIGNMENTS OF PEAKS OBSERVED IN THE CARBON K-SHELL ENERGY LOSS SPECTRUM OF CARBON DISULFIDE AND THE CARBON AND OXYGEN K-SHELL ENERGY LOSS SPECTRA OF CARBONYL SULFIDE.

CARBON DISULFIDE CARBON K-SHELL			POSSIBLE[a] ORBITAL ASSIGNMENT	CARBONYL SULFIDE				
				CARBON K-SHELL			OXYGEN K-SHELL	
PEAK	ENERGY	ΔE		PEAK	ENERGY	ΔE	ENERGY	ΔE
1	286.1	0	π^*	1	288.2	0	533.7	0
2	289.6	3.5	ns?	2	291.0	2.8		
3	290.6	4.5	np?	3	291.5	3.3		
				4	∿ 293.7	5.5		
				5	294.4	6.2		
K-EDGE[b]	293.1	7.0	∞	K-EDGE[b]	295.2	7.0	540.3	6.6
4	293.4	7.3		6	297.5	9.3		
5	295.8	9.7		7	298.3	10.1		
6	∿ 299.4	∿ 13.3						

a Only the outer orbitals involved in the K-excitations have been included.

b These values are from X-ray PES[125].

The position of the carbon K-edge indicated on our spectrum is based on the experimental X-ray PES value[125] of 293.1 ± 0.1 eV. Peak four with a maximum at 293.4 ± 0.2 eV has two possible explanations: i. the peak may be associated with the shake-up and/or shake-off of valence electrons in conjunction with the excitation of a carbon K-shell electron to the $3\pi_u$ molecular orbital and, ii. the carbon disulfide molecule may have an effective potential barrier in the regions of the sulfur atoms (see References 131-134). Discrete levels can occur up to the top of the barrier which may be well above the ionization limit. The first interpretation is supported by the shake-up lines observed in conjunction with carbon K-shell ionization in carbon disulfide as determined[125] by X-ray PES. The two lowest shake-up states, $(C^{K-1}S_2)^{+*}$ states, occur at 6.5 and 9.1 eV above the K-shell ion state[125] (see Figure 29) with relative intensities (with respect to the main K-shell ion peak) of 7 and 16.4% respectively. The shake-up states associated with the discrete excitation of a carbon K-shell electron are expected to have similar relative energies (with respect to the main discrete peak) and intensities roughly 5 to 20% of that of the main peak. Therefore, peaks four and five, which are observed at 7.3 eV and 9.7 eV respectively above the intense $3\pi_u$ peak are consistent with a shake-up interpretation. Similarly the broad structure (peak 6) located at approximately 299.4 eV could be associated with the shake-up of valence electrons in conjunction with K-shell excitation to the $3\pi_u$ orbital and/or K-shell ionization. Similar shake-up structures were observed in the K-shell spectra (carbon, nitrogen and oxygen) of the diatomic molecules, nitrogen, Section (5.1.1), and carbon monoxide, Section (5.1.2), and the triatomic molecules, carbon dioxide, Section (6.1.1), and nitrous

oxide, Section (6.1.2). However, in these cases the shake-up bands are rather broad in contrast to the relatively sharp nature of peak four. The second interpretation, that there is an effective potential barrier, is based on the observation that the carbon K-shell spectrum of carbon disulfide has properties similar to those observed in the inner shell absorption spectra of SF_6[16-19], BF_3[20-22] and other molecules[15,21,23-25] consisting of a central atom "surrounded" by electronegative atoms. For these molecules the inner shell absorption spectra of the central atom (and in some cases the surrounding atoms) are generally characterized by strong discrete peaks both above and below the ionization limit, as well as weak Rydberg series and small K-jumps. These effects have been attributed to the existence[131-134] of an effective potential barrier on the outer rim of these molecules. This barrier separates an inner potential well from an outer, shallow well of large radius[132]. Calculations[133] for the excited states of BF_3 support a potential barrier in this molecule. This phenomenon is not limited to molecules which consist of a central atom completely surrounded by electronegative atoms. In fact the sulfur $L_{II,III}$ absorption spectrum[115] of SO_2 has some of the characteristics which are usually associated with a potential barrier[131]. Dehmer[131] has pointed out that the sulfur $L_{II,III}$ photoabsorption spectrum[15,21] of carbon disulfide is not consistent with the existence of a potential barrier. However, this result does not negate the possibility of a potential barrier to the promotion of a carbon K-shell electron (i.e., from the central atom) of carbon disulfide. The fact that peaks four and five in the carbon K-shell spectrum are located above the K-edge and are relatively narrow structures indicates the possible existence of a potential barrier.

The presence of a barrier is not expected to significantly reduce the overlap between Rydberg orbitals (outer-well) and the inner-well carbon K-shell orbital since the barrier would not completely surround the molecule. Therefore, Rydberg excitations are also expected to be observed (see Reference 131). With the exception of the NF_3, BF_3 and BCl_3 molecules, characteristics attributed to a potential barrier have only been observed (see Reference 131) in molecules containing sulfur or silicon In these molecules, the participation of d-orbitals in the bonding may be an important factor. The carbon K-shell energy loss spectrum of carbon dioxide, Section (6.1.1), does not support such an interpretation for this molecule. These results suggest that the electronegativity of the peripheral atoms is not the only consideration, since oxygen is more electronegative than sulfur.

c. Sulfur $L_{II,III}$ (2p) Shell Excitation.

The sulfur $L_{II,III}$-shell energy loss spectrum of carbon disulfide is shown in Figure 30 and the energies and possible assignments of peaks are listed in Table 10. The optical absorption spectrum of carbon disulfide in this energy region has previously been obtained[15] using a Bremstrahlung continuum. The instrumental resolution was $\sim$ 0.4 eV (i.e. the same as in our spectrum) and the absolute calibration is reported to be $\pm$ 0.1 eV. The optical results are listed in Table 10. Below the $L_{II,III}$-edge, the optical spectrum[15] and our energy loss spectrum show identical structure, although the absolute calibrations differ by 0.4 eV (this is 0.1 eV larger than the sum of the experimental uncertainties). The spectra do not show characteristics which are usually associated with a potential barrier. It has been suggested[131] that the discrete structure observed in the optical spectrum

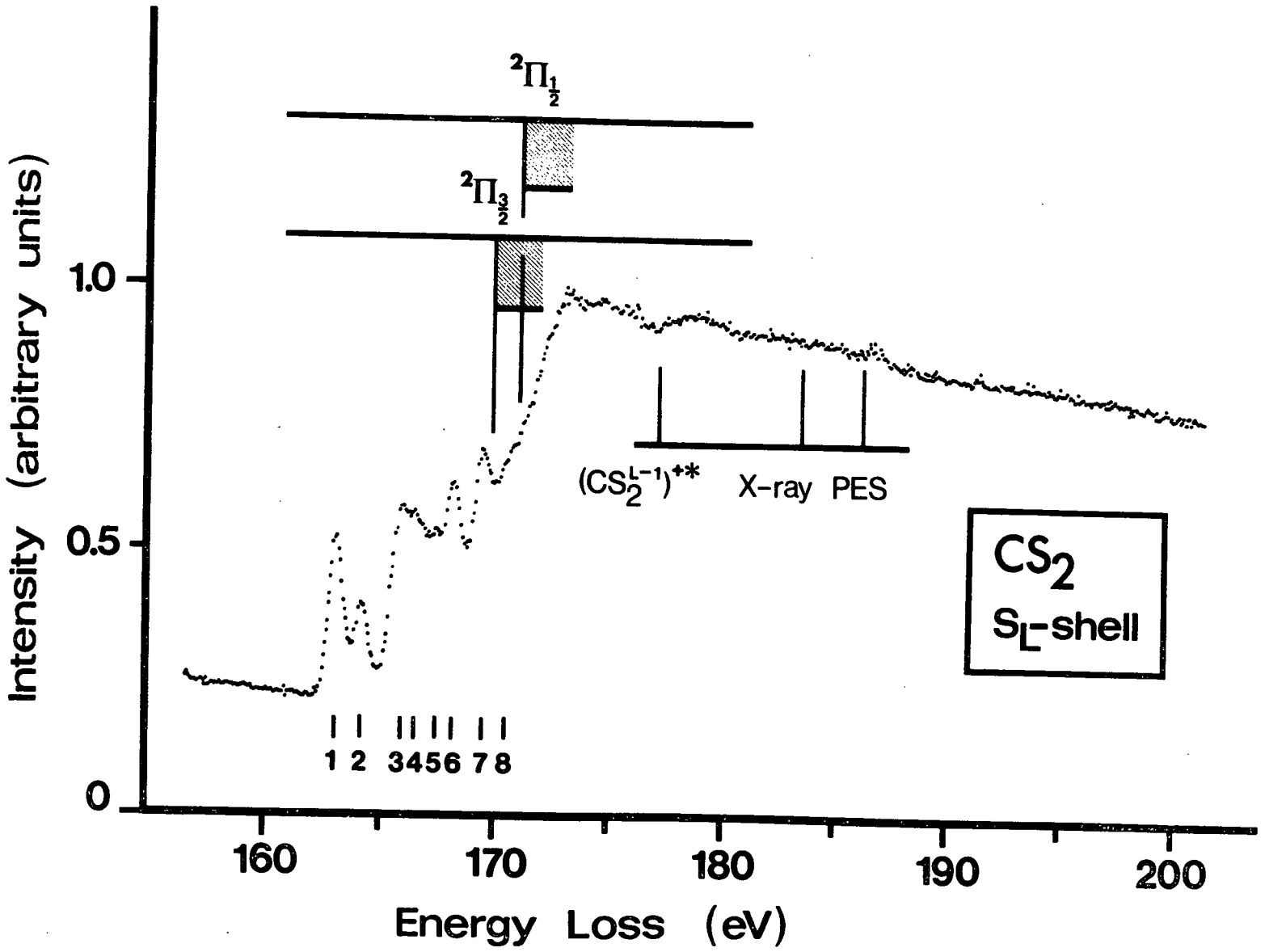

FIGURE 30. Sulfur $L_{II,III}(2p)$ energy loss spectrum of carbon disulfide.

TABLE 10

ABSOLUTE ENERGIES (eV), RELATIVE ENERGIES AND POSSIBLE ASSIGNMENTS OF PEAKS OBSERVED IN THE SULFUR 2p ($L_{II,III}$-SHELL) ENERGY LOSS SPECTRA OF CARBON DISULFIDE AND CARBONYL.

	CARBON DISULFIDE					CARBONYL SULFIDE		
	THIS WORK		OPTICAL[a]		POSSIBLE[b] ORBITAL	THIS WORK		
PEAK	ENERGY	ΔE	ENERGY	ΔE	ASSIGNMENT	PEAK	ENERGY	ΔE
1	163.1	0	163.5	0	π^*	1	164.2	0
2	164.2	1.1	164.6	1.1	π^*	2	165.6	1.4
3	165.9	2.8	166.4	2.9	π^*	3	166.9	2.7
4	166.5	3.4	167.0	3.5		4	168.1	3.9
5	167.4	4.3	167.7	4.2		5	168.6	4.4
6	168.2	5.1	168.6	5.1		6	170.0	5.8
7	169.5	6.4	169.9	6.4				
L-EDGE[c] ($^2\Pi_{3/2}$)	169.8	6.7			∞	L-EDGE[c] ($^2\Pi_{3/2}$)	170.6	6.4
8	170.8	7.4	171.1	7.6			≈171.0	6.8
L-EDGE[c] ($^2\Pi_{1/2}$)	171.0	7.9			∞	L-EDGE[c] ($^2\Pi_{1/2}$)	171.8	7.6
	≈177.1	≈14.0			SHAKE-UP		≈191	≈26.8

a. Reference 15.
b. Only the outer orbital involved in the transition is given.
c. Reference 125.

probably derives from superimposed Rydberg lines, but an individual assignment of the peaks has not been attempted. Spin-orbit coupling in the sulfur 2p shell of carbon disulfide is large, as shown by the 1.2 eV splitting observed[125] by X-ray PES between the $^2\Pi_{3/2}$ and $^2\Pi_{1/2}$ sulfur 2p ion states of carbon disulfide. Therefore Russell-Saunders coupling does not apply and (ω,ω) coupling gives a more appropriate description (see Reference 75). The lowest energy discrete peaks observed in the sulfur 2p spectrum are expected to be associated with the promotion of a sulfur 2p electron to the $3\pi_u$ valence molecular orbital (cf. the carbon K-shell spectrum of carbon disulfide). Six groups of molecular states are expected[75] as a result of this excitation, since the lone sulfur 2p electron may be a $\sigma^+_{1/2}$, $\pi_{3/2}$ or $\pi_{1/2}$. Peaks one and two are probably associated with $3\pi_u$ excitation. Peak one is approximately the same energy below the $^2\Pi_{3/2}$ edge, as the first discrete peak in the carbon K-shell spectrum of carbon disulfide is below the carbon K-edge. Peaks three to seven are probably associated with Rydberg excitations, although some of the intensity (particularly in the low energy region of this group of peaks) may be associated with $3\pi_u$ excitation.

The positions of the $^2\Pi_{3/2}$ and $^2\Pi_{1/2}$ L-edges indicated in our spectrum are based on the X-ray PES values[125] of 169.8 ± 0.1 and 171.0 ± 0.1 eV respectively. The band of structure with an onset at ∿ 177 eV is probably associated with the shake-up of valence electrons in conjunction with sulfur 2p ionization. The onset is 7.3 eV above the $^2\Pi_{3/2}$ edge in exact agreement with the energy of the lowest shake-up state observed by X-ray PES for the sulfur 2p shell of carbon disulfide. The positions of the shake-up states, $(CS_2^{L-1})^{+*}$, observed[125] by X-ray PES are indicated in

Figure 30.

6.2.2. Carbonyl Sulfide.

The carbonyl sulfide molecule is linear in its ground electronic state and has the electron configuration:

$$S_{1s}^2\ O_{1s}^2\ C_{1s}^2\ S_{2s}^2\ S_{2p}^6\ (6\sigma)^2\ (7\sigma)^2\ (8\sigma)^2\ (9\sigma)^2\ (2\pi)^4\ (3\pi)^4,\ {}^1\Sigma^+.$$

We have studied the oxygen 1s (K), carbon 1s (K) and sulfur 2p ($L_{II,III}$) shell energy loss spectra. Cross-sections for discrete transitions in the region of the sulfur 2s (L_I) edge appear to be small and a spectrum was not recorded. The valence shell of carbonyl sulfide is isoelectronic with those of carbon dioxide, nitrous oxide and carbon disulfide. A valence shell spectrum was recorded.

a. Valence Shell Spectrum.

The valence shell spectrum of carbonyl sulfide is shown in Figure 31. The locations of peaks are consistent with higher resolution electron impact[118] and optical spectra[119]. The weak broad band, A, with a maximum at approximately 5.7 eV is probably associated with the transition $2\pi \rightarrow 3\pi\ (\pi^*)\ [{}^1\Sigma^+ \rightarrow {}^1\Delta({}^1A')]$, see Reference 119. The higher energy peaks observed in our spectrum are; B (7.4 eV), C (8.1 eV), D (9.5 eV), E (12.1 eV), F (13.2 eV) and G (13.8 eV). In the higher resolution electron impact spectrum[118] the corresponding peaks have been assigned to Rydberg transitions. However, in the optical spectrum[119], peaks corresponding to B and C in our spectrum have been assigned to non-Rydberg, ${}^1\Sigma^+ \rightarrow {}^1\Pi$ and ${}^1\Sigma^+ \rightarrow {}^1\Sigma^+$ transitions respectively. The location of the first ionization potential shown in Figure 31 is based on the optical[120] and experimental

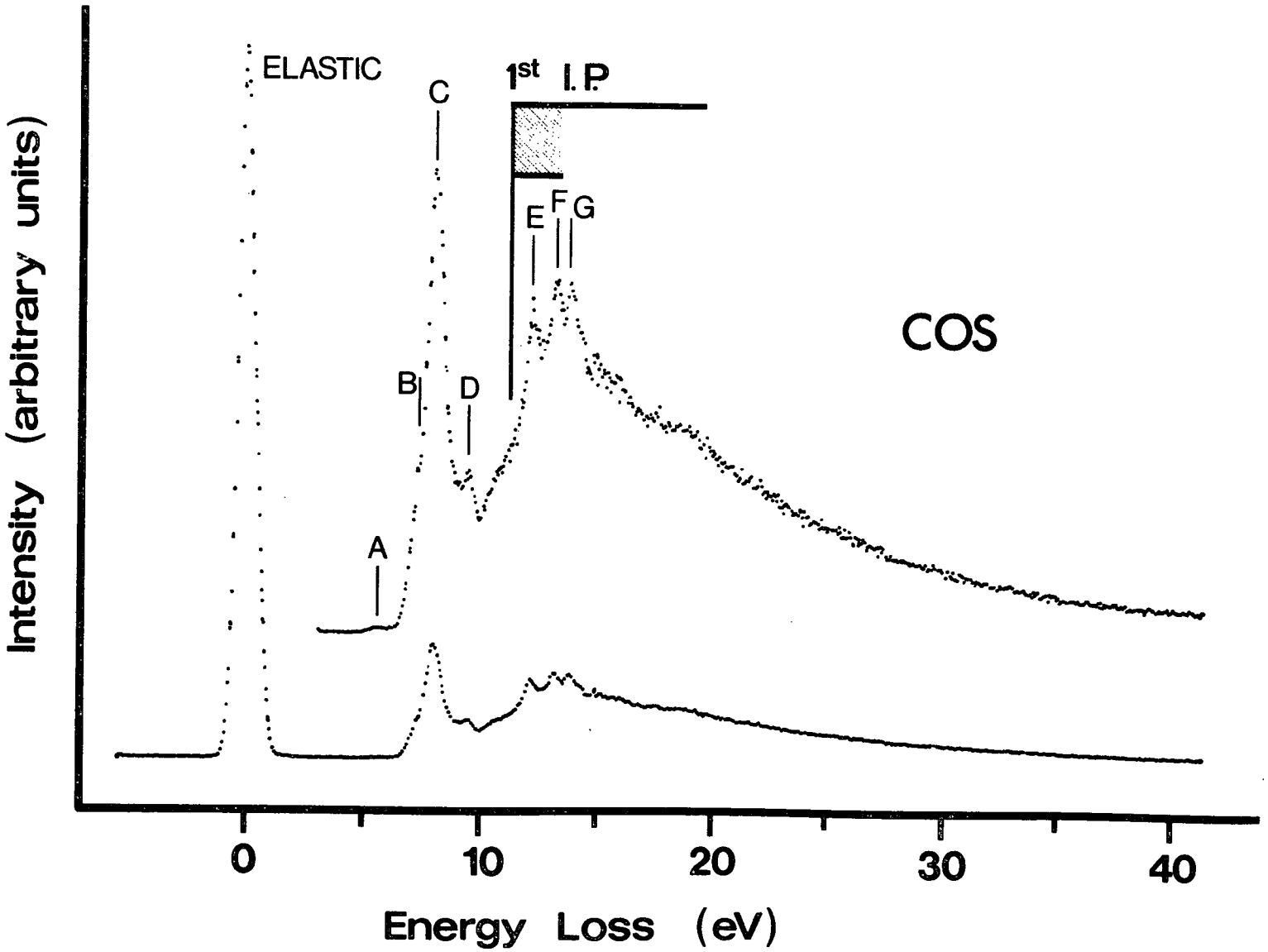

FIGURE 31. Valence shell energy loss spectrum of carbonyl sulfide.

UV-PES value[78] of 11.2 eV.

b. Oxygen K-shell Excitation.

The oxygen K-shell energy loss spectrum of carbonyl sulfide is shown in Figure 32 and the energies and possible assignments of structures are listed in Table 9. The calibration accuracy of the spectrum is ± 0.3 eV. The poor signal to noise and signal to background ratios are partially due to the fact that for fast electron impact and forward scattering, the inelastic scattering intensity decreases[11] by a factor, $\propto$ (energy loss)$^{-3}$. The broad peak with a maximum at 533.7 ± 0.3 eV is interpreted as arising from the promotion of an oxygen K-shell electron to the lowest unfilled molecular orbital, the 4π (π^*). The peak has a FWHM of 1.2 eV (elastic FWHM 0.5 eV) indicating the excitation of a number of vibrational levels.

The position of the oxygen K-edge indicated on our spectrum is based on the X-ray PES value[125] of 540.3 ± 0.1 eV.

c. Carbon K-shell Excitation.

The carbon K-shell energy loss spectrum of carbonyl sulfide is shown in Figure 33 and the energies and possible assignments of peaks are listed in Table 9. The general appearance of the spectrum is similar to the carbon K-shell spectrum of carbon disulfide, although the relative energies of structures are different. The intense discrete peak observed at 288.2 eV is interpreted as arising from the promotion of a carbon K-shell electron to the lowest unfilled molecular orbital of carbonyl sulfide, the 4π (π^*). This interpretation is analogous to that of the first discrete peak observed in the carbon K-shell spectrum of carbon disulfide, Section (6.2.1), and carbon dioxide, Section (6.1.1). In each case the

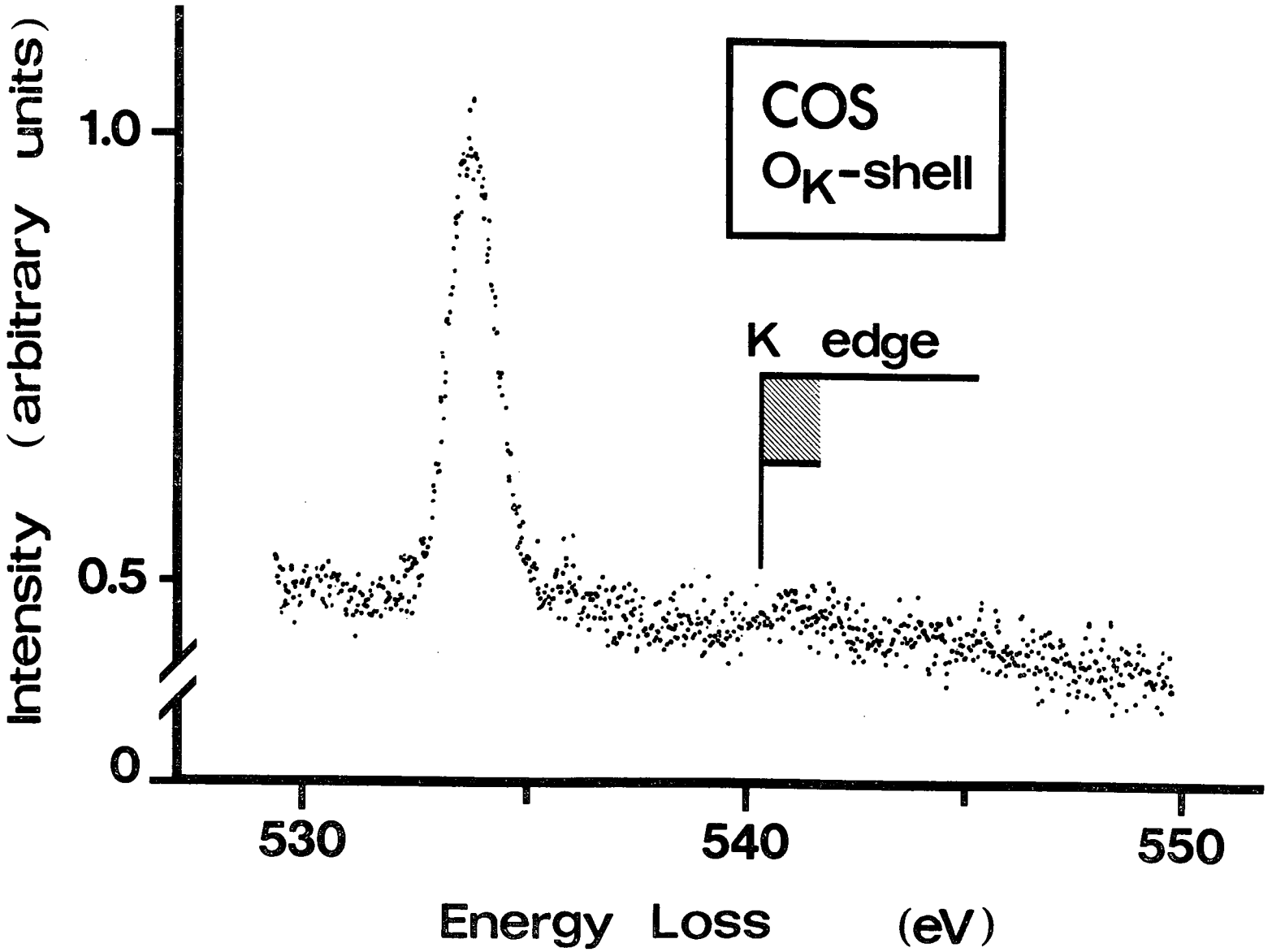

FIGURE 32. Oxygen K-shell energy loss spectrum of carbonyl sulfide.

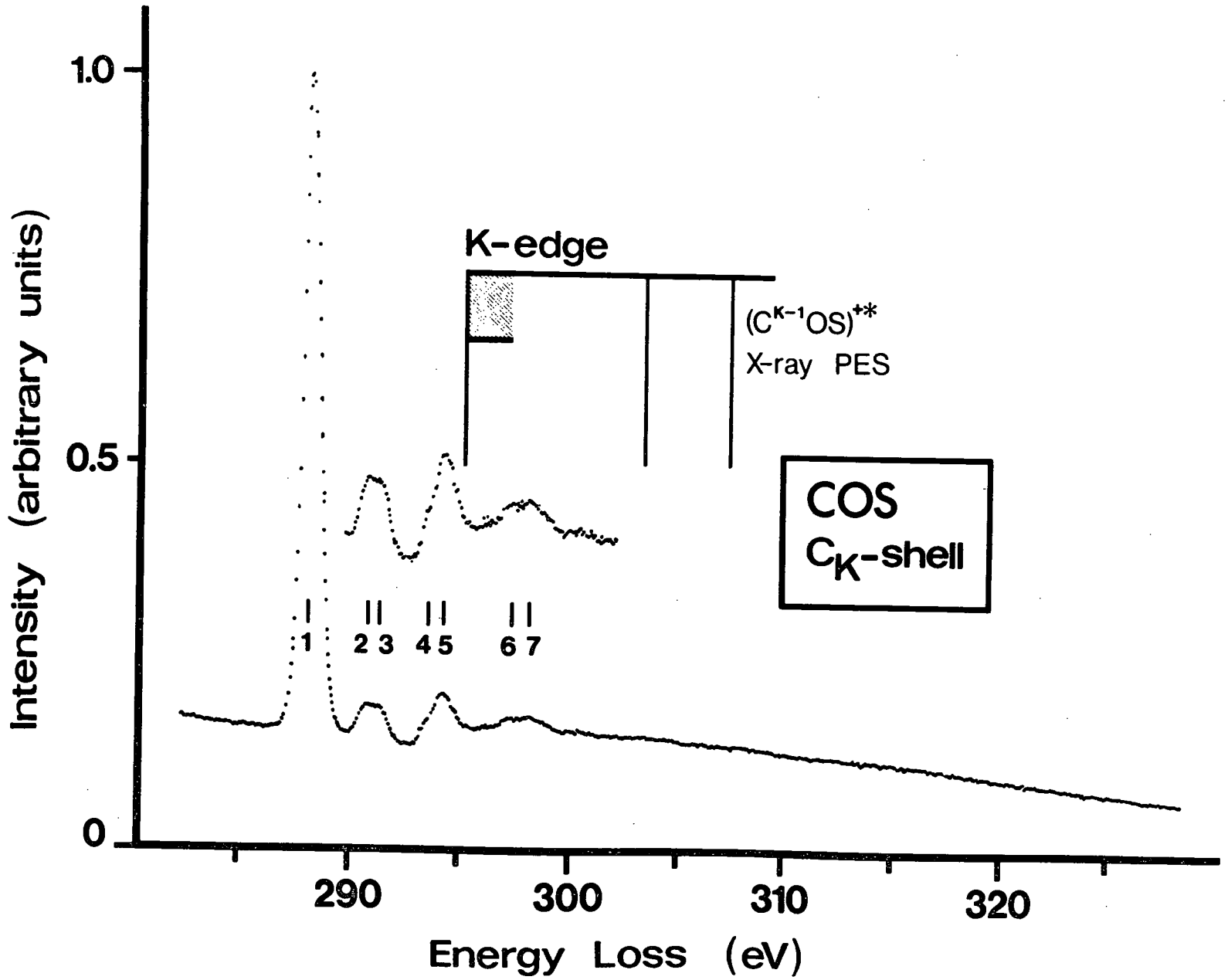

FIGURE 33. Carbon K-shell energy loss spectrum of carbonyl sulfide.

peak is approximately the same energy below the respective K-edge. The peak in the carbonyl sulfide spectrum has a FWHM of 0.85 eV (elastic FWHM 0.56 eV) indicating the excitation of a number of vibrational levels. Higher energy discrete structures below the K-edge are probably associated with the promotion of a carbon K-shell electron to Rydberg orbitals. The derived quantum defects of peaks two and three (assuming n = 3) are 1.2 and 1.08 respectively. Therefore peaks two and three could represent promotion to the 3s and 3p Rydberg orbitals respectively. The quantum defect of 1.08 is somewhat large for a 3p Rydberg excitation and suggests that this Rydberg orbital has more penetration into the sulfur core than does the 3s. In addition to Rydberg excitations, peak five may have a contribution from the shake-up of valence electrons in conjunction with the promotion of a carbon K-shell electron to the 4π molecular orbital. It is also possible that the carbonyl sulfide molecule has an effective potential barrier (cf. the possible interpretation of the carbon K-shell spectrum of carbon disulfide). If this is the case, the excited states are expected to be a mixture of Rydberg (outer-well states) and inner-well states.

The position of the K-edge indicated in our spectrum is based on the X-ray PES value[125] of 295.2 ± 0.1 eV. The broad structure observed above the K-edge (peaks six and seven) may be associated with shake-up states where the promotion of a carbon K-shell electron to the 4π molecular orbital is involved. The relative energies of these structures with respect to the first discrete peak is $\sim$ 9 eV which is consistent with the lowest shake-up state observed[125] in conjunction with carbon K-shell ionization (i.e. 8.3 eV above the K-edge). The X-ray PES[125] shake-up

lines corresponding to $C^{K-1}OS)^{+*}$ states have been included in Figure 33. Alternatively, peaks six and seven may represent discrete states raised above the K-edge by an effective potential barrier.

d. Sulfur $L_{II,III}$ (2p)-shell Excitation.

The sulfur $L_{II,III}$-shell energy loss spectrum of carbonyl sulfide is shown in Figure 34 and the energies and possible assignments of peaks are listed in Table 10. Figure 35 shows the discrete structure below the edge on an expanded scale. The interpretation of the spectrum is similar to that of the sulfur $L_{II,III}$ spectrum of carbon disulfide. The first three peaks are relatively intense and are probably associated with the promotion of a sulfur 2p electron to the 4π (π^*) molecular orbital. In exact analogy to carbon disulfide, the promotion of a sulfur 2p electron to the 4π molecular orbital results in six groups of molecular state in (ω,ω) coupling[120]. Higher energy discrete peaks (four-six) are probably associated with Rydberg transitions. Should an effective potential barrier exist in the carbonyl sulfide molecule, it is unlikely (as in the case of carbon disulfide) that it would have a significant effect on the excitation of a sulfur 2p electron.

The positions of the $^2\Pi_{3/2}$ and $^2\Pi_{1/2}$ L-edges indicated in Figures 34 and 35 are based on the experimental[125] X-ray PES values of 170.6 ± 0.1 eV and 171.8 ± 0.1 eV respectively. The shake-up lines observed[125] in conjunction with sulfur 2p ionization corresponding to $(COS^{L-1})^{+*}$ states, have been included in Figure 34. The broad band of structure with an onset at approximately 191 eV is probably associated with the excitation of shake-up/shake-off states. The X-ray PES spectrum[125], showing shake-up structures, is not reported above 190 eV.

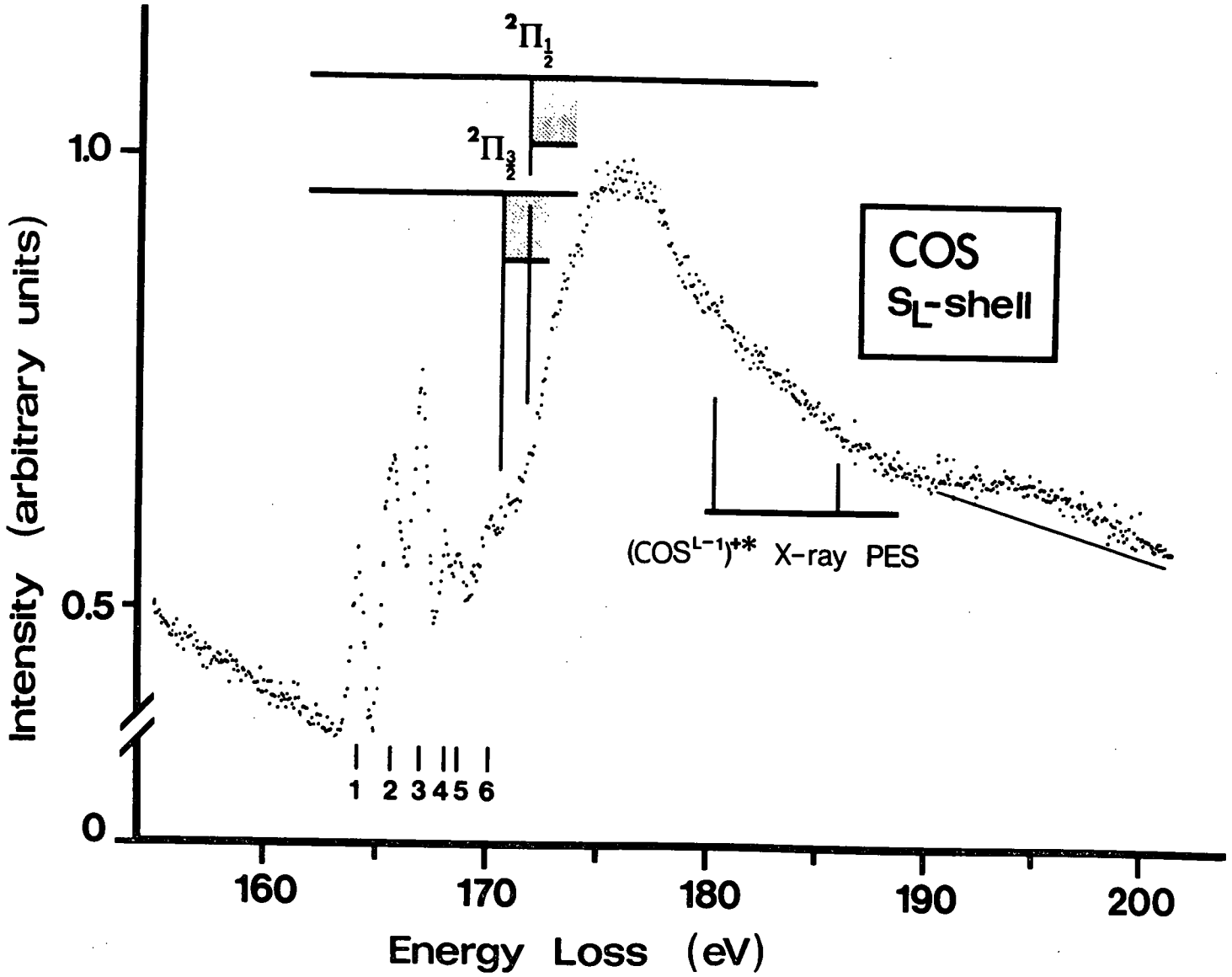

FIGURE 34. Sulfur $L_{II,III}(2p)$ energy loss spectrum of carbonyl sulfide.

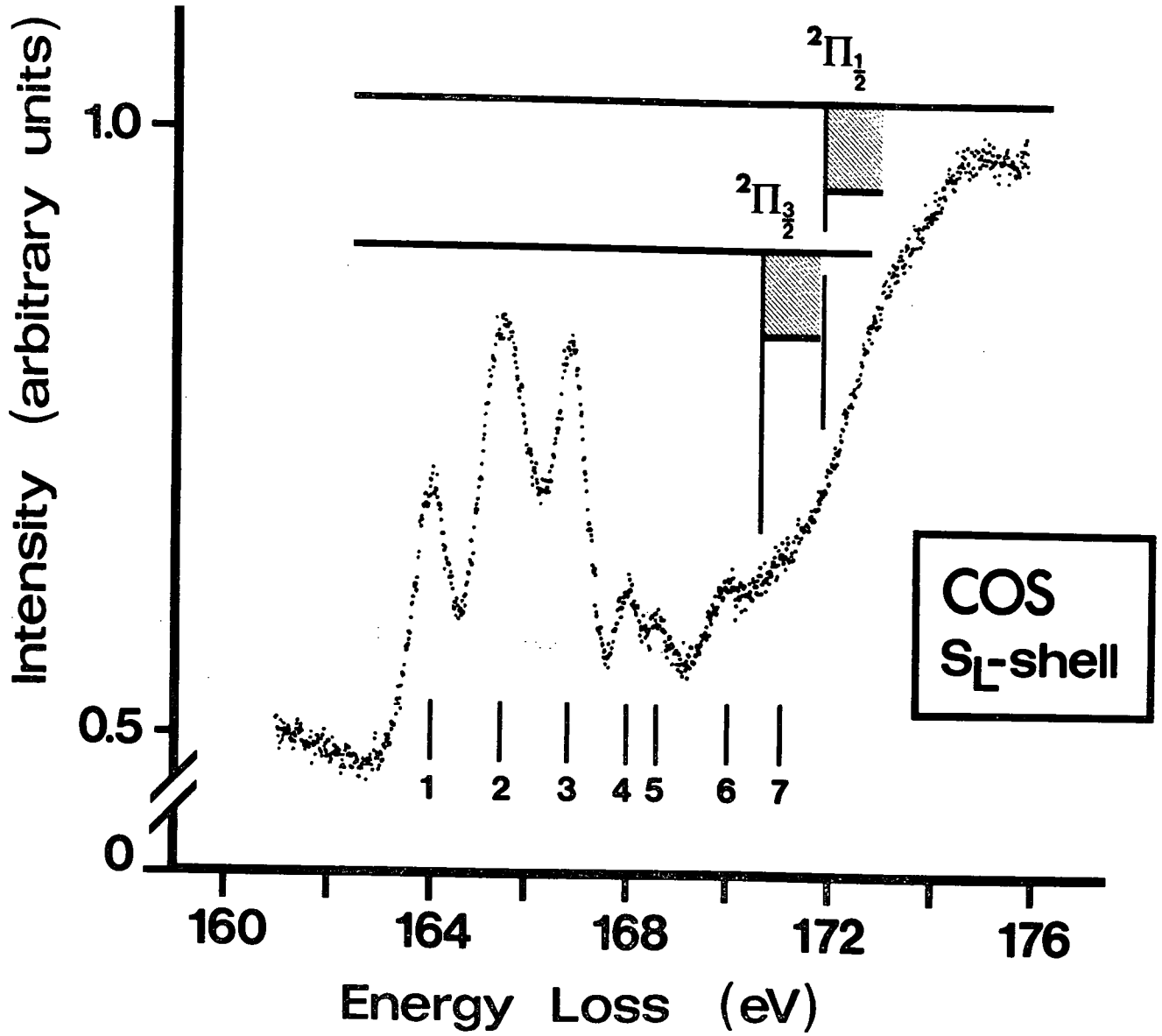

FIGURE 35. Sulfur $L_{II,III}(2p)$ energy loss spectrum of carbonyl sulfide with an expanded energy scale in the region of the $L_{II,III}$ edges.

CHAPTER SEVEN

POLYATOMIC MOLECULES.

7.1. Introduction.

The prominent features observed in the absorption spectra (valence shell regions) of saturated polyatomic molecules are usually associated with Rydberg transitions (for examples see Reference 120). On this basis, Rydberg transitions are also expected to dominate the K-shell spectra of these molecules. In comparing the Rydberg states observed as a result of K-shell promotion with those observed in the promotion of a valence shell electron, it is convenient to use the term values (difference between the excitation energy and the corresponding ionization potential) since they have been extensively used in interpreting the valence shell spectra. For the same principal quantum number, n, a discussion of the quantum defect, δ, or the term value is equivalent since the term value is equal to $R/(n - \delta)^2$ where R is the Rydberg constant. For valence shell excitation to 3p and 3d Rydberg levels, it has been found that the term values are approximately constant in a wide range of compounds, while the 3s term values vary considerably[135]. The observed 3s deviations correlate with the nature of the substituent groups of the molecule and occur because the penetration of the 3s orbital either increases (the binding energy increases and therefore the term value increases) or decreases (lower term value) for the addition of an electronegative or electropositive substituent respectively. The 3p and 3d Rydberg orbitals are much less sensitive to the nature

of the substituents since they have much less penetration than the 3s. In principle, for K-shell excitation to Rydberg orbitals, we expect to observe larger term values than those observed for valence shell excitation in the same molecule. This result is expected since, as a result of a K-shell excitation, one of the cores (nucleus + K-shell) of the molecule has effectively one more positive charge. A penetrating orbital such as a 3s Rydberg is therefore expected to be more tightly bound (higher term value) for a molecule with a K-shell vacancy than it is when the molecule has a valence vacancy.

7.2. Methane, Ammonia, Water, Methanol, Dimethyl Ether and Monomethylamine.

7.2.1. Methane.

The ground electronic state of the methane molecule has tetrahedral symmetry and the electron configuration:

$$(1a_1)^2\ (2a_1)^2\ (1t_2)^6,\ {}^1A_1.$$

The $1a_1$ molecular orbital is formed from the carbon 1s atomic orbital and is essentially localized on the carbon nucleus. In recognition of this "atomic" character the electrons filling this orbital are designated carbon K-shell electrons.

a. Valence Shell Spectrum.

The valence shell electron energy loss spectrum of methane is shown in Figure 36. The locations of peaks are consistent with a higher resolution spectrum[136], where a Rydberg assignment has been proposed. The peak positions in our spectrum are: A (10.0 eV), B (11.6 eV) and C (13.4 eV). The location of the first ionization potential shown in Figure 36 is based

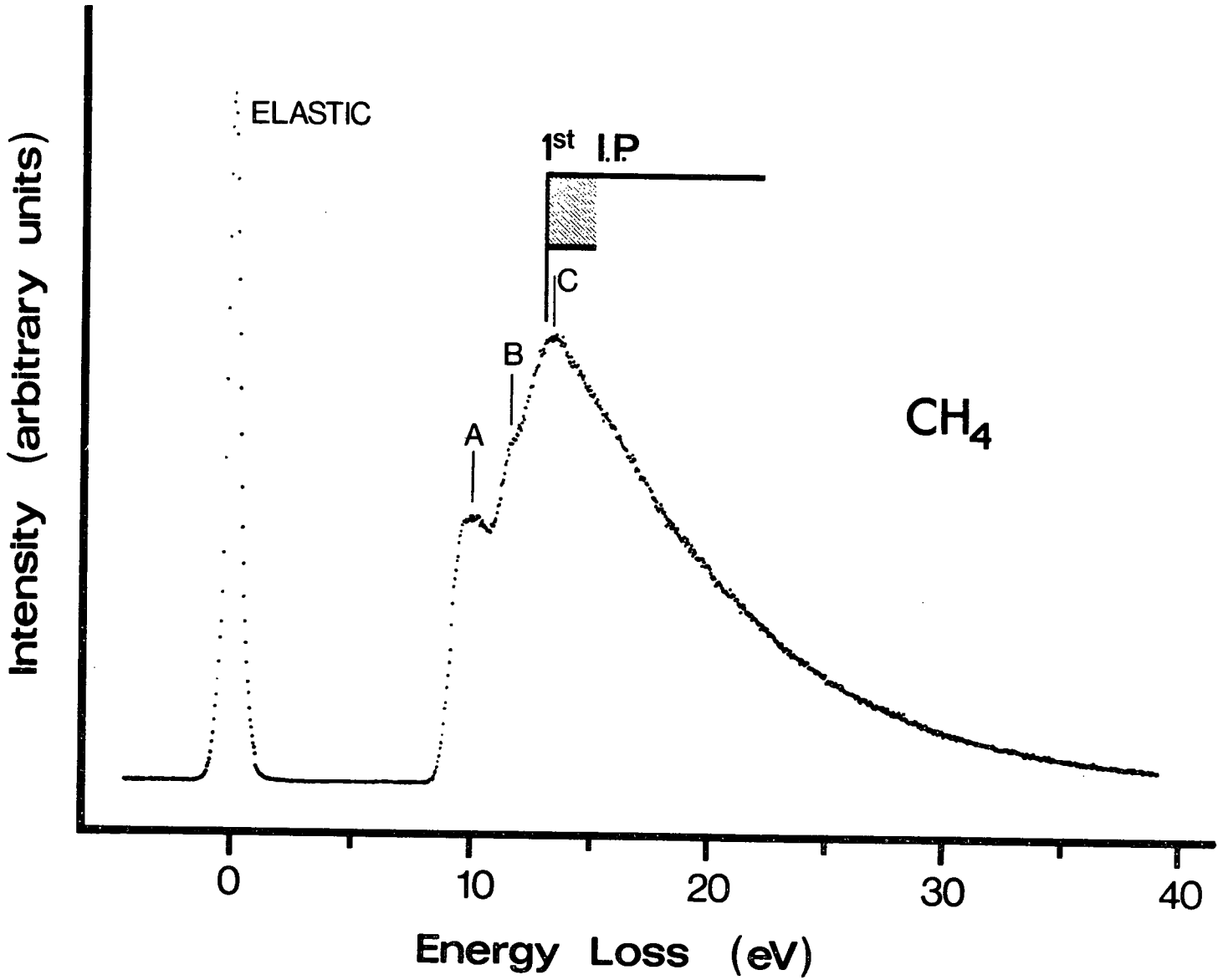

FIGURE 36. Valence shell energy loss spectrum of methane.

on the adiabatic value[120] of 13.0 eV.

b. Carbon K-shell Excitation.

Absorption in the region of the carbon K-edge in methane has been investigated using Bremsstrahlung continuua[137-140] and more recently with the continuous radiation produced by an electron synchrotron[28]. The spectra obtained with Bremsstrahlung radiation are characterized by weak absorptions superimposed by the second order spectrum of the lower wavelength region, making it difficult to identify carbon-K absorption bands. However, the much "cleaner" synchrotron spectrum[28] shows two discrete absorptions. Energy levels for some of the core excited states of methane have also been calculated[141.142].

The carbon K-shell energy loss spectrum of methane is shown in Figure 37 and the energies and tentative assignments of peaks are listed in Table II. Table II also includes excitation energies observed using electron synchrotron radiation[28] and calculated values using SCF wavefunctions[142]. Our spectrum shows more discrete structure than the optical spectrum[28] and extends further into the continuum region. The first discrete peak observed at 287.0 eV is interpreted as arising from the promotion of a carbon K-shell electron ($1a_1$) to the $3sa_1$ Rydberg level. This experimental value for the excitation energy and the X-ray PES[32] value of 290.7 eV for the K-shell ionization potential implies a quantum defect of 1.08 for the 3s Rydberg state. The magnitude of the quantum defect is consistent with those observed for excitations to an ns Rydberg level[130]. The transition $1a_1 \rightarrow 3sa_1$ is optically forbidden and is forbidden in our experiment if the first Born approximation is valid (the impact energy is 8 times the excitation energy and $\theta \sim 0°$). However, both the initial and final states

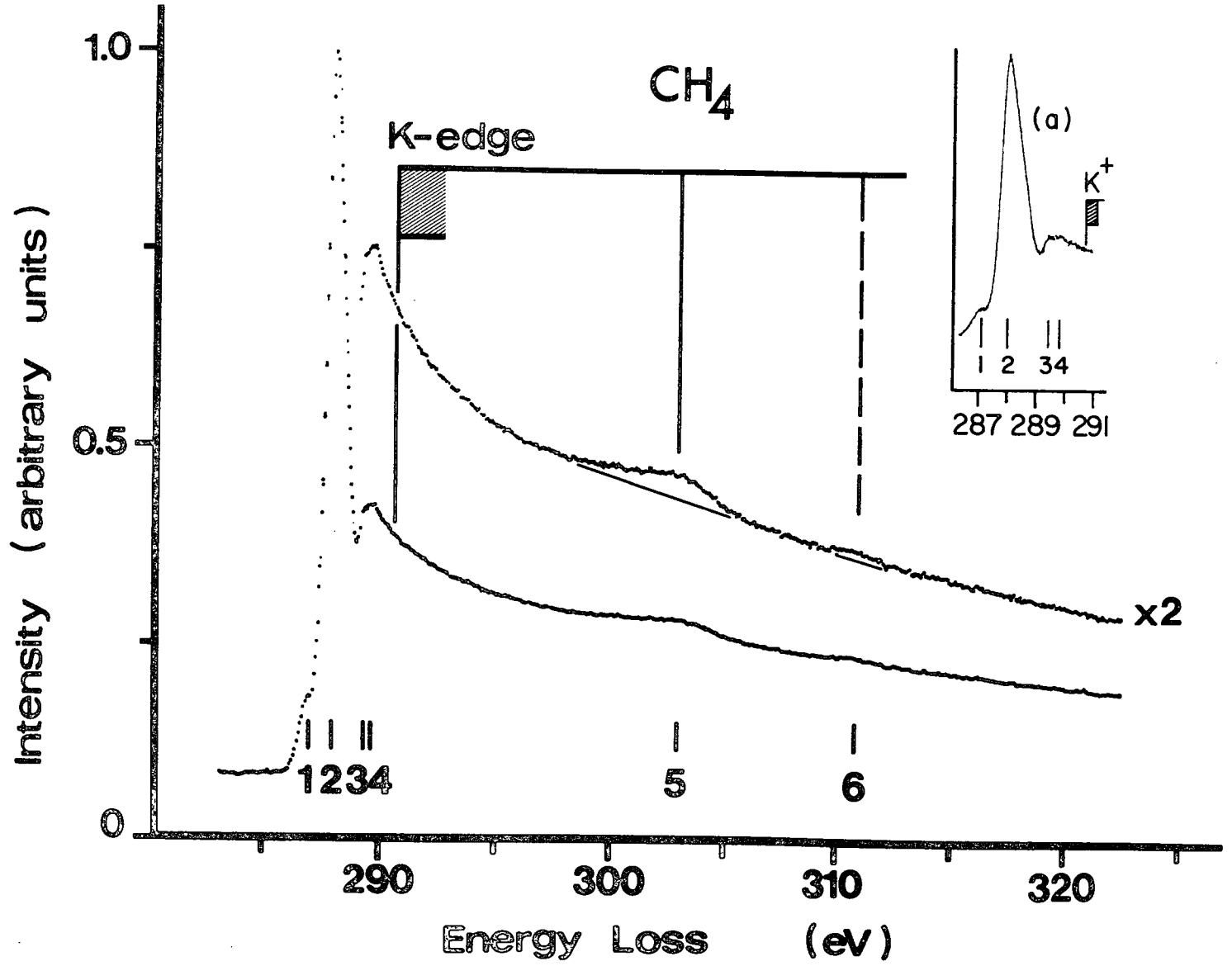

FIGURE 37. Carbon K-shell energy loss spectrum of methane.

TABLE 11

ABSOLUTE ENERGIES (eV), RELATIVE ENERGIES AND TENTATIVE ASSIGNMENTS OF PEAKS OBSERVED IN THE CARBON K-SHELL SPECTRUM OF METHANE.

PEAK	ENERGY	ΔE	TERM VALUE[a]	ASSIGNMENT[b]	CALCULATED ENERGY[c]	OPTICAL DATA[d]	SCF[e]
1	287.0	0	3.7	$3sa_1$	-	287.2	287.3
2	288.0	1.0	2.7	$3pt_2$	-	288.3	288.4
				$4sa_1$	289.1	-	-
				3d	289.2	-	-
3	289.4	2.4	1.3	$4pt_2$	289.4	-	-
4	289.8	2.8	0.9	$5pt_2$	289.9	-	-
K-EDGE[f]	290.7	3.7	0	∞			
5	∿303	∿16		SHAKE-UP AND SHAKE-OFF			
6	∿311	∿24					

a. Defined as the difference between the ionization potential and the excitation energy.
b. Only the final orbital is listed (initial orbital is $1a_1$ ≡ carbon K).
c. Calculated using the Rydberg formula $E_n = A-R/(n-\delta)^2$ where E_n is the excitation energy for the Rydberg level having quantum number n and quantum defect δ, A is the carbon K-shell ionization potential and R is the Rydberg constant. The quantum defects used for ns and np were derived from the energy positions of the first two peaks. δ(nd) was assumed to be 0.
d. From Reference 28.
e. From Reference 142.
f. X-ray PES value (Reference 32).

belong to the same symmetry species and therefore deviations from the Born theory are expected.[53] The first absorption in the electron synchrotron spectrum[28] was observed at 287.2 eV. Bagus et al.[142] have calculated a value of 287.3 eV for the Rydberg transition, $1a_1 \rightarrow 3sa_1$. From intensity considerations and the calculated results, they suggest that the first absorption peak in the synchrotron spectrum should be assigned to the $1a_1 \rightarrow 3sa_1$ Rydberg transition, the transition being observed because of vibronic coupling between the ground state and the $3sa_1$ Rydberg state due to the two, T_2, vibrational modes, ν_3 and ν_4. Finally, the term value for this transition is 3.7 eV in comparison with a term value of 3.95 eV observed[136] for the corresponding transition in the valence shell spectrum of methane, $1t_2 \rightarrow 3sa_1$. The second peak in our spectrum observed at 288.0 eV is assigned to the promotion of a $1a_1$ electron to the first p-Rydberg orbital, $1a_1 \rightarrow 3pt_2$, $^1T_2$. This transition is electric dipole allowed and the large intensity relative to that of the first peak is therefore expected. The excitation energy implies a quantum defect of 0.75 which is reasonable for a 3p Rydberg level (see Reference 130). The peak has a FWHM of 1.0 eV (in contrast to a FWHM of 0.5 eV for the peak associated with elastically scattered electrons) and is asymmetric on the high energy side (see the insert in Figure 37). In addition to vibrational excitation, some of the broadening and asymmetry could be associated with a Jahn-Teller splitting of the degenerate $^1T_2$ electronic state. The first two peaks observed in the electron impact spectrum of the valence shell energy region of methane[136,143] (corresponding to peak A in Figure 36) have an energy difference of 0.68 eV and have been interpreted as Jahn-Teller components of the $^1T_2$ state arising from the transition $1t_2 \rightarrow 3sa_1$. A

Jahn-Teller splitting of 0.8 eV has been observed for the first ion state of methane by PES[144]. The observed energies for peak 2 in our spectrum and the second peak in the synchrotron spectrum[28] are in good agreement. Bagus et al.[142] have calculated a value of 288.4 eV for the $1a_1 \rightarrow 3pt_2$ transition and have suggested that this is the correct interpretation of the photoabsorption peak observed by Chun[28] at 288.3 eV. A one-centre Hartree-Fock calculation[141] of the $1a_1 \rightarrow 3pt_2$ transition energy gave a value of 284.7 ± 0.3 eV, which is appreciably lower than our experimental result. Finally, a term value of 2.7 eV is obtained from our data for this transition. The magnitude of this term value is similar to those observed in the valence shell spectra of the fluoromethane molecules[136] for the promotion of an outermost electron to a 3p Rydberg orbital (e.g. CF_4: $1t_1 \rightarrow 3p$, term value 2.61 eV). We have calculated the expected excitation energies for higher nsa_1 and npt_2 Rydberg levels using the quantum defects derived from our experimental values for the n = 3 levels and a value of 290.7 eV for the carbon K-edge of methane[32]. The results are listed in Table 11 and have been used as an aid in interpreting the higher energy discrete structure in the spectrum. This structure consists of a peak (number 4) with a maximum at 289.8 eV and a lower energy shoulder (peak number 3) at 289.4 eV. The observed energies are in excellent agreement with the calculated values for the $4pt_2$ and $5pt_2$ Rydberg levels, suggesting that these peaks could have contributions from transitions to these orbitals. The relative intensity of the 3p transition to that of the 3s transition indicates that transitions to higher quantum number ns states would be very weak. Finally, $1a_1$ to 3d transitions could contribute to structure in this region, as indicated by the calculated transition energy

(the quantum defect was assumed to be zero).

The position of the K-edge indicated in our spectrum is based on the value of 290.7 eV for the K-shell ionization potential determined by X-ray PES[32]. The very broad structures located at approximately 303 and 311 eV are associated with the simultaneous transitions of a K-shell and valence shell electrons (i.e. the shake-up and shake-off of valence electrons in conjunction with K-shell excitation or ionization. Similar structures have been observed in the case of the diatomic and triatomic molecules (see Section (5.1.1) for details).

7.2.2. Ammonia.

The ground electronic state of the ammonia molecule has pyramidal geometry, but is more appropriately described by D_{3h} symmetry because of inversion. However, the small inversion splitting of the $\nu_2'' = 0$ vibrational level into a symmetric and antisymmetric level results in selection rules which are effectively the same as those for C_{3v} symmetry[145]. The electron configuration of the ground electronic state of ammonia in C_{3v} symmetry is

$$(1a_1)^2\ (2a_1)^2\ (1e)^4\ (3a_1)^2,\ {}^1A_1.$$

The $1a_1$ molecular orbital is formed from the nitrogen 1s atomic orbital. Promotion of a $1a_1$ electron to nsa_1, npe and npa_1 Rydberg orbitals is electric dipole allowed. One interesting feature of the valence shell spectrum of ammonia is that all of the states (both Rydberg and ion), resulting from the promotion of a $3a_1$ electron, are either planar or very nearly planar[146]. This produces long progressions in ν_2 and is a result of

the loss of an electron from an orbital which strongly stabilizes pyramidal geometry. Such large changes in geometry are not expected for the promotion of a $1a_1$ electron (essentially atomic and nonbonding) to Rydberg orbitals and, therefore, these transitions are expected to result in less vibrational excitation.

a. Valence Shell Spectrum.

The valence shell electron energy loss spectrum of ammonia is shown in Figure 38. The locations of peaks are consistent with higher resolution photoabsorption[120,145] and electron impact results[49,50,56] where the peaks have been associated with Rydberg transitions. In our spectrum, corresponding peaks are observed at: A (6.3 eV), B ($\sim$ 8.0 eV), C (9.2 eV), D (11.3 eV) and E (15.2 eV). The location of the first ionization potential in Figure 38 is based on the experimental value[120,147] of 10.2 eV.

b. Nitrogen K-shell Excitation.

The nitrogen K-shell energy loss spectrum of ammonia is shown in Figure 39 and the energies and tentative assignments of peaks are listed in Table 12. The general appearance of the spectrum resembles that of the carbon K-shell spectrum of methane and the spectrum has been interpreted in terms of the excitation of a nitrogen "K-shell" electron ($1a_1$) to Rydberg orbitals. Transition energies estimated using quantum defects derived from the valence shell spectrum[120,145] of ammonia have been included in Table 12. The first discrete peak observed at 400.6 eV has been assigned to the transition, $1a_1 \rightarrow 3sa_1$. The peak has a FWHM of 0.8 eV (compared with an elastic peak FWHM of 0.5 eV) indicating that a number of vibrational levels are excited. The 5.0 eV term value implies a quantum

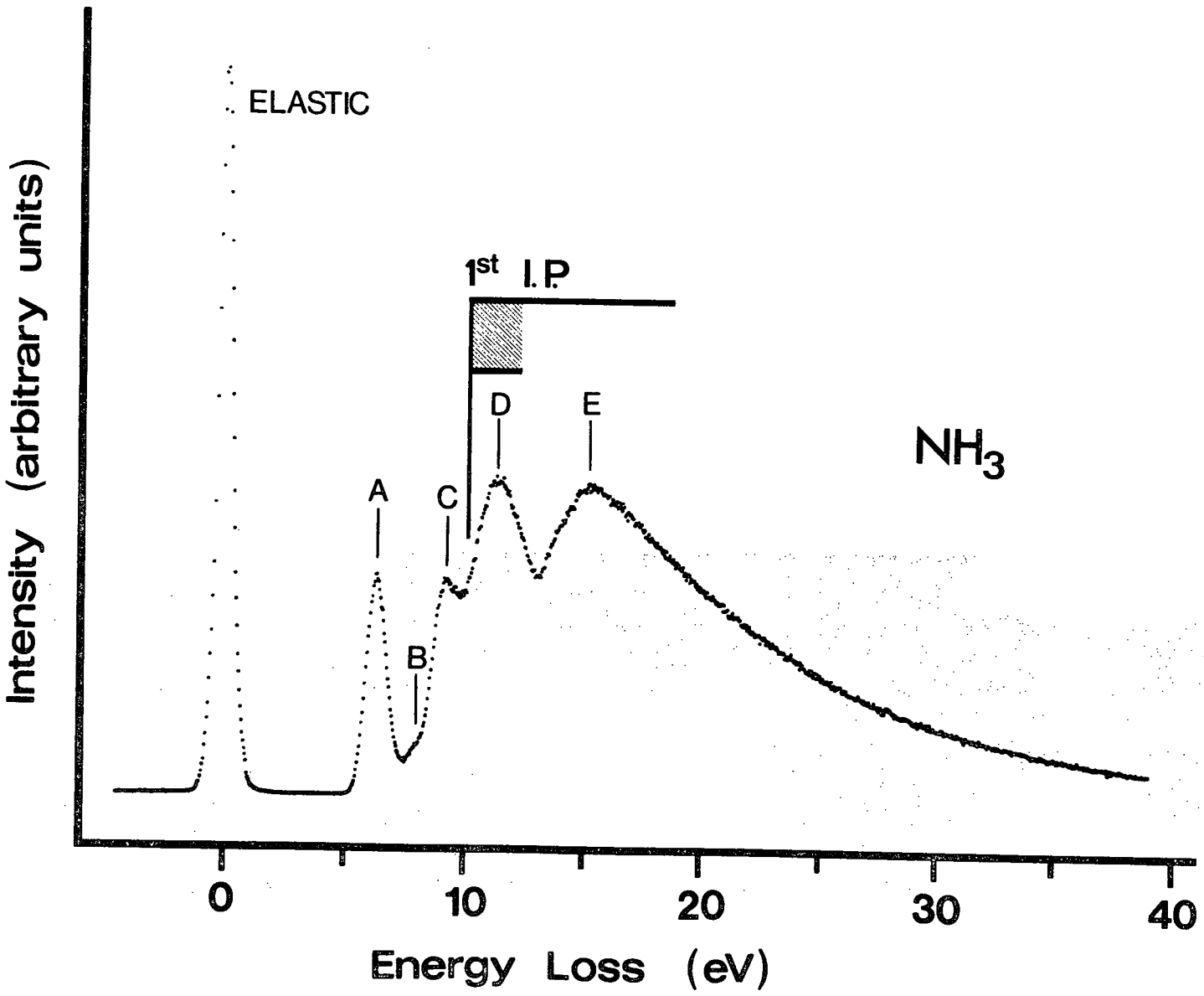

FIGURE 38. Valence shell energy loss spectrum of ammonia.

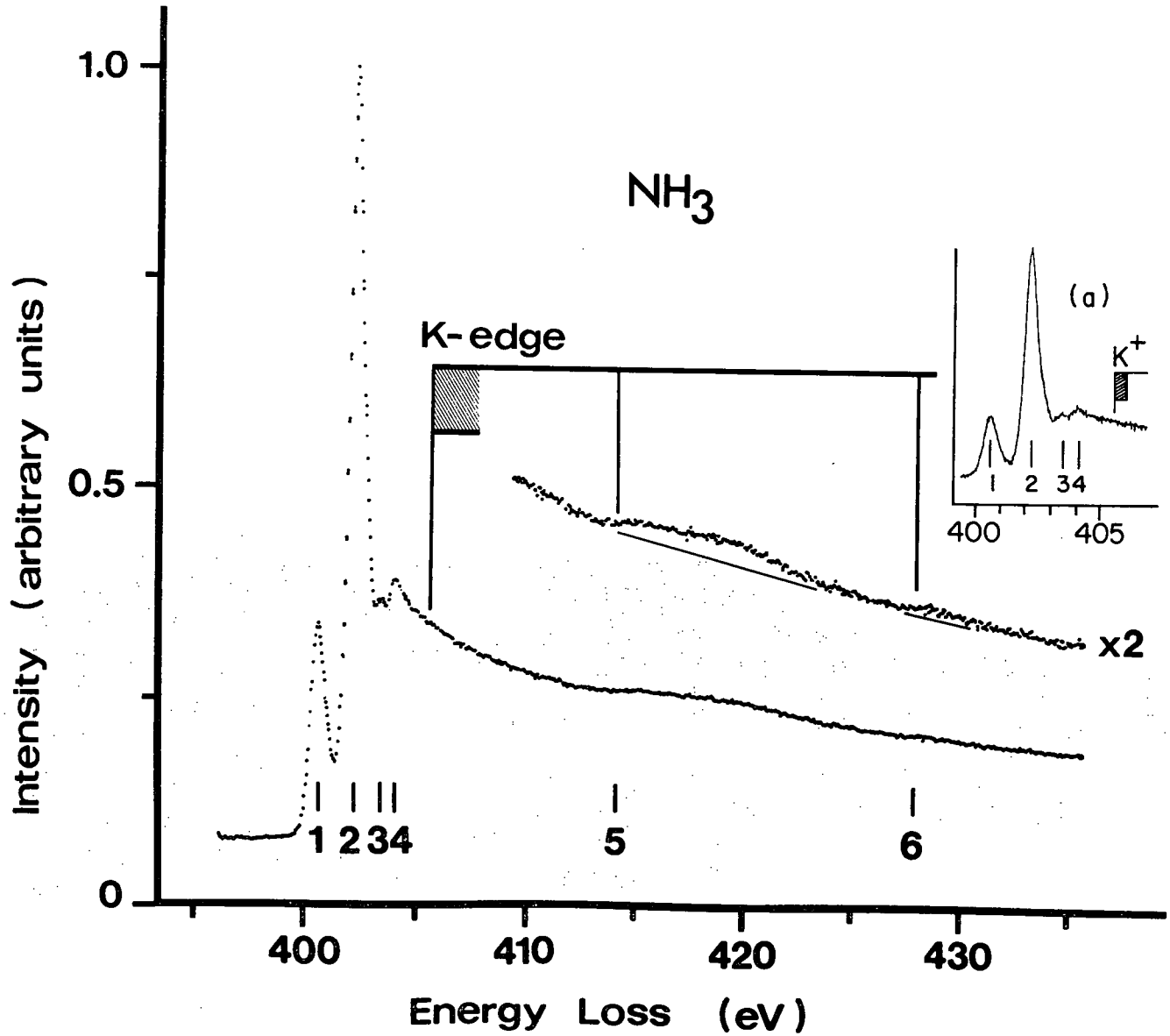

FIGURE 39. Nitrogen K-shell energy loss spectrum of ammonia.

TABLE 12

ABSOLUTE ENERGIES (eV), RELATIVE ENERGIES AND TENTATIVE ASSIGNMENTS OF THE PEAKS OBSERVED IN THE NITROGEN K-SHELL SPECTRUM OF AMMONIA

PEAK	ENERGY	ΔE	TERM VALUE	ASSIGNMENT[a]	ESTIMATED ENERGY[b]
1	400.6	0	5.0	$3sa_1$	401.2
2	402.2	1.6	3.4	3pe	402.8
3	403.5	2.9	2.1	$3pa_1$	403.4
4	404.1	3.5	1.5	$4sa_1/3d$	404.1
				4pe	404.3
	∿ 404.6	4.0	1.0	5pe	404.8
K-EDGE[c]	405.6	5.0	0	∞	
5	∿ 414[d]	∿ 13.5		SHAKE-UP AND SHAKE-OFF	
6	∿ 428[d]	∿ 27.5			

a. Only the final orbital involved in the excitation is given (the initial orbital is $1a_1$ ≡ Nitrogen K).

b. Estimated using quantum defects derived from the valence shell spectrum[50,143,145]; $\delta(nsa_1) = 1.25$ $n = 3$; 1.02 $n > 3$, $\delta(npe) = 0.8$, $\delta(npa_1) = 0.54$, and $\delta(nd)$ was assumed to be 0.

c. From X-ray PES[32].

d. Onset.

defect of 1.35 which is comparable with the 1.25 quantum defect observed[145] in the valence shell spectrum for the transition $3a_1 \rightarrow 3sa_1$. It is normal for the 3s quantum defect to be appreciably higher than that determined for the higher members of the series in polyatomic molecules. In fact, for valence shell excitation in ammonia, the $3sa_1$ orbital is not a pure Rydberg orbital and shows appreciable antibonding character[56]. Peak number 2, observed at 404.2 eV, is assigned to the promotion of a $1a_1$ electron to the lowest energy 3p Rydberg orbital (3pe). This peak has a FWHM of 0.7 eV and a quantum defect (peak maximum) of 1.0 in contrast to the quantum defect of 0.8 (calculated from the adiabatic transition energy reported in Reference 50) for the promotion of a $3a_1$ electron to the 3pe Rydberg orbital. The energy difference observed for the two valence shell transitions $3a_1 \rightarrow 3pe$ and $3a_1 \rightarrow 3pa_1$ ($\delta = 0.54$) is $\lesssim 0.6$ eV[50]. The observed FWHM of the second peak in our spectrum does not support a contribution from the transition $1a_1 \rightarrow 3pa_1$ unless for K-shell excitation the 3pe and $3pa_1$ energy difference is small or the intensity of one transition is weak. We suggest that the third peak at 403.5 eV could represent the transition $1a_1 \rightarrow 3pa_1$. This implies a 3p splitting of 1.3 eV for K-shell excitation. The observed energy of the fourth peak, 401.1 eV, is consistent with the energy calculated for the excitation of a $1a_1$ electron to 3d, 4s and 4p Rydberg orbitals. The high energy shoulder probably has contributions from the excitation of $n = 5$ and higher Rydberg orbitals.

The position of the K-edge in our spectrum is based on the experimental X-ray PES value[32] of 405.6 eV for the $1a_1$ binding energy in ammonia. The broad structures with onsets at $\sim$ 414 eV and $\sim$ 428 eV are identified with the simultaneous transitions of a K-shell and valence shell electrons.

7.2.3. Water.

The ground electronic state of the water molecule has C_{2v} symmetry and the electron configuration:

$$(1a_1)^2\ (2a_1)^2\ (1b_2)^2\ (3a_1)^2\ (1b_1)^2,\ ^1A_1.$$

The $1a_1$ orbital is formed from the oxygen 1s orbital and is localized on the oxygen nucleus. The three p-orbitals are nondegenerate in C_{2v} symmetry and have a_1, b_1 and b_2 symmetries. Transitions involving the promotion of a $1a_1$ electron to ns and np Rydberg orbitals are electric dipole allowed.

a. Valence Shell Spectrum.

The valence shell energy loss spectrum of water is shown in Figure 40. The locations of peaks; A (7.5 eV), B (9.7 eV), C (10.1 eV), D (11.1 eV), E (13.6 eV) and F (17.2 eV) are consistent with higher resolution optical[120] and electron impact results[49,148,149]. These spectra have been interpreted in terms of Rydberg transitions[120,150,151]. The location of the first ionization potential in Figure 40 is based on the experimental value[120] of 12.61 eV.

b. Oxygen K-shell Excitation.

The K-shell energy loss spectrum of water is shown in Figure 41 and the energies and tentative assignments of peaks are listed in Table 13. The general appearance of the spectrum is similar to that observed for the K-shell spectra of methane and ammonia. The spectrum is interpreted in terms of Rydberg excitations and excitation energies estimated using the quantum defect method are included in Table 13. The first peak observed at 534.0 eV is assigned to the promotion of an oxygen K-shell electron ($1a_1$) to the $3sa_1$ Rydberg orbital. The peak has a FWHM of 1.0 eV,

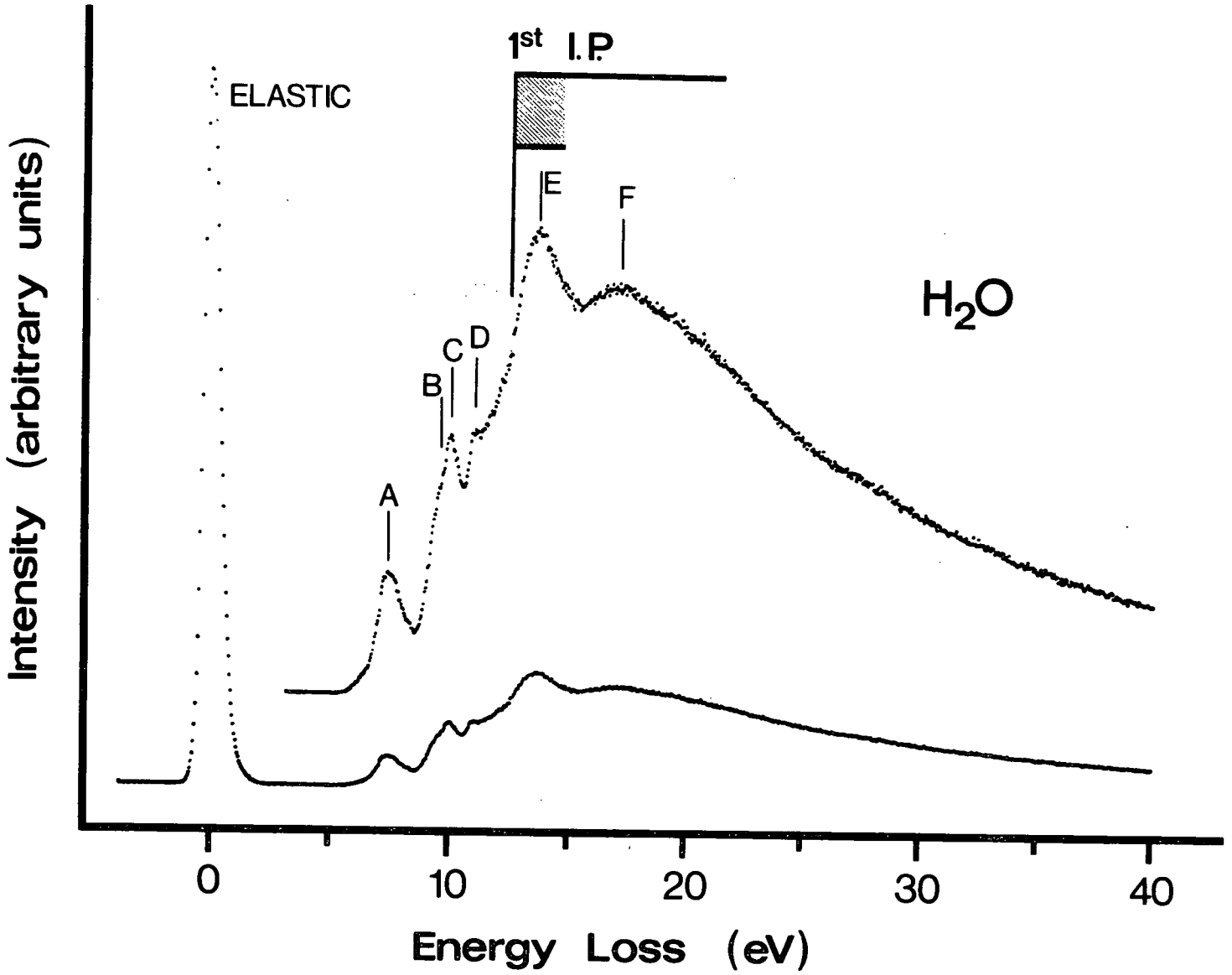

FIGURE 40. Valence shell energy loss spectrum of water.

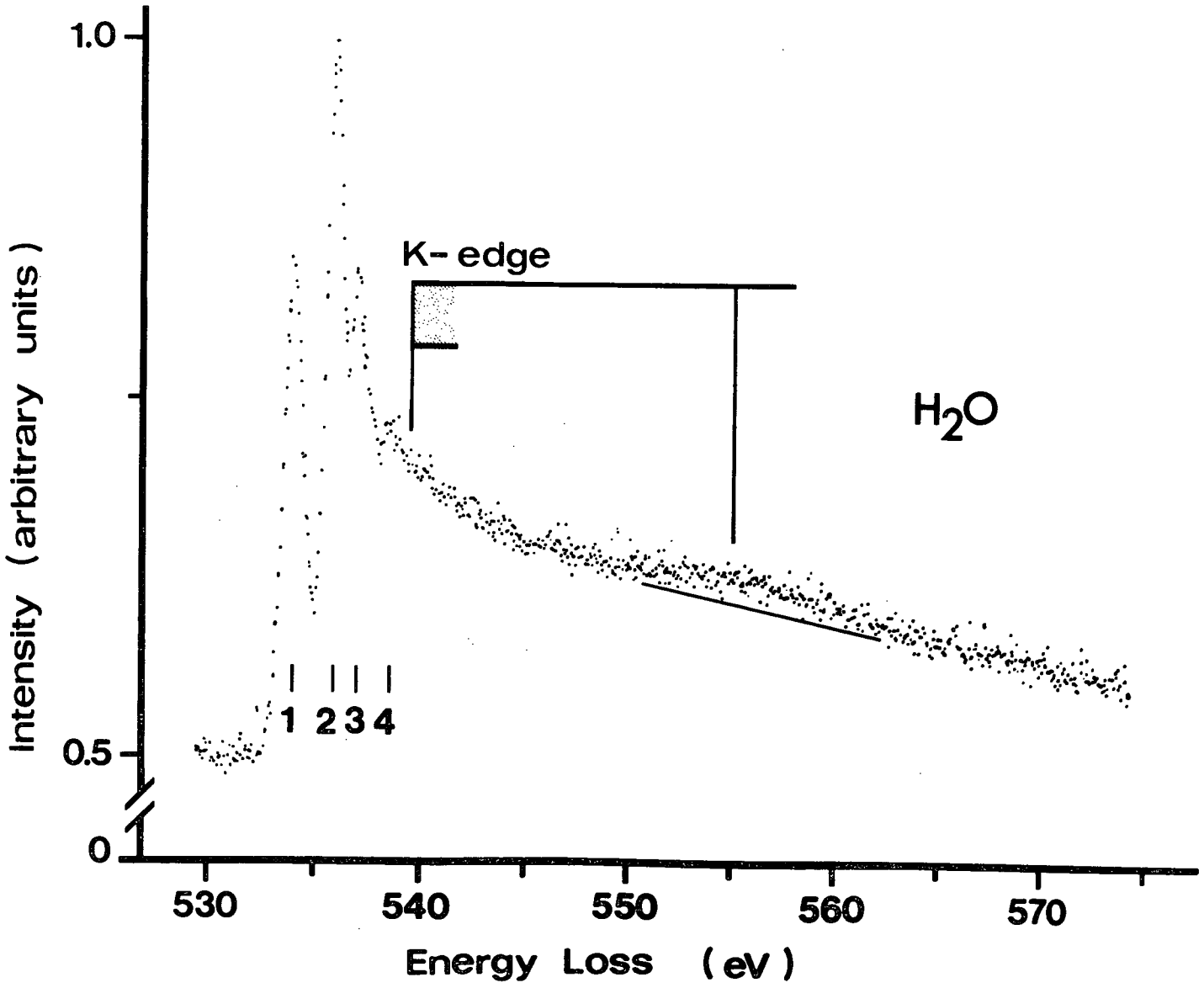

FIGURE 41. Oxygen K-shell energy loss spectrum of water.

TABLE 13

ABSOLUTE ENERGIES (eV), RELATIVE ENERGIES AND POSSIBLE ASSIGNMENTS OF PEAKS OBSERVED IN THE OXYGEN K-SHELL SPECTRUM OF WATER.

PEAK	ENERGY	ΔE	TERM VALUE	POSSIBLE ASSIGNMENT[a]	ESTIMATED ENERGY[b]
1	534.0	0	5.7	$3sa_1$	534.5
2	535.9	1.9	3.8	$3pb_2$	-
3	537.1	3.1	2.6	$3pa_1$	537.1
				$3pb_1$	
				3d	537.5
4	538.5	4.5	1.2	4s	538.1
				4p	538.5
K-EDGE[c]	539.7	5.7		∞	
	~ 555			SHAKE-UP AND SHAKE-OFF	

a. Only the final orbitals involved in the K-excitations have been included.

b. Estimated using the quantum defect method with quantum defects from the valence shell spectrum of water[146]. (3s) = 1.38 (from the term value of 5.2 eV reported by Reference 150, $\delta(ns) = 1.05$ $n > 3$, $\delta(npa_1/b_1) = 0.7$, $\delta(nd) = 0.05$.

c. From X-ray PES[32].

indicating that a number of vibrational levels are excited. The term value is 5.7 eV which implies a quantum defect of 1.45 for the 3s Rydberg state. This term value is comparable with the term value of 5.2 eV observed[150] in the valence shell spectrum of water for the promotion of an electron from the outermost orbital to the 3s Rydberg level, i.e. $1b_1 \rightarrow 3sa_1$. The second peak, observed at 535.9 eV, has a FWHM of 0.9 eV (different data run) which indicates the excitation of a number of vibrational levels. This peak is assigned to the transition $1a_1 \rightarrow 3pb_2$ and has a term value of 3.8 eV. The corresponding transition in the valence shell spectrum $1b_1 \rightarrow 3pb_2$ is electric dipole forbidden and has not been observed. However, the $1b_1 \rightarrow 3pb_2$ excitation energy has been calculated by the INDO[152] and the IVO[153] methods. Both calculations indicate that the lowest energy 3p Rydberg excitation should result from promotion to the b_2 component. The third peak in our spectrum at 537.1 eV is then associated with promotion of a $1a_1$ electron to the $3pa_1$ and $3pb_1$ Rydberg orbitals and has a term value of 2.6 eV. The energy difference between these orbitals in the valence shell spectrum[150] ($1b_1$ promotion) is 0.16 eV (term values 2.62 eV and 2.46). The term value for the K-shell transition is in good agreement with the term values for the corresponding valence transitions. The fourth peak observed at 538.5 eV (term value 1.2 eV) is probably associated with 4s and 4p Rydberg transitions (cf. the estimated values in Table 13).

The position of the K-edge shown on our spectrum is based on the X-ray PES[32] value of 539.7 eV for the K-shell binding energy of water. The broad structure observed in the continuum region $\sim$ 555 eV is associated with the simultaneous transitions of a K-shell and valence shell electrons.

7.2.4. Methanol.

The ground electronic state of the methanol molecule has C_s symmetry and the electronic configuration[150];

$(1a')^2\ (2a')^2\ (3a')^2\ (4a')^2\ (5a')^2\ (1a'')^2\ (6a')^2\ (7a')^2\ (2a'')^2,\ ^1A'$.

The 1a' and 2a' molecular orbitals represent the oxygen 1s and carbon 1s atomic orbitals respectively. The 3s and 3p Rydberg orbital symmetries in the C_s point group are 3sa', 3pa' (twice) and 3pa". The promotion of an electron from any of the occupied molecular orbitals of methanol to each of these Rydberg orbitals is electric dipole allowed. We have investigated both the carbon and oxygen K-shell regions of methanol. A valence shell spectrum was recorded.

a. Valence Shell Spectrum.

The valence shell energy loss spectrum of methanol is shown in Figure 42. The locations of peaks, A (6.8 eV), B(7.9 eV), C (8.3 eV), D (9.8 eV), E (12.0 eV), F (13.8 eV) and G (15.8 eV), are consistent with higher resolution electron impact results[148,150], where the peaks have been associated with Rydberg transitions. The location of the first ionization potential in Figure 42 is based on the adiabatic value[120] of 10.85 eV.

b. Carbon K-shell Excitation.

The carbon K-shell energy loss spectrum of methanol is shown in Figure 43 and the energies and tentative assignments of peaks are listed in Table 14. We have interpreted the spectrum in terms of Rydberg transitions. Transition energies estimated using term values observed in the valence shell spectrum[150] for 2a" promotion (mainly an oxygen lone pair orbital[150]) are also listed in Table 14. The first discrete peak observed

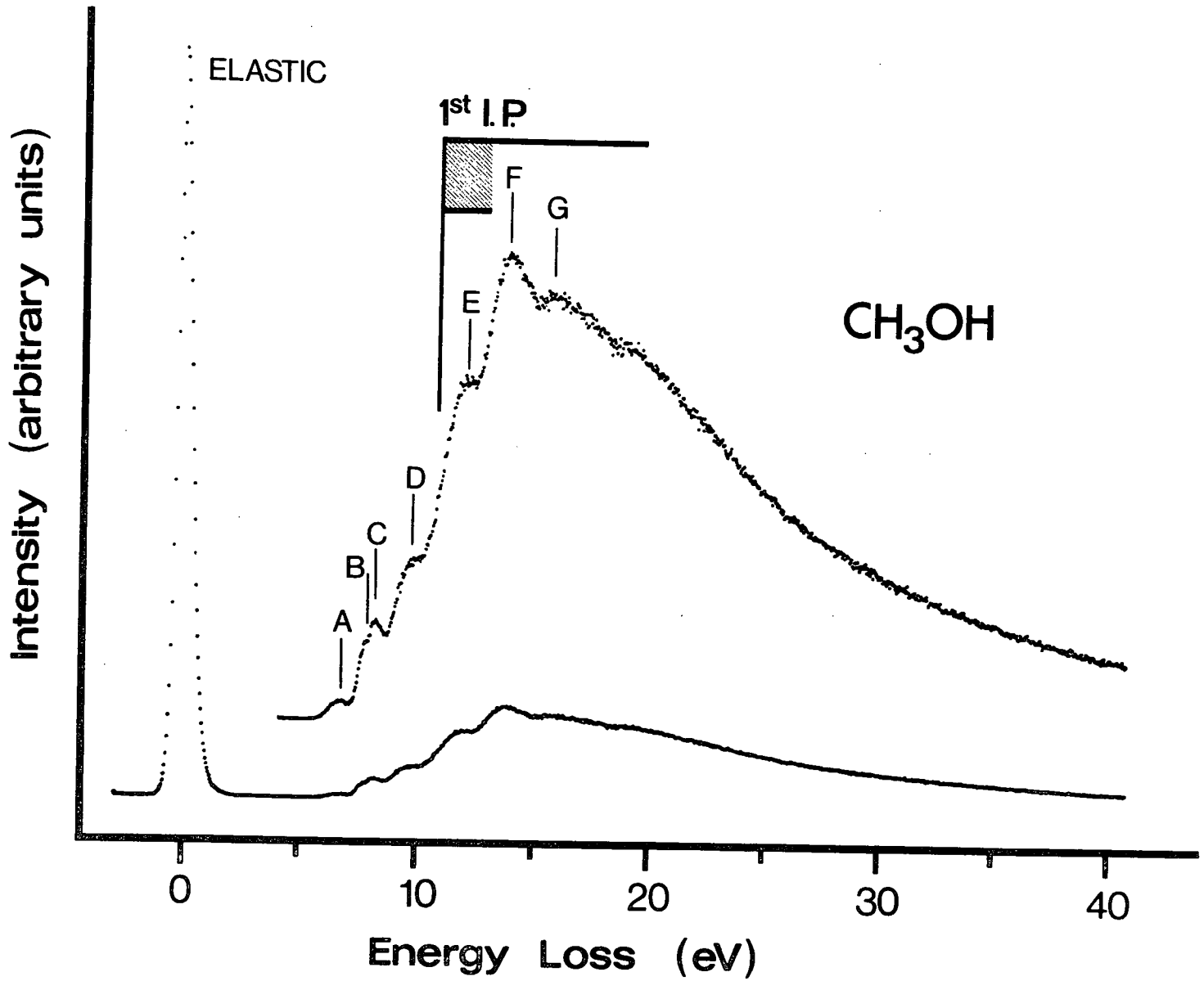

FIGURE 42. Valence shell energy loss spectrum of methanol.

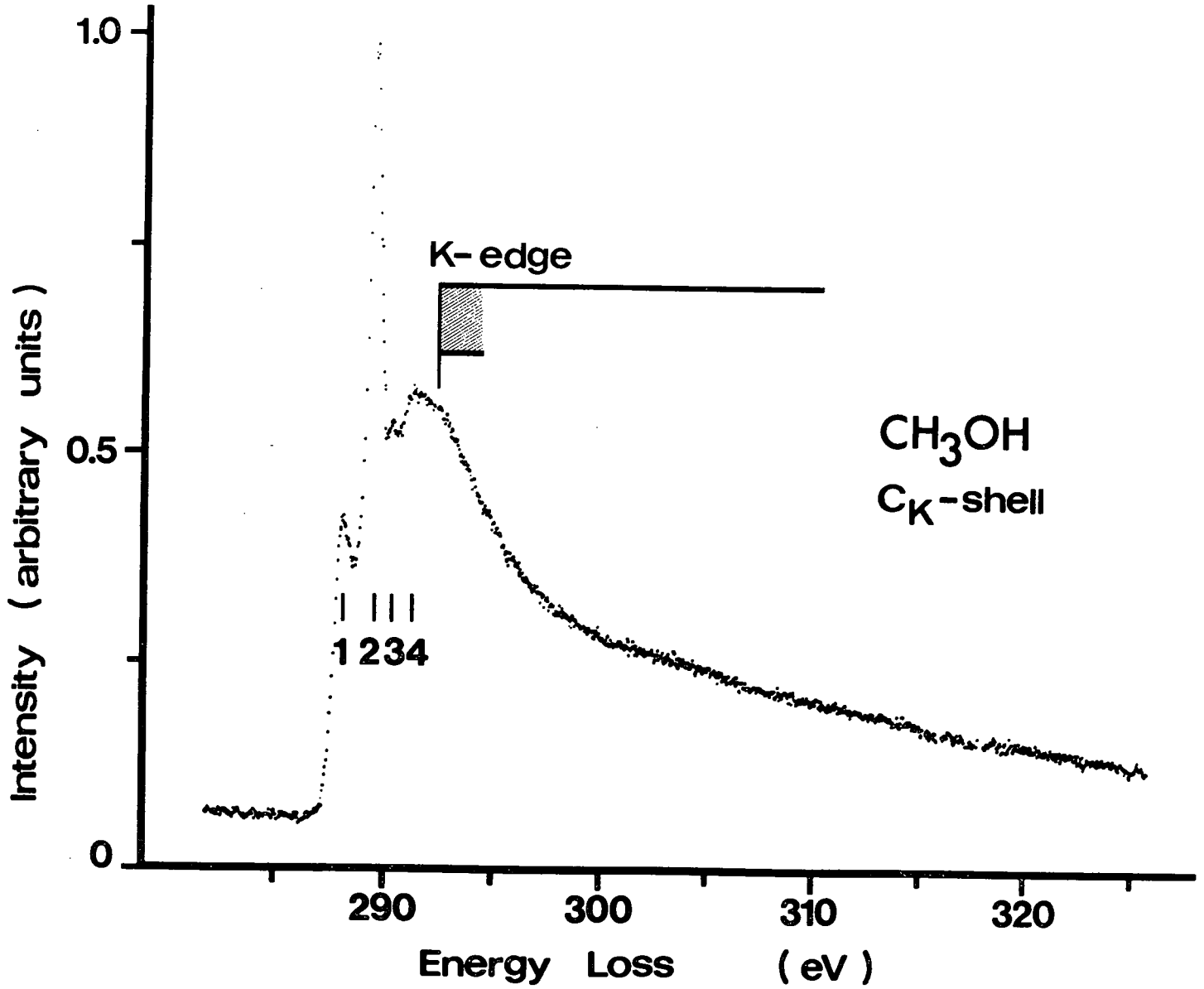

FIGURE 43. Carbon K-shell energy loss spectrum of methanol.

TABLE 14

ABSOLUTE ENERGIES (eV), RELATIVE ENERGIES AND TENTATIVE ASSIGNMENTS OF PEAKS OBSERVED IN THE CARBON AND OXYGEN K-SHELL SPECTRUM OF METHANOL.

CARBON K-SHELL					OXYGEN K-SHELL					ASSIGNMENT[b]
PEAK	ENERGY	ΔE	TERM VALUE	ESTIMATED VALUE[a]	PEAK	ENERGY	ΔE	TERM VALUE	ESTIMATED VALUE[a]	
1	288.1	0	4.2	288.1	1	534.1	0	4.8	534.6	3sa'
2	289.4	1.3	2.9	289.1						3p
3	290.3	2.2	2.0	289.7 290.6	2	537.1	3.0	1.8		3p 3d
4	291.3	3.2	1.0	291.0[d]						4s/4p
K-EDGE[c]	292.3	4.2			K-EDGE[c]	538.9	4.8			∞

a. Estimated using the term values observed in the valence shell spectrum.[150]

b. Only the final orbital involved in the excitation is given.

c. X-ray PES value.[32]

at 288.1 eV has a term value of 4.2 eV and is assigned to the promotion of a carbon 1s electron (2a') to the 3sa' Rydberg orbital, 2a' → 3sa' (δ = 1.2). The term value for this transition is very close to the term value of 4.22 eV observed[150] for the corresponding valence shell transition, 2a" → 3sa'. The second and third discrete peaks in our spectrum are assigned to the promotion of a 1a' electron to 3p Rydberg orbitals. The observed energy difference between the two 3p levels is 0.8 eV. In the valence shell electron impact spectrum of methanol[150] (obtained with much higher resolution) two peaks with an energy difference of 0.4 eV (corresponding to peaks B and C in Figure 42) have been assigned to 3p Rydberg excitations, 2a" → 3p. The observed term values were 3.24 eV and 2.64 eV which are somewhat higher than those observed in our K-shell spectrum (2.9 and 2.0 eV). The fourth band of structure with a maximum at 291.3 eV probably has contributions from 3d, 4s and 4p Rydberg transitions.

The position of the carbon K-edge in our spectrum is based on the X-ray PES value[32] of 292.3 eV for the K-shell ionization energy. Structures arising from the simultaneous promotion of a K-shell and valence shell electrons appear to be weak.

c. Oxygen K-shell Excitation.

The oxygen K-shell energy loss spectrum of methanol is shown in Figure 44 and the energies and tentative assignments of peaks are listed in Table 14. The spectrum has a sloping baseline which is instrumental, arising from the large continuous background of secondary emitted and apparatus scattered electrons. This background is monotonically decreasing as a function of energy loss and was checked by recording the signal from background scattered electrons without any target gas. The background is

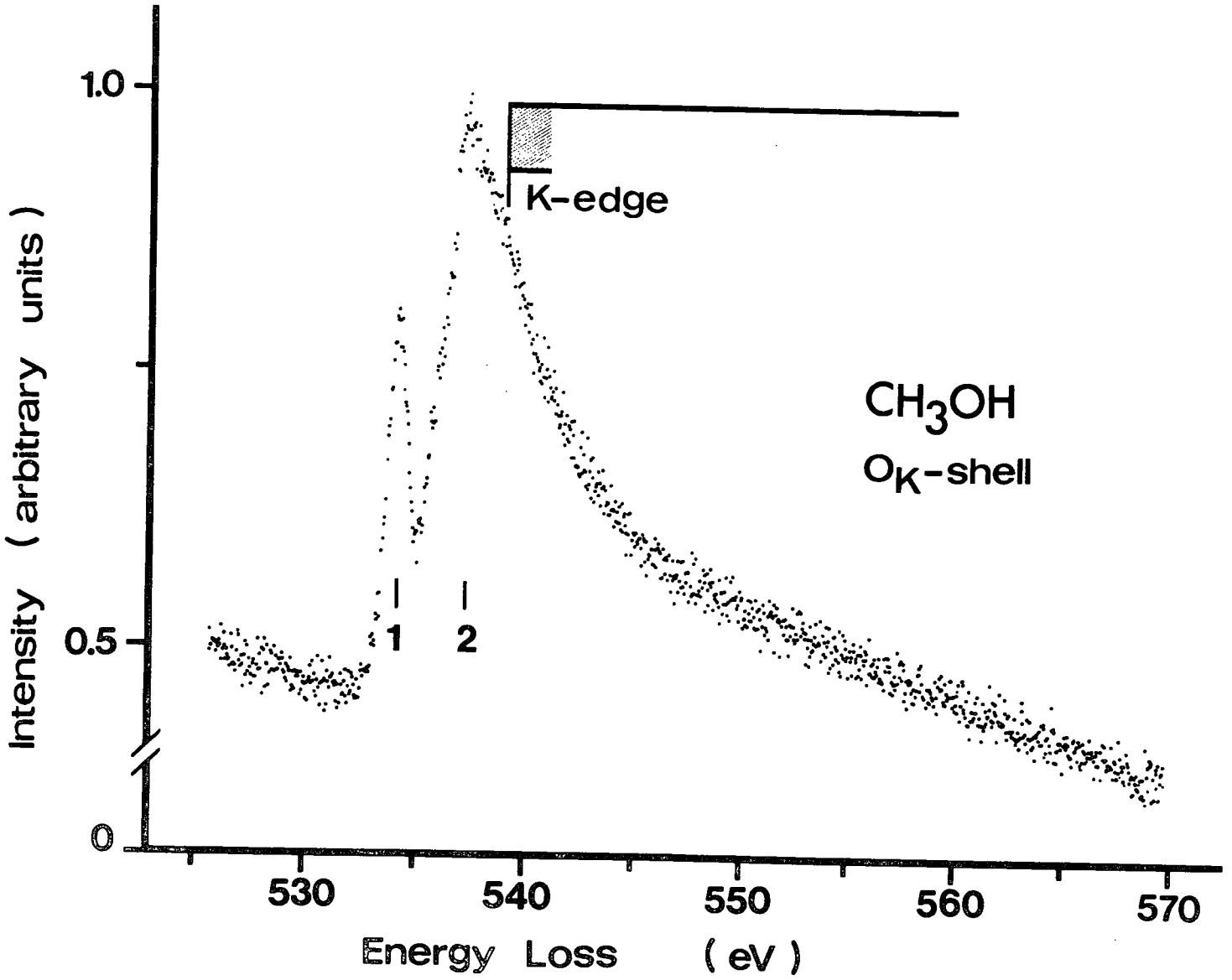

FIGURE 44. Oxygen K-shell energy loss spectrum of methanol.

more prominent in the oxygen K-shell energy region because of the rapid decrease in scattering intensity with energy loss[11], i.e. at least as fast as (energy loss)$^{-3}$. The appearance of the spectrum is appreciably different from that for the carbon K-shell (Figure 43). The first peak at 534.1 eV has a term value of 4.6 eV and is interpreted as arising from the promotion of an oxygen K-shell electron to the 3sa' Rydberg orbital, 1a' → 3sa'. The peak has a FWHM of 1.2 eV indicating the excitation of many vibrational levels. Higher energy structure consists of a broad peak with a maximum at 537.1 eV. On the basis of the assignments of the previous spectra, we expect 3p Rydberg excitations to contribute the most intensity to this broad structure. If this is the case, the relative intensities of the 3p components must be significantly different from those observed in the carbon K-shell spectrum of methanol. Transitions to 3d, 4s and 4p Rydberg orbitals are also expected to contribute intensity in the region of the band maximum.

The position of the K-edge indicated on our spectrum is based on the X-ray PES value[32] of 538.9 eV for the oxygen K-shell binding energy of methanol.

7.2.5. Dimethyl Ether.

The ground electronic state of the dimethyl ether molecule has C_{2v} symmetry and the electron configuration[154]:

$$(1a_1)^2\ (2a_1)^2\ (1b_2)^2\ (CH_{bonding})^{12}\ (2b_2)^2\ (3a_1)^2\ (1b_2)^2,\ ^1A_1.$$

The $1a_1$ and $2a_1/1b_2$ molecular orbitals represent oxygen 1s and carbon 1s orbitals respectively. In the excitation of an oxygen 1s electron, the

final Rydberg states have the same symmetries as the corresponding states in water [see Section (7.2.3.)]. The promotion of a carbon 1s electron should result in a lowering of the molecular symmetry to C_s. In either point group, excitation of a K-shell electron (carbon or oxygen) to all 3s and 3p Rydberg levels is electric dipole allowed.

a. Valence Shell Spectrum.

The valence shell energy loss spectrum of dimethyl ether is shown in Figure 45. The locations of peaks, A (6.7 eV), B (7.6 eV), C (8.5 eV), D (9.2 eV), E (11.0 eV) and F (12.9 eV), are consistent with a higher resolution energy loss spectrum[148], where structures have been assigned to Rydberg transitions. Peaks G (14.0 eV) and H (15.5 eV) are associated with nitrogen impurity (verified by UV-PES) and peaks D and F also have a contribution from this source. The location of the first ionization potential shown in Figure 45 is based on the experimental, adiabatic value[120] of 9.96 eV.

b. Carbon K-shell Excitation.

The carbon K-shell energy loss spectrum of dimethyl ether is shown in Figure 46 and the energies and tentative assignments of peaks are listed in Table 15. The first energy loss structure appears as a shoulder at approximately 288.5 eV (term value 3.75 eV) on the more intense second peak and is assigned to the promotion of a carbon K-shell electron (2a' in C_s point group) to the 3sa' Rydberg orbital. The second peak observed at 289.4 eV (term value 2.85 eV) is assigned to the promotion of a carbon K-shell electron (2a') to a 3p Rydberg orbital. The third peak in the spectrum observed at 291.1 eV (term value 1.15 eV) probably has contributions from 4s and 4p Rydberg transitions.

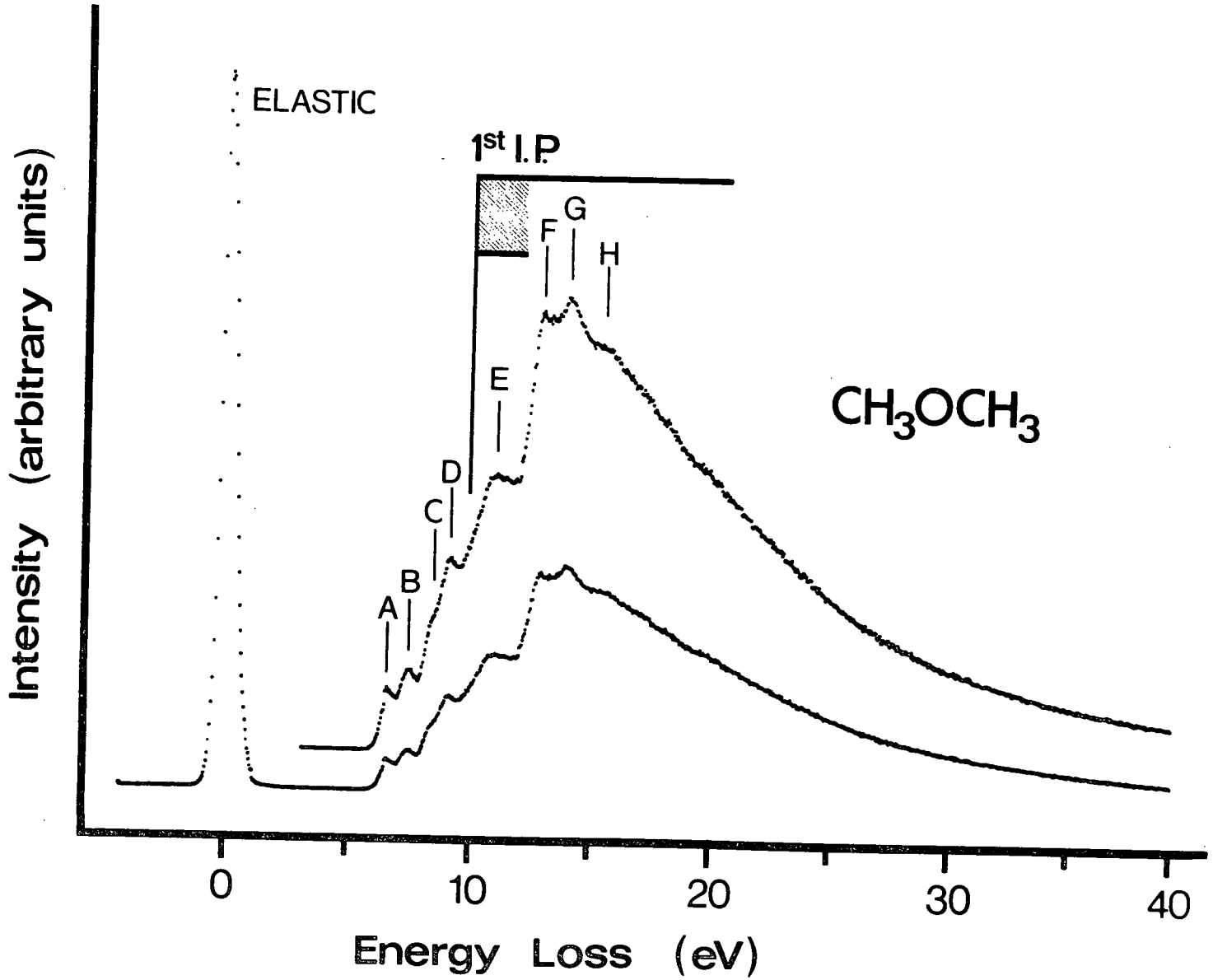

FIGURE 45. Valence shell energy loss spectrum of dimethyl ether.

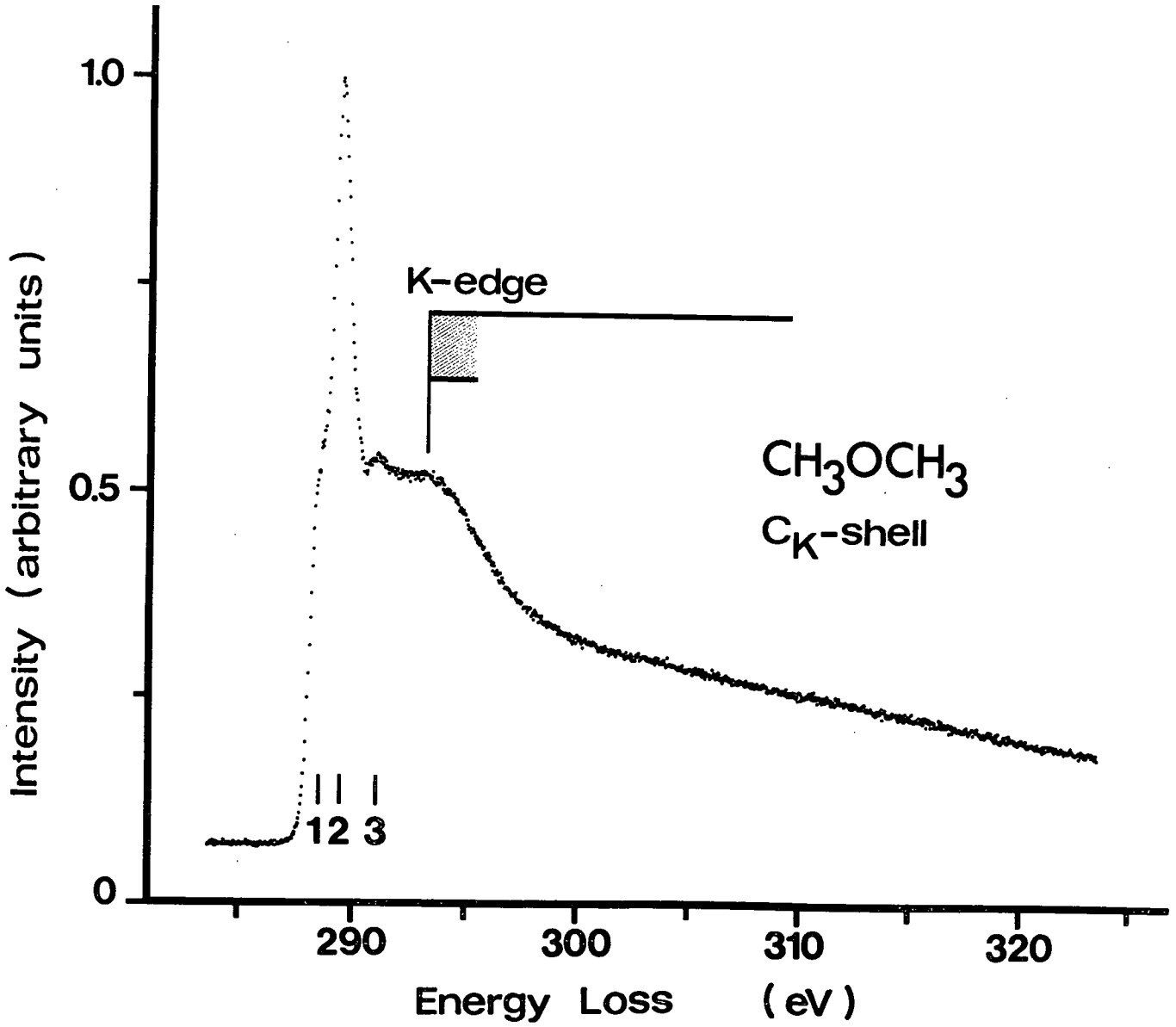

FIGURE 46 Carbon K-shell energy loss spectrum of dimethyl ether.

TABLE 15

ABSOLUTE ENERGIES (eV), RELATIVE ENERGIES AND TENTATIVE ASSIGNMENTS OF PEAKS OBSERVED IN THE CARBON AND OXYGEN K-SHELL SPECTRA OF DIMETHYL ETHER (CH_3OCH_3).

CARBON K-SHELL					OXYGEN K-SHELL					ASSIGNMENT[b]
PEAK	ENERGY	ΔE	TERM VALUE	ESTIMATED VALUE[a]	PEAK	ENERGY	ΔE	TERM VALUE	ESTIMATED VALUE[a]	
1	288.5	0	3.75	288.9	1	535.5	0	3.1	535.2	$3sa_1$
2	289.4	0.9	2.85	289.6 289.8 290.7					535.9 536.2 537.0	3p 3d
3	291.1	2.6	1.15		2	538.6	3.1			4s/4p
K-EDGE[c]	292.25	3.75			K-EDGE[c]	538.59	3.1			∞

a. Estimated using the term values observed in the valence shell spectrum of dimethyl ether[148].

b. Only the final orbital involved in the excitation is listed.

c. X-ray PES values[155].

The position of the carbon K-edge indicated in our spectrum is based on the X-ray PES value[155] of 292.25 0.05 eV.

c. Oxygen K-shell Excitation.

The oxygen K-shell energy loss spectrum of dimethyl ether is shown in Figure 47 and the energies and tentative assignments of peaks are listed in Table 15. The spectrum is very different from the carbon K-shell spectrum of dimethyl ether (Figure 46) and resembles the oxygen K-shell spectrum of methanol (Figure 44).

The first peak at 535.5 eV (term value 3.1 eV) is assigned to the promotion of an oxygen K-shell electron to the $3sa_1$ Rydberg orbital. The broad band of structure with a maximum at 538.6 eV presumably has contributions from 3p and higher quantum number Rydberg transition.

The position of the oxygen K-edge indicated on our spectrum is based on the X-ray PES value[155] of 538.6 ± 0.05 eV.

7.2.6. Monomethylamine.

The ground electronic state of the monomethylamine molecule has C_s symmetry (staggered conformation) and the electron configuration[156];

$(1a')^2\ (2a')^2\ (3a')^2\ (4a')^2\ (1a'')^2\ (5a')^2\ (6a')^2\ (2a'')^2\ (7a')^2\ (3a'')^2,\ ^1A'$.

The 1a' and 2a' orbitals represent nitrogen 1s and carbon 1s orbitals respectively.

a. Valence Shell Spectrum.

The valence shell electron energy loss spectrum of monomethylamine is shown in Figure 48. Electron impact data for monomethylamine has not been reported in the literature and, optically, only the $X \rightarrow A$ transition, with an onset at 5.2 eV, has been observed[120]. This transition has been assigned[120] to the excitation of a nitrogen lone pair electron (3a") to the

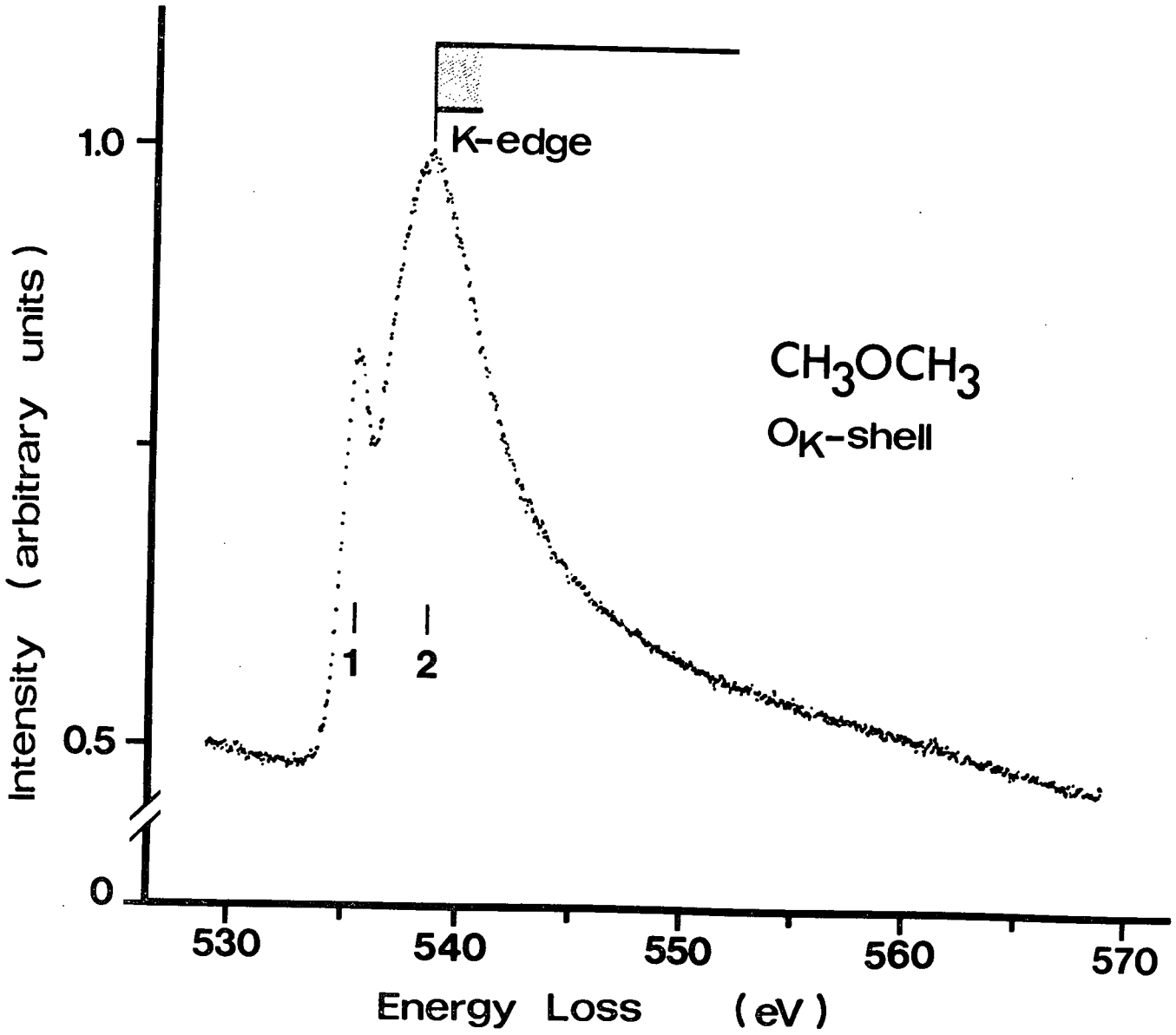

FIGURE 47. Oxygen K-shell energy loss spectrum of dimethyl ether.

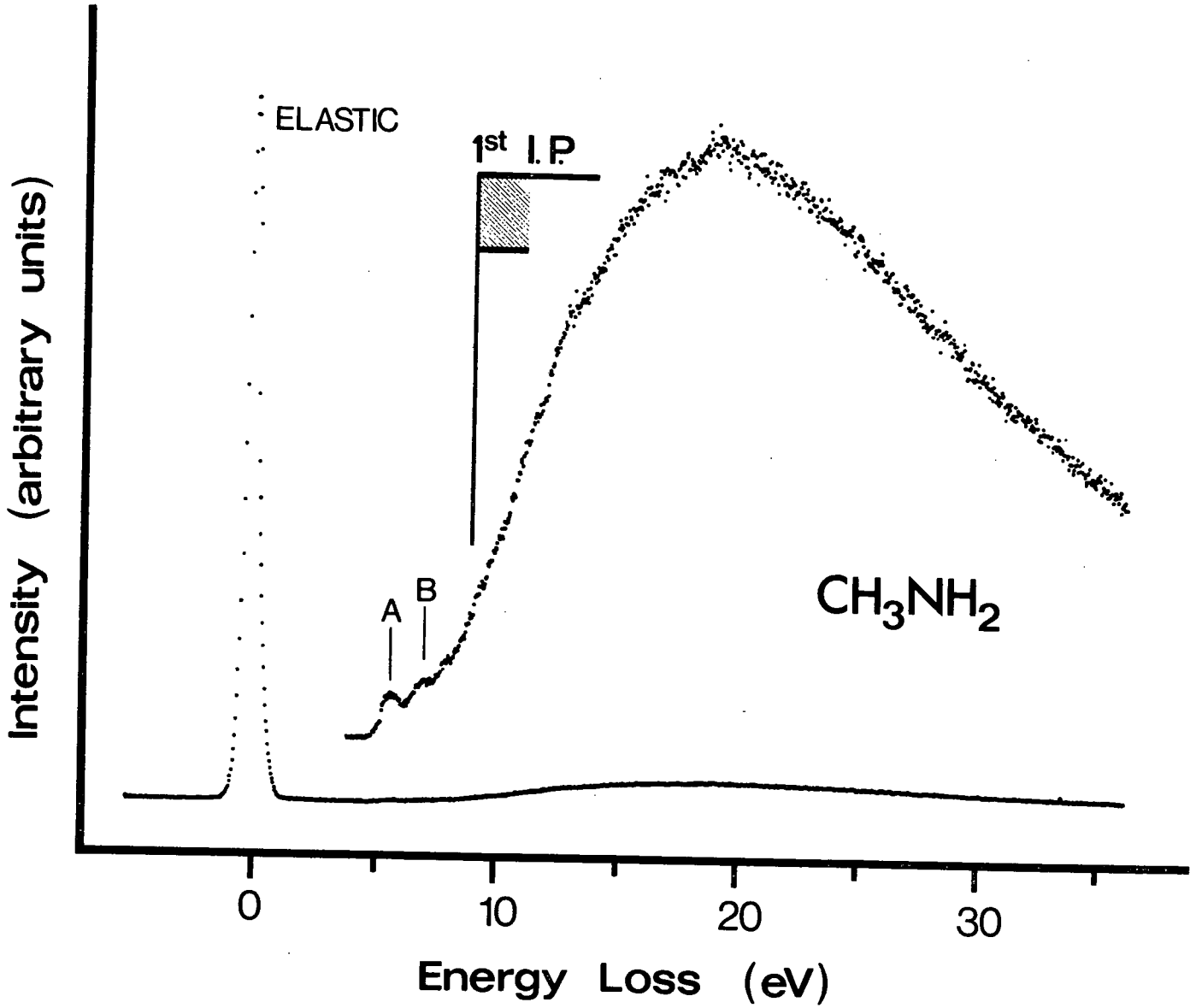

FIGURE 48. Valence shell energy loss spectrum of monomethylamine.

3s Rydberg orbital, analogous to the first band in the ammonia valence shell spectrum (peak A in Figure 38). Peak A, with a maximum at approximately 5.7 eV in our spectrum, is therefore associated with the $X \rightarrow A$ transition. Peak B ($\sim$ 7.0 eV) probably represents the excitation of a higher energy Rydberg state. The location of the first ionization potential shown in Figure 48 is based on the adiabatic value[120] of 8.97 eV.

b. Carbon K-shell Excitation.

The carbon K-shell energy loss spectrum of monomethylamine is shown in Figure 49 and the energies and tentative assignments of peaks are listed in Table 16. The first peak observed at 287.5 eV (term value 4.1 eV) is interpreted as representing the promotion of a carbon 1s electron to the 3sa' Rydberg orbital, while the second peak observed at 288.5 eV (term value 3.1 eV) is associated with carbon 1s excitation to a 3p Rydberg level. Finally, the broad band with a peak maximum at 291.5 eV and shoulder $\sim$ 290.4 eV is probably associated with 3d and higher quantum number ns and np Rydberg transitions.

The position of the carbon K-edge indicated in our spectrum is based on the X-ray PES value[155] of 291.6 $\pm$ 0.05 eV.

c. Nitrogen K-shell Excitation.

The nitrogen K-shell energy loss spectrum of monomethylamine is shown in Figure 50 and the energies and tentative assignments of peaks are listed in Table 16. The first peak at 400.6 eV has a term value of 4.5 eV (δ = 1.3) and is assigned to the promotion of a nitrogen 1s electron to the 3sa' Rydberg orbital. The second peak at 401.9 eV has a term value of 3.2 eV (δ = 0.9) and is associated with the promotion of a nitrogen 1s electron to a 3p Rydberg orbital. The broad structure with a peak maximum at 404.6 eV

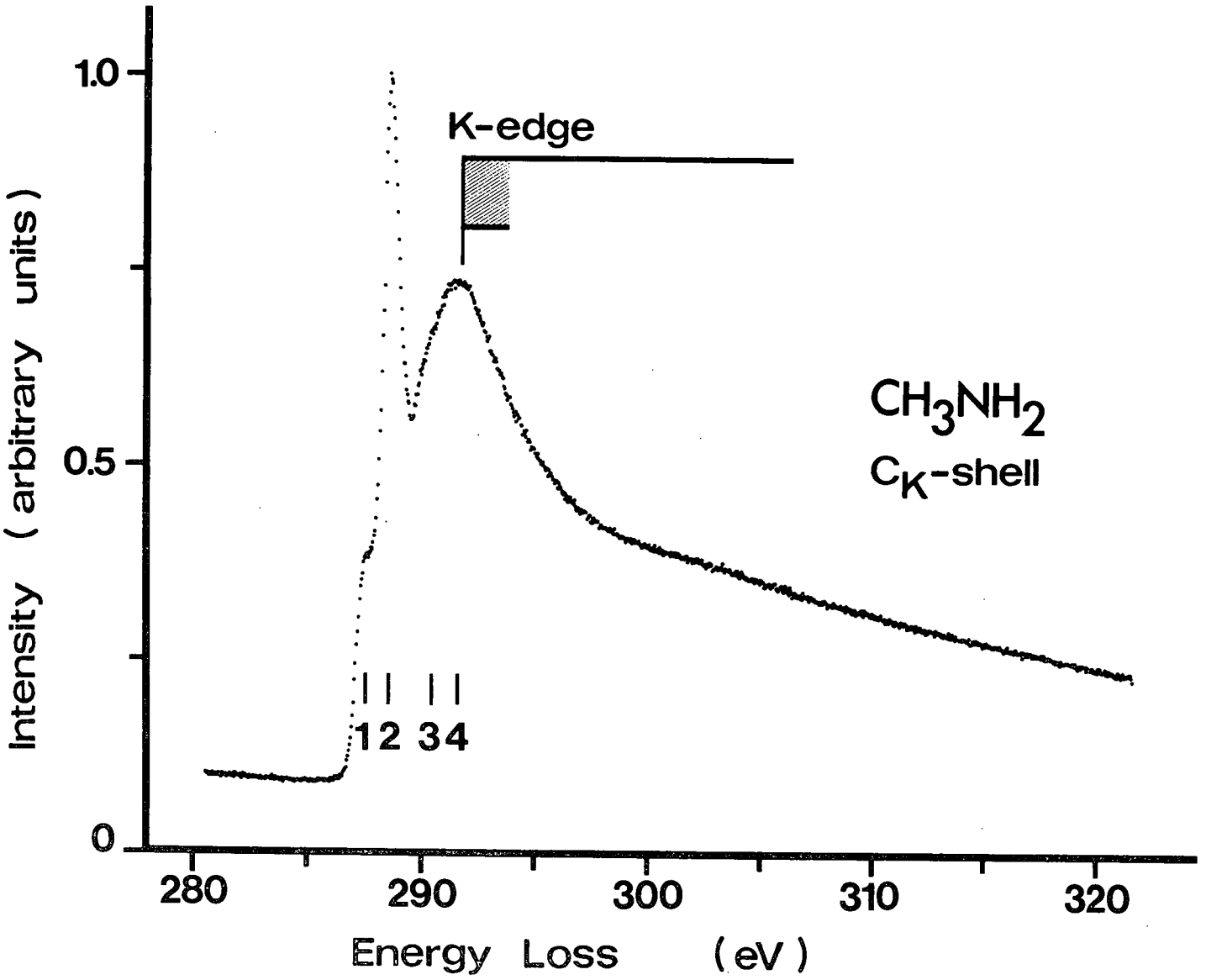

FIGURE 49. Carbon K-shell energy loss spectrum of monomethylamine.

TABLE 16

ABSOLUTE ENERGIES (eV), RELATIVE ENERGIES AND TENTATIVE ASSIGNMENTS OF PEAKS OBSERVED IN THE CARBON AND NITROGEN K-SHELL SPECTRA OF MONOMETHYLAMINE (CH_3NH_2).

CARBON K-SHELL					NITROGEN K-SHELL					ASSIGNMENT[b]
PEAK	ENERGY	E	TERM VALUE	ESTIMATED VALUE[a]	PEAK	ENERGY	E	TERM VALUE	ESTIMATED VALUE[a]	
1	287.5	0	4.1	-	1	400.6	0	4.5	-	3s
2	288.5	1.0	3.1	-	2	401.9	1.3	3.2	-	3p
	shoulder	~1.8?	2.3							
3	290.4	2.9	1.2	289.2 290.2	3	~403.4	~2.8	1.7	403.3 403.6	4s 3d/4p
4	291.5	4.0	0.1		4	404.6	4.0	0.5		
K-EDGE[c]	291.6	4.1			K-EDGE[d]	405.1	4.5			

a. Estimated from the quantum defects derived from the energy positions of the first two peaks. $\delta(nd)$ was assumed to be 0.

b. Only the final orbital involved in the excitation is given.

c. X-ray PES value[155].

d. X-ray PES value[155,157].

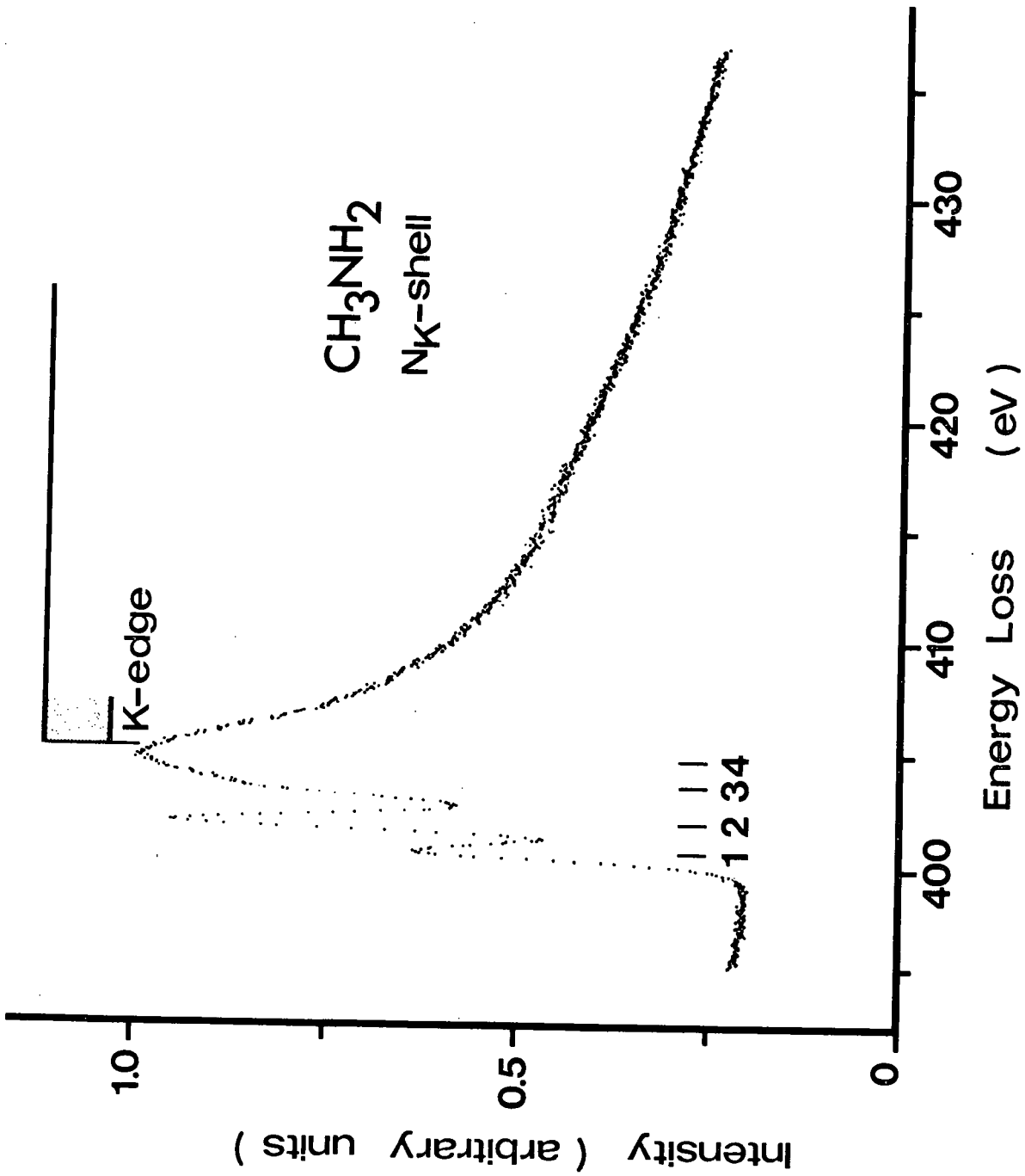

FIGURE 50. Nitrogen K-shell energy loss spectrum of monomethylamine.

(term value 0.5 eV) and a shoulder at ∿ 403.4 (term value ∿ 1.7 eV) is probably associated with 3d, and higher quantum number ns and np Rydberg transitions. Table 16 includes estimates of these excitation energies on the basis of the quantum defects derived from the observed energies of the 3s and 3p peaks in our spectrum.

The position of the nitrogen K-edge indicated in our spectrum is based on the X-ray PES value of 405.1 eV for the nitrogen 1s binding energy in monomethylamine[155,157].

7.2.7. Term Values.

The 3s term values in the K-shell spectra of methane, ammonia and water follow the same order as the 3s term values derived from the valence shell spectra of the same molecules[120,136,145,148,150] (for promotion of the least tightly bound electron) with CH_4 < NH_3 < H_2O (see Table 17). This result is expected, since term values increase with increasing effective nuclear charge. In the series, water, methanol and dimethyl ether, the 3s term values derived from both the valence shell spectra and the K-shell spectra follow the same order with CH_3OCH_3 < CH_3OH < H_2O. The trend in the valence shell spectra has been explained[135] on the basis that the 3s Rydberg orbital increases its carbon character with increasing alkylation, which results in less penetration into the core and, therefore, a lower term value. A similar trend is observed in the K-shell spectra of ammonia and monomethylamine with the term values in the expected order, CH_3NH_2 < NH_3.

7.3. Carbon Tetrafluoride.

The carbon tetrafluoride molecule is tetrahedral in its ground

TABLE 17.

3s AND 3p RYDBERG TERM VALUES OBSERVED FOR K-SHELL EXCITATION AND VALENCE SHELL EXCITATION (OUTERMOST ELECTRON) IN CH_4, NH_3, H_2O, CH_3OH, CH_3OCH, AND CH_3NH_2.

Ne	CH_4			NH_3		H_2O		Final
K-Shell[a]	C_K		$1t_2$	N_K	$3a_1$[c]	O_K	$1b_1$[d]	Orbital
-	3.7	3.95	4.29 3.61	5.0	4.43	5.7	5.2	3s
3.04	2.7	-	-	3.4 2.1	2.81 2.24	3.8 2.6	- 2.62 2.46	

CH_3NH_2		CH_3OH			
N_K	C_K	O_K	C_K	$2a''$[d]	
4.5	4.1	4.8	4.2	4.22	3s
3.2	3.1 2.3		2.9 2.1	3.24 2.64	3p

CH_3OCH_3			
O_K	C_K	$1b_1$[e]	
3.1	3.75	3.37	3s
	2.85	2.70 2.41	3p

a. Reference 158; b. Reference 136; c. References 120,145
d. Reference 150; e. Reference 148.

electronic state and has the electron configuration[144]:

$$(1t_2)^6\ (1a_1)^2\ (2a_1)^2\ (3a_1)^2\ (2t_2)^6\ (4a_1)^2\ (3t_2)^6\ (1e)^4\ (4t_2)^6\ (1t_1)^6,\ {}^1A_1.$$

The $1t_2$ and $1a_1$ molecular orbitals are formed from linear combinations of fluorine 1s (K) atomic orbitals. The calculated energy difference[32,144] between the $1a_1$ and $1t_2$ orbitals is negligible ($\sim$ 0.001 eV). The two orbitals will be designated fluorine-K because of their atomic character and assumed to be degenerate. Similarly the $2a_1$ molecular orbital is formed from the carbon 1s (K) atomic orbital and the electrons filling this orbital will be designated carbon K-shell electrons.

It has already been pointed out in Section 6.2. that the inner shell absorption spectra for molecules composed of a central atom "surrounded" by electronegative atoms, show analomous features which have been attributed to an effective potential barrier on the outer rim of these molecules (see Reference 131). Therefore, a potential barrier may exist in the carbon tetrafluoride molecule. The fluorine K-shell absorption spectra of the fluoromethanes, including carbon tetrafluoride, have been obtained[26] using Bremsstrahlung radiation. However, absorption spectra in the region of the carbon K-edges, which are the most interesting from the point of view of a possible potential barrier, were not reported.

a. Valence Shell Spectrum.

The valence shell energy loss spectrum of carbon tetrafluoride is shown in Figure 51 and the energies of peaks are given in Table 18. The valence shell spectrum of carbon tetrafluoride has previously been obtained[136] with 400 eV incident electrons, zero degree scattering angle and a resolution of $\sim$ 0.045 eV. The observed peaks have been assigned[136]

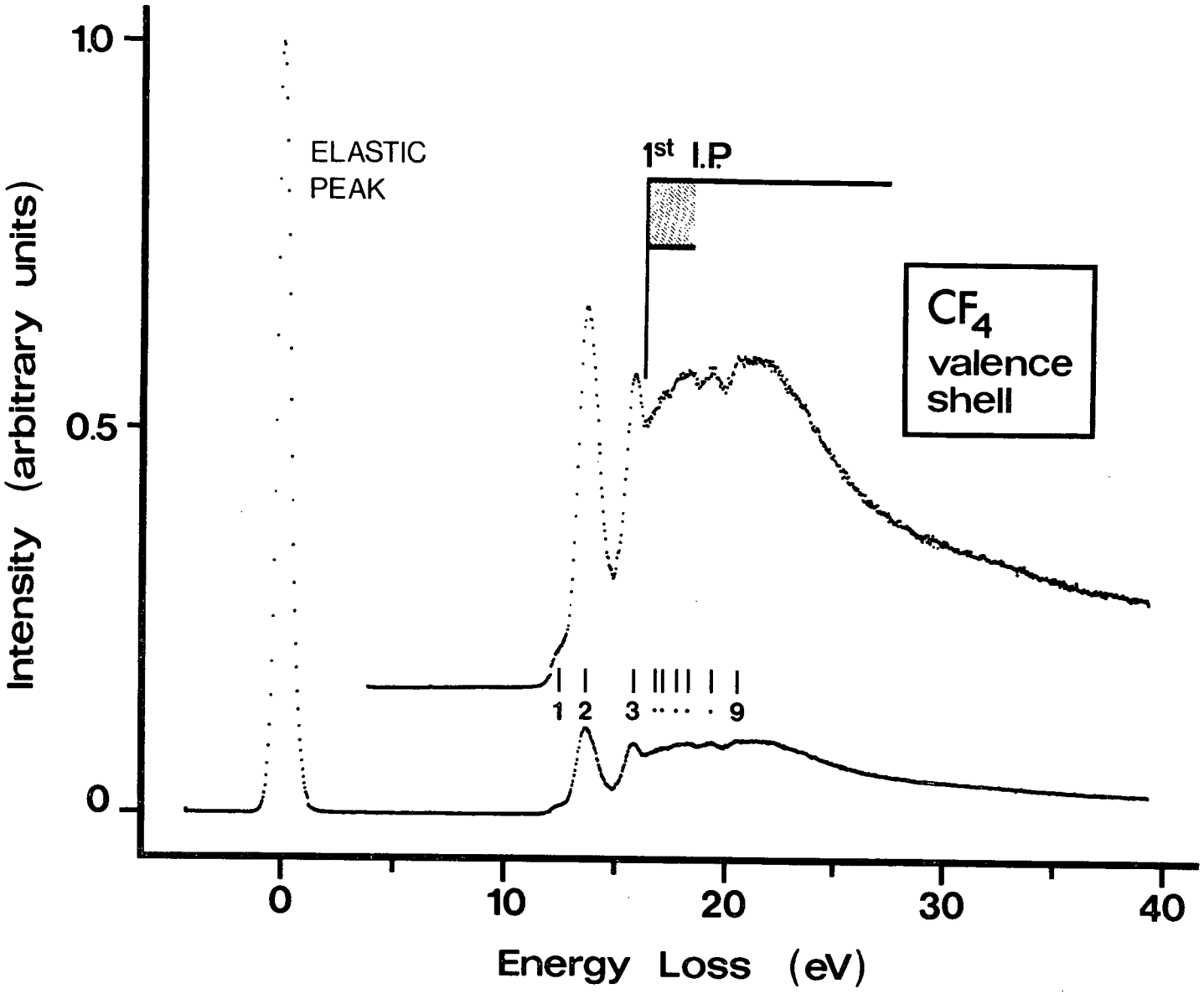

FIGURE 51. Valence shell electron energy loss spectrum of carbon tetrafluoride.

TABLE 18

ABSOLUTE ENERGIES (eV) OF PEAKS OBSERVED IN THE VALENCE SHELL ENERGY LOSS SPECTRUM OF CARBON TETRAFLUORIDE.

THIS WORK[a]		REFERENCE 136[b]
PEAK	ENERGY	ENERGY
1	12.5	12.51
2	13.7	13.59, 13.89
3	15.9	15.81
4	16.8	16.86
5	17.2	
6	17.8	18.01
7	18.4	
8	19.3	19.42
9	20.6	20.53

a. 2.5 keV incident energy, 0.5 eV FWHM elastic peak and average scattering angle 2×10^{-2} rad.

b. 400 eV incident energy, 0.045 FWHM elastic peak and zero degree scattering angle. The spectrum has been assigned in Reference 136.

to Rydberg transitions using the term value scheme and this interpretation is consistent with that of the other fluoromethane molecules[136]. Our spectrum compares favourably with the higher resolution spectrum[136] (see Table 18).

b. Carbon K-shell Excitation.

The carbon K-shell energy loss spectrum of carbon tetrafluoride is shown in Figure 52 and the energies and possible assignments of peaks are listed in Table 19. The spectrum is dominated by a broad band of structure located just below the carbon K-edge. This band of structure has a number of components which are clearly visible in the expanded spectrum shown in the insert in Figure 52. On the basis of the Rydberg interpretations of the carbon K-shell spectrum of methane (see Section 7.2.1) and the valence shell spectra of methane and the fluoromethanes[136], we expect the lowest energy transition in the carbon K-shell spectrum of carbon tetrafluoride to be, $2a_1$ (carbon-K) $\rightarrow$ $3sa_1$. This transition is optically forbidden and is forbidden in our experiment if the first Born approximation is valid (the incident energy is eight times the excitation energy). However, both initial and final states belong to the same symmetry species and deviations from the Born theory are expected[53]. The spectrum is expected to resemble the carbon K-shell spectrum of methane (see Figure 37) where the 3s peak has much less intensity than the 3p. As shown by Figure 52, this is not observed. Moreover, the first four structures on the band have quantum defects of 1.2, 1.1, 1.0 and 0.9 (term values, 4.0, 3.7, 3.4 and 3.1 eV respectively), all consistent with 3s excitation. The term value observed for the first carbon K-shell absorption in the methane spectrum (Figure 37) was 3.7 eV. In the valence shell

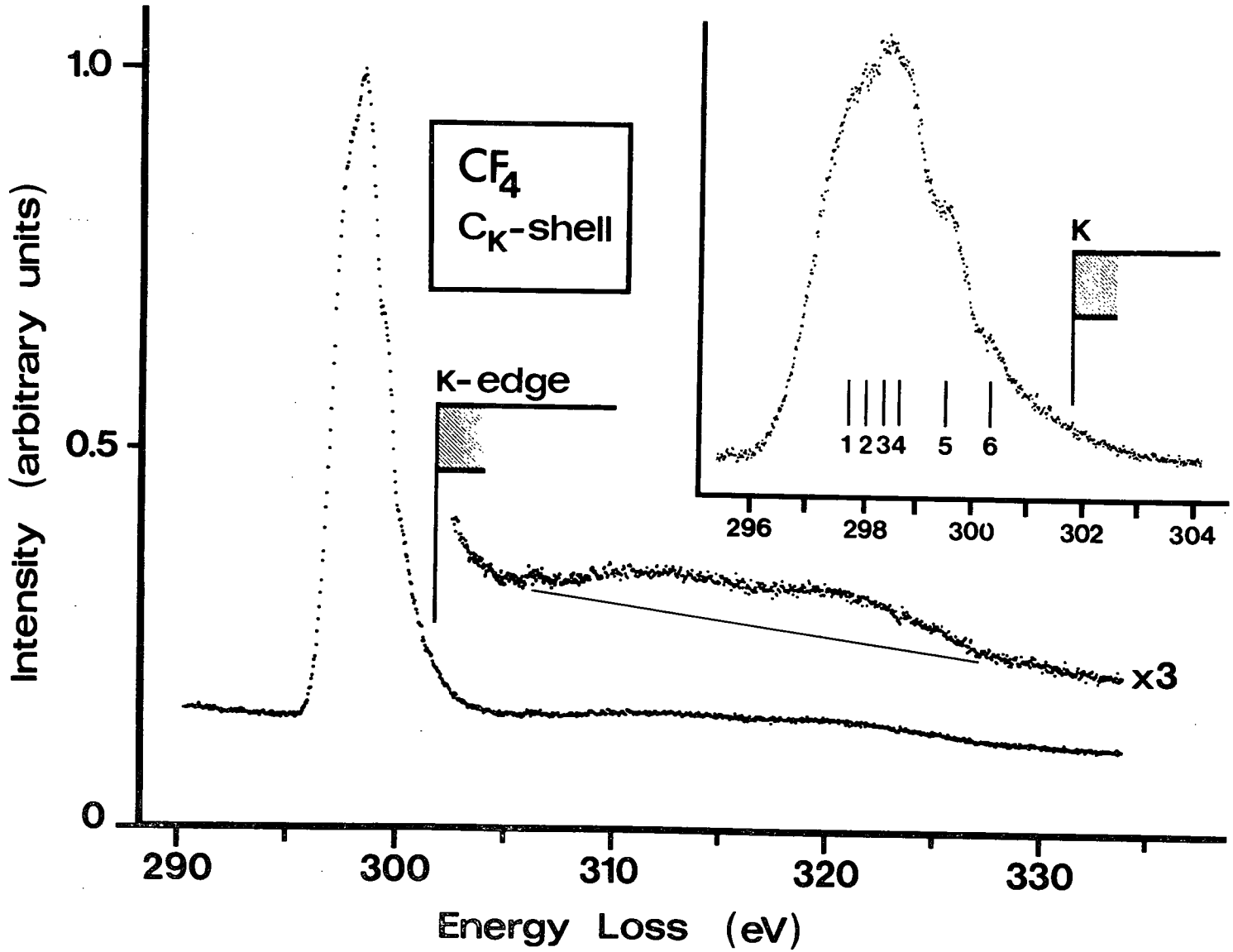

FIGURE 52. Carbon K-shell energy loss spectrum of carbon tetrafluoride.

TABLE 19

ABSOLUTE ENERGIES (eV), RELATIVE ENERGIES AND POSSIBLE ASSIGNMENTS OF PEAKS OBSERVED IN THE CARBON AND FLUORINE K-SHELL ENERGY LOSS SPECTRA OF CARBON TETRAFLUORIDE.

CARBON K-SHELL				FLUORINE K-SHELL				POSSIBLE[b] ORBITAL ASSIGNMENT
PEAK	ENERGY	ΔE	TERM VALUE[a]	PEAK	ENERGY	ΔE	TERM VALUE[a]	
1	297.8	0	4.0	shoulder			∿4	3s[c]
2	298.1	0.3	3.7					
3	298.4	0.6	3.4					
4.	298.7	0.9	3.1					
5	299.3	1.5	2.5	1	692.9	0	2.3	3p
6	300.2	2.7	1.6	2	∿694	1.1	1.2	3d
K-EDGE[d]	301.8	4.0		K-EDGE[d]	695.2	2.3		∞

a. Defined as the difference between the excitation energy and the ionization potential (i.e. the binding energy of the electron in the excited orbital).

b. Only the final orbital is given.

c. This assignment does not apply to the carbon K-shell spectrum (see text).

d. X-ray PES values [32].

spectrum of carbon tetrafluoride[136], 3s term values were in the range 4.1 - 3.5 eV. However, the energy spacings between the first four components of the band, $\sim$ 0.3 eV, are too large to be associated with vibrational structure.† Therefore, the appearance of these multiplet features in the region where a single peak is expected is highly unusual. Features five and six have quantum defects of 0.67 and 0.08 respectively (term values 2.5 and 1.6 eV. These features may be associated with the promotion of a carbon K-shell electron to 3p and 3d Rydberg orbitals respectively. The term values are consistent with those observed for corresponding Rydberg excitations in the valence shell spectra of the fluoromethane molecules[136] (e.g. CF_4, $1t_1 \rightarrow 3p$ and $1e \rightarrow 3d$ have term values of 2.6 and 1.6 eV respectively).

The location of the carbon K-edge indicated on our spectrum is based on the experimental X-ray PES value[32] of 301.8 eV. The extremely broad structure observed above the K-edge is possibly associated with shake-up and shake-off processes in conjunction with K-shell excitation and/or ionization.

With regard to the possible existence of a potential barrier, the carbon K-shell energy loss spectrum of carbon tetrafluoride has two features not observed in the K-shell spectra of molecules such as methane, ammonia, and water, where a potential barrier is not expected (see Figures 37, 39 and 41):

i. an unusual number of components are observed in the energy region where a single peak associated with 3s Rydberg excitation is expected. This

† The largest vibrational spacing for CF_4 in its ground electronic state is $\nu_3 = 0.16$ eV[159].

is apparently not vibrational structure and it is also unlikely that any of the higher energy components (i.e. peaks 3 and 4) are associated with a Jahn-Teller splitting of the $^1T_2$ state arising from the transition, $2a_1 \rightarrow 3pt_2$, which has been associated with peak five. Jahn-Teller instability is larger in methane than in carbon tetrafluoride. This is illustrated by the valence shell spectra[136] where a distinct splitting has been observed in methane ($1t_2 \rightarrow 3s$, $\Delta E = 0.68$ eV) while a splitting is not apparent in the carbon tetrafluoride spectrum. Since a Jahn-Teller splitting is not obvious in the carbon K-shell spectrum of methane, (see Figure 37) we do not expect to observe a splitting in the carbon K-shell spectrum of carbon tetrafluoride. However, even if there is appreciable Jahn-Teller splitting, there can only be a maximum of three features associated with the $^1T_2$ state.

ii. the ratio of the intensity in the continuum region of the K-edge to that of discrete structures is small in comparison with similar ratios observed in the K-shell spectra of methane, ammonia and water (see Figures 37, 39 and 41). This feature is common to all inner shell spectra in molecules where the existence of a potential barrier has been proposed. It arises because the intensity associated with direct ionization is suppressed until the ejected electron has enough energy to overcome the barrier (see Reference 131). Using this model, the increase in intensity on the K-continuum at approximately 308 eV may be associated with the onset of "direct" ionization.

c. Fluorine K-shell Excitation.

The fluorine K-shell electron energy loss spectrum of carbon tetrafluoride is shown in Figure 53 and the energies and possible

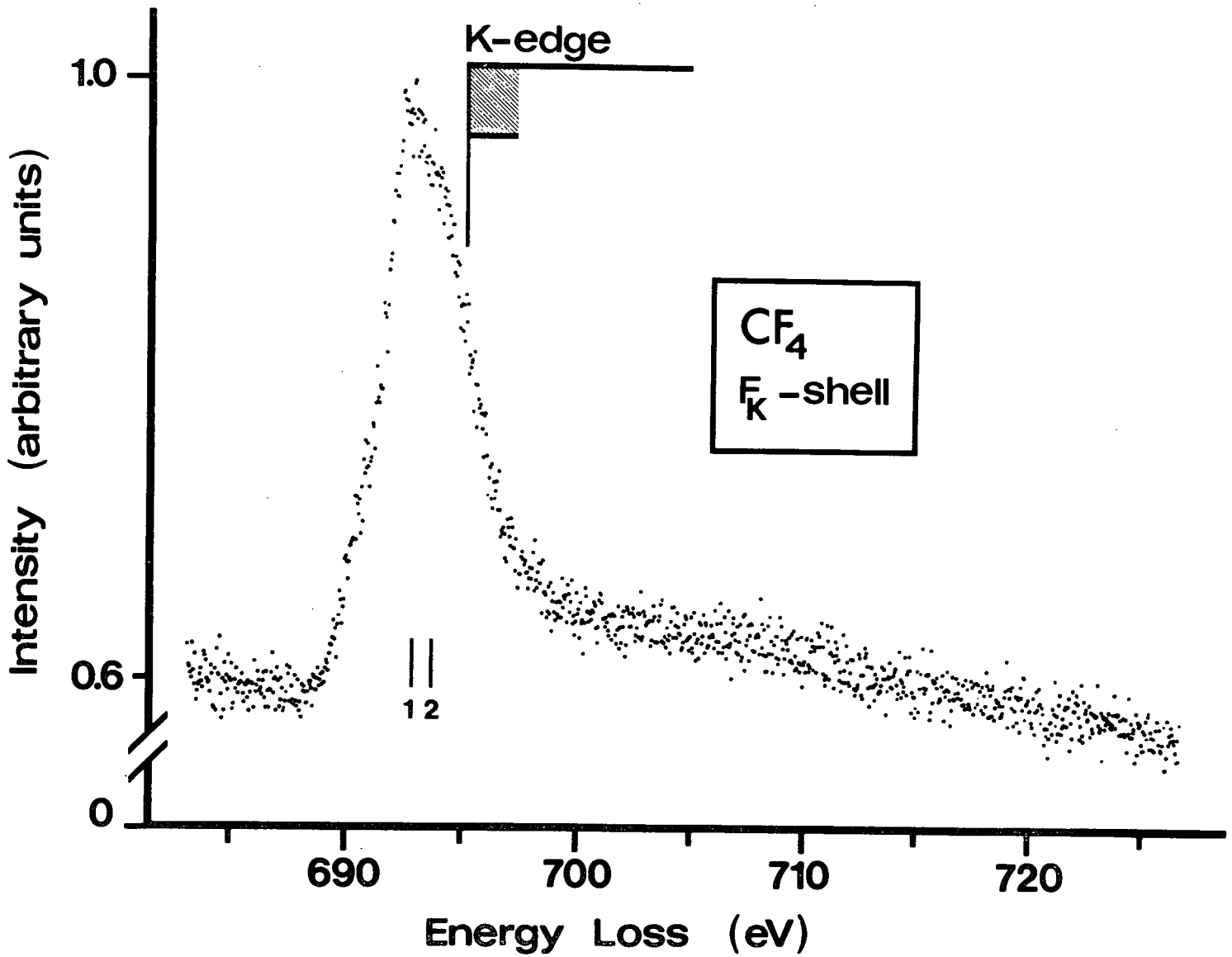

FIGURE 53. Fluorine K-shell energy loss spectrum of carbon tetrafluoride.

assignments of structures are given in Table 19. The optical absorption spectrum has previously been obtained using Bremsstrahlung radiation[26]. It consists of one broad absorption band located just below the K-edge and several broad bands in the continuum region. Our spectrum shows a broad band below the K-edge with a maximum located at 692.9 eV and a high energy shoulder located at approximately 694 eV. The low energy side of the peak is asymmetric and appears to have a contribution from unresolved structure. The discrete structure observed in the K-shell photoabsorption spectrum[26] was attributed to the promotion of a fluorine K-shell electron to anti-bonding valence orbitals. We suggest that a Rydberg interpretation is more likely. The quantum defects derived from the locations of the peak maximum and high energy shoulder are 0.57 and 0 respectively (term values 2.3 and 1.2 eV), consistent with those expected for 3p and 3d Rydberg excitation. The structure on the low energy side of the peak may be associated with 3s Rydberg excitation. This interpretation is consistent with that of the carbon K-shell spectrum of methane (see Table 11) and the valence shell spectra of the fluoromethanes[136] (including CF_4).

The location of the fluorine K-edge indicated on our spectrum is based on the X-ray PES value[32] of 695.2 eV. The intensity of structure just beyond the K-edge is approximately one-half that of the main discrete peak (see also the optical absorption spectrum[26]). This is in sharp contrast to the low ratio of continuum to discrete structure observed in the carbon K-shell spectrum of carbon tetrafluoride and the fluorine K-shell spectrum[16] of SF_6. This suggests that if a potential barrier exists in the carbon tetrafluoride molecule (see the carbon K-shell discussion) it probably has little effect on the excitation of a fluorine K-shell electron.

7.4. Carbon K-shell Energy Loss Spectrum of Acetone.

The ground electronic state of the acetone molecule has C_{2v} symmetry and the electron configuration:

$$(1a_1)^2\ (2a_1)^2\ (3a_1)^2\ (1b_2)^2\ (\text{valence shell})^{24},\ {}^1A_1$$

The $1a_1$ and $2a_1$ molecular orbitals are formed from the 1s (K) atomic orbitals of oxygen and the carbonyl carbon respectively. Similarly, the $3a_1$ and $1b_2$ molecular orbitals represent linear combinations of the 1s (K) atomic orbitals of the two methyl carbons. The electrons filling these orbitals are designated K-shell electrons because they are localized on their respective nuclei (nonbonding) and are mainly atomic in character. The X-ray PES spectrum of acetone[32] consists of two peaks in the region of the carbon K-edge separated by 2.6 eV (intensity ratio 2:1). These peaks represent the ionization of $3a_1/1b_2$ and $2a_1$ electrons respectively, with the methyl carbon associated with the lower K-shell binding energy and the larger intensity peak. On the basis of the X-ray PES spectrum, the $3a_1$ and $1b_2$ molecular orbitals are considered to be effectively degenerate[†] at our experimental resolution ($\sim$ 0.5 eV).

The valence shell electron energy loss spectrum of acetone has recently been reported[160,161] and prominent features have been assigned to Rydberg transitions. On this basis we expect Rydberg transitions to dominate the K-shell spectrum.

The carbon K-shell energy loss spectrum of acetone is shown in Figure 54 and the energies and possible assignments of peaks are given in

[†] Theoretically a small energy difference is expected. A similar situation occurs[32] in the CF_4 molecule for the fluorine 1s (K) electrons. In this case, the calculated[32,144] energy splitting is very small ($\sim$ 0.001 eV).

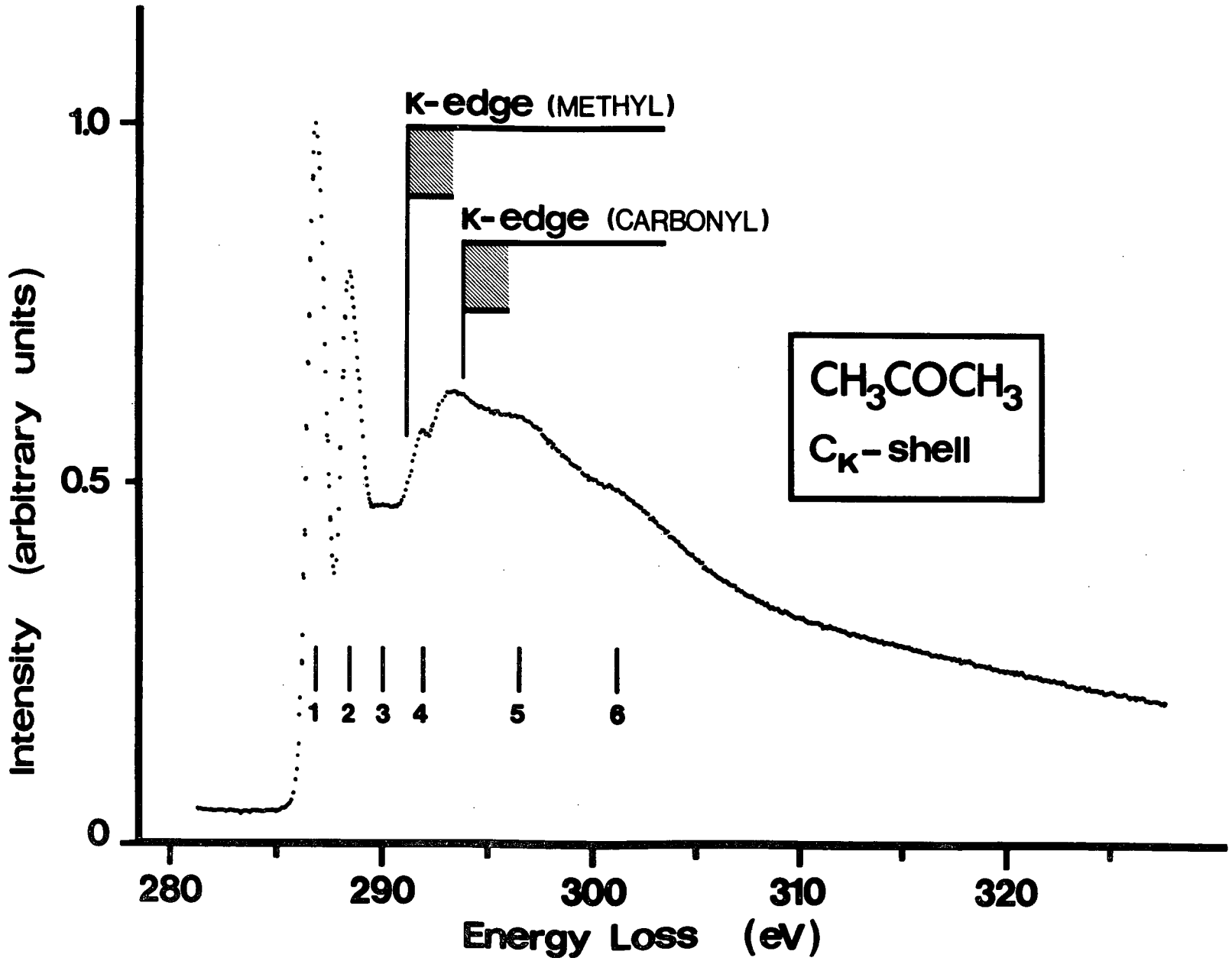

FIGURE 54. Carbon K-shell energy loss spectrum of acetone.

Table 20. The first discrete peak with a maximum at 286.8 eV is interpreted as arising from the promotion of a carbon K-shell electron (methyl), $3a_1/1b_2$, to the $3sa_1$ Rydberg orbital. The observed excitation energy and the X-ray PES value[32] for the series limit implies a quantum defect of 1.2. The magnitude of this quantum defect is consistent with that expected[130] for a 3s Rydberg state and similar to the quantum defect derived for the ns Rydberg series in the valence shell spectrum of acetone (1.03, Reference 160 and 1.09, Reference 161). The first peak observed in our spectrum has a FWHM of 1.0 eV compared with a FWHM of 0.6 eV for the peak associated with elastically scattered electrons. This indicates the excitation of a number of vibrational levels. It is unlikely that any of this broadening is associated with an energy difference between the $3a_1$ and $1b_2$ orbitals. Peak two, with a maximum at 288.4 eV, may be associated with the excitation of a carbon K-shell electron (methyl) to one or more components of the 3p Rydberg orbital (a_1, b_1 and b_2). The derived quantum defect is 0.8, consistent with the quantum defect observed for the np Rydberg series in the valence shell spectrum of acetone (0.81, Reference 160 and 0.76, Reference 161). In addition, we expect the promotion of a $2a_1$ electron (carbonyl carbon K-shell) to the $3sa_1$ Rydberg orbital to contribute to the intensity observed in this region of the spectrum. The derived quantum defect of peak two with respect to the carbonyl carbon K-edge is 1.4. The magnitude of this quantum defect is possible for a 3s Rydberg state.

Assignments of structure located above the first peak in our spectrum are clearly speculative. However, peaks associated with the promotion of a methyl carbon K-shell electron are expected to be approximately twice as intense as those associated with the excitation of a carbonyl K-shell

TABLE 20

ABSOLUTE ENERGIES (eV), RELATIVE ENERGIES AND POSSIBLE ASSIGNMENTS OF PEAKS OBSERVED IN THE CARBON K-SHELL ENERGY LOSS SPECTRUM OF ACETONE.

PEAK	ENERGY	ΔE	POSSIBLE[a] ASSIGNMENT	DERIVED[b] QUANTUM DEFECT
1	286.8	0	$C_1 \rightarrow 3sa_1$	1.2
2	288.4	1.6	$C_1 \rightarrow 3p$	0.8
			$C_2 \rightarrow 3sa_1$	1.4
3	290.0	3.2		
K-EDGE (C_1)[c]	291.2	4.4	$C_1 \rightarrow \infty$	
4	291.9	5.5	$C_2 \rightarrow 4s$	1.3
			$C_2 \rightarrow 3d$	0.32
K-EDGE (C_2)[c]	293.8	7.0	$C_2 \rightarrow \infty$	
5	$\sim$ 296.4	$\sim$ 9.6	SHAKE-UP AND SHAKE-OFF	
6	$\sim$ 301	$\sim$ 14.2		

a. C_1 = Carbon K (methyl), C_2 = Carbon K (carbonyl)

b. Derived from the Rydberg formula, $E = A - R/(n-\delta)^2$ where E is the observed excitation energy; A, the ionization potential; R, the Rydberg constant; n, the principal quantum number and δ, the quantum defect.

c. X-ray PES values[32].

electron (cf. the X-ray PES spectrum of acetone[32]).

The locations of the two carbon K-edges shown on our spectrum are based on the experimental[32] carbon 1s binding energies determined by X-ray PES. Peak 4, located between the two edges, may be associated with the transition carbon K (carbonyl) → 4s (δ = 1.3) and/or carbon-K (carbonyl) → 3d (δ = 0.32). In the valence shell spectrum of acetone, the 3d Rydberg series has a quantum defect[160] of 0.32 (0.28, Reference 161). The broad structures observed above the K-edges (peaks 5 and 6) are attributed to the simultaneous transitions of a carbon 1s and valence shell electrons (i.e. shake-up and shake-off processes).

7.5. Estimation of the Excitation and Ionization Energies of NH_4, H_3O and H_2F Radicals Using Core Analogies Applied to K-shell Electron Energy Loss Spectra.

Nakamura et al.[27] have interpreted the K-shell photoabsorption spectrum of molecular nitrogen (obtained using synchrotron radiation) using a core analogy model. The K-shell excited nitrogen molecule is expected to resemble nitric oxide in two respects; i. the outer electronic configurations of K-shell excited nitrogen states and valence nitric oxide states are identical, and, ii. the core potential (nuclei plus K-shells) in both molecules is expected to be similar, since a hole in one of the K-shells of nitrogen increases the effective core charge by one positive unit. Thus the energy spacings of valence shell excited states of nitric oxide and K-shell excited states of nitrogen are found to be very similar. The results presented in this thesis demonstrate that inner shell absorption spectra can be more easily obtained using techniques of energy loss, electron

impact spectroscopy at high (2.5 keV) impact energies. The K-shell energy loss spectra of nitrogen and carbon monoxide (carbon-K) are almost identical (see Figures 9 and 13) as expected on the basis of the core analogy model (both K-shell excited molecules should "resemble" nitric oxide). Furthermore, the oxygen K-shell spectrum of carbon monoxide (Figure 14) is consistent with a "CF description" of the oxygen K-shell excited molecule. Thus, satisfactory estimates of the excited state energies and ionization potential of the carbon monofluoride radical were obtained. However, in the case of the linear triatomic molecules, nitrous oxide and carbon dioxide (see Section 6.1.) there is poor agreement between the energy spacings of the K-shell excited states and those expected on the basis of the core analogy model (i.e. excitation of the terminal nitrogen K-shell electron in N_2O and the carbon K-shell electron in CO_2 should produce "NO_2-like" species). The breakdown of the model in these cases may be partially associated with the large changes in molecular geometry which occur as a result of electronic excitation in these molecules. In favourable cases it should be possible to predict the excited state and ionization energies of radical species using core analogies applied to inner shell absorption spectra.

The core analogy model is expected to apply to the K-shell "hole" states of the methane, ammonia and water molecules because they have one "central" heavy nucleus which is expected to dominate the potential field. This "atomic-like" structure is evident from the well-behaved Rydberg levels observed in the K-shell spectrum of methane (see Table 11). Therefore, the relative energies of the K-shell excited states of methane (with respect to the lowest energy K-shell excited state);

$(1a_1)^1\ (2a_1)^2\ (2t_2)^6\ (3sa_1)^1,\ ^1A_1$

are expected to be similar to the relative energies of the excited states of the ammonium radical, NH_4, (with respect to the ground state:

$(1a_1)^2\ (2a_1)^2\ (2t_2)^6\ (3sa_1)^1,\ ^2A_1,$

assuming tetrahedral symmetry) produced by the excitation of a 3s electron. Similarly, the relative energies of the K-shell excited states of ammonia and water are expected to be similar to those observed for states resulting from 3s electron promotion in the hydrogen oxide radical, H_3O, and the hypothetical fluoronium radical, H_2F, respectively.

The ammonium and hydrogen oxide radicals have been investigated both experimentally and theoretically. Mass spectrometry has provided experimental evidence suggesting that NH_4[162] and H_3O[162,163] could exist in the gas phase. The formation of NH_4 on solid surfaces has also been claimed[164,165] and H_3O has been postulated as an intermediate in water radiolysis experiments[166,167]. A recent report[168] of the ESR spectra of matrix-stabilized H_3O and D_3O radicals has been challenged on both experimental[169] and theoretical grounds[170]. Theoretically, the stability of gas phase NH_4 and H_3O with respect to dissociation into NH_3 + H· and H_2O + H· respectively, has not been clearly established. The calculations of Gangi and Bader[171] for H_3O indicate a barrier of 6.6 Kcals/mole along the dissociation path, suggesting the possibility of low temperature isolation. However, the calculations by Lathan et al.[172] indicate that NH_4 and H_3O are unstable with respect to dissociation, since potential minima were not found. Experimental evidence to support the existence of the H_2F radical has not been reported and theoretical calculations[172] indicate that the radical does not have a tightly bound structure. The fluoronium

ion, H_2F^+, has recently been observed[173] in a solid mixture and in solution by (low temperature) infrared spectroscopy.

Table 21 lists the predicted excitation and ionization energies of the NH_4, H_3O and H_2F radicals using the core analogy model. Theoretical values[174] for the ammonium radical have also been included. The theoretical and core analogy values for the excited states of NH_4 agree within experimental accuracy. This is illustrated in Figure 55, where we have indicated the relative energies of the calculated NH_4 states on the carbon K-shell electron energy loss spectrum of methane. The zero of the NH_4 energy scale corresponds to its ground electronic state. The position of the methane K-edge indicated on the spectrum is based on the experimental value determined by X-ray photoelectron spectroscopy[32]. Other calculations of the ionization potential of NH_4 give values of 3.92[172], 3.94[175,176], 3.97[175] and 3.8 eV[162,177], in good agreement with our predicted value of 3.7 ± 0.3 eV. The experimental value of 5.9 eV estimated by surface ionization techniques[162] is much larger than the predicted core analogy and theoretical values. Excited state calculations for the H_3O radical[171] give values of 4.4 and 5.2 eV for the two lowest excited states, which do not agree with our predicted values. The calculated ionization potential[171] (using a larger basis set) is 4.6 eV and is in better agreement with our predicted value of 5.0 ± 0.3 eV. Other calculated values for the ionization potential of H_3O give values of 5.8[172], 4.6[171], 4.4[175], 4.2[175,178] and 3.9 eV[162]. The experimental value[162] of ∿ 10.9 eV estimated from the appearance potential of H_3O^+ is appreciably larger than our predicted value. Calculations for excited states of the fluoronium radical, H_2F, have not

TABLE 21

ESTIMATED ENERGY LEVELS (eV) OF THE NH_4, H_3O AND HYPOTHETICAL H_2F RADICALS.

EXCITED ORBITAL	NH_4		H_3O	H_2F
	THIS WORK ΔE (eV)	THEORY[a] ΔE (eV)	THIS WORK ΔE (eV)	THIS WORK ΔE (eV)
GROUND STATE	0	0	0	0
3p	1.0	1.3	1.6 2.9	1.9 3.1
3d/4s		2.2		
4p	2.4	2.6	3.5	4.5
5p	2.8		4.0	
∞ (IP)	3.7	3.8[b]	5.0[c]	5.7[d]

a. Reference 174, the calculated ionization potential increased to 4.0 eV with a larger basis set.

b. Other calculations of the ionization potential of NH_4 give values of 3.92[172], 3.94[175],[176], 3.97[175], and 3.8 eV[162],[177].

c. Calculations of the ionization potential of H_3O give values of 5.8[172], 4.6[171], 4.4[175], 4.2[175],[178] and 3.9 eV[162].

d. A value of 8.57 eV has been calculated[172]

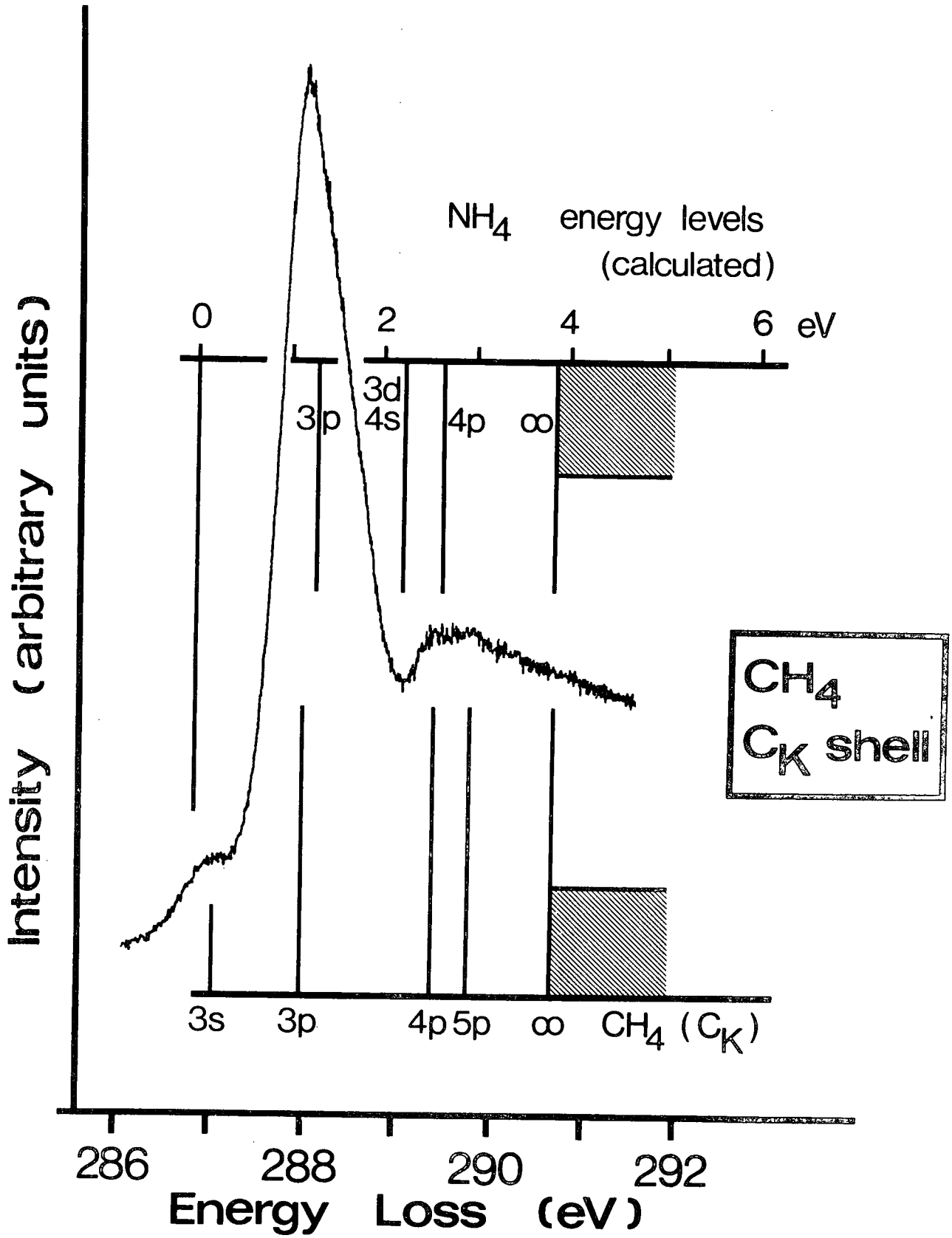

FIGURE 55. The carbon K-shell electron energy loss spectrum of methane and calculated energy levels of the ammonium radical (NH_4).

been reported. The calculated ionization potential[172], 8.57 eV, is larger than our predicted value, 5.7 ± 0.3 eV.

CHAPTER EIGHT

CONCLUSION

The K-shell energy loss spectra for a variety of small molecules have been studied using fast electron impact. The results demonstrate that high impact energy, electron energy loss spectroscopy is a viable alternative to the use of photoabsorption techniques for studying excitation processes in the soft X-ray and X-ray regions. In fact, there are some practical advantages to the use of electron impact spectroscopy, and with only modest energy selection of the incident beam, the resolution would be the same magnitude as the natural line widths of these highly excited states.

It has been shown that the K-shell spectra of the diatomic molecules, nitrogen and carbon monoxide, are consistent with the results expected on the basis of a simple core analogy model. This model has been used to estimate excitation and ionization energies for some exotic chemical species from the relative energies observed in the K-shell energy loss spectra of a number of molecules.

Finally, evidence for the possible existence of effective potential barriers in the carbon disulfide, carbonyl sulfide and carbon tetrafluoride molecules has been obtained. However, additional experiments (with higher resolution) complimented by theoretical calculations are necessary in order to substantiate these proposals.

REFERENCES

1. J. Franck and G. Hertz, Verhandl. Deut. Phys. Ges., 16 (1914) 457.
2. E. Rudberg, Proc. Roy. Soc. (London), A 27 (1930) 628.
3. J. Geiger and M. Topschowsky, Z. Naturforsch., 21a (1966) 626.
4. E. N. Lassettre, Rad. Res. Suppl. 1 (1959) 530.
5. E. N. Lassettre, Can. J. Chem., 47 (1969) 1733.
6. R. S. Berry, Ann. Rev. Rhys. Chem., 20 (1969) 357.
7. S. Trajmar, J. K. Rice and A. Kuppermann, Adv. Chem. Phys., 18 (1970) 15.
8. C. E. Brion, in A. Macoll (editor), MTP Int. Rev. of Sci., Phys. Chem., Ser. one, 5 (1972) 55, Butterworth, London.
9. J. B. Hasted, Cont. Phys., 14 (1973) 357.
10. U. Fano, Phys. Rev., 95 (1954) 1198.
11. M. Inokuti, Rev. Mod. Phys., 43 (1971) 297.
12. M. J.-A. Prins, Physica, 1 (1934) 1174.
13. T. Magnusson, Nova Acta Regiae Soc. Sci. Upsaliensis ser. III, 11 No. 3, (1938).
14. L. N. Mazolov, A. P. Sadovskii, V. M. Bertenev, K. E. Mironov, T. I. Guzhavina and L. I. Chernyavskii, Zh. Struk. Khim., 13 (1972) 859 [J. Struct. Chem., 13 (1972) 802].
15. A. S. Vinogradov and T. M. Zimkina, Optika I Spektrosk., 31 (1971) 685 [Optics and Spectrosc. 31 (1971) 364].
16. R. E. LaVilla and R. D. Deslattes, J. Chem. Phys., 44 (1966) 4399.
17. T. M. Zimkina and V. A. Fomichev, Doklady Akad. Nauk SSSR., 169 (1966) 1304 [Soviet Physics-Doklady, 11 (1967) 726].
18. A. S. Vinogradov, T. M. Zimkina and V. A. Fomichev, Zh. Struk. Khim., 12 (1971) 899 [J. Struct. Chem., 12 (1971) 823].
19. R. E. LaVilla, J. Chem. Phys., 57 (1972) 899.

20. V. A. Fomichev, Fiz. Tverd. Tela., 9 (1971) 3167 [Sov. Phys. Solid State, 9 (1968) 2496].

21. T. M. Zimkina and A. S. Vinogradov, Izv. Akad. Nauk SSSR. Ser. Fiz., 36 (1972) 248 [Bull. Acad. Sci. USSR. Physical Ser., 36 (1972) 229].

22. W. Hayes and F. C. Brown, J. Phys. B, 4 (1971) L85.

23. T. M. Zimkina and A. S. Vinogradov, J. de Physique, 32 Suppl. 10 (1971) C4-3.

24. A. S. Vinogradov and T. M. Zimkina, Optika I. Spektrosk., 31 (1971) 542 [Optics and Spectrosc., 31 (1971) 288].

25. W. Hayes and F. C. Brown, Phys. Rev. A, 6 (1972) 21.

26. R. E. LaVilla, J. Chem. Phys., 58 (1973) 3841.

27. M. Nakamura, M. Sasanuma, S. Sato, M. Watanabe, H. Yamashita, Y. Iguchi, A. Ejiri, S. Nakai, S. Yamaguchi, T. Sagawa, Y. Nakai and T. Oshio, Phys. Rev., 178 (1969) 80.

28. H.-U. Chun, Phys. Letters, 30 A (1969) 445.

29. M. J. van der Wiel, Th. M. El-Sherbini and C. E. Brion, Chem. Phys. Letters, 7 (1970) 161.

30. M. J. van der Wiel and Th. M. El-Sherbine, Physica, 59 (1972) 453.

31. M. Isaacson, J. Chem. Phys., 56 (1972) 1813.

32. K. Siegbahn, C. Nordling, G. Johansson, J. Hedman, P. F. Hedén, K. Hamrin, U. Gelius, T. Bergmark, L. O. Werme, R. Manne and Y. Baer, ESCA Applied to Free Molecules (North-Holland, Amsterdam, 1969).

33. D. Stalherm, B. Cleff, H. Hillig and W. Mehlhorn, Z. Naturforsch., 24a (1969) 1728.

34. T. A. Carlson, W. E. Moddeman, B. P. Pullen and M. O. Krause, Chem. Phys. Letters, 5 (1970) 390.

35. W. E. Moddeman, T. A. Carlson, M. O. Krause, B. P. Pullen, W. E. Bull and G. K. Schweitzer, J. Chem. Phys., 55 (1971) 2317.

36. F. Wuilleumier and M. O. Krause, Paper presented at "International Conference on Inner Shell Ionization Phenomena", 1972, Georgia Institute of Technology, Atlanta, Georgia.

37. R. E. LaVilla, J. Chem. Phys., 56 (1972) 2345.

38. L. O. Werme, B. Grennberg, J. Nordgren, C. Nordling and K. Siegbahn, Uppsala University report, Uppsala, Sweden, UUIP-803, 1972.

39. L. O. Werme, B. Grennberg, J. Nordgren, C. Nordling and K. Siegbahn, Phys. Rev. Letters, 30 (1973) 523.

40. R. A. Mattson and R. C. Ehlert, J. Chem. Phys., 48 (1968) 5465.

41. C. E. Kuyatt, in B. Bederson and W. L. Fite (editors), Methods of Experimental Physics, 7 A (1968) 1, Academic Press, New York, 1968.

42. L. G. Christophorou, Atomic and Molecular Radiation Physics, Wiley-Interscience, London - New York, 1971.

43. H. Bethe, Ann. Physik, 5 (1930) 325.

44. H. S. W. Massey and E. H. S. Burhop, Electronic and Ionic Impact Phenomena, Vol. 1, second edition, Oxford University Press, London, 1969.

45. B. L. Moiseiwitsch and S. J. Smith, Rev. Mod. Phys., 40 (1968) 238.

46. N. F. Mott and H. S. W. Massey, The Theory of Atomic Collisions, third edition, Oxford University Press, London, 1965.

47. H. S. W. Massey, Electronic and Ionic Impact Phenomena, Vol. II, second edition, Oxford University Press, London, 1969.

48. V. D. Meyer, A. Skerbele and E. N. Lassettre, J. Chem. Phys., 43,(1965) 805.

49. E. N. Lassettre, A. Skerbele, M. A. Dillon and K. J. Ross, J. Chem. Phys., 48 (1968) 5066.

50. W. R. Harshbarger, J. Chem. Phys., 54 (1971) 2504.

51. R. A. Bonham and J. Geiger, J. Chem. Phys., 51 (1969) 5246.

52. E. N. Lassettre, A. Skerbele and M. A. Dillon, J. Chem. Phys., 50 (1969) 1829.

53. A. Skerbele and E. N. Lassettre, J. Chem. Phys., 55 (1971) 424.

54. W. A. Goddard III, D. L. Huestis, D. C. Cartwright,and S. Trajmar, Chem. Phys. Letters, 11 (1971) 329.

55. E. N. Lassettre and A. Skerbele, J. Chem. Phys., 54 (1971) 1597.

56. W. R. Harshbarger, A. Skerbele and E. N. Lassettre, J. Chem. Phys., 54 (1971) 3784.

57. I. V. Hertel and K. J. Ross, J. Phys. B (Proc. Phys. Soc.), 1 (1968) 697.

58. I. V. Hertel and K. J. Ross, J. Phys. B (Atom. Mol. Phys.) 2 (1969) 285

59. J. Geiger and K. Wittmaack, Z. Naturforsch., 20 a (1965) 628.

60. J. Geiger and W. Stickel, J. Chem. Phys., 43 (1965) 4535.

61. J. Geiger and B. Schröder, J. Chem. Phys., 49 (1968) 740.

62. J. Geiger and B. Schröder, J. Chem. Phys., 50 (1969) 7.

63. M. J. van der Wiel, Physica, 49 (1970) 411.

64. A. Skerbele and E. N. Lassettre, J. Chem. Phys., 53 (1970) 3806.

65. K. Siegbahn, C. Nordling, A. Fahlman, R. Nordberg, K. Hamrin, J. Hedman, G. Johansson, T. Bergmark, S.-E. Karlsson, I. Lindgren and B. Lindberg, ESCA, Atomic, Molecular and Solid State Structure by means of Electron Spectroscopy, Almqvist and Wiksells, Uppsala, 1967.

66. K. Siegbahn, L. Werme, B. Grennberg, J. Nordgren and C. Nordling, Phys. Letters, 41 A (1972) 111.

67. J. A. Simpson, in V. W. Hughes and H. L. Schultz, editors, Methods of Experimental Phys., 4 A (1967) 127.

68. H. Z. Sar-El, Rev. Sci. Instr., 41 (1970) 561.

69. B. Wannberg, U. Gelius and K. Siegbahn, J. Phys. E., Sci. Instr., 7 (1974) 149.

70. E. M. Purcell, Phys. Rev., 54 (1938) 818.

71. J. A. Simpson, Rev. Sci. Instr., 35 (1964) 1698.

72. J. A. Simpson and C. E. Kuyatt, J. Appl. Phys., 37 (1966) 3805.

73. C. E. Kuyatt and J. A. Simpson, Rev. Sci. Instr., 38 (1967) 103.

74. J. B. Hasted, Physics of Atomic Collisions, second edition, Butterworth and Co., London, 1972.

75. G. Hertzberg, Molecular Spectra and Molecular Structure I. Spectra of Diatomic Molecules, (second edition) Van Nostrand Reinhold Co., New York, 1950.

76. J. T. Vanderslice, P. G. Wilkinson and S. G. Tilford, J. Chem. Phys., 42 (1965) 2681.

77. R. A. Bonham, personal communication.

78. D. W. Turner, C. Baker, A. D. Baker and C. R. Brundle, Molecular Photoelectron Spectroscopy, Wiley-Interscience, London, 1970.

79. O. Edqvist, E. Lindholm, L. E. Selin, H. Sjögren and L. Åsbrink, Arkiv. för Fysik, 40, (1970) 439.

80. B. L. Henke, R. White and B. Lundberg, J. Appl. Phys., 28 (1957) 98.

81. T. A. Carlson, M. O. Krause and W. E. Moddeman, J. Phys. (Paris), Coll. C4, Supp. 10, 32 (1971) C4-76.

82. F. Wuilleumier and M. O. Krause, Electron Spectroscopy, D. A. Shirley, (editor) North Holland Publishing Co., Amsterdam, London, 1972, page 259.

83. A. Skerbele and E. N. Lassettre, J. Chem. Phys., 42 (1965) 395.

84. A. P. Lukirskii, I. A. Brytov and T. M. Zimkina, Opt. Spectrosc. (USSR), 17 (1964) 234.

85. R. W. Shaw and T. D. Thomas, Chem. Phys. Letters, 14 (1972) 121.

86. E. B. Andrews and R. F. Barrow, Proc. Phys. Soc. A, 64 (1951) 481.

87. B. A. Thrush and J. J. Zwolenik, Trans. Faraday Soc., 59 (1963) 582.

88. T. L. Porter, D. E. Mann and N. Acquista, J. Molec. Spectrosc. 16 (1965) 228.

89. P. K. Carroll and T. P. Grennan, J. Phys. B, 3 (1970) 865.

90. J. A. Hall and W. G. Richards, Mol. Phys., 23 (1972) 331.

91. J. W. C. Johns and R. F. Barrow, Proc. Phys. Soc. A, 71 (1958) 476.

92. P. A. G. O'Hare and A. C. Wahl, J. Chem. Phys., 55 (1971) 666.

93. D. W. Davis and D. A. Shirley, J. Chem. Phys., 56 (1972) 669.

94. D. W. Davis, R. L. Martin, M. S. Banna, and D. A. Shirley, J. Chem. Phys., 59 (1973) 4235.

95. R. K. Nesbet, J. Math. Phys., 2 (1961) 701.

96. J. B. Mann, "Atomic Structure Calculations. I. Hartree-Fock Energy Results for the Elements Hydrogen to Lawrencium", Los Almos Scientific Laboratory Report LA-3690.

97. W. L. Jolly and D. N. Hendrickson, J. Am. Chem. Soc., 92 (1970) 1863.

98. W. L. Jolly, J. Amer. Chem. Soc., 92 (1970) 3260.

99. L. J. Aarons and I. H. Hillier, J. Chem. Soc. Faraday II, 69 (1973) 1510.

100. O. Edqvist, E. Lindholm, L. E. Selin, and L. Åsbrink, Physica Scripta, 1 (1970) 25.

101. K. Dressler and E. Miescher, Astrophys. J., 141 (1965) 1266.

102. D. C. Cartwright, W. J. Hunt, W. Williams, S. Trajmar, and W. A. W. A. Goddard, III, Phys. Rev. A, 8 (1973) 2436.

103. J. A. Pople and D. L. Beveridge, Approximate Molecular Orbital Theory, McGraw-Hill, New York, 1970.

104. A. E. Douglas and W. E. Jones, Can. J. Phys., 44 (1966) 2251.

105. W. E. Jones, Can. J. Phys., 45 (1967) 21.

106. P. A. G. O'Hare and A. C. Wahl, J. Chem. Phys., 54 (1971) 4563.

107. J. T. Herron and V. H. Dibeler, J. Res. Natl. Bur. Std., 65 A (1961) 405.

108. R. M. Reese and V. H. Dibeler, J. Chem. Phys., 24 (1956) 1175.

109. U. Gelius, E. Basilier, S. Svensson, T. Bergmark, and K. Siegbahn, J. Electron Spectrosc., 2 (1973) 405.

110. A. Arkell, R. R. Reinhard, and L. P. Larson, J. Am. Chem. Soc., 87 (1965) 1016.

111. I. J. Solomon, A. J. Kacmarek, and J. Raney, J. Phys. Chem. 72 (1968) 2262.

112. L. Andrews, J. Chem. Phys., 57 (1972) 51.

113. M. A. A. Clyne and R. T. Watson, Chem. Phys. Letters, 12 (1971) 344.

114. P. A. G. O'Hare and A. C. Wahl, J. Chem. Phys., 53 (1970) 2469.

115. T. J. Malone and H. A. McGee, Jr., J. Phys. Chem., 69 (1965) 4338.

116. S. Trajmar, W. Williams and A. Kuppermann, J. Chem. Phys., 56 (1972) 3759.

117. P. S. Bagus and H. F. Schaefer III, J. Chem. Phys., 56 (1972) 224.

118. V. Y. Foo, C. E. Brion and J. B. Hasted, Proc. Roy. Soc. (London), A 322 (1971) 535.

119. J. W. Rabalais, J. M. McDonald, V. Scherr, and S. P. McGlynn, Chemical Reviews, 71 (1971) 73.

120. G. Herzberg, Molecular Spectra and Molecular Structure III. Electronic Spectra and Electronic Structure of Polyatomic Molecules, D. Van Nostrand Co., New York, N.Y., 1966.

121. J. L. Hardwick and J. C. D. Brand, Chem. Phys. Letters, 21 (1973) 458.

122. O. Edquist, E. Lindholm, L. E. Selin, L. Åsbrink, C. E. Kuyatt, S. R. Mielczarek, J. A. Simpson and I. Fischer-Hjalmars, Physica Scripta 1 (1970) 172.

123. P. C. Killgoar, Jr., G. E. Leroi, W. A. Chupka and J. Berkowitz, J. Chem. Phys., 59 (1973) 1370.

124. E. Lindholm, Arkiv för Fysik, 40 (1969) 125.

125. C. J. Allan, U. Gelius, D. A. Allison, G. Johansson, H. Siegbahn and K. Siegbahn, J. Electron Spectrosc., 1 (1972/73) 131.

126. E. N. Lassettre, J. Chem. Phys., 53 (1970) 3801.

127. E. Lindholm, Arkiv för Fysik, 40 (1969) 129.

128. C. J. Allan, personal communication.

129. C. Jungen, D. N. Malm and A. J. Merer, Can. J. Phys., 51 (1973) 1471.

130. E. Lindholm, Arkiv för Fysik, 40 (1969) 97.

131. J. L. Dehmer, J. Chem. Phys., 56 (1972) 4496.

132. U. Fano, Comments Atomic and Molecular Physics, III #3 (1972) 75.

133. B. Cadioli, U. Pincelli, E. Tosatti, U. Fano and J. L. Dehmer, Chem. Phys. Letters, 17 (1972) 15.

134. V. I. Nefedov, Zh. Strukt. Khim. 11 (1970) 292 [J. Struct. Chem. 11 (1970) 272].

135. M. B. Robin, International J. Quantum Chem., 6 (1972) 257.

136. W. R. Harshbarger, M. B. Robin and E. N. Lassettre, J. Electron Spectrosc. 1 (1972/73) 319.

137. H. Hartmann and H.-U. Chun, Theoret. Chim. Acta, 2 (1964) 1.

138. H.-U. Chun, T.-K. Ha and R. Mann, Z. Phys. Chem. (Frankfurt), 47 (1965) 313.

139. H.-U. Chun and H. Gebelein, Z. Naturforsch. 22a (1967) 1813.

140. H.-U. Chun, Z. Naturforsch., 23a (1968) 1415.

141. P. W. Deutsch and A. B. Kunz, J. Chem. Phys., 59 (1973) 1155.

142. P. S. Bagus, M. Krauss and R. E. LaVilla, Chem. Phys. Letters, 23 (1973) 13.

143. W. R. Harshbarger and E. N. Lassettre, J. Chem. Phys., 58 (1973) 1505.

144. C. R. Brundle, M. B. Robin and H. Basch, J. Chem. Phys., 53 (1970) 2196.

145. A. D. Walsh and P. A. Warsop, Trans. Faraday Soc., 57 (1961) 345.

146. A. B. F. Duncan, Rydberg Series in Atoms and Molecules, Academic Press, New York, 1971. Physical Chemistry, Vol. 23, E. M. Loebel, editor.

147. J. W. Rabalais, L. Karlsson, L. O. Werme, T. Bergmark and K. Siegbahn, J. Chem. Phys., 58 (1973) 3370.

148. W.-C. Tam and C. E. Brion, J. Electron Spectrosc., 3 (1974) 263.

149. S. Trajmar, W. Williams, and A. Kuppermann, J. Chem. Phys., 58 (1973) 2521.

150. M. B. Robin and N. A. Kuebler, J. Electron Spectrosc., 1 (1972/73) 13.

151. W. A. Goddard III and W. J. Hunt, Chem. Phys. Letters, 24 (1974) 464.

152. C. R. Claydon, G. A. Segal and H. S. Taylor, J. Chem. Phys., 54 (1971) 3799.

153. W. J. Hunt and W. A. Goddard III, Chem. Phys. Letters, 3 (1969) 414.

154. S. Cradock and R. A. Whiteford, J. Chem. Soc. Faraday II, 68 (1972) 281.

155. J. S. Jen and T. D. Thomas, J. Electron Spectrosc., in press.

156. W. H. Fink and L. C. Allen, J. Chem. Phys., 46 (1967) 2276.

157. P. Finn, R. K. Pearson, J. M. Hollander and W. L. Jolly, Inorganic Chemistry, 10 (1971) 378.

158. F. Wuilleumier, C. R. Acad. Sc. (Paris) 270 B (1970) 825.

159. T. Shimanouchi, Tables of Molecular Vibrational Frequencies Part I, National Bureau of Standards, NSRDS - NBS 6 1967.

160. R. H. Huebner, R. J. Celotta, S. R. Mielczarek and C. E. Kuyatt, J. Chem. Phys., 59 (1973) 5434.

161. W.-C. Tam and C. E. Brion, J. Electron Spectrosc., in press.

162. C. E. Melton and H. W. Joy, J. Chem. Phys., 46 (1967) 4275.

163. C. E. Melton and P. S. Rudolph, J. Catalysis, 5 (1966) 387.

164. C. E. Melton, J. Amer. Chem. Soc., 84 (1962) 1491.

165. C. E. Melton, J. Chem. Phys., 45 (1966) 4414.

166. J. L. Magee, Rad. Res. Suppl., 4 (1964) 20.

167. T. J. Sworski, J. Amer. Chem. Soc., 86 (1964) 5034.

168. T. W. Martin and L. L. Swift, J. Amer. Chem. Soc., 93 (1971) 2788.

169. J. A. Wargon and F. Williams, Chem. Phys. Letters, 13 (1972) 579.

170. N. D. Chuvylkin and G. M. Zhidomirov, Chem. Phys. Letters, 14 (1972) 70.

171. R. A. Gangi and R. F. W. Bader, Chem. Phys. Letters, 11 (1971) 216.

172. W. A. Lathan, W. J. Hehre, L. A. Curtiss and J. A. Pople, J. Amer. Chem. Soc., 93 (1971) 6377.

173. M. Couzi, J.-C. Cornut, and P. V. Huong, J. Chem. Phys., 56 (1972) 426.

174. W. Strehl, H. Hartmann, K. Hensen and W. Sarholz, Theor. Chim. Acta., 18 (1970) 290.

175. D. M. Bishop, J. Chem. Phys., 48 (1968) 5285.

176. D. M. Bishop, J. Chem. Phys., 40 (1964) 432.

177. C. E. Melton and H. W. Joy, J. Chem. Phys., 48 (1968) 5286.

178. D. M. Bishop, J. Chem. Phys., 45 (1966) 2474.